

Redox-switchable Copolymerization: Transforming Underutilized Monomer Feedstocks to Complex Copolymers

Matthew Scott Thompson

A dissertation
submitted to the Faculty of
the department of Chemistry
in partial fulfillment
of the requirements for the degree of
Doctor of Philosophy

Boston College
Morrissey College of Arts and Sciences
Graduate School

December 2021

Redox-switchable Copolymerization: Transforming Underutilized Monomer Feedstocks to Complex Copolymers

Matthew S. Thompson

Advisor: Jeffrey A. Byers, Ph.D.

Abstract: This dissertation covers the development of redox-switchable ring-opening polymerizations for the synthesis of copolymers of underutilized monomers. In Chapter one, the progress in the development of switchable methods for ring-opening polymerization and ring-opening copolymerizations. Chapter two describes a method for the redox-switchable copolymerization of *L*-lactide, propylene oxide and carbon dioxide. The benefits of this method are demonstrated through the facile synthesis of blocky and statistical copolymers of the three monomers. In Chapter three, a method for the redox-switchable polymerization of *N*-carboxyanhydrides is presented. A mechanistic analysis and copolymerizations of *N*-carboxyanhydrides and either lactones or epoxides follow the initial findings. Chapter four further expands the uses of *N*-carboxyanhydride redox-switchable polymerizations by immobilizing the catalysts onto semiconductor surfaces for the synthesis of surface bound polyamides.

TABLE OF CONTENTS

Table of Contents	iv
Abbreviations	vii
List of Schemes	x
List of Figures	xvi
List of Tables	xxii
Acknowledgements	xiii
1. Chapter 1. Switchable Ring-opening Polymerization and Ring-opening Copolymerizations: Methods and Applications	1
1.1 Introduction.....	1
1.2 Chemically-switchable Ring-opening Polymerization.....	4
1.21 Acid/base-switchable Ring-opening Polymerization.....	12
1.22 Pressure-switchable Ring-opening polymerization.....	15
1.3 Photoswitchable Ring-opening Polymerization.....	20
1.4 Redox-switchable Ring-opening Polymerization.....	27
1.5 Conclusion.....	39
1.6 References.....	40
2. Chapter 2. Redox-switchable Polymerization by Chain-transfer (ReSPCT): A Versatile Method for the Copolymerization of Lactones, Epoxides and Carbon Dioxide	58
2.1 Introduction.....	58

2.2 Initial Screening of Catalysts for <i>L</i> -lactide ROP.....	65
2.3 Optimizing Homopolymerization Conditions.....	73
2.4 Kinetics of <i>L</i> -lactide Ring-opening polymerization and Propylene Oxide-CO ₂ Ring-opening Copolymerization During Redox Switches.....	77
2.5 Sequential Copolymerization of <i>L</i> -Lactide, Propylene Oxide and CO ₂ for Multi-block Copolymers	81
2.6 Synthesis of Statistical Copolymers of <i>L</i> -Lactide, Propylene Oxide and CO ₂	93
2.7 Conclusion.....	102
2.8 Experimental.....	103
2.9 References.....	112
3.0 Chapter 3. Redox-switchable, <i>N</i>-carboxyanhydride Polymerization and Applications for Copolymerization	125
3.1 Introduction.....	125
3.2 Polymerization of <i>N</i> -Carboxyanhydrides by Redox-switchable Iron Bis(imino)pyridine Alkoxide Complexes.....	129
3.3 Redox-switchable Polymerization of NCAs, the Unexpected Effect of Lewis Acid Additives and the Subsequent Mechanistic Investigation	130
3.4 Copolymerization of Caprolactone and Sarcosine-NCA.....	145
3.5 Copolymerization of Sarcosine-NCA and Cyclohexene Oxide.....	149
3.6 Conclusion	157
3.7 Experimental	158
3.8 References	174

4.0 Chapter 4: Redox-switchable, <i>N</i>-carboxyanhydride Polymerization from Surface-anchored Catalysts.....	188
4.1 Introduction.....	188
4.2 Synthesis of Iron on Titania Nanoparticles and their Activity for NCA Polymerization.....	190
4.3 Anchoring Iron Complexes onto Electrode Surfaces and Their Activity for Sarcosine-NCA Polymerization.....	197
4.4 Redox behavior of Anchored Iron Complexes on Electrode Surfaces.....	203
4.5 Conclusion.....	206
4.6 Experimental.....	207
4.7 References.....	212
5.0 Appendix A. NMR Spectra for All Complexes and Polymers.....	222
6.0 Appendix B. GPC Chromatograms for All Polymers.....	257
7.0 Appendix C. MALDI Mass Spectrums and Control Reactions from Chapter 3	264

Abbreviations

2-MeTHF	2-methyltetrahydrofuran
δ	Chemical shift (NMR)
Ω	Ohm
A	ampere
Å	Angstrom
Ar	Aryl
atm	atmosphere
ATR	Attenuated Total Reflectance
BAr ^{F24}	tetrakis[3,5-bis(trifluoromethyl)phenyl] borate
BAr ^{F20}	tetrakis(2,3,4,5,6-pentafluoro)phenyl] borate
BIP	2,6-Bis(iminomethyl)pyridine
Bu	butyl
CHO	Cyclohexene oxide
CL	ϵ -Caprolactone
CoCp ₂	cobaltocene
Conv.	Conversion
Cp	Cyclopentadienyl
Cp*	Decamethylcyclopentadienyl
CTA	chain transfer agent

Equiv.	equivalents
DOSY	Diffusion Ordered Spectroscopy
Et	Ethyl
g	grams
GPC	Gell Permeation Chromatography
h	hour
ICP-OES	Inductively Coupled Plasma Optical Emission Spectroscopy
iPr	isopropyl
Fc	Ferrocene
FTIR	Fourier Transform Infrared Spectroscopy
L	liter
m	meter
<i>m</i>	meta
M	Molarity (mol/ L)
M_n	Number average molecular weight
M_w	Weight average molecular weight
M_w/M_n	polymer dispersity
Me	methyl
Mes	2,4,6-trimethylphenyl
min	min
mol	mole
Np	neopentyl

NMR	Nuclear magnetic resonance
<i>o</i>	ortho
OMRP	Organometallic mediate radical polymerizations
<i>p</i>	para
PC	propylene carbonate
Ph	phenyl
s	second
salen	3,5-di-tert-butyl-salicaldehyde
SAM	simple amine method
^t Bu	tert-butyl
THF	tetrahydrofuran
V	volt

List of Schemes

Scheme 1.1. Copolymer synthesis from monomer mixtures using switchable catalysis. a) Polymerization of monomer 1 selectively in a mixed monomer solution. b) Polymerization of monomer 2 selectively in a mixed monomer solution. c) Polymerization of monomer 1 selectively then monomer 2 to produce diblock copolymers from a mixed monomer solution. d) Synthesis of a blocky copolymer with a catalyst active for both monomers 1 and 2, but more reactive for 1. e) Synthesis of a statistical copolymer with a catalyst equally active for both monomers 1 and 2.	2
Scheme 1.2 Chloride controlled, chemically-switchable polymerization of ϵ -caprolactone through the allosteric inhibition of a triple-layer aluminum catalyst.....	5
Scheme 1.3 Chemically-switchable copolymerization of valerolactone and propylene oxide using iterative additions of Lewis acids and bases to synthesize a pentadecablock poly(ester-b-ether).	6
Scheme 1.4 Chemically-switchable, terpolymerization of cyclohexene oxide, CO ₂ and diglycolic anhydride by a zinc carboxylate catalyst, 1.3.....	7
Scheme 1.5 Representative catalysts that have demonstrated chemically-switchable, terpolymerization of epoxides, anhydrides and CO ₂	7
Scheme 1.6 Doubly chemically-switchable terpolymerization of cyclohexene oxide, CO ₂ and phthalic anhydride.....	8
Scheme 1.7 Four component chemically-switchable polymerization of cyclohexene oxide, phthalic anhydride, ϵ -caprolactone and CO ₂ catalyzed by a dizinc catalyst, 1.4.....	9
Scheme 1.8 Synthesis of isosikaiheptablock copolymers of propylene oxide, phthalic anhydride and lactide through chemically-switchable catalysts.....	10
Scheme 1.9 Self-switchable, quadripolymerization of <i>L</i> -phenylalanine OCA, phthalic anhydride, nbutyl-glycidyl ether and L-lactide by a simple, organobase catalyst.....	12
Scheme 1.10 Acid-switchable ROMP by inhibition of a Grubbs 1st generation catalyst, 1.10, with <i>N</i> -methylimidazole to form 1.11 which is inactive for ROMP. Catalyst is reactivated through In-situ synthesis of a highly active catalyst, 1.12 upon the addition of phosphoric acid.....	12
Scheme 1.11 Acid-switchable, norbornene ROMP with tunable E/Z ratio through the addition of hydrochloric acid to a pH-sensitive, Hoveyda-Grubbs type complex, 1.13.....	13
Scheme 1.12 One-pot synthesis of copolymers of ϵ -caprolactone or trimethylene carbonate and γ -benzyl-L-aspartate NCA through acid/base-switchable polymerization.....	14
Scheme 1.13 Copolymerization of propylene oxide, CO ₂ and lactide in one-pot using a two catalyst system.....	16
Scheme 1.14 Pressure-switchable copolymerization of lactide, propylene oxide and CO ₂	17

Scheme 1.15 One-pot copolymerization of cyclohexene oxide, ϵ -decalactone and CO ₂ to produce triblock copolymers with widely-tunable, mechanical properties.....	18
Scheme 1.16. Copolymerization of propylene oxide and phthalic anhydride by cobalt salen catalyst, 1.17, followed by the one cyclization driven by the addition of carbon monoxide and then white light organometallic mediated controlled radical cyclization. Synthesis of tadpole-shaped copolymers from pre-formed cobalt(III) alkyl cyclic polyester, 1.18, and methyl acrylate by OMRP.....	19
Scheme 1.17 Synthesis of poly(valerolactone) by the photoswitchable polymerization of valerolactone by 2-trans-cinnamoyl- α -cyclodextrin 1.20.....	20
Scheme 1.18 Photoisomerization of azo-benzene containing thiourea 1.21 to sterically-congested species 1.22 and its influence on lactide ROP in the presence of an amine base PMDTA.	21
Scheme 1.19 Light and base driven photocyclization of phenolic species 1.23 to keto-tautomer 1.25 and the difference in catalyst reactivity towards valerolactone and trimethylene carbonate ROP.....	22
Scheme 1.20 Photoisomerization of a zinc half-salen catalyst 1.26 bearing a pendant azobenzene group to change the reactivity of the catalysts towards lactide ROP.....	23
Scheme 1.21 Photocyclization of dithiophene bearing <i>N</i> -heterocyclic carbene precatalyst 1.28 to 1.29 and its influence on valerolactone ROP.....	24
Scheme 1.22 (a) Photoacid, 1.30 , catalyzed polymerization of valerolactone. (b) Dual photocatalysts for the Janus-type copolymerization of methacrylate and valerolactone.....	25
Scheme 1.23 Metal-free ROMP of norbornene catalyzed by a pyrillium photocatalyst 1.34 initiated by vinyl ethers.....	26
Scheme 1.24 Photoswitchable ROMP of cyclooctadiene catalyzed by a Hoveyda-Grubbs variant 1.35 bearing a photoswitchable thiazole ligand.....	26
Scheme 1.25 Stereolithography by ROMP of DCPD with a deactivated catalyst Grubbs II type catalyst 1.37. UV light activates the catalyst to induce cross-linking of dicyclopentadiene.....	27
Scheme 1.26 Redox-switchable, catalyst consisting of a titanium-salen complex 1.38 containing pendant ferrocene moieties. When the ferrocene moieties are reduced the complex is active for lactide polymerization, while the polymerization is much slower when the ferrocene moieties are oxidized.....	28
Scheme 1.27 Site of oxidation for various redox-active lactide polymerization catalysts. Reduced moiety is in red and oxidized moieties are in blue. For all catalyst redox pairs, the reduced species were more active for lactide ROP than the oxidized species.....	29
Scheme 1.28 Redox-switchable copolymerization of <i>L</i> -lactide and ϵ -caprolactone by titanium-salen complex 1.46 containing a pendant ferrocene moiety.....	30
Scheme 1.29 Redox-switchable iron bis(imino)pyridine alkoxide catalyst 1.48 displays orthogonal reactivity towards <i>rac</i> -lactide and cyclohexene oxide depending on oxidation state. Catalyst	

oxidation state can be altered with both chemical redox reagents and electrochemistry reversibly.....	31
Scheme 1.30 Redox-switchable zirconium salfan alkoxide catalyst 1.50 displays orthogonal reactivity towards L-lactide and cyclohexene oxide depending on oxidation state of the ferrocene moiety.....	32
Scheme 1.31 Polymerization and in-situ crosslinking of a cyclic diester-epoxide through redox-switchable polymerization.....	33
Scheme 1.32 Redox-switchable initiation of norbornene ROMP with a Hoveyda-Grubbs type catalyst containing a ferrocene moiety on the alkylidene initiating ligand.....	34
Scheme 1.33 a) Redox-switchable initiation of norbornene ROMP with a modified Hoveyda-Grubbs II catalysts containing a ferrocene moiety on the NHC spectator ligand. b) Redox-switchable ROMP of a derivative containing a silyl ether by a cationic palladium complex bearing a ferrocene-containing ligand.....	35
Scheme 1.34 a) Electrochemically redox-switchable polymerization of <i>rac</i> -lactide and cyclohexene oxide. b) Magnification of pre-existing polymer dispersity by mass-transport to the electrode during electrochemical redox-switchable polymerization.....	36
Scheme 1.35 a) The anchoring of redox-active, iron(II) bis(imino)pyridine alkyl complex 1.58 onto TiO ₂ nanoparticles. B) The anchoring of redox-active, iron(II) bis(imino)pyridine alkyl complex 1.58 onto layered surfaces consisting of TiO ₂ nanoparticles on a layer of FTO on glass slides. Complex was active for separate polymerizations in each redox-state.....	38
Scheme 2.1 Previous methods for the copolymerization of lactide, propylene oxide and CO ₂ in one-pot. a) CO ₂ -switchable copolymerization of propylene oxide and CO ₂ and then lactide by sequential addition of monomers. b) CO ₂ -switchable copolymerization of lactide then propylene oxide and CO ₂ . c) Statistical copolymerization of propylene oxide, CO ₂ and lactide by a three component catalyst system.....	62
Scheme 2.2 Formation of active catalyst for propylene oxide-CO ₂ ROCOP through <i>in-situ</i> oxidation of cobalt(II) catalyst 2.4 in the presence of a nucleophilic cocatalyst.....	63
Scheme 2.3 Accessing blocky and statistical copolymers of L-lactide, propylene oxide and CO ₂ through redox-switchable polymerization by chain transfer (ReSPCT). A) Selectivity of catalysts for lactide ROP or propylene oxide-CO ₂ ROCOP depending on oxidation state of the cobalt salen catalyst. b) Demonstration of how ReSPCT can be utilized to synthesize blocky and statistical copolymers of lactide, propylene oxide and CO ₂ . Sliders represent the relative ratio of cobalt(II)-based to cobalt(III)-based catalyst in the reaction mixture at any given point in the reaction with the top position being 100% cobalt (II) and the bottom representing 100% cobalt(III).....	64
Scheme 2.4 Representative cocatalysts used for epoxide-CO ₂ ROCOP with cobalt salen complexes.....	65
Scheme 2.5 Original design for redox-switchable polymerization by chain-transfer (ReSPCT) for the copolymerization of L-lactide, propylene oxide and CO ₂	67

Scheme 2.6 a) Polymerization of <i>L</i> -lactide by 18-crown-6 potassium tert-butoxide with and without 2.4. b) <i>In-situ</i> oxidation of 2.4 during <i>L</i> -lactide ROP. c) <i>In-situ</i> oxidation of 2.4 during <i>L</i> -lactide ROP.....	68
Scheme 2.7 Proposed mechanism for the deactivation of cobalt(III) catalysts during the ring-opening copolymerization of epoxides and carbon dioxide consistent with the detection of acetaldehyde.....	69
Scheme 2.8 Cobalt(III) salen complexes for epoxide-anhydride ROCOP. Fluorine-containing cobalt(III) salen complex 2.8 is resistant to autoreduction to inactive cobalt(II) species 2.9.....	69
Scheme 2.9 Synthesis of cobalt(II) salen-F complex 2.9.....	70
Scheme 2.10 Redox-switchable polymerization of <i>L</i> -lactide using FcBF ₄ and a) cobaltocene (CoCp ₂) or b) decamethylcobaltocene (CoCp* ₂).....	72
Scheme 2.11 Modified design for redox-switchable polymerization by chain-transfer for the copolymerization of <i>L</i> -lactide, propylene oxide and CO ₂	77
Scheme 2.12 Procedure for the ReSPCT copolymerization of <i>L</i> -lactide, propylene oxide and CO ₂ for the synthesis of diblock copolymers. (a) Synthesis of poly(<i>L</i> -lactic acid- <i>b</i> -propylene carbonate). (b) Synthesis of poly(propylene carbonate- <i>b</i> - <i>L</i> -lactic acid).....	82
Scheme 2.13 Procedure for the ReSPCT copolymerization of <i>L</i> -lactide, propylene oxide and CO ₂ for the synthesis of asymmetric, tri-block copolymers. (a) Synthesis of poly(<i>L</i> -lactic acid- <i>b</i> -propylene carbonate- <i>b</i> - <i>L</i> -lactic acid). (b) Synthesis of poly(propylene carbonate- <i>b</i> - <i>L</i> -lactic acid- <i>b</i> -propylene carbonate).....	86
Scheme 2.14 Procedures for the ReSPCT copolymerization of <i>L</i> -lactide, propylene oxide and CO ₂ with 1,8-octanediol as an initiator.....	91
Scheme 2.15 Statistical copolymerization of <i>L</i> -lactide, propylene oxide and CO ₂ by mixed species of cobalt(II) and cobalt(III)-based salen complexes.....	93
Scheme 2.16 Procedure for ReSPCT copolymerization of <i>L</i> -lactide, propylene oxide and CO ₂ to synthesize statistical copolymers.....	94
Scheme 2.17 Procedure for ReSPCT of <i>L</i> -lactide, propylene oxide and CO ₂ to synthesize mixed-blocky and statistical copolymers. (a) Synthesis of poly(<i>L</i> -lactic acid- <i>b</i> -(<i>L</i> -lactic acid- <i>s</i> -propylene carbonate)- <i>b</i> - <i>L</i> -lactic acid). (b) Synthesis of poly(propylene carbonate- <i>b</i> -(<i>L</i> -lactic acid- <i>s</i> -propylene carbonate)- <i>b</i> -propylene carbonate). 99	99
Scheme 3.1 Synthesis of NCAs from amino acids and the polymerization of NCAs through the simple amine method.....	126
Scheme 3.2 Previous methods to produce copolymers of polyamides and other polymers: (a) End group deprotection of a macroinitiator. (b) Sequential addition of strong acids and bases. Methods reported in this work using iron-based catalysts: (c) Sequential addition of monomers using; and (d) Redox-switchable copolymerization.....	127

Scheme 3.3 Iron bis(iminopyridine) alkoxide complexes used in redox-switchable copolymerizations of (left) lactide and cyclohexene oxide and (right) N-carboxyanhydride (NCAs) and cyclohexene oxide.....	130
Scheme 3.4 Proposed coordination-insertion mechanism for γ -benzyl-L-glutamate-NCA (BLG-NCA) or and sarcosine-NCA (Sar-NCA) polymerization catalyzed by 3.1 and co-catalyzed by a Lewis acid co-catalyst (A). The Lewis acidic co-catalyst could serve two functions: to activate the NCA monomer for insertion and/or to prevent product inhibition by inhibiting polyamide binding to the catalyst.....	141
Scheme 3.5 a) Diblock copolymerization of ϵ -caprolactone (CL) then sarcosine-NCA (Sar-NCA) by 3.1 and $[\text{CoCp}_2][\text{BAR}^{\text{F}24}]$ through sequential addition of monomers. b) Attempted copolymerization of sarcosine-NCA then ϵ -caprolactone, but only poly(sarcosine) was observed. (c) Telechelic, triblock copolymerization of ϵ -caprolactone then sarcosine-NCA by 3.7 and $[\text{CoCp}_2][\text{BAR}^{\text{F}24}]$ through sequential addition of monomers.....	145
Scheme 3.6 Polymerization of cyclohexene oxide (CH) by 3.2.....	150
Scheme 3.7 Attempted synthesis of polyether-polyamide diblock copolymers using a 3.1/3.2 catalyzed redox-switchable polymerization in a solution of mixed monomers.....	151
Scheme 3.8 Synthesis of polyether-polyamide diblock copolymers using a 3.1/3.2 catalyzed redox-switchable polymerization a) Poly(sarcosine- <i>b</i> -cyclohexene oxide) and b) poly(cyclohexene oxide- <i>b</i> -sarcosine) synthesis required the sequential addition of redox reagents and monomers.....	152
Scheme 3.9 Synthesis of polyether-polyamide triblock copolymers using a 3.1/3.2 catalyzed redox-switchable polymerization. (a) Poly(sarcosine- <i>b</i> -cyclohexene oxide- <i>b</i> -sarcosine) and (b) poly(cyclohexene oxide- <i>b</i> -sarcosine- <i>b</i> -cyclohexene oxide').....	155
Scheme 4.1 The anchoring of redox-active, iron(II) bis(imino)pyridine alkyl complex 1.58 onto TiO_2 nanoparticles and the oxidation of these solid-supported iron complexes.....	190
Scheme 4.2 Polymerization of <i>rac</i> -lactide or cyclohexene oxide off of titanium nanoparticles by surface anchored iron complexes.....	194
Scheme 4.3 Cleavage of poly(sarcosine) from TiO_2 nanoparticles by treatment with methyl iodide.....	195
Scheme 4.4. Comparison of molecular and surface bound catalysts for ROP a) Polymerization of sarcosine-NCA by molecular catalyst 3.1. b) polymerization of sarcosine-NCA by surface-bound catalyst 4.1. c) Polymerization of <i>rac</i> -lactide by molecular catalyst 1.48. d) polymerization of <i>rac</i> -lactide by surface-bound catalyst 1.59.....	196
Scheme 4.5. The anchoring of redox-active, iron(II) bis(imino)pyridine alkyl complex 1.58 onto layered surfaces consisting of TiO_2 nanoparticles on a layer of FTO on glass slides. Complex was active for separate polymerizations in each redox-state.....	198
Scheme 4.6. Synthesis of electrode and anchoring of iron bis(imino)pyridine alkyl complexes onto electrode surfaces. a) Anchoring iron bis(imino)pyridine complexes onto P25 TiO_2 -FTO	

electrodes. b) Synthesis of hydroxyl functionalized self-assembled monolayers (SAM) onto P25 TiO₂-FTO electrodes. Anchoring iron complexes onto the TiO₂ SAM..... 200

Scheme 4.7. Stability of iron(I)-based complex 3.1 (a) before polymerization (b) after ϵ -caprolactone polymerization (c) after γ -benzyl-*L*-glutamate-NCA polymerization..... 204

Scheme 4.8. (a) Stability of iron(I)-based complex 4.4 under cyclic voltammetry (b) Stability of iron(I)-based complex 4.4 under cyclic voltammetry after polymerizing sarcosine-NCA..... 206

List of Figures

Figure 2.1 Mass spectra of cobalt(II) complex 2.9 and dioxygen adduct 2.11.....	70
Figure 2.2 Redox-switchable polymerization of L-lactide by catalysts 2.9 and 2.12-KONp. Red is the catalyst in the reduced cobalt(II) oxidation state while blue is in the oxidized cobalt(III) oxidation state. FcBF ₄ is added at 10 min ($M_n(\text{GPC}) = 5.8$ kDa, $M_w/M_n = 1.20$), and CoCp* ₂ at 70 min ($M_n(\text{GPC}) = 6.5$ kDa, $M_w/M_n = 1.24$). At the final time point ($M_n(\text{GPC}) = 11.9$ kDa, $M_w/M_n = 1.28$). A polymerization of L-lactide by 2.9 and 2.12-KONp in the presence of 1 equivalent of [CoCp* ₂][BF ₄] without redox-switching was included for comparison.....	78
Figure 2.3 Redox-switchable polymerization of propylene oxide and CO ₂ by catalyst 2.9, 2.12-KONp and FcBF ₄ . Red is the catalyst in the reduced cobalt(II) oxidation state while blue is in the oxidized cobalt(III) oxidation state. CoCp* ₂ is added at 8 h and FcBF ₄ at 12 h. Sampling required the reactor to be depressurized and pressurized.....	80
Figure 2.4 GPC chromatograms of poly(L-lactic acid) ($M_n(\text{GPC}) = 2.7$ kDa, $M_w/M_n = 1.22$, blue) and poly(L-lactic acid- <i>b</i> -propylene carbonate) ($M_n(\text{GPC}) = 4.6$ kDa, $M_w/M_n = 1.03$, orange) from Scheme 2.12A.....	83
Figure 2.5 DOSY NMR of poly(L-lactic acid- <i>b</i> -propylene carbonate) from Scheme 2.12a.....	84
Figure 2.6 GPC chromatograms of poly(propylene carbonate) ($M_n(\text{GPC}) = 5.1$ kDa, $M_w/M_n = 1.10$, blue), poly(propylene carbonate- <i>b</i> -L-lactic acid) ($M_n(\text{GPC}) = 11.0$ kDa, $M_w/M_n = 1.09$, orange) from Scheme 2.12b. High molecular weight peak is likely caused by initiation with adventitious water.....	85
Figure 2.7 DOSY-NMR spectrum of poly(propylene carbonate- <i>b</i> -L-lactic acid) from Scheme 2.12b.....	85
Figure 2.8 DOSY NMR of poly(L-lactic acid- <i>b</i> -propylene carbonate- <i>b</i> -L-lactic acid') from Scheme 2.13a.....	87
Figure 2.9 GPC chromatograms of poly(L-lactic acid) ($M_n(\text{GPC}) = 9.5$ kDa, $M_w/M_n = 1.04$, blue), poly(L-lactic acid- <i>b</i> -propylene carbonate) ($M_n(\text{GPC}) = 12.2$ kDa, $M_w/M_n = 1.08$, orange) and poly(L-lactic acid- <i>b</i> -propylene carbonate- <i>b</i> -L-lactic acid') ($M_n(\text{GPC}) = 20.6$ kDa, $M_w/M_n = 1.01$, green) from Scheme 2.14a.....	88
Figure 2.10 GPC chromatograms of poly(propylene carbonate) ($M_n(\text{GPC}) = 8.6$ kDa, $M_w/M_n = 1.04$, blue), poly(propylene carbonate- <i>b</i> -L-lactic acid) ($M_n(\text{GPC}) = 13.0$ kDa, $M_w/M_n = 1.08$, orange) and poly(propylene carbonate- <i>b</i> -L-lactic acid- <i>b</i> -propylene carbonate') ($M_n(\text{GPC}) = 14.4$ kDa, $M_w/M_n = 1.11$, green) from Scheme 2.14b.....	89
Figure 2.11 DOSY NMR of poly(propylene carbonate- <i>b</i> -L-lactic acid- <i>b</i> -propylene carbonate') from Scheme 2.13a.....	90

Figure 2.12 (top) GPC chromatograms of poly(propylene carbonate) ($M_n(\text{GPC}) = 8.0$ kDa, $M_w/M_n = 1.01$, blue) and poly(<i>L</i> -lactic acid- <i>b</i> -propylene carbonate- <i>b</i> - <i>L</i> -lactic acid) ($M_n(\text{GPC}) = 13.6$ kDa, $M_w/M_n = 1.10$, orange) from Scheme 2.14.....	92
Figure 2.13 DOSY NMR spectrum of telechelic poly(<i>L</i> -lactic acid- <i>b</i> -propylene carbonate- <i>b</i> - <i>L</i> -lactic acid) from Scheme 2.14.....	92
Figure 2.14 GPC chromatogram of poly(<i>L</i> -lactic acid- <i>s</i> -propylene carbonate) ($M_n(\text{GPC}) = 7.7$ kDa, $M_w/M_n = 1.07$) from Scheme 2.16a.....	94
Figure 2.15 DOSY NMR spectrum of poly(<i>L</i> -lactic acid- <i>s</i> -propylene carbonate) from Scheme 2.16a.....	95
Figure 2.16 GPC chromatogram of poly(<i>L</i> -lactic acid- <i>s</i> -propylene carbonate) ($M_n(\text{GPC}) = 12.0$ kDa, $M_w/M_n = 1.04$) from Scheme 2.16b.....	96
Figure 2.17 DOSY NMR spectrum of poly(<i>L</i> -lactic acid- <i>s</i> -propylene carbonate) from Scheme 2.16b.....	97
Figure 2.18 ^1H NMR Spectra of poly(<i>L</i> -lactic acid- <i>s</i> -propylene carbonate) from Scheme 2.16a (red), poly(<i>L</i> -lactic acid- <i>s</i> -propylene carbonate) from scheme 2.16b and poly(propylene carbonate- <i>b</i> - <i>L</i> -lactic acid) from Scheme 2.12b.....	98
Figure 2.19 GPC Chromatogram of poly(<i>L</i> -lactic acid) ($M_n(\text{GPC}) = 6.0$ kDa, $M_w/M_n = 1.12$, blue), poly(<i>L</i> -lactic acid- <i>b</i> -(<i>L</i> -lactic acid- <i>s</i> -propylene carbonate)) ($M_n(\text{GPC}) = 8.8$ kDa, $M_w/M_n = 1.06$, orange) and poly(<i>L</i> -lactic acid- <i>b</i> -(<i>L</i> -lactic acid- <i>s</i> -propylene carbonate)- <i>b</i> - <i>L</i> -lactic acid) ($M_n(\text{GPC}) = 12.5$ kDa, $M_w/M_n = 1.09$, green) from Scheme 2.17a.....	100
Figure 2.20 DOSY NMR spectrum of poly(<i>L</i> -lactic acid- <i>b</i> -(<i>L</i> -lactic acid- <i>s</i> -propylene carbonate)- <i>b</i> - <i>L</i> -lactic acid) from Scheme 2.17a.....	100
Figure 2.21 GPC Chromatogram of poly(propylene carbonate) ($M_n(\text{GPC}) = 4.6$ kDa, $M_w/M_n = 1.01$, blue), poly(propylene carbonate- <i>b</i> -(<i>L</i> -lactic acid- <i>s</i> -propylene carbonate)) ($M_n(\text{GPC}) = 8.1$ kDa, $M_w/M_n = 1.11$, orange) and poly(propylene carbonate- <i>b</i> -(<i>L</i> -lactic acid- <i>s</i> -propylene carbonate)- <i>b</i> -propylene carbonate) ($M_n(\text{GPC}) = 15.4$ kDa, $M_w/M_n = 1.19$, green) from Scheme 2.17b.....	101
Figure 2.22 DOSY NMR spectrum of poly(propylene carbonate- <i>b</i> -(<i>L</i> -lactic acid- <i>s</i> -propylene carbonate)- <i>b</i> -propylene carbonate) from Scheme 2.17b.....	102
Figure 3.1 The conversion of γ -benzyl- <i>L</i> -glutamate-NCA vs. time for complexes 1.48 (red) and 3.1 (blue). Reactions were set up with a 1:100 equivalents [Catalyst]:[NCA] in THF.....	133
Figure 3.2 MALDI mass spectrum of poly(γ -benzyl- <i>L</i> -glutamate) polymerized by 3.1 from Table 3.1, entry 4. $M_n(\text{theo}) = 2.4$ kDa, $M_n(\text{GPC}) = 3.3$ kDa, $M_w/M_n = 1.19$	134
Figure 3.3 Redox-switchable polymerization of γ -benzyl- <i>L</i> -glutamate-NCA by complex 3.1 in THF at room temperature. Oxidation and reduction of the catalyst are represented with dotted lines and are enacted with the addition of $\text{FcBAr}^{\text{F24}}$ and CoCp_2 , respectively. The red and blue data points indicate when the catalyst is in the reduced and oxidized oxidation states, respectively. Number averaged molecular weights (M_n) and molecular weight distributions (M_w/M_n) for the indicated data points were determined by GPC relative to polystyrene standards.....	136

Figure 3.4 600 MHz, ¹ H NMR spectrum of 1:1 sarcosine-NCA:[CoCp ₂][BAr ^{F24}] in CDCl ₃	138
Figure 3.5 Redox-switchable polymerization of γ -benzyl- <i>L</i> -glutamate-NCA by complex 3.1 in THF at room temperature. Oxidation and reduction of the catalyst are represented with dotted lines and are enacted with the addition of FcBAr ^{F24} and CoCp ₂ , respectively. The red and blue data points indicate when the catalyst is in the reduced and oxidized oxidation states, respectively. M_n and M_w/M_n for the indicated data points were determined by GPC.....	140
Figure 3.6 GPC chromatogram of poly(ϵ -caprolactone) (M_n (GPC) = 31.2 kDa, M_w/M_n = 1.08, blue) and poly(ϵ -caprolactone- <i>b</i> -sarcosine) (M_n (GPC) = 31.2 kDa, M_w/M_n = 1.08, red) from Scheme 3.5A. Measurement taken in THF at 40 °C and recorded by a LS detector.....	146
Figure 3.7 600 MHz, DOSY NMR spectra of poly(ϵ -caprolactone- <i>b</i> -sarcosine) from Scheme 3.5A in CDCl ₃	147
Figure 3.8 GPC chromatogram from the telechelic copolymerization poly(ϵ -caprolactone) (blue, M_n = 58.8 kDa, M_w/M_n = 1.17) and poly(sarcosine- <i>b</i> - ϵ -caprolactone- <i>b</i> -sarcosine) (red, M_n = 75.9 kDa, M_w/M_n = 1.16) from Scheme 3.5c.....	148
Figure 3.9 600 MHz, ¹ H DOSY NMR spectra of poly(sarcosine- <i>b</i> - ϵ -caprolactone- <i>b</i> -sarcosine) from Scheme 4c in CDCl ₃	149
Figure 3.10 GPC chromatogram from the copolymerization of CHO (blue, M_n = 18.1 kDa, M_w/M_n = 1.79) then sarcosine-NCA (red, M_n = 22.1 kDa, M_w/M_n = 1.32) from Scheme 3.7B.....	153
Figure 3.11 (Top) GPC chromatogram of triblock copolymers of cyclohexene oxide (CHO) and sarcosine-NCA (Sar-NCA). Poly(cyclohexene oxide) (M_n = 17.6 kDa, M_w/M_n = 2.16, blue), poly(cyclohexene oxide- <i>b</i> -sarcosine) (M_n = 27.9 kDa, M_w/M_n = 1.39, orange) and poly(cyclohexene oxide- <i>b</i> -sarcosine- <i>b</i> -cyclohexene oxide') (M_n = 48.4 kDa, M_w/M_n = 1.40, green) from Scheme 3.8A. (Bottom) GPC chromatogram of poly(sarcosine- <i>b</i> -cyclohexene oxide) (M_n = 32.2 kDa, M_w/M_n = 1.38, blue) and poly(sarcosine- <i>b</i> -cyclohexene oxide- <i>b</i> -sarcosine') (M_n = 62.2 kDa, M_w/M_n = 1.15, red) from Scheme 3.8B.....	156
Figure 4.1 GPC chromatograms of poly(sarcosine) (M_n = 2.5 kDa, M_w/M_n = 1.58) in the supernatant (blue) and poly(sarcosine) (M_n = 2.2 kDa, M_w/M_n = 1.78) cleaved from TiO ₂ nanoparticles (orange) for entry 1, Table 4.1.....	197
Figure 4.2 CV of [24.4 mM]: [0.49 mM] 3.1: monomer in 0.1 M TBAPF ₆ in THF, scan rate = 20 mV/s. Electrochemical potential is measured relative to ferrocene. The iron (I) complex 3.1 without any monomer (red) is not redox-reversible. The addition of ϵ -caprolactone (CL) (yellow) is quasi-reversible electrochemically. The mixture of 3.1 and γ -benzyl- <i>L</i> -glutamate-NCA (BLG-NCA) is fully reversible.....	203
Figure 4.3 CVs of anchored complex 4.4 (ref) and complex 4.4 after polymerizing sarcosine-NCA 4.15 (blue) in 0.1 M TBAPF ₆ in THF, scan rate = 50 mV/s. The large feature from (1.35-1.15 mv) is the reduction of the TiO ₂ substrate.....	205
Figure A.1 500 MHz, ¹ H NMR spectrum for complex 2.9 in CDCl ₃	222
Figure A.2 470 MHz, ¹⁹ F NMR spectrum for complex 2.9 in CDCl ₃	223

Figure A.3 500 MHz, ¹ H NMR spectrum for poly(<i>L</i> -lactic acid- <i>b</i> -propylene carbonate) from Scheme 2.12a in CDCl ₃	224
Figure A.4 500 MHz, ¹ H NMR spectrum for poly(propylene carbonate- <i>b</i> - <i>L</i> -lactic acid) from Scheme 2.12b in CDCl ₃	225
Figure A.5 500 MHz, ¹ H NMR spectrum for poly(<i>L</i> -lactic acid- <i>b</i> -propylene carbonate- <i>b</i> - <i>L</i> -lactic acid') from Scheme 2.13a in CDCl ₃	226
Figure A.6 500 MHz, ¹ H NMR spectrum for poly(propylene carbonate- <i>b</i> - <i>L</i> -lactic acid- <i>b</i> -propylene carbonate') from Scheme 2.13b in CDCl ₃	227
Figure A.7 500 MHz, ¹ H NMR spectrum for telechelic poly(<i>L</i> -lactic acid- <i>b</i> -propylene carbonate- <i>b</i> - <i>L</i> -lactic acid) from Scheme 2.14 in CDCl ₃	228
Figure A.8 500 MHz, ¹ H NMR spectrum for poly(<i>L</i> -lactic acid- <i>s</i> -propylene carbonate) from Scheme 2.16a in CDCl ₃	229
Figure A.9 125 MHz, ¹³ C NMR spectrum for poly(<i>L</i> -lactic acid- <i>s</i> -propylene carbonate) from Scheme 2.16a in CDCl ₃	230
Figure A.10 500 MHz, ¹ H NMR spectrum for poly(<i>L</i> -lactic acid- <i>b</i> -(<i>L</i> -lactic acid- <i>s</i> -propylene carbonate)- <i>b</i> - <i>L</i> -lactic acid') from Scheme 2.17a in CDCl ₃	231
Figure A.11 125 MHz, ¹³ C NMR spectrum for poly(<i>L</i> -lactic acid- <i>b</i> -(<i>L</i> -lactic acid- <i>s</i> -propylene carbonate)- <i>b</i> - <i>L</i> -lactic acid') from Scheme 2.17a in CDCl ₃	232
Figure A.12 500 MHz, ¹ H NMR spectrum for poly(propylene carbonate- <i>b</i> -(<i>L</i> -lactic acid- <i>s</i> -propylene carbonate)- <i>b</i> - <i>L</i> -lactic acid) from Scheme 2.17b in CDCl ₃	233
Figure A.13 125 MHz, ¹³ C NMR spectrum for poly(propylene carbonate- <i>b</i> -(<i>L</i> -lactic acid- <i>s</i> -propylene carbonate)- <i>b</i> - <i>L</i> -lactic acid) from Scheme 2.17b in CDCl ₃	234
Figure A.14 500 MHz, ¹ H NMR spectrum for complex 3.2 in CD ₂ Cl ₂	235
Figure A.15 470 MHz, ¹⁹ F NMR spectrum for complex 3.2 in CD ₂ Cl ₂	236
Figure A.16 128 MHz, ¹¹ B NMR spectrum for complex 3.2 in CD ₂ Cl ₂	237
Figure A.17 500 MHz, ¹ H NMR spectrum of precipitated poly(γ-benzyl- <i>L</i> -glutamate) in CDCl ₃ and 5 % trifluoroacetic acid from entry 6, Table 3.1.....	238
Figure A.18 500 MHz, ¹ H NMR spectrum of poly(sarcosine) from entry 1, Table 3.3 in CDCl ₃	239
Figure A.19 500 MHz, ¹ H NMR spectrum of poly(ε-caprolactone) from Scheme 3.5a in CDCl ₃	240
Figure A.20 600 MHz, ¹ H NMR spectrum of poly(ε-caprolactone- <i>b</i> -sarcosine) from Scheme 3.5a in CDCl ₃	241
Figure A.21 500 MHz, ¹ H NMR spectrum of poly(ε-caprolactone) from Scheme 3.5c in CDCl ₃	242
Figure A.22 600 MHz, ¹ H NMR spectra of telechelic poly(sarcosine- <i>b</i> -ε-caprolactone- <i>b</i> -sarcosine) from Scheme 3.5c in CDCl ₃	243
Figure A.23 600 MHz, ¹ H DOSY NMR spectra of poly(sarcosine- <i>b</i> -ε-caprolactone- <i>b</i> -sarcosine) from Scheme 3.5c in CDCl ₃	244
Figure A.24 500 MHz, ¹ H NMR spectrum of poly(sarcosine- <i>b</i> -cyclohexene oxide) from Scheme 3.8a in CDCl ₃	245

Figure A.25 500 MHz, ¹³ C NMR spectrum of poly(sarcosine- <i>b</i> -cyclohexene oxide) from Scheme 3.8a in CDCl ₃	246
Figure A.26 500 MHz, ¹ H DOSY NMR spectrum of poly(sarcosine- <i>b</i> -cyclohexene oxide) from entry Scheme. 3.8a in CDCl ₃	247
Figure A.27 600 MHz, ¹ H NMR spectrum of poly(cyclohexene oxide- <i>b</i> -sarcosine) from Scheme 3.8b in CDCl ₃	248
Figure A.28 125 MHz, ¹³ C NMR spectrum of poly(cyclohexene oxide- <i>b</i> -sarcosine) from Scheme 3.8b in CDCl ₃	249
Figure A.29 600 MHz, ¹ H DOSY NMR spectrum of poly(cyclohexene oxide- <i>b</i> -sarcosine) from Scheme 3.8b in CDCl ₃	250
Figure A.30 500 MHz, ¹ H NMR spectrum of poly(cyclohexene oxide- <i>b</i> -sarcosine- <i>b</i> -cyclohexene oxide') from Scheme 3.9a in CDCl ₃	251
Figure A.31 125 MHz, ¹³ C NMR spectrum of poly(cyclohexene oxide- <i>b</i> -sarcosine- <i>b</i> -cyclohexene oxide') from Scheme 3.9a in CDCl ₃	252
Figure A.32 500 MHz, ¹ H DOSY NMR spectrum of (top) poly(cyclohexene oxide- <i>b</i> -sarcosine) and (bottom) poly(cyclohexene oxide- <i>b</i> -sarcosine- <i>b</i> -cyclohexene oxide') from Scheme 3.9a in CDCl ₃	253
Figure A.33 500 MHz, ¹ H NMR spectrum of poly(sarcosine- <i>b</i> -cyclohexene oxide- <i>b</i> -sarcosine') from Scheme 3.9b CDCl ₃	254
Figure A.34 125 MHz, ¹³ C NMR spectrum of poly(sarcosine- <i>b</i> -cyclohexene oxide- <i>b</i> -sarcosine') from Scheme 3.9b in CDCl ₃	255
Figure A.35 500 MHz, ¹ H DOSY NMR spectrum of (top) poly(sarcosine- <i>b</i> -cyclohexene oxide) and (bottom) poly(sarcosine- <i>b</i> -cyclohexene oxide- <i>b</i> -sarcosine') from Scheme 3.9b in CDCl ₃	256
Figure B.1 GPC chromatogram of poly(γ-benzyl- <i>L</i> -glutamate) polymerized by complexes 1.48 (green), 3.1 (red) and 1.49 (blue) from entries 3 (green) ,6 (red) and 7 (blue), Table 3.1 in DMF at 50 °C recorded by a RI detector.....	257
Figure B.2 GPC chromatogram of poly(γ-benzyl- <i>L</i> -glutamate) from entry 2, Table 3.2 in DMF at 50 °C recorded by a RI detector.....	257
Figure B.3 GPC chromatogram of poly(γ-benzyl- <i>L</i> -glutamate) polymerized by 3.1 with different additives from entries 1,2, 4 and 5, Table 3.2. Polymers were measured in DMF at 50 °C recorded by a RI detector.....	258
Figure B.4 GPC chromatogram of poly(BLG) from entry 19, Table 3.2 in DMF at 50 C recorded by a RI detector.....	258
Figure B.5 GPC chromatogram of poly(sarcosine) at various loadings of complex 3.1 to Sar-NCA from entries 1 (1:100 3.1:[Sar-NCA], red), 4 (1:50 3.1:[Sar-NCA], green) and 5 (1:200 3.1:[Sar-NCA], blue), from Table 3.3. Polymers were measured in DMF at 50 °C and recorded by an RI detector.....	259

Figure B.6 GPC chromatogram of poly(sarcosine) from entry 6, Table 3.3 in DMF at 50 °C recorded by an RI detector.....	259
Figure B.7 GPC chromatogram of poly(ϵ -caprolactone) from Scheme 3.4A in THF at 40 °C recorded by a LS detector.....	260
Figure B.8 GPC chromatogram of telechelic poly(ϵ -caprolactone) sequential poly(sarcosine- <i>b</i> - ϵ -caprolactone- <i>b</i> -sarcosine) from Scheme 3.4c in THF at 40 °C recorded by a LS detector.....	260
Figure B.9 GPC chromatogram of poly(sarcosine) (top) and poly(sarcosine- <i>b</i> -cyclohexene oxide) (bottom) from Scheme 3.8a. Top spectra was recorded using RI detector in DMF at 50 °C. Bottom spectra was recorded using a LS detector in THF at 40 °C.....	261
Figure B.10 GPC chromatogram of poly(cyclohexene oxide) and poly(cyclohexene oxide- <i>b</i> -sarcosine) from Scheme 3.8b in THF at 40 °C recorded by LS detector.....	262
Figure B.11 GPC chromatogram of poly(cyclohexene oxide) (blue), poly(cyclohexene oxide- <i>b</i> -sarcosine) (red) and poly(cyclohexene oxide- <i>b</i> -sarcosine- <i>b</i> -cyclohexene oxide') (green) from Scheme 3.9a.....	262
Figure B.12 GPC chromatogram of poly(sarcosine) (top) and poly(sarcosine- <i>b</i> -cyclohexene oxide) and poly(sarcosine- <i>b</i> -cyclohexene oxide- <i>b</i> -sarcosine') (bottom) from Scheme 3.9b. Top spectrum was recorded by RI detector in DMF at 50 °C. Bottom spectra were recorded by a LS detector in THF at 40 °C.....	263
Figure C.1 MALDI spectrum of sarcosine-NCA polymerized by 1 mol % complex 3.1 for 10 min in THF. Sample was prepared in CHCl ₃ at a 1:10 ratio of polymer to trans-2-[3-(4-tert-Butylphenyl)-2-methyl-2-propenylidene]malononitrile with no added cationizing agent. Potentially, excess benzoic acid from quenching of polymerization is acting as the cation source.....	264

List of Tables

Table 2.1 Copolymerization of propylene oxide and CO ₂ by cobalt salen, 2.9, with 2.2.2-cryptand potassium alkoxide cocatalysts, 2.12-KONp.....	74
Table 2.2 Polymerization of <i>L</i> -lactide by 2.2.2 cryptand potassium neopentoxide 2.12-KONp in the presence of cobalt(II) salen complex 2.9.....	75
Table 3.1 Polymerization of γ -benzyl- <i>L</i> -glutamate N-carboxyanhydride (BLG-NCA) by various iron bis(iminopyridine) alkoxide complexes.....	132
Table 3.2 Polymerization of γ -benzyl- <i>L</i> -glutamate-NCA (BLG-NCA) by iron bis(iminopyridine) alkoxide complex, 3.1, with additives.....	137
Table 3.3 Polymerization of sarcosine-NCA by iron bis(iminopyridine) complexes 3.1 and 3.2...144	144
Table 4.1 Parameters tested for anchoring iron bis(imino)pyridine complexes onto TiO ₂ nanoparticles and the subsequent activity during NCA polymerization.....	193
Table 4.2 Sarcosine-NCA polymerization activity of iron(I)-based complexes anchored on electrodes.....	202
Table C.1 Polymerization of cyclohexene oxide by complex 3.2 in various solvents.....	265

Acknowledgements

Graduate school was a journey and certainly not one I embarked on alone. At Boston College I really had an excellent lab full of clever and hardworking colleagues who became my friends through the toil. I would like to specifically mention Dr. Chet Tyrol who immediately became one of my closest friends, and there is no one else I would have wanted to bring along on this journey. Jeffery Byers was an excitable and responsive advisor that made me really enjoy contributing to group meetings and coming up with new ideas.

Outside of the Byers group I was also fortunate to have formed a network stretching all throughout the school, y'all really made those Kilsyth parties wild. Special thanks must go to my many roommates and their dogs as I managed to stay in the same house for five years with little conflict or hassle. Alex and Ben (and Charli) were my last roommates, and you really helped this last year finish with a bang. Rest in Peace, Jim Thorne, you were the first to greet me in Boston and it was heartbreaking to hear you were gone. To anyone reading this do not allow yourself to suffer in silence, help is out there even if it may not be easy to find.

I am fortunate to have made so many friends both in Boston and around the world who I could go to when I needed to get out of the lab. Maddie, I may have met you in college, but we really became so much closer when you moved to Boston and I am glad you could introduce me to fantastic people like Mary and Bri, you are all truly fabulous. Eric M. and Becca, my dear exclusive friend, our yearly visits rejuvenated me and filled my life with exciting stories.

Rosalyn, Avelina and Eric S. I am glad we have remained close despite my great distance in both time and geography and I promise to make more time to see you after graduation.

My family has been a bedrock of support, even on days when I felt like my projects were going nowhere and I did not deserve to receive my PhD. Spoiler alert, things got better and they were right (Thanks Mom!), I will always keep my most hallowed faith. Mom, you are absolutely wonderful (which my friends can attest to) and I have always felt so loved and supported. You always bought me books, and encouraged my love of learning. My pursuit of chemistry came from all the times you let me experiment in the kitchen, even when some recipes were straight up duds. Dad, you have always taught me to find out what is true, and even when it leads us to disagree and I must thank you for forcing me to look outside of my comfort zone. Ryan, your influence gave me an independent streak that has benefitted me throughout my academic pursuits. Also, your niece is one of the best things you ever made and made me overjoyed to hear “Uncle Matthew”. Sarah, you are an endless source of fun and adventure, thanks for always thinking I am “smartical”. Outside of the immediate family, I have been blessed with so many grandparents, aunts, uncles and cousins who were out there believing in me and I truly wish to see you more often than this grad schedule has permitted.

Of course, none of this would have been possible without funding specifically I would like to thank the National Science Foundation (NSF) for the NSF CAREER (CHE-1454807) and the NSF-CIC center for integrated catalysis (CHE-2023955) as well as the US Army (66672-CH(W911NF-15-1-0454) for providing the resources that make this science possible.

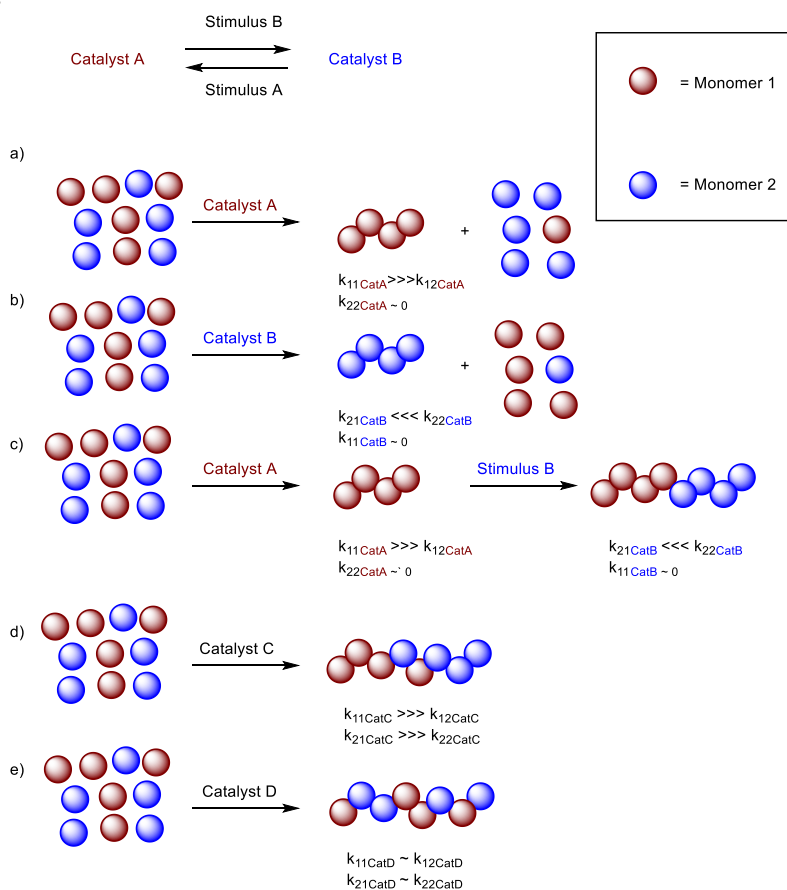
Chapter 1. Switchable Ring-opening Polymerization and Ring-Opening Copolymerization: Methods and Applications

1.1 Introduction

The diversity of polymer microstructures in both shape and composition translates to the macroscopic versatility of polymeric materials.¹⁻³ The ability to control these specific microstructures is an active area of research that has led to the creation of valuable blocky and random copolymers that find uses as adhesives,⁴⁻⁷ packaging,⁸⁻¹⁰ drug delivery devices¹¹⁻¹³ among countless other applications. Still these structures are simple in design compared to the polymers routinely created by biology. Living cells contain complex copolymers that enable the catalysis,^{14,15} replication,^{16,17} movement,^{18,19} and all other living processes that synthetic advances have only begun to scratch the surface of through complex polymer synthesis. Stepwise copolymer synthesis can require intermediate purification steps that are impractical for polymers with more than two blocks.¹ Meanwhile, conventional methods for designing copolymers from monomer mixtures can be rather complex,²⁰ which limits the potential structures one can access.

Switchable polymerization is a method to more readily create complex and predictable polymer structures through the addition or removal of stimuli (Scheme 1.1).²¹ With a single switchable catalyst, one can easily synthesize diblock copolymers by first polymerizing one monomer then applying a stimuli to change the reactivity of the catalyst to favor monomer 2 (Scheme 1.1a-c). With conventional catalysts one would need to find a catalyst that is reactive towards both monomers, but much more reactive towards one monomer and even then some tapering can be observed when the concentration of one monomer is low (Scheme 1.1d). If the

Scheme 1.1. Copolymer synthesis from monomer mixtures using switchable catalysis. a) Polymerization of monomer 1 selectively in a mixed monomer solution. b) Polymerization of monomer 2 selectively in a mixed monomer solution. c) Polymerization of monomer 1 selectively then monomer 2 to produce diblock copolymers from a mixed monomer solution. d) Synthesis of a blocky copolymer with a catalyst active for both monomers 1 and 2, but more reactive for 1. e) Synthesis of a statistical copolymer with a catalyst equally active for both monomers 1 and 2.



catalyst is equally active for both monomers one can instead observe statistical copolymerizations from a solution of mixed monomers (Scheme 1.1e). Stepwise addition of monomers can be used to synthesize well-defined block copolymers, but high conversions of the 1st monomer are generally required before the second monomer can be added.²² Switchable catalysts have the advantage of being able to produce blocky copolymers without the full consumption of monomers which can be beneficial for solvent free copolymerizations.²³ The stimuli can be light,^{24–27} electricity,^{28–30} pressure^{31,32} and chemical additives.^{33–35} These switchable reactions have been developed to induce morphological changes including branching^{36–38} or cross-linking^{39,40} as well as the synthesis of complex, blocky copolymers.²¹

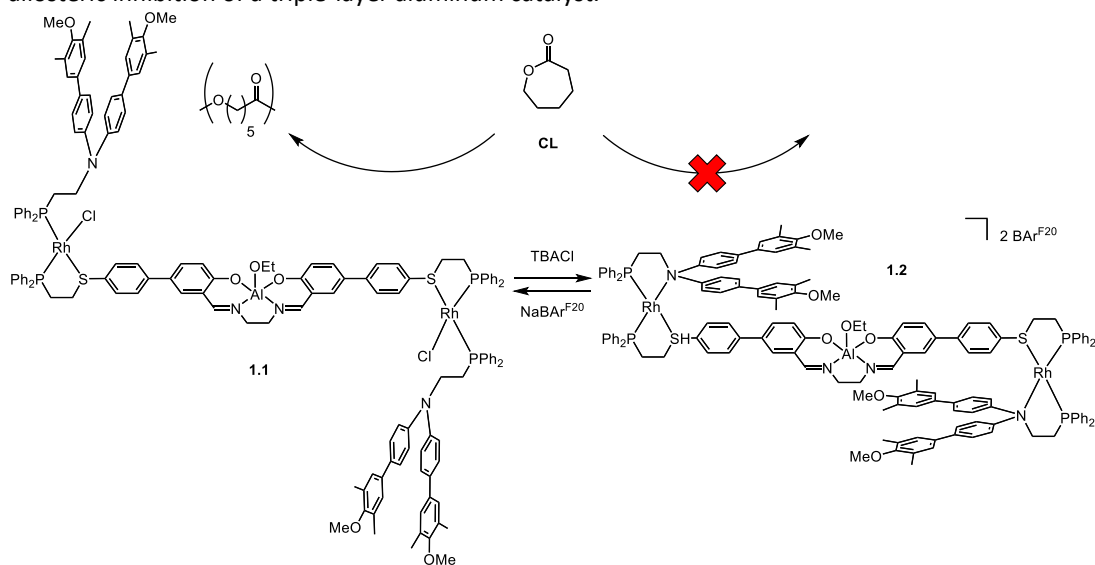
Ring-opening polymerization (ROP) and ring-opening copolymerization (ROCOP) are especially suitable to switchable polymerization conditions as the various monomer classes from lactones and cyclic carbonates to epoxides and *N*-carboxyanhydrides can require vastly different activation conditions.²¹ Ring-opening polymerization has been growing in popularity as the resulting polymers largely have reactive polymer backbones which can enable further functionalization, (bio)degradation or even chemical recycling.³³ In comparison to commercial polyolefin homopolymers, commercial biodegradable polymers like poly(lactic acid) that are accessible through conventional ROP tend to have poor mechanical and thermal properties. This justifies the use of switchable polymerization to introduce branches, crosslinks or copolymers to produce more valuable materials.

1.2 Chemically-switchable Ring-opening Polymerization

The addition of chemical stimuli is a common technique for modulating the activity of a catalyst.^{21,41} Catalysts can be modified with pH sensitive^{42,43} or ligand sensitive moieties⁴⁴ that change catalyst reactivity. Another method involves the addition of certain monomers that after ring-opening are kinetically or thermodynamically unable to initiate other monomers in the reaction mixture.^{23,31,32,45,46} These techniques have been utilized by numerous groups to easily synthesize copolymers from diverse monomer streams.^{21,41}

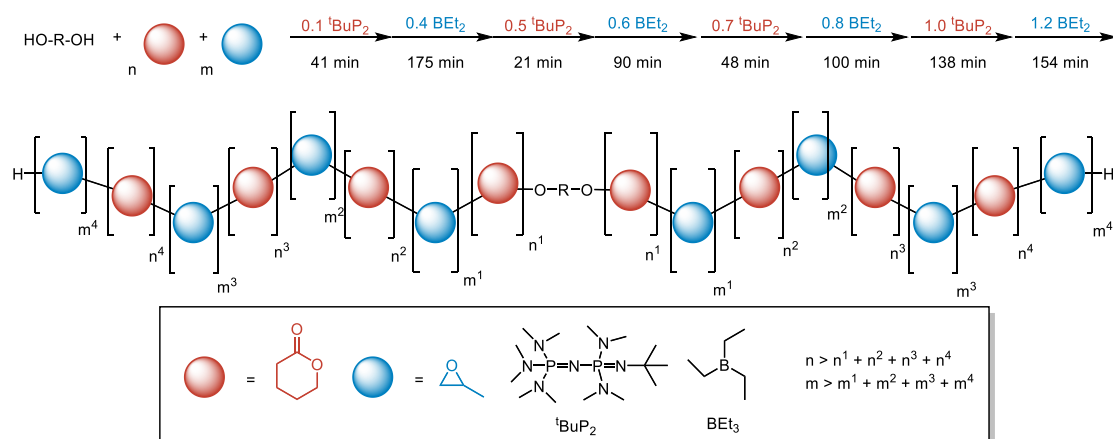
Conformational changes can cause significant changes in catalyst reactivity as was observed by Mirkin and coworkers with their aluminum-salen catalyst bearing two bulky rhodium, phosphinoamine complexes, **1.1** (Scheme 1.2).⁴⁴ When the rhodium centers are bound to chloride ligands, the two amine arms are no longer blocking the active site and the complex can polymerize ϵ -caprolactone. Upon the addition of sodium tetrakis(perfluorophenyl) borate (NaBAr^{F20}) the chlorides are removed and the two rhodium-containing arms rearrange into a sandwiched structure, **1.2**, The aluminum active site is now blocked, which shuts down ϵ -caprolactone polymerization. This type of allosteric inhibition resembles the regulatory mechanisms for many enzymes, including hemoglobin, which opens and closes in response to oxygen.⁴⁷

Scheme 1.2. Chloride controlled, chemically-switchable polymerization of ϵ -caprolactone through the allosteric inhibition of a triple-layer aluminum catalyst.



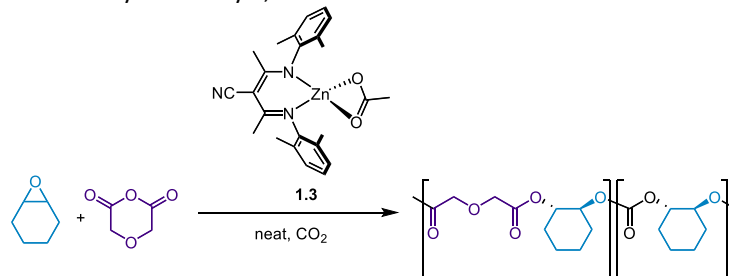
Zhang and coworkers demonstrated that a Lewis acid/base pair could be switched between ROP of lactones/ cyclic carbonates and the ROP of epoxides by changing the ratio of the Lewis acid, triethylborane, to the Lewis base, phosphazane $t\text{BuP}_2$.⁴⁸ When there was an excess of the Lewis base, lactone or cyclic carbonate polymerization proceeded, and when there was excess Lewis acid, epoxide polymerization was possible. Multi-block copoly(ester-*b*-ether)/copoly(carbonate-*b*-ether)s could be synthesized in this way, but each subsequent switch would require more Lewis acid/Lewis base to maintain high selectivity and activity (Scheme 1.3). The excess of Lewis acid/base is needed because the Lewis pairs will first quench each other until an excess is formed and polymerization can continue. This catalytic system was tolerant of a wide variety of lactones, cyclic carbonates and epoxides while maintaining high selectivity, short reaction times and living characteristics.

Scheme 1.3. Chemically-switchable copolymerization of valerolactone and propylene oxide using iterative additions of Lewis acids and bases to synthesize a pentadecablock poly(ester-*b*-ether).

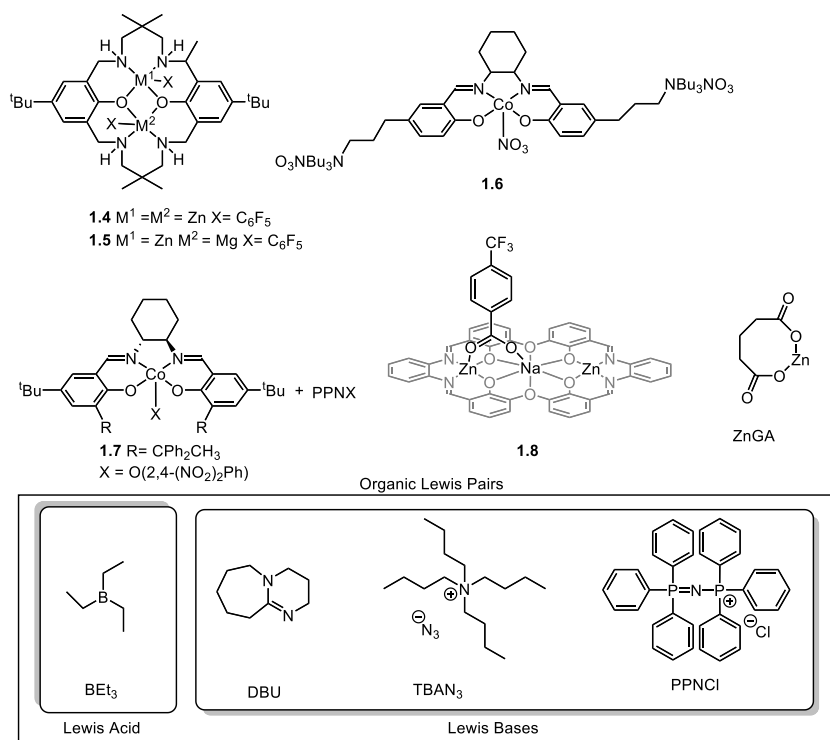


The ROCOP of epoxides and cyclic anhydrides was first demonstrated in 1979 by Manasek *et al.* using amine initiators leading to polymers with significant polyether segments, broad dispersities and low molecular weights.⁴⁹ Coates and coworkers made a significant advance when they discovered that a zinc diketimidate acetate catalyst **1.3** that they had previously used for epoxide-CO₂ ROCOP was also efficient for the ROCOP of cyclohexene oxide and diglycolic anhydride.⁵⁰ This catalyst was so selective for epoxide-anhydride ROCOP that even in the presence of CO₂ the anhydride would be consumed first (Scheme 1.4).⁵¹ The addition of anhydrides has since been used as a switch between epoxide-anhydride copolymerization and the ROCOP of epoxides and CO₂ by many groups with a variety of catalysts (Scheme 1.5).^{40,52–56} These other systems have been able to achieve improved stereoselectivities,⁵³ control cross-linking⁴⁰ and even access non-blocky polymer microstructures.⁵⁴

Scheme 1.4. Chemically-switchable, terpolymerization of cyclohexene oxide, CO₂ and diglycolic anhydride by a zinc carboxylate catalyst, **1.3**.

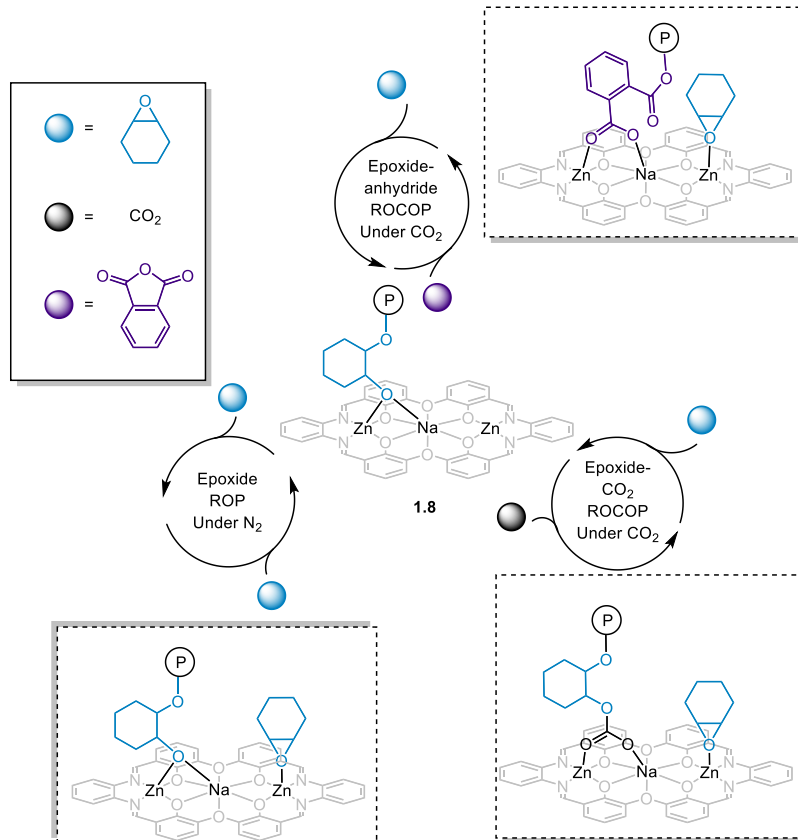


Scheme 1.5. Representative catalysts that have demonstrated chemically-switchable, terpolymerization of epoxides, anhydrides and CO₂.



Many catalysts used for epoxide-anhydride ROCOP are often inactive or very slow for the ROP of epoxides, preventing the incorporation of nondegradable polyether in the degradable polycarbonate or polyester blocks. Some notable exceptions were demonstrated by Feng and coworkers,⁵⁴ and Williams and coworkers,⁵⁶ which could switch between epoxide-anhydride ROCOP, epoxide-CO₂ ROCOP and epoxide ROP after complete consumption of the anhydride and

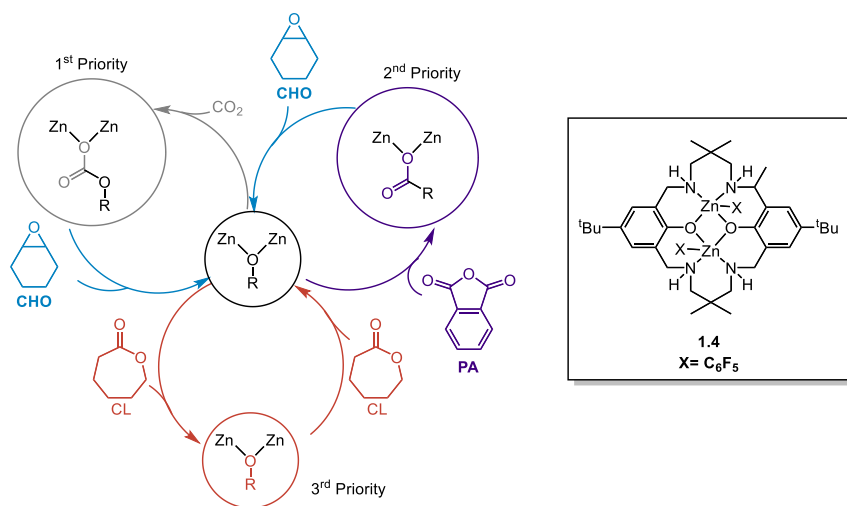
Scheme 1.6. Doubly chemically-switchable terpolymerization of cyclohexene oxide, CO₂ and phthalic anhydride.



then CO₂. A heterotrimetallic, dizinc and sodium catalyst, **1.8**, could be added to a solution of cyclohexene oxide and phthalic anhydride under a CO₂ atmosphere and selectively produce blocky copolymers. First epoxide-anhydride ROCOP would occur, then epoxide-CO₂ ROCOP and finally epoxide ROP if the CO₂ was replaced with nitrogen (Scheme 1.6).⁵⁶ This catalyst was also thermally switchable, which enabled the synthesis of random copolymers of epoxide and CO₂ if the temperature was raised from 80 °C to 120 °C demonstrating another method to tune the polymer composition.

In 2016, Williams and coworkers first demonstrated the selective copolymerization of epoxides, CO₂, anhydrides and lactones with a single catalyst.²³ The selectivity of each monomer could be understood in terms of relative priorities to govern selectivity which could be easily mapped (Scheme 1.7). In a solution of mixed monomers, all anhydride was first consumed because the ROCOP of epoxides and anhydrides was most favored. The ROCOP of epoxides and CO₂ is the next favorable reaction for polycarbonate formation. They did not that at high lactone concentrations, neither the ROCOP of epoxides and CO₂ or the ROP of lactones occurred which is believed to be due to competitive binding of lactones blocking open sites for epoxides. In the absence of cyclic anhydrides or CO₂ the ROP of lactones can take place. This switch relies on a common metal alkoxide intermediate in each of the three cycles. This common intermediate allows for simple transitions between the different polymerization mechanisms depending on which monomer had the lowest barrier for insertion, which was supported by DFT calculations. Other groups have explored chemically-switchable copolymerization between epoxides,

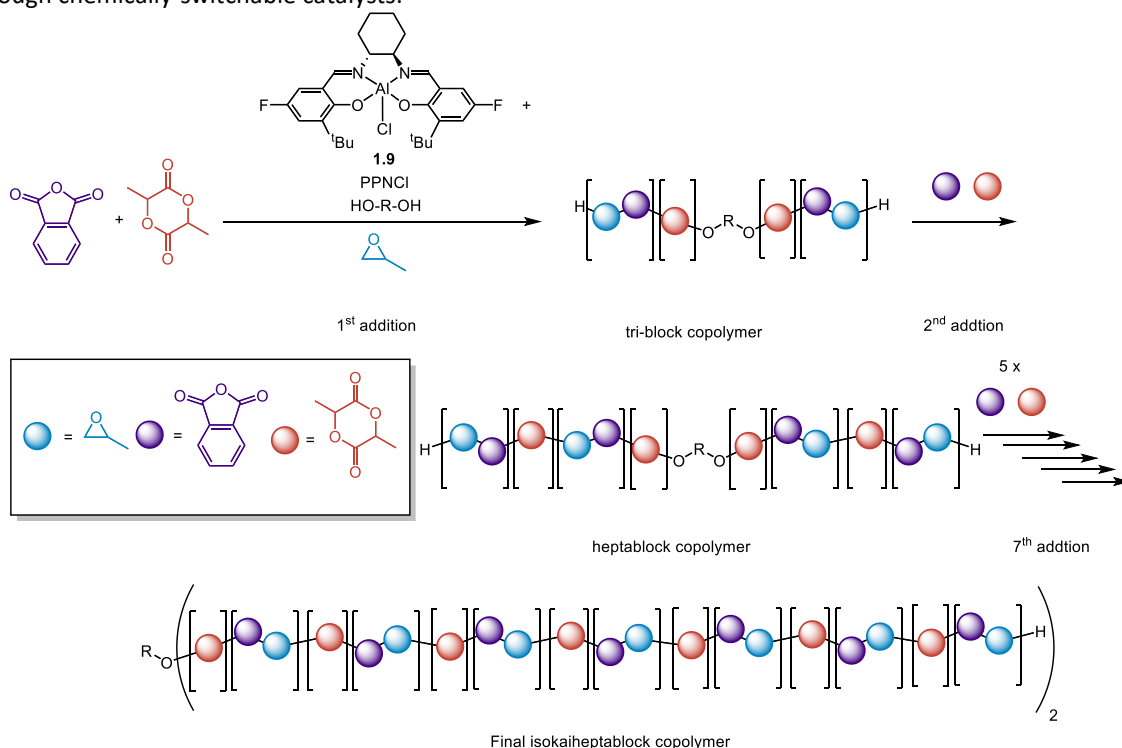
Scheme 1.7. Four component chemically-switchable polymerization of cyclohexene oxide, phthalic anhydride, ε-caprolactone and CO₂ catalyzed by a dizinc catalyst, **1.4**.



anhydrides, lactones^{57–59} (and CO₂⁶⁰) that each rely on this preferential consumption of anhydrides, then CO₂ if present, and finally lactones.

The Williams group has since expanded upon this work by achieving this type of chemical selectivity with other bimetallic catalysts,⁶¹ metal salen complexes,^{34,62,63} and industrially viable tin carboxylates.⁶⁴ A variety of epoxides, anhydrides and lactones, many of which are derived from biomass, have all been copolymerized.^{7,34,45,65} This excellent monomer compatibility has enabled the synthesis of structurally diverse and flexible polymers ranging from elastomers^{45,65} to hard plastics⁶⁴ and adhesives.^{7,41} A notable accomplishment for the Williams group has been the facile synthesis of polymers of propylene oxide, phthalic anhydride and lactide with up to 27 different blocks solely through the addition of phthalic anhydride and lactide (Scheme 1.8).⁶⁵ This copolymer would be completely impractical through conventional copolymerization methods.

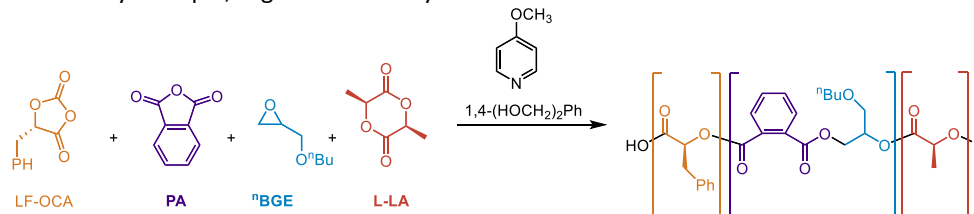
Scheme 1.8. Synthesis of isosikaiheptablock copolymers of propylene oxide, phthalic anhydride and lactide through chemically-switchable catalysts.



Multi-block copolymers with 2-3 blocks are already known to be valuable as elastomers^{66,67} and compatibilizers,^{68,69} but higher order copolymers are underexplored despite their differences in morphology.

Anhydride-like monomers, such as *O*-carboxyanhydrides (OCAs) have also proven to be useful for chemically switchable polymerization.^{46,70} Williams and coworkers demonstrated the copolymerization of OCAs and epoxides to make polyester-polycarbonate copolymers.⁷¹ OCAs release one unit of CO₂ for every unit of monomer incorporated into the polymer, and the Williams group paired this polymerization with a catalyst **1.5** that is active for epoxide-CO₂ ROCOP at low concentrations of CO₂. The ROP of an OCA, like its anhydride counterpart, is more thermodynamically favorable than insertion of CO₂. The catalyst first consumes all of the OCA before the ROCOP of epoxides and CO₂ can begin. By coupling a CO₂-generating process with a CO₂-consuming polymerization through switchable polymerization, the atom economy of both reactions are improved. Y. Li and coworkers also demonstrate the potential of OCAs in switchable polymerizations with anhydrides, epoxides and lactide.⁴⁶ Notably, they observed that the OCA is fully consumed before epoxide-anhydride ROCOP can begin, and when the anhydride is fully consumed lactide ROP can begin. OCA ROP is a rare example of a monomer being consumed before epoxide-anhydride ROCOP in a mixed solution. Additionally, the use of an organobase catalyst that is inactive for epoxide-CO₂ ROCOP or cyclization precludes any polycarbonate formation. Through this remarkably selective polymerization, a tri-block copolymer of *L*-phenylalanine-OCA, phthalic anhydride, *n*-butyl-glycidyl ether and *L*-lactide was synthesized without intermediate addition of monomers (Scheme 1.9). It was noted that the use of lactones

Scheme 1.9. Self-switchable, quadripolymerization of *L*-phenylalanine OCA, phthalic anhydride, ⁿbutyl-glycidyl ether and *L*-lactide by a simple, organobase catalyst.

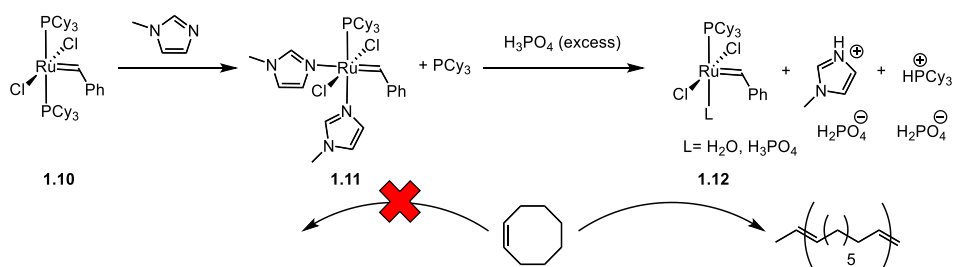


besides *L*-lactide leads to uncontrolled polymerizations with these initiators, which could be an area for future catalyst development.

1.2.1 Acid/Base-switchable Ring-opening Polymerization

An early example of an acid used to modify a catalyst for ROP was demonstrated by P'Pool and Schanz with the reversible inhibition of ROMP (Scheme 1.10).⁴³ *N*-methylimidazole was first added to Grubbs first generation catalyst **1.10** to produce inactive species **1.11**. The addition of excess phosphoric acid would restore polymerization activity by protonating the imidazole producing catalyst **1.12** which contains a weakly coordinating water or phosphate ligand that can leave behind an open site for cyclooctene coordination. This species is then active for cyclooctene ROMP.

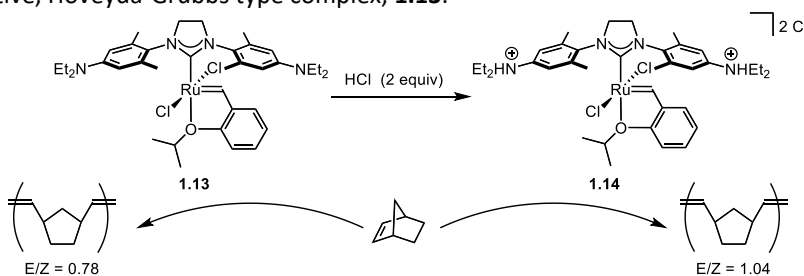
Scheme 1.10. Acid-switchable ROMP by inhibition of a Grubbs 1st generation catalyst, **1.10**, with *N*-methylimidazole to form **1.11** which is inactive for ROMP. Catalyst is reactivated through in-situ synthesis of a highly active catalyst, **1.12** upon the addition of phosphoric acid.



Plenio and coworkers were able to alter the stereoselectivity of a modified Hoveyda-Grubbs catalyst **1.13** by protonating the amine groups on the aryl substituents of the *N*-heterocyclic carbene (NHC) ligand to form complex **1.14** (Scheme 1.11).⁴² **1.13** polymerized norbornene with an *E/Z* of 0.78 while the acidified variant **1.14** led to an *E/Z* of 1.04. By controlling the addition time of the acid, the ratio could be further fine-tuned in the final polymer. The difference in selectivity is attributed to electronic differences rather than the comparatively minor difference in sterics. These findings were supported by DFT calculations as well as by comparing the stereoselectivities of other Hoveyda-Grubbs-type catalysts containing electron deficient NHC ligands.

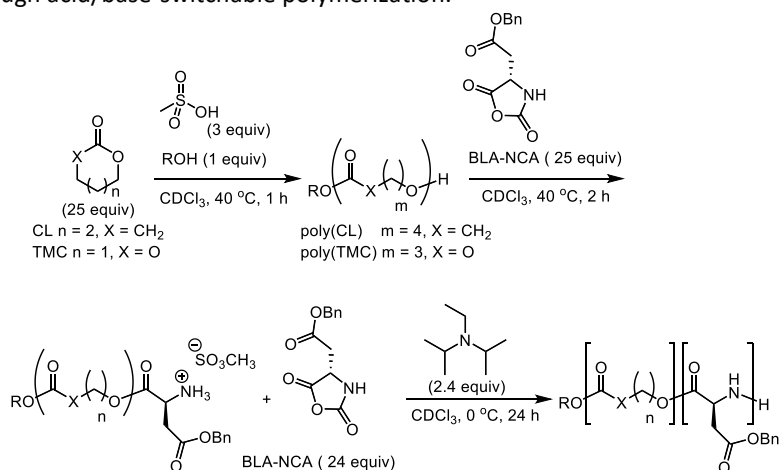
For the copolymerization of epoxides and lactones/cyclic carbonates, Hadjichristidis and coworkers reported a metal free switch using a phosphazene base and a phosphoric acid catalyst.⁷² The phosphazene base could initiate epoxide ROP, while the addition of excess acid not only turned off epoxide polymerization, but could then activate lactones/cyclic carbonate ROP to synthesize various diblock copolymers. Due to the high nucleophilicity of the phosphazene base, the monomers had to be added stepwise to achieve clean copolymer without significant transesterification.

Scheme 1.11. Acid-switchable, norbornene ROMP with tunable *E/Z* ratio through the addition of hydrochloric acid to a pH-sensitive, Hoveyda-Grubbs type complex, **1.13**.



A similar method was demonstrated by Pahovnik and coworkers for the one-pot synthesis of copolymers of ϵ -caprolactone/trimethylene carbonate and *N*-carboxyanhydrides (NCAs) through acid and base-switchable polymerizations (Scheme 1.12).⁷³ ϵ -caprolactone or trimethylene carbonate was first polymerized by triflic acid in the presence of alcohol initiators. The addition of γ -benzyl-*L*-aspartate NCA lead to the ring-opening of 1 equivalent of NCA, which formed an amine that was immediately quenched by the acid. To control NCA polymerization, the bulky base diisopropylethylamine was then added to regenerate the amine nucleophile that was then active for NCA polymerization. In this two-part switchable polymerization, the acid prevents the early propagation of the NCA while the base was added only after all of the alcohol macronitiator was consumed. This strategy produced clean block copolymers.

Scheme 1.12. One-pot synthesis of copolymers of ϵ -caprolactone or trimethylene carbonate and γ -benzyl-*L*-aspartate NCA through acid/base-switchable polymerization.

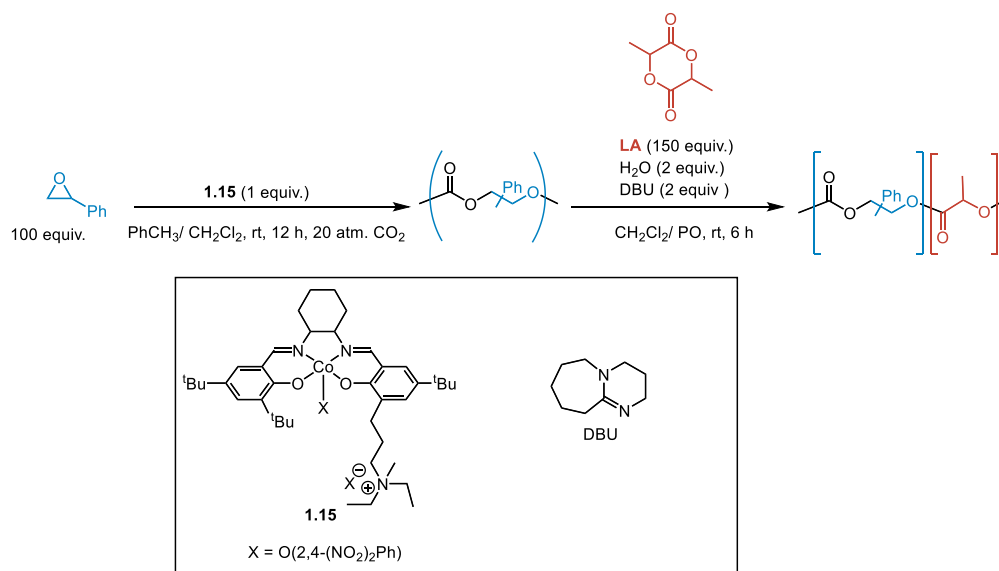


1.2.2 Pressure-switchable Ring-opening Polymerization

Gaseous additives can either be thermodynamic modulators to make polymerization favorable or they can be reactive monomers in their own right like epoxide-CO₂ ROCOP.^{6,31,32,74–78} CO₂ can also be used to deactivate nucleophilic catalysts through the formation of carboxylate derivatives that are then much weaker nucleophiles.⁴¹ The decomposition of this carboxylate derivative at low CO₂ concentrations can then regenerate the nucleophilic initiator. This principle lies at the center of CO₂ pressure-switchable polymerization.

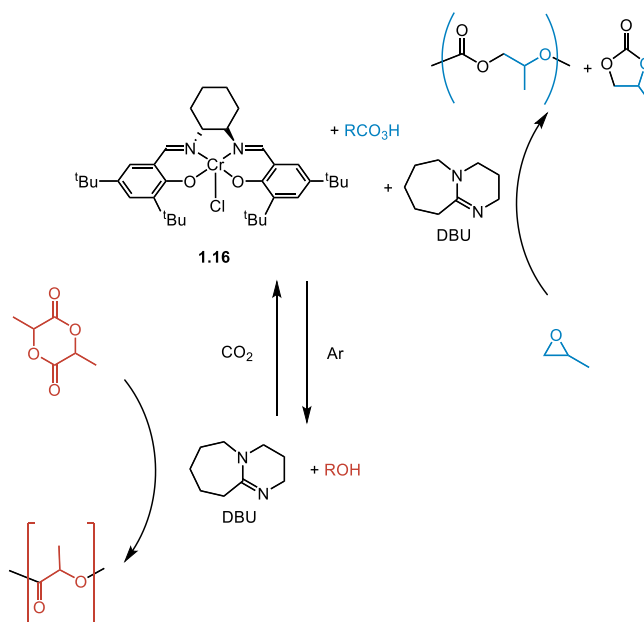
In 2012, Darensbourg and coworkers demonstrated that one could produce copolymers of styrene oxide, CO₂ and lactide in one pot with a combination of a bifunctional cobalt salen, **1.15**, and an organobase, 1-8-diazabicyclo[5.4.0]-undec-7-ene (DBU) as catalysts. **1.15** catalyzed propylene oxide-CO₂ ROCOP could be directly quenched with water in air and then combined with DBU, and lactide to synthesize diblock copolymers in one-pot (Scheme 1.13).⁷⁹ By removing the CO₂, the consumption of additional epoxide was prevented as well as any unwanted addition of the organobase to CO₂. They were later able to expand this work towards the synthesis telechelic triblock copolymers by introducing water during propylene oxide-CO₂ ROCOP to generate diol chain-transfer agents *in-situ* leading to α,ω -hydroxy terminated poly(propylene carbonate).⁸⁰ After the removal of CO₂, lactide and DBU were then added to form the desired triblock copolymer.

Scheme 1.13. Copolymerization of propylene oxide, CO₂ and lactide in one-pot using a two catalyst system.



In 2014, Dubois and coworkers were able to deactivate the organobase catalyzed polymerization using CO₂.⁸¹ A 10: 1 mixture of organobase catalysts 1,5,7-triazabicyclododecene (TBD) and DBU were first added to alcohol initiators, then a CO₂ atmosphere was applied. The combination of base and CO₂ produced weakly nucleophilic carbonate end groups which were inactive for ϵ -caprolactone ROP. After removing the CO₂ with excess nitrogen the polymerization can proceed. Chen and coworkers went even further by demonstrating CO₂-switchable lactone ROP and epoxide-CO₂ ROCOP with a mixture of chromium salen chloride, DBU cocatalysts and alcohol initiators (Scheme 1.14).⁷⁶ CO₂ can react with the organobase and alcohol initiator to form carbonate groups active which are active for ROCOP, while the CO₂ can be purged with argon to decompose the carbonate initiators into alkoxides for lactide ROP. This copolymerization can be run in a mixed solution of monomers and start with either ROCOP or ROP and still synthesize blocky copolymers. A drawback of this method is the formation of large

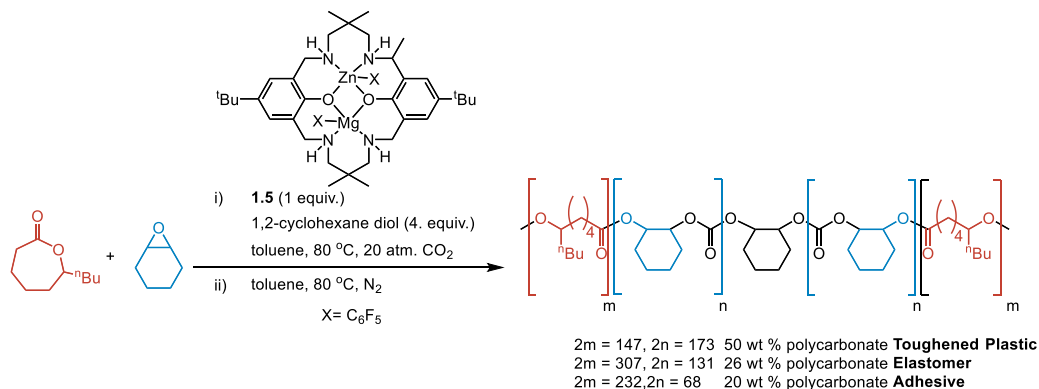
Scheme 1.14. Pressure-switchable copolymerization of lactide, propylene oxide and CO₂



amounts (35 % of all epoxide conversion) of high-boiling point cyclic carbonate from back-biting of the polycarbonate during ROCOP.

As mentioned earlier, the Williams group has demonstrated the selective copolymerization of lactones, epoxides and CO_2 , using CO_2 to deactivate the alkoxide initiator for lactone ROP.^{74,75} The difficulty of fully removing or consuming a gaseous reagent as opposed to fully consuming an anhydride often requires extensive purging steps with a neutral gas like nitrogen or argon. Nevertheless, with one combination of monomers, their group was able to use switchable catalysis to easily synthesize triblock copolymers of cyclohexene oxide, ϵ -decalactone and CO_2 with vastly different physical properties (Scheme 1.15).⁶ By varying the total weight percentage of the rigid polycarbonate blocks in relation to the amorphous polyester blocks they were able to easily tune the mechanical properties. At 50 wt. % polycarbonate content the copolymer was a tough plastic, but at 20 wt. % polycarbonate the copolymer was a sticky adhesive. Other groups have also used CO_2 pressure to switch between lactone ROP and

Scheme 1.15. One-pot copolymerization of cyclohexene oxide, ϵ -decalactone and CO₂ to produce triblock copolymers with widely-tunable, mechanical properties.



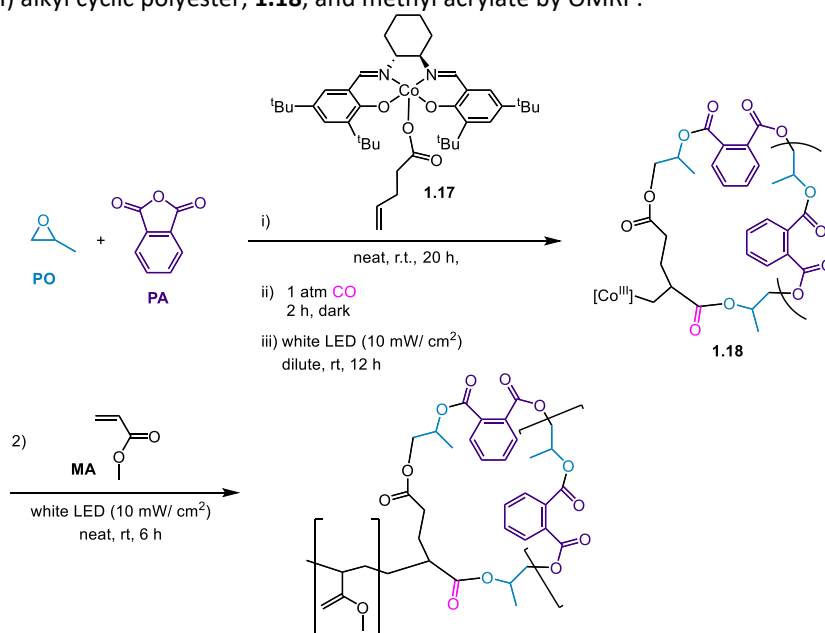
epoxide-CO₂ ROCOP to make blocky^{31,32,78} or statistical^{31,32} copolymers of polyesters and polycarbonates from a variety of monomers.

Chemically-switchable polymerization has also been applied in systems that can switch between ring-opening polymerizations and other polymerization mechanisms by changing the nature of the initiator or the active catalyst. Poli and coworkers demonstrated the one-way switch from cobalt salen catalyzed epoxide-anhydride ROCOP to acrylate organometallic mediated controlled radical polymerization (OMRP) through the addition of carbon monoxide and 2,2,6,6-tetramethylpiperidine-1-oxyl (TEMPO).³⁵ The addition of carbon monoxide forms a cobalt-acyl initiator that in the presence of TEMPO can initiate methyl or *n*-butyl acrylate polymerization. The OMRP of acrylates was only active in the presence of light, thus making this system both chemically and photo-switchable.

A similar reaction was demonstrated by the Tang *et al.* for the cyclization of polycarbonates derived from epoxide and CO₂/anhydrides (Scheme 1.16).²⁶ When vinyl-terminal carboxylates are used as initiators with cobalt-salen catalysts for epoxide-anhydride ROCOP the polymerization can first be chemically switched off using carbon monoxide which inserts into the

metal alkoxide. The newly formed cobalt-acyl species can then undergo organometallic mediated controlled radical cyclization under white light. Cyclization was favorable for polymers of low to moderate molecular weights (3.9-16.2 kDa) with only small shoulder peaks observed by size-exclusion chromatography (SEC) for intermolecular rather than intramolecular coupling. Tadpole polymers could also be formed after cyclization upon the addition of methyl acrylate to the cobalt alkyl, representing a novel way to synthesize cyclic and tadpole shaped polymers.

Scheme 1.16. Copolymerization of propylene oxide and phthalic anhydride by cobalt salen catalyst, **1.17**, followed by the one cyclization driven by the addition of carbon monoxide and then white light organometallic mediated controlled radical cyclization. Synthesis of tadpole-shaped copolymers from pre-formed cobalt(III) alkyl cyclic polyester, **1.18**, and methyl acrylate by OMRP.



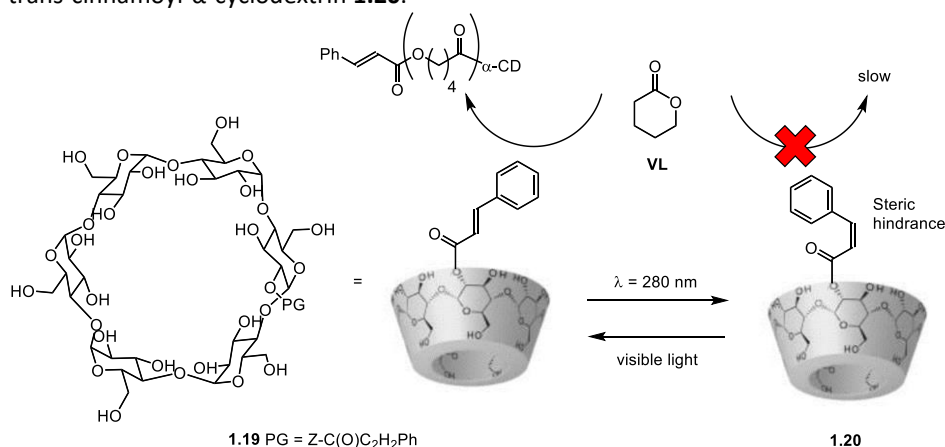
1.3 Photoswitchable Ring-opening Polymerization

While photoswitchable ROP and ROMP is not as well developed and industrially adopted as light-controlled radical polymerization,²⁷ there has been progress designing catalysts suitable for a wide-range of monomers.^{82,83} Photoswitchable catalysis generally relies on either inducing structural changes in a catalyst that change its reactivity or by promoting an electron to a redox-active excited state that can activate a monomer or catalyst.^{21,27}

Harada and coworkers synthesized a photoswitchable catalyst that utilized the trans/ cis isomerization of a cinnamoyl group-functionalized α -cyclodextrin to control the steric environment of the active site.⁸⁴ The trans isomer, **1.19**, was active for valerolactone ROP leading to a high monomer conversion (82 %). The sterically crowded cis isomer, **1.20**, that could form under UV radiation ($\lambda_{irr} = 280$ nm) was less active for the polymerization leading to lower conversions of (12 %) (Scheme 1.17).

A thiourea catalyst **1.21**, in conjunction with tertiary amine base pentamethyldiethylenetriamine (PMDTA) was shown by Wu *et al.* to be photoswitchable through

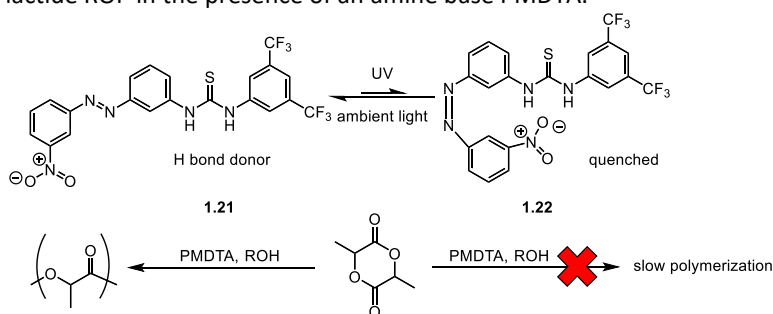
Scheme 1.17. Synthesis of poly(valerolactone) by the photoswitchable polymerization of valerolactone by 2-trans-cinnamoyl- α -cyclodextrin **1.20**.



E/Z isomerization of the azo group (Scheme 1.18).⁸⁵ The more stable catalyst was also the more active catalyst for lactide polymerization, which lead to complications during the photoswitching. Rather than fully deactivating the catalyst in presence of blue light ($\lambda_{irr} = 450-480$ nm), the polymerization rate was only decreased from 94 % conv. to 30% conv. in 24 h. To determine if the cause of the inefficient switching was the activity of **1.22** or incomplete isomerization the authors examined the isotacticity of the polymer produced with and without light. The Z-isomer **1.21** and the E-isomer **1.22** would likely have different selectivities but the difference between the polymers produced in the light and in the dark were minor ($P_m = .72-0.76$ vs $0.73-0.75$). These results suggest that the E-isomer is completely inactive and the difference in polymerization rate is caused by inefficient photoisomerization of the Z-isomer.

In 2018, Diaconescu and coworkers and Hecht and coworkers each reported the photoswitchable ROP of various lactones and cyclic carbonates occurred with the photocatalyst **1.23** and various organobases.^{86,87} The catalyst, in conjunction with a tertiary amine base cocatalyst, is active for L-lactide, valerolactone and trimethylene carbonate ROP under visible light. In the presence of UV light and the amine base, the catalyst rearranges to the inactive keto-tautomer **1.25** (Scheme 1.19). The difference is **1.23** is a hydrogen bond donor that can activate

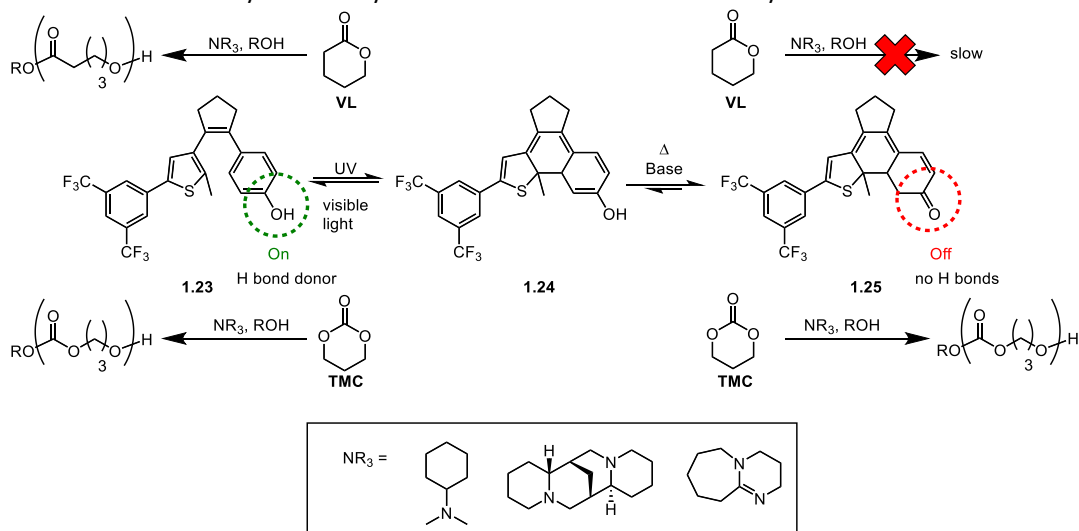
Scheme 1.18. Photoisomerization of azo-benzene containing thiourea **1.21** to sterically-congested species **1.22** and its influence on lactide ROP in the presence of an amine base PMDTA.



the monomer carbonyl, while **1.25** is not a hydrogen bond donor leading to a slight difference in monomer activation. No matter the choice of amine base the catalysts were slow to polymerize any of the monomers and only oligomers were formed after multiple days. **1.23** was more active for valerolactone ROP than **1.25**, and both catalysts were equally reactive for trimethylene carbonate ROP. The relative ratio of poly(valerolactone) in copolymers of valerolactone and trimethylene carbonate could be slightly tuned from 10: 7 trimethylene carbonate: valerolactone in UV light to 3: 4 trimethylene carbonate: valerolactone in visible light.⁸⁶

Chen and coworkers reported that zinc half-salen catalysts **1.26** was able to undergo photoisomerization through a pendant azo group to induce photoswitchable polymerization (Scheme 1.20). Catalyst **1.26** is less electron rich due to conjugation into the distant azobenzene group, while photoisomerization should break this conjugation and lead to more electron rich **1.27**. Unfortunately, the monomer conversions were only slightly impacted for a variety of lactones and cyclic carbonates in presence or absence of light ($\lambda_{irr} = 365$ nm). Even for the copolymerization of ϵ -caprolactone and trimethylene carbonate there were only slight

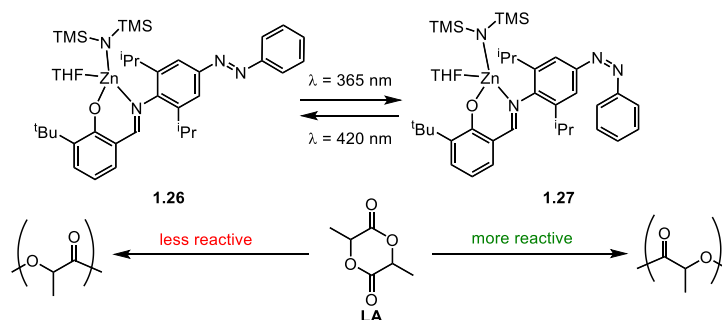
Scheme 1.19. Light and base driven photocyclization of phenolic species **1.23** to the keto-tautomer **1.25** and the difference in catalyst reactivity towards valerolactone and trimethylene carbonate ROP.



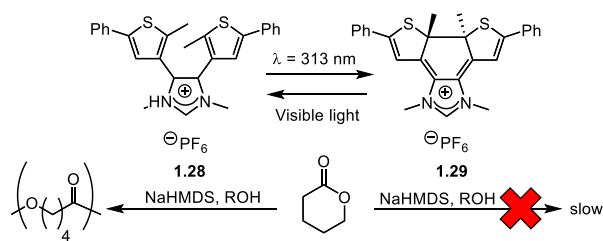
differences in overall monomer incorporation depending on if the polymerization was performed in the light (6: 13 ϵ -caprolactone: trimethylene carbonate) or dark (15: 44 ϵ -caprolactone: trimethylene carbonate). Similarly to Wu and coworkers' findings with a photoisomerizable azobenzene installed on thiourea catalysts,⁸⁵ it was possible that not all of the catalyst was undergoing isomerization. If only a small proportion of **1.26** is isomerizing to **1.27** under irradiation that could explain the minor reactivity differences in light and dark conditions.

Photocyclization is another common method for inducing structural and electronic changes^{24,88} and Bielawski and coworkers were able to modify NHCs bearing photoactive thiophene groups to control valerolactone ROP.²⁴ The cyclization of the thiophene groups of precatalyst **1.28** forms **1.29** (Scheme 1.21), which is less electron rich due to increased conjugation. After deprotonation with sodium hexamethyldisilazane (NaHMDS), **1.28** is active for valerolactone ROP, while **1.29** is inactive. This catalyst pair displayed low reversibility as 13 % of **1.28** decomposes to insoluble byproducts after 1 hour of UV radiation ($\lambda_{\text{irr}} = 313 \text{ nm}$) and 2 hours of visible light irradiation ($\lambda_{\text{irr}} > 500 \text{ nm}$). This degradation over time limits the total number of

Scheme 1.20. Photoisomerization of a zinc half-salen catalyst **1.26** bearing a pendant azobenzene group to change the reactivity of the catalysts towards lactide ROP.



Scheme 1.21. Photocyclization of dithiophene bearing *N*-heterocyclic carbene precatalyst **1.28** to **1.29** and its influence on valerolactone ROP.



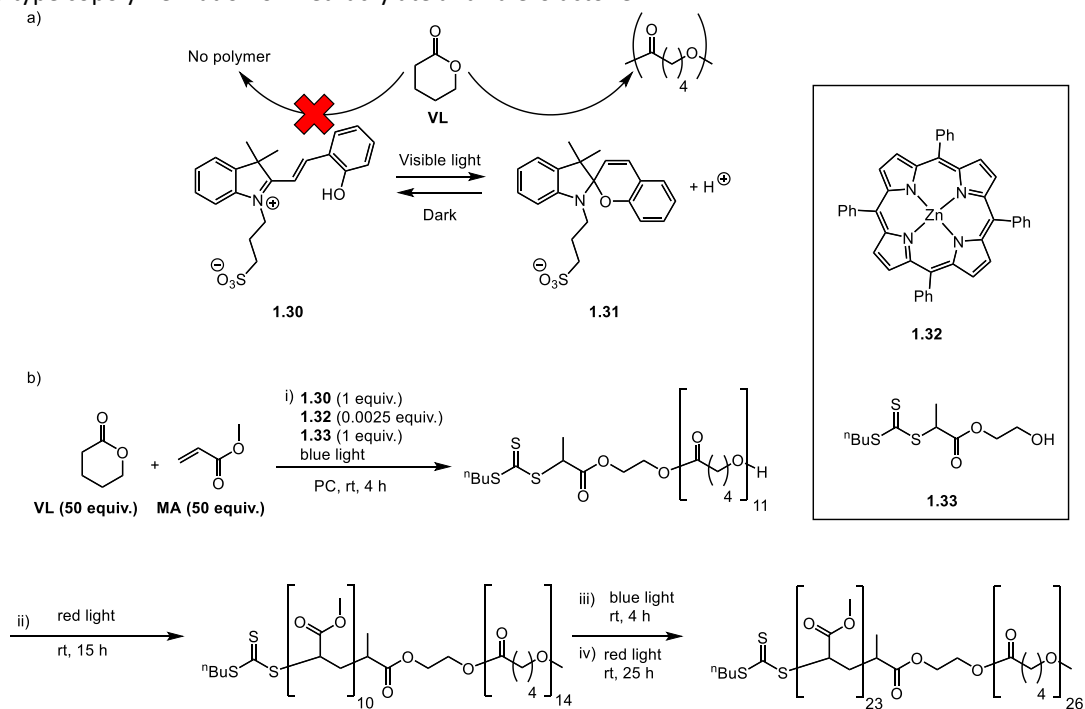
times this system could be switched before significant reductions of catalyst activity were observed.

Boyer and coworkers utilized a photoacid **1.30** for the photoswitchable polymerization of valerolactone (Scheme 1.22a).⁸⁸ Under a blue light ($\lambda_{\text{irr}} = 460 \text{ nm}$, 0.7 mW/cm^2), photocyclization of **1.30** to **1.31** was induced, which creates a potent Brønsted acid. The acid activated valerolactone for ROP by alcohol initiators and the polymerization reaches high conversions of 88 % in 22 hours with a modest degree of polymerization ($\text{DP} = 44$). Under ambient light (0.1 mW/cm^2) the conversion is lower (25 %, $\text{DP} = 13$) and the dispersity is broader ($M_w/M_n = 1.18$ vs. 1.27) indicating a smaller amount of **1.31** is being formed. Photocatalyst **1.30** was then paired with another photocatalyst tetraphenylporphyrin zinc **1.32** for simultaneous photo-induced energy transfer reversible addition-fragmentation transfer (PET RAFT) polymerization of methacrylate and the ROP of valerolactone. For this Janus-type copolymerization a bifunctional thiocarbonate-alcohol initiator **1.33** was used to provide sufficient initiators for both monomers. Under blue light the photoacid **1.31** is produced while **1.32** is inactive (Scheme 1.22b). Under red light, both catalysts are active and both methyl acrylate and valerolactone are consumed, but the rate of ROP for valerolactone is slower. After a second switch from red light to blue light, methacrylate polymerization is halted and the rate of ROP for valerolactone increases. A final

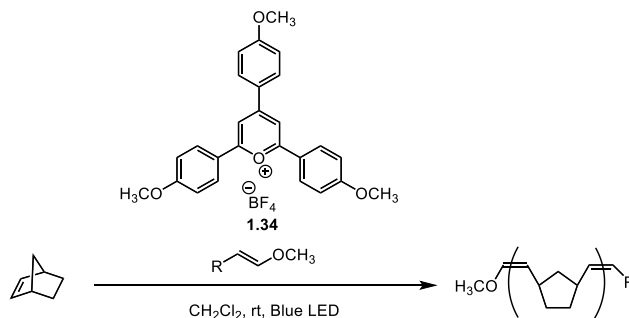
switch from blue light to red light was performed and again both methacrylate and valerolactone continue polymerizing, showing that both catalyst remain active. This dual photocatalyst offers insights into the challenges inherent in finding two photocatalysts with sufficiently different absorption ranges for well-defined photo switches. Nevertheless, these results could lead to future copolymerizations with multiple photocatalysts undergoing mechanistically distinct copolymerizations for complex copolymer synthesis.

Boydston and coworkers demonstrated that exposing 2,4,6-tri-(4-methoxy)pyrylium tetrafluoroborate **1.34** to light leads to an effective catalyst for the ROMP of norbornene (Scheme 1.23).²⁵ At a 1000: 1.0: 0.03 ratio of norbornene: vinyl ether: photocatalyst with a blue LED light ($\lambda_{\text{irr}} = 450\text{-}480\text{ nm}$), 88 % conversion was obtained in only 30 minutes, displaying excellent molecular weight control and a relatively narrow dispersity for ROMP ($M_n = 60.2\text{ kDa}$, $M_w/M_n =$

Scheme 1.22. (a) Photoacid **1.30** catalyzed polymerization of valerolactone. (b) Dual photocatalysts for the Janus-type copolymerization of methacrylate and valerolactone.



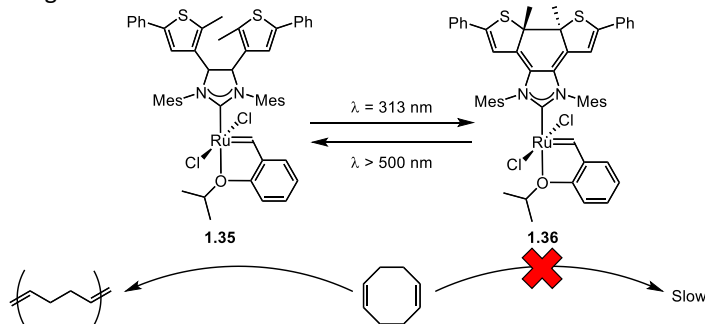
Scheme 1.23. Metal-free ROMP of norbornene catalyzed by a pyrrilium photocatalyst **1.34**, initiated by vinyl ethers.



1.6). In the absence of light, no polymer is formed and the polymerization could be turned on and off without a noticeable loss in activity.

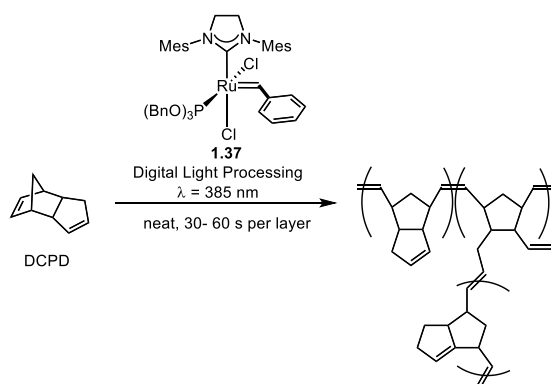
Bielawski and coworkers developed a variant of the Hoveyda-Grubbs second generation catalyst **1.35** bearing pendant thiophene moieties on the NHC for photocyclization.⁸⁹ Under visible light, the spectator NHC ligand is not cyclized and the catalyst is active for the ROMP of cyclooctadiene (Scheme 1.24). UV light induced cyclization on the spectator ligand which led to a less reactive catalyst and a long induction period was observed for ROMP. This catalyst could be switched *in-situ* between the more active open catalyst and the less active cyclized species, because the photoswitchable moiety was located on the spectator ligand rather than the initiator.

Scheme 1.24. Photoswitchable ROMP of cyclooctadiene catalyzed by a Hoveyda-Grubbs variant **1.35** bearing a photoswitchable thiazole ligand.



Lemcoff and coworkers were able to develop inactive variants of the Grubbs second generation catalysts **1.37** containing bulky tribenzyl phosphite ligands that forces the alkylidene ligand into a cis orientation (Scheme 1.25).⁹⁰ Upon the application of UV light ($\lambda_{\text{irr}} = 385 \text{ nm}$) the catalyst is believed to rearrange into the more reactive transalkylidene that is then active for ROMP. UV light was then applied to a neat solution of dicyclopentadiene and **1.37** to initiate ROMP cross-linking. By using digital light processing to program patterns, **1.37** was used for stereolithography to design patterned surfaces.

Scheme 1.25. Stereolithography by ROMP of DCPD with a deactivated catalyst Grubbs II type catalyst **1.37**. UV light activates the catalyst to induce cross-linking of dicyclopentadiene.



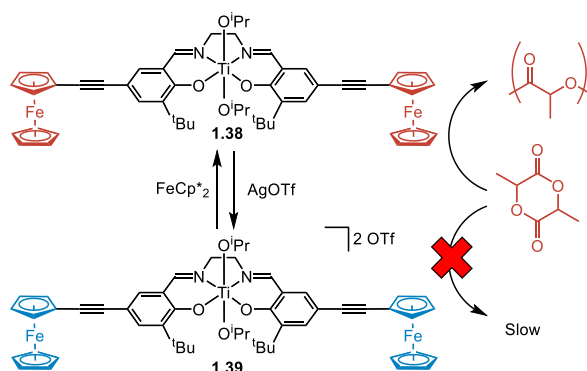
1.4 Redox-switchable Ring-opening Polymerization

The variety of easily accessible oxidation states that many metal complexes can accommodate has supported a number of redox-switchable polymerization reactions. Chemical oxidants and reductants have enabled rapid switching to produce blocky copolymers,^{39,91} initiate *in-situ* crosslinking⁹² and produce patterned surfaces.³⁰ An increasing focus has been replacing

chemical oxidants and reductants with more sustainable alternatives.^{29,30} Electrochemical redox reactions have been demonstrated both in solution²⁹ and on surfaces,³⁰ which could allow programmable copolymerizations in the future.

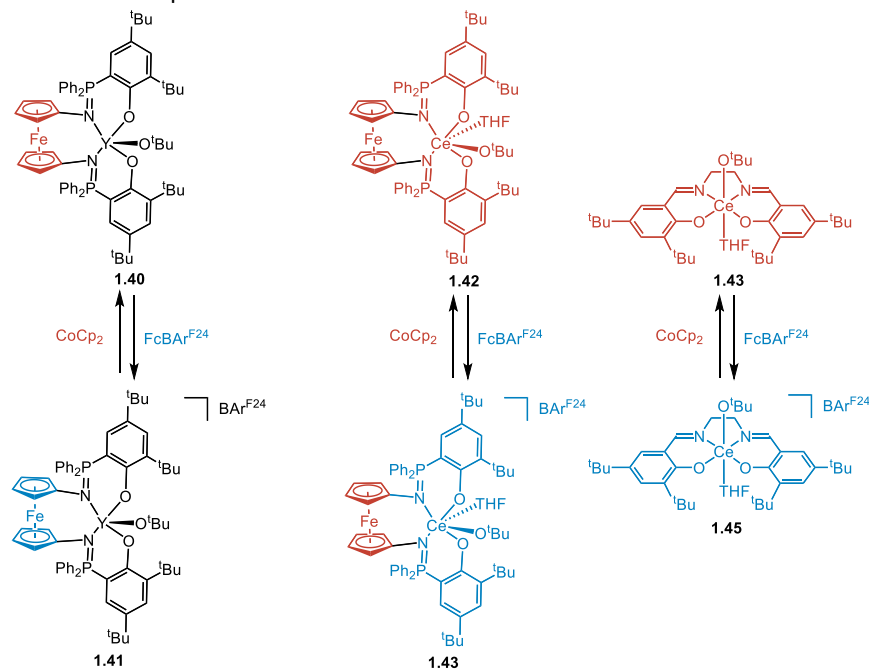
The earliest example of a redox-switchable ROP was demonstrated by Gibson and coworkers with a titanium salen bisalkoxide catalyst **1.38** that had variable reactivity toward lactide ROP depending on the oxidation state of ferrocene moieties bound to the salen ligand (Scheme 1.26). This catalyst was more active in its reduced form and less active in the oxidized form **1.39**.

Scheme 1.26. Redox-switchable, catalyst consisting of a titanium-salen complex **1.38** containing pendant ferrocene moieties. When the ferrocene moieties are reduced the complex is active for lactide polymerization, while the polymerization is much slower when the ferrocene moieties are oxidized.



In 2011, Diaconescu and coworkers developed the first, completely orthogonal redox-switchable polymerization with yttrium phosphasalen catalysts **1.40** and **1.41** containing pendant ferrocene moieties.⁹³ Similarly to Gibson's catalyst, the oxidation and reduction of the ferrocene changed the electron density of the bound transition metal catalyst (Scheme 1.27). Lactide polymerization proved to be highly sensitive to the oxidation state as both catalysts were active in their more nucleophilic reduced forms and inactive in their more electrophilic oxidized forms. The Diaconescu group noted the same trend with a similar cerium(III)-ferrocenylphosphasalen

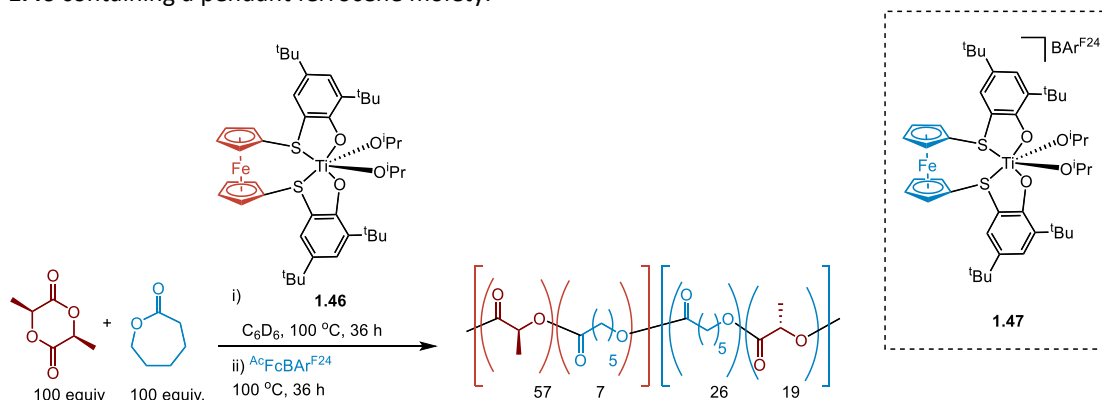
Scheme 1.27. Site of oxidation for various redox-active lactide polymerization catalysts. Reduced moiety is in red and oxidized moieties are in blue. For all catalyst redox pairs, the reduced species were more active for lactide ROP than the oxidized species.



catalyst **1.42** and **1.43** as well as a cerium(III) salen **1.44** and **1.45** where both sets of complexes displayed completely orthogonal lactide polymerization, being active in the reduced form and inactive in the oxidized form.⁹⁴ X-ray absorption near-edge structure (XANES) analysis of both sets of complexes indicate that the oxidation takes place at cerium and not on ferrocene for **1.42**. These results were corroborated by Mossbauer spectroscopy for **1.42** whose isomer shift is similar to ferrocene and is only slightly shifted from **1.42** at 0.53 mm^{-1} to **1.43** at 0.55 mm^{-1} . Notably, these are the first examples where the metal being subject to the redox-switches was also the metal at the active site for ring-opening polymerization. These two design principles offer complementary methods for designing redox-active catalysts

In 2014, Diaconescu and coworkers demonstrated the redox-switchable copolymerization of *L*-lactide and ϵ -caprolactone with titanium salphen alkoxide catalyst **1.46** and

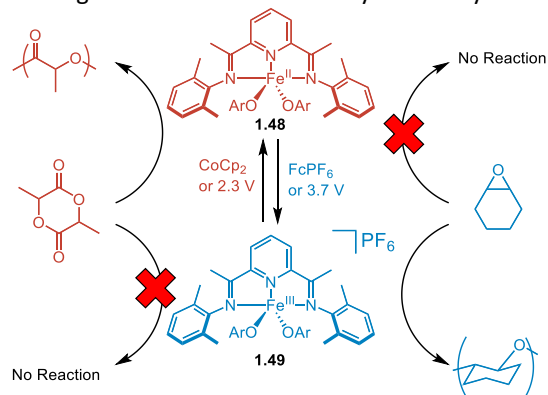
Scheme 1.28. Redox-switchable copolymerization of *L*-lactide and ϵ -caprolactone by titanium-salen complex **1.46** containing a pendant ferrocene moiety.



1.47 (Scheme 1.28).⁹¹ **1.46** was more active for *L*-lactide polymerization than **1.47** and less active for ϵ -caprolactone ROP and vice versa for ϵ -caprolactone. Neither catalyst was completely orthogonal in reactivity towards the homopolymerization of either monomer, regardless, the differences in reactivity depending allowed the Diaconescu group to synthesize blocky copolymers from a mixed monomer solution through redox-switching (Scheme 1.28). While the first block was predominantly composed of poly(lactic acid) the second block had an almost 1: 1 incorporation of *L*-lactide and ϵ -caprolactone, demonstrating the challenges of designing catalysts that can effectively switch between similar monomers as well as more complicated reactivity ratios for mixed solutions.

In 2013, Byers and coworkers synthesized iron bis(imino)pyridine alkoxides catalyst **1.48** that could be oxidized with chemical redox-reagents to **1.49**. This catalyst pair was also active for *rac*-lactide polymerization in the reduced form of the catalyst and completely inactive in the oxidized form.⁹⁵ The Byers group later noted that this catalyst pair was competent for the doubly orthogonal redox-switchable ROP of *rac*-lactide and the cyclohexene oxide (Scheme 1.29).⁹⁶ The ROP of *rac*-lactide was active for **1.48** and inactive for **1.49** while the inverse was true for the ROP

Scheme 1.29. Redox-switchable iron bis(imino)pyridine alkoxide catalyst **1.48** displays orthogonal reactivity towards *rac*-lactide and cyclohexene oxide depending on oxidation state. Catalyst oxidation state can be altered with both chemical redox reagents and electrochemistry reversibly.



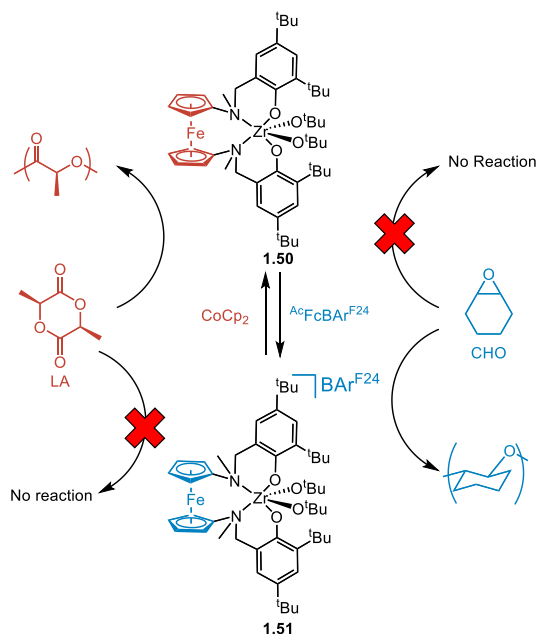
of cyclohexene oxide. The selectivity for each monomer matched expectations as previous catalysts for the ROP of cyclohexene oxide have been catalyzed by electrophilic metal centers or organic Lewis acids. It was noted that *rac*-lactide ROP had living characteristics, while cyclohexene oxide ROP was notably less controlled as seen from the higher than expected molecular weights and the broad dispersity of the polymer ($M_w/M_n = 2.2$). Nevertheless, with this catalyst block copolymers of *rac*-lactide and cyclohexene oxide were synthesized cleanly from a solution of mixed monomers for the first time.

Subsequently, the Diaconescu group published a synthesis of tri-block copolymers of *L*-lactide and cyclohexene oxide using zirconium salfan **1.50** (Scheme 1.30).⁹⁷ Following a similar trend as those observed by the Byers and Diaconescu groups had previously reported, the reduced catalyst **1.50** was active for *L*-lactide polymerization while **1.51** was completely inactive, and the oxidized catalyst **1.51** was active for epoxide polymerization while **1.50** was completely inactive. When the copolymerization was carried out, clean tri-block copolymers could be synthesized starting from either monomer. It was noted that the oxidant, ferrocenium tetrakis[bis(trifluoromethyl)phenyl] borate ($\text{FcBAR}^{\text{F}24}$), was an excellent initiator for cyclohexene

oxide polymerization, so copolymerizations were achieved through sequential addition of monomers and oxidants to prevent unwanted cyclohexene oxide homopolymerization during oxidant addition, unlike the copolymerization reaction reported by Byers and coworkers which used ferrocenium hexafluorophosphate as the oxidant.

The Diaconescu group have since developed a family of ferrocene containing, redox-active complexes^{98–105} in order to better understand the relationship between ligand, design, metal choice and monomer reactivity through both from experimental results and DFT calculations.^{99,104} Currently, these models have not been applied to make predictions for future catalyst development due to complications involving the large number of variables from both the diverse ligand frameworks as well as the metal active sites. A more systematic variation of ligand parameters involving a single metal center may prove to be more efficient for developing predictive models.

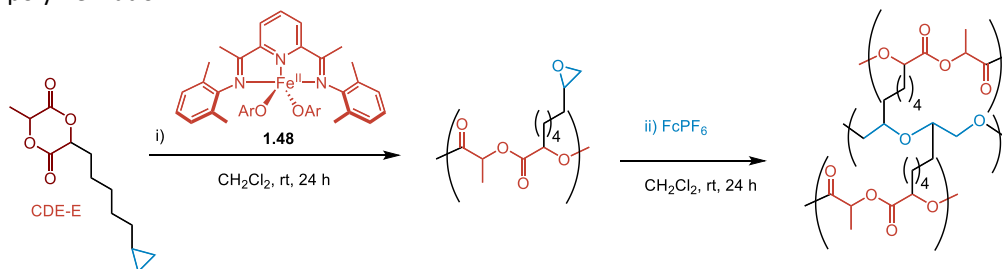
Scheme 1.30. Redox-switchable zirconium salfan alkoxide catalyst **1.50** displays orthogonal reactivity towards L-lactide and cyclohexene oxide depending on oxidation state of the ferrocene moiety.



The Byers group was able to use the same catalyst used for *rac*-lactide-cyclohexene oxide copolymerization, **1.48**, for the redox-switchable ROP of a monomer containing both a lactide-like cyclic diester and a pendant epoxide to demonstrate *in-situ* cross-linking (Scheme 1.31).⁹² Pre-polymer length was controlled from the catalyst ratio of the bifunctional monomer to **1.48** while cross-linking could be initiated by oxidation to **1.49**. The cross-linking density correlated with amount of time **1.49** spent in solution allowing the glass transition temperature (T_g) to be increased from 15 °C of the prepolymer to 74 °C for the cross-linked polymer.

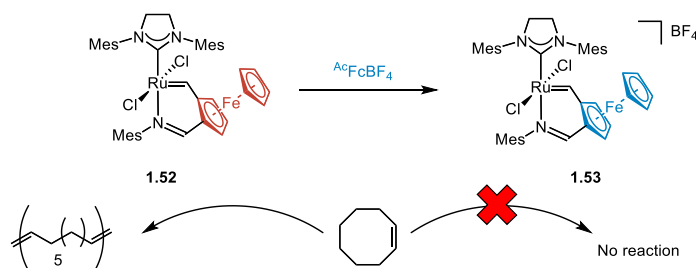
Redox-switchable ROMP was first demonstrated when Plenio and coworkers synthesized a catalyst inspired by the Hoveyda modification to Grubbs second generation olefin polymerization catalyst.¹⁰⁶ The initiator was a modified alkylidene bound to a ferrocene imine. When the ferrocene was oxidized the imine would more loosely coordinate to ruthenium making the catalyst more reactive for the ROMP of norbornene. By placing the redox-active moiety on the initiator this system was not able to be switched on and off mid-polymerization which limits the potential applications for switchable polymerizations.

Scheme 1.31. Polymerization and in-situ crosslinking of a cyclic diester-epoxide through redox-switchable polymerization.



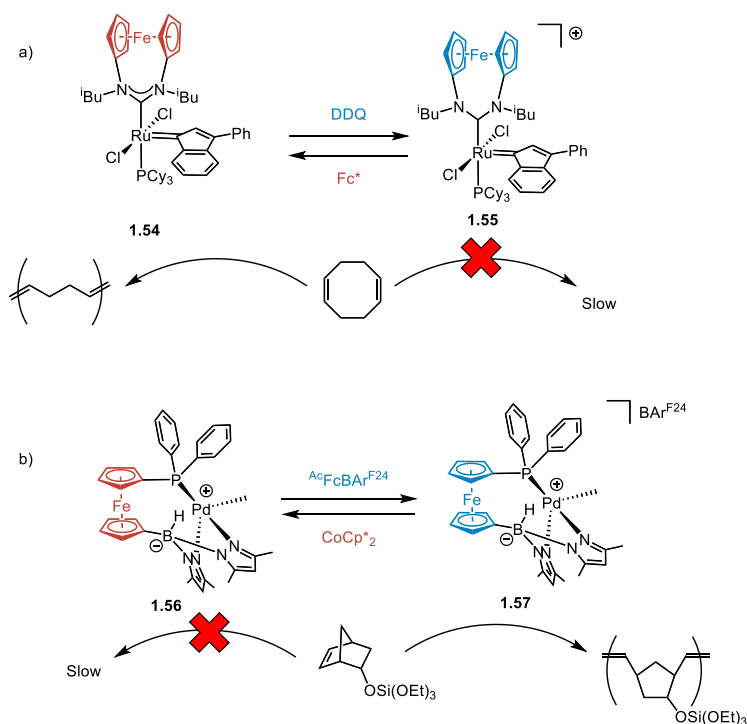
Spectator ligand and metal-centered oxidations have also been investigated and these systems can be switched on or off mid-reaction. Bielawski and coworkers discovered that metal centered oxidations of commercial Ruthenium catalysts would induce catalyst precipitation and thus allow the catalyst to be easily removed and recycled.¹⁰⁷ To modify reactivity, the Bielawski group modified a Grubbs second generation catalyst with a ferrocene appended to the NHC **1.54** (Scheme 1.33a).¹⁰⁸ The reduced complex was a better catalyst for ROMP because the NHC is a better donor promoting phosphine dissociation, while the oxidized complex **1.55** has a worse NHC donor ligand and the catalyst is less active for metathesis. In 2016, Diaconescu and coworkers reported a palladium-ferrocene catalyst **1.56** that can be turned on and off for different norbornene derivatives (Scheme 1.33b). For this catalyst an electron deficient palladium is needed to activate the olefin and thus the electron-deficient oxidized catalyst **1.57** is more active and the electron-rich reduced species **1.56** is less active for ROMP.¹⁰⁹ While the above catalysts both demonstrated orthogonal reactivity for catalysts in different oxidation states, this type of redox-switchable ROMP has not been used to make novel materials in the same way that photoswitchable ROMP has been utilized which could be an exciting avenue for future studies.

Scheme 1.32. Redox-switchable initiation of norbornene ROMP with a Hoveyda-Grubbs type catalyst containing a ferrocene moiety on the alkylidene initiating ligand.

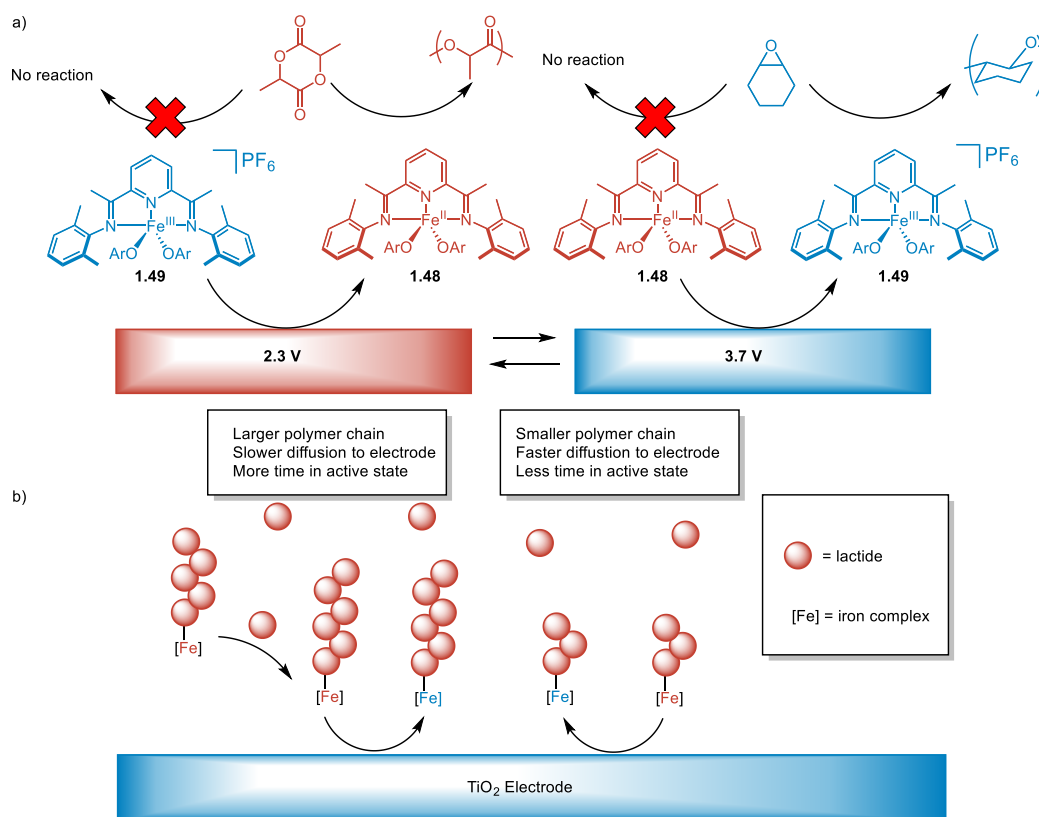


While previous systems have all involved chemical redox-reagents for both ROP and ROMP reactions, Byers and coworkers demonstrated the ability to use electrochemistry to replace chemical redox reagents for redox-switchable ROP of *rac*-lactide and cyclohexene oxide (Scheme 1.34a).²⁹ When **1.48** was electrochemically oxidized to **1.49** the resulting complex was active for cyclohexene oxide ROP and inactive for *rac*-lactide ROP. When **1.49** was electrochemically oxidized to **1.48** the resulting complex was active for *rac*-lactide ROP and inactive for cyclohexene oxide ROP. These results correlate to the reactivity of each complex after chemically oxidation/ reduction. When **1.48** was oxidized and reduced repeatedly during *rac*-lactide polymerization the dispersity of the polymers were always broader after a cycle of electrochemical switching. This is believed to be due to mass-transport to the electrode amplifying the natural dispersities of the polymerization reaction (Scheme 1.34b). The

Scheme 1.33. a) Redox-switchable initiation of norbornene ROMP with a modified Hoveyda-Grubbs II catalysts containing a ferrocene moiety on the NHC spectator ligand. b) Redox-switchable ROMP of a silyl ether containing norbornene derivative containing a silyl ether by a cationic palladium complex bearing a ferrocene-containing ligand.



Scheme 1.34. a) Electrochemically redox-switchable polymerization of *rac*-lactide and cyclohexene oxide. b) Magnification of pre-existing polymer dispersity by mass-transport to the electrode during electrochemical redox-switchable polymerization.



polymerization of lactide by **1.48** may be living, but the dispersity of the polymers is not exactly 1.0 before electrochemical oxidation, therefore some iron catalysts will have slightly longer poly(lactic acid) chains. These complexes will be more massive and therefore diffuse more slowly and polymerize more lactide before being oxidized at the electrode than iron catalysts with shorter poly(lactic acid) chains. With each subsequent oxidation and reduction cycle this disparity grows wider as does the polymer dispersity.

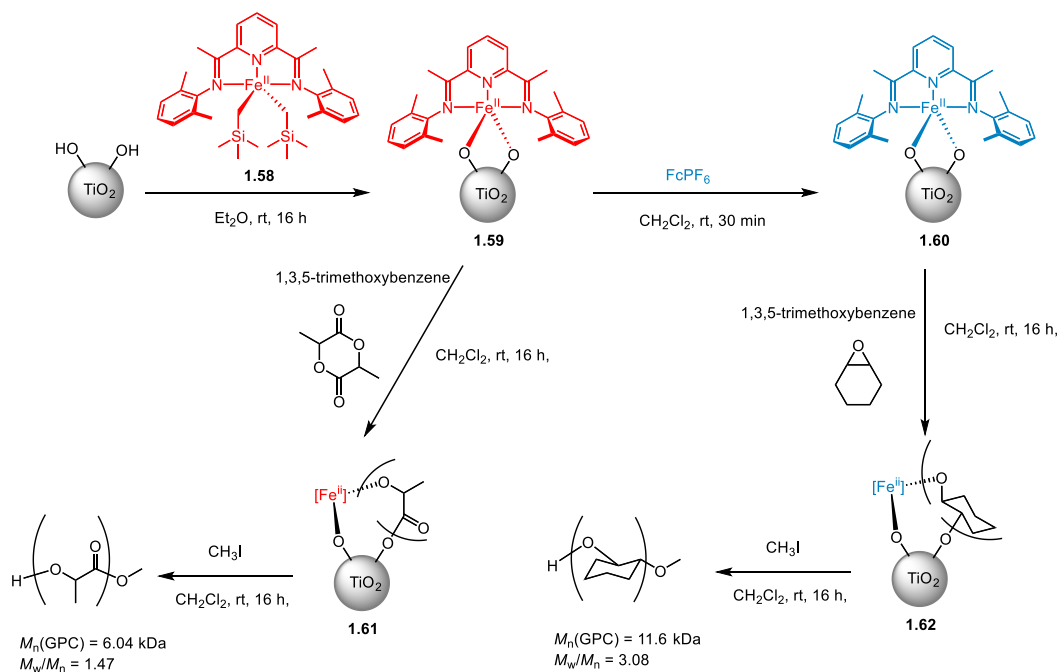
An application of electrochemically redox-switchable ROP was the synthesis of patterned surfaces.³⁰ By reacting the hydroxyl groups on the TiO₂ surface with iron bis(imino)pyridine dialkyl **1.58**, surface-bound Iron catalysts could be synthesized onto both solid TiO₂ nanoparticles and

TiO₂ coated plates (Scheme 1.35). Surface-bound iron nanoparticles **1.59** were active for lactide ROP, and the polymer could be cleaved off of the surface by reacting the titanium carboxylate end groups with methyl iodide (Scheme 1.35a). The resulting polymer had a slightly broader dispersity ($M_w/M_n = 1.46$) than was previously reported for homogenous iron bis(imino)pyridine alkoxide catalyst **1.48** ($M_w/M_n = 1.16$)⁹⁵ which we attribute to mass transport of monomer to the catalyst surface. Upon the chemical oxidation of **1.59** with ferrocenium hexafluorophosphate, the oxidized complex **1.60** was formed. This species was active for cyclohexene oxide ROP and this polymer could also be removed through treatment with methyl iodide. Again this polymer possessed a broader dispersity ($M_w/M_n = 3.08$). than had previously been observed for poly(cyclohexene oxide) produced from homogenous catalyst **1.49** ($M_w/M_n = 2.20$).⁹⁶

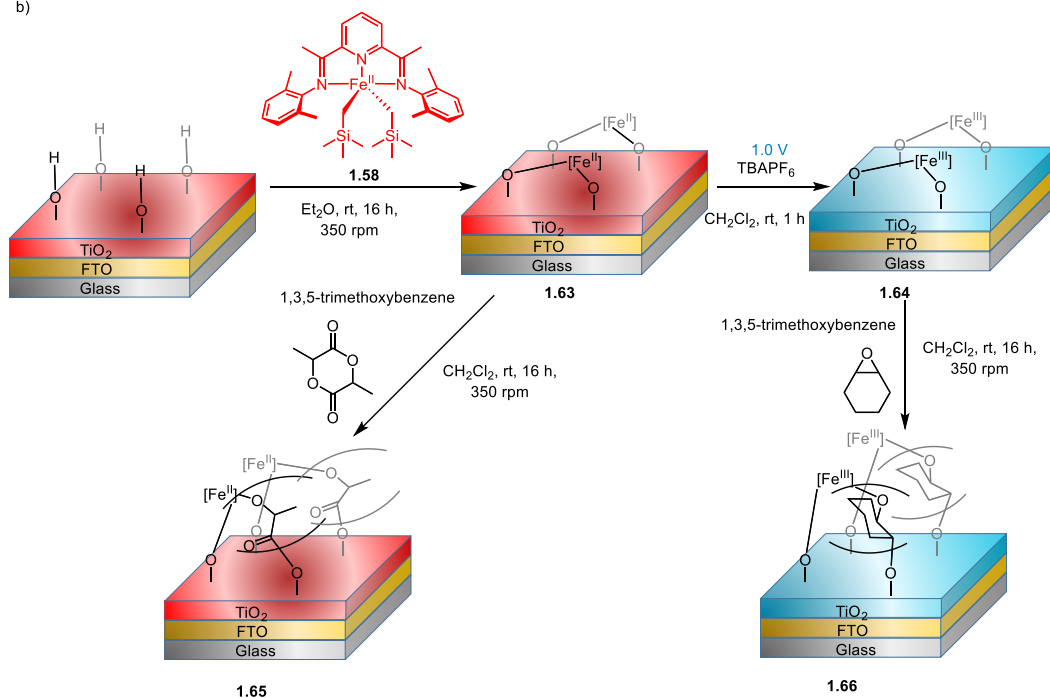
The **1.59** and **1.60**. iron complexes were analyzed through Mossbauer spectroscopy to determine the oxidation state of the surface bound species. **1.59** consisted of a major species with an isomer shift of 1.09 mm/s which is similar to molecular iron (II) species **1.48**. The minor species had an isomer shift of 0.42 mm/s which is similar to the cationic, formally iron (III) species **1.49**. This may indicate some electron transfer from the titania surface to iron complexes on the surface.¹¹⁰ **1.60** consisted of a major species with an isomer shift of 0.49 mm/s which is similar to the cationic formally iron (III) species **1.49** and a minor species with an isomer shift of 1.28 mm/s which is similar to the molecular iron (II) species **1.48**. The persistence of iron (II) species after oxidation is attributed to Inefficient oxidation of the titania nanoparticles as some of iron (II) complex could be inaccessible to the ferrocenium oxidant.¹¹⁰

Scheme 1.35. a) The anchoring of redox-active, iron(II) bis(imino)pyridine alkyl complex **1.58** onto TiO₂ nanoparticles. B) The anchoring of redox-active, iron(II) bis(imino)pyridine alkyl complex **1.58** onto layered surfaces consisting of TiO₂ nanoparticles on a layer of FTO on glass slides. Complex was active for separate polymerizations in each redox-state.

a)



b)



The iron bound catalysts on titania plates **1.63** was also reactive for lactide polymerization leading to surface bound polymer **1.65** (Scheme 1.35b). **1.63** could be electrochemically oxidized to **1.64** which was reactive towards cyclohexene oxide. By oxidizing only half of a plate containing anchored iron complex **1.63** to **1.64**, both lactide and cyclohexene oxide could be selectively polymerized on their respective section of the plate. There were minor impurities of polyether on the reduced section of the plate and polyester on the oxidized section. This was believed to be due to incomplete oxidation/ reduction of iron catalyst on the titania surface as was observed on the surface anchored nanoparticles. These redox-active surfaces could be used in the future to synthesize complex patterned surfaces for sensors or electronic devices through more sophisticated and precise patterning.

1.5 Conclusion

Switchable, ring-opening polymerization was only developed in the last 20 years, but, already, it has proven to be a versatile technique for producing copolymers, especially block copolymers.^{21,111} While chemically-switchable polymerization has been utilized to make copolymers with large block sizes and up to four monomers,⁴¹ the architectures and monomer scope demonstrated for photoswitchable and redox-switchable polymerizations is still being developed. Although light is an operationally simple stimulus to apply to reactions, photoswitchable polymerizations have not yet demonstrated the ability to produce unique polymers using ROP.⁸² Photo-switchable ROMP, in contrast, has been used to effectively demonstrate its potential for *in-situ* cross-linking and surface functionalization.⁸³ Redox-

switchable ROP is currently limited to lactones, cyclic carbonates, epoxides while no switchable ROCOP methods have yet been demonstrated. Accessing a wider variety of monomers will allow for a greater diversity of copolymers. Additionally, non-stoichiometric redox switching could be an important technique in the future for synthesizing tunable gradient or even statistical copolymers of normally incompatible monomers. Exciting future directions include the expansion of photoredox reactions to ring-opening polymerizations to replace stoichiometric chemical reagents and mass-transport-limited electrochemical stimuli. Switchable, ring-opening polymerization will continue to be a promising area of research as more unique copolymers and applications are developed.

In the following chapters I will cover my efforts towards expanding the monomer scope of redox-switchable copolymerizations. The second chapter will cover redox-switchable *L*-lactide ROP and propylene oxide-CO₂ ROCOP using cobalt salen catalysts and potassium cryptand alkoxides. The third chapter will cover the redox-switchable polymerization of *N*-carboxyanhydrides as well as their copolymerization with ϵ -caprolactone and cyclohexene oxide using iron bis(imino)pyridine catalysts. The final chapter will detail the efforts made to expand redox-switchable *N*-carboxyanhydride polymerization to semiconductor surfaces.

1.6 References

- (1) Feng, H.; Lu, X.; Wang, W.; Kang, N. G.; Mays, J. W. Block Copolymers: Synthesis, Self-Assembly, and Applications. *Polymers* **2017**, *9* (10).

<https://doi.org/10.3390/polym9100494>.

- (2) Verduzco, R.; Li, X.; Pesek, L.; Stein, G. E. Structure, Function, Self-Assembly, and Applications of Bottlebrush Copolymers. *Chem. Soc* **2015**, *44*, 2405–2420. <https://doi.org/10.1039/c4cs00329b>.
- (3) Li, L.; Raghupathi, K.; Song, C.; Prasad, P.; Thayumanavan, S. Self-Assembly of Random Copolymers. *Chem. Commun.* **2015**, *50* (88), 13417–13432. <https://doi.org/10.1039/c4cc03688c>.Self-assembly.
- (4) Peykova, Y.; Lebedeva, O. V; Diethert, A.; Peter, M.; Willenbacher, N. International Journal of Adhesion & Adhesives Adhesive Properties of Acrylate Copolymers : Effect of the Nature of the Substrate and Copolymer Functionality. *Internation Journal of Adhesion and Adhesives of Adhesion & Adhesives* **2012**, *34*, 107–116. <https://doi.org/10.1016/j.ijadhadh.2011.12.001>.
- (5) Staeger, M.; Finot, E. Surface Investigation of Adhesive Formulation Consisting of UV Sensitive Triblock Poly (Styrene – b-Butadiene – b-Styrene) Copolymer. **2002**, *185*, 231–242.
- (6) Sulley, G. S.; Gregory, G. L.; Chen, T. T. D.; Peña Carrodeguas, L.; Trott, G.; Santmarti, A.; Lee, K. Y.; Terrill, N. J.; Williams, C. K. Switchable Catalysis Improves the Properties of CO₂-Derived Polymers: Poly(Cyclohexene Carbonate- b-ε-Decalactone- b-Cyclohexene Carbonate) Adhesives, Elastomers, and Toughened Plastics. *Journal of the American Chemical Society* **2020**, *142* (9), 4367–4378. <https://doi.org/10.1021/jacs.9b13106>.
- (7) Chen, T. T. D.; Carrodeguas, L. P.; Sulley, G. S.; Gregory, G. L.; Williams, C. K. Bio-Based and Degradable Block Polyester Pressure-Sensitive Adhesives. *Angewandte Chemie* -

<https://doi.org/10.1002/anie.202006807>.

- (8) Kim, S. W.; Cha, S. Thermal , Mechanical , and Gas Barrier Properties of Ethylene – Vinyl Alcohol Copolymer-Based Nanocomposites for Food Packaging Films : Effects of Nanoclay Loading. *Journal of Applied Polymer Science* **2014**, *131* (11), 40289–40297. <https://doi.org/10.1002/app.40289>.
- (9) Guidotti, G.; Soccio, M.; Siracusa, V.; Salatelli, E.; Munari, A.; Lotti, N. Novel Random PBS-Based Copolymers Containing Aliphatic Side Chains for Sustainable Flexible Food Packaging. *Polymers* **2017**, *9* (724), 1–16. <https://doi.org/10.3390/polym9120724>.
- (10) Zhu, J.; Tang, X.; Etxeberria, A.; Chen, E. Y. Packaging Materials with Desired Mechanical and Barrier Properties and Full Chemical Recyclability. *Nature Communications* **2019**, 1–7. <https://doi.org/10.1038/s41467-019-11525-x>.
- (11) Gillies, E. R.; Fréchet, J. M. J. A New Approach towards Acid Sensitive Copolymer Micelles for Drug Delivery. *Chem. Commun.* **2003**, 1640–1641.
- (12) Cerritelli, S.; Velluto, D.; Hubbell, J. A. PEG-SS-PPS : Reduction-Sensitive Disulfide Block Copolymer Vesicles for Intracellular Drug Delivery. **2007**, *8*, 1966–1972.
- (13) He, C.; Wan, S.; Sung, D. In Situ Gelling Stimuli-Sensitive Block Copolymer Hydrogels for Drug Delivery. *Journal of Controlled Release* **2008**, *127*, 189–207. <https://doi.org/10.1016/j.jconrel.2008.01.005>.
- (14) Gonzalo, G. De; Colpa, D. I.; Habib, M. H. M.; Fraaije, M. W. Bacterial Enzymes Involved in Lignin Degradation. *Journal of Biotechnology* **2016**, *236*, 110–119. <https://doi.org/10.1016/j.jbiotec.2016.08.011>.

- (15) Chung, Y.; Chris, D.; Kwon, Y. Glucose Biofuel Cells Using Bi-Enzyme Catalysts Including Glucose Oxidase , Horseradish Peroxidase and Terephthalaldehyde Crosslinker. *Chemical Engineering Journal* **2018**, *334*, 1085–1092. <https://doi.org/10.1016/j.cej.2017.10.121>.
- (16) Cech, T. R. A Model for the RNA-Catalyzed Replication of RNA. *Proc. Natl. Acad. Sci. USA* **1986**, *83* (June), 4360–4363.
- (17) Fan, J.; Pavletich, N. P. Structure and Conformational Change of a Replication Protein A Heterotrimer Bound to SsDNA. *Genes & Development* **2012**, 2337–2347. <https://doi.org/10.1101/gad.194787.112.nucleotide>.
- (18) Veit, B.; Heinlein, M.; Epel, B. L.; Padgett, H. S.; Beachyt, R. N. Interaction of Tobarnovirus Movement Proteins with the Plant Cytoskeleton. *Science* **1995**, *270* (5244), 1983–1985.
- (19) Xiong, R.; Wu, J.; Zhou, Y.; Zhou, X. Identification of a Movement Protein of the Tenuivirus Rice Stripe Virus □. **2008**, *82* (24), 12304–12311. <https://doi.org/10.1128/JVI.01696-08>.
- (20) Whittington, S. G. Random Copolymers. *Physica A: Statistical Mechanics and its Applications* **2002**, *314* (1–4), 214–219. [https://doi.org/10.1016/S0378-4371\(02\)01055-5](https://doi.org/10.1016/S0378-4371(02)01055-5).
- (21) Teator, A. J.; Lastovickova, D. N.; Bielawski, C. W. Switchable Polymerization Catalysts. *Chemical Reviews* **2016**, *116*, 1969–1992.
- (22) Id, K. N.; Alzahrany, Y.; Polymeropoulos, G.; Gnanou, Y.; Hadjichristidis, N. Anionic Polymerization of Styrene and 1,3-Butadiene in the Presence of Phosphazene Superbases. *Polymers* **2017**, *9* (538), 1–14. <https://doi.org/10.3390/polym9100538>.
- (23) Romain, C.; Zhu, Y.; Dingwall, P.; Paul, S.; Rzepa, H. S.; Buchard, A.; Williams, C. K. Chemoselective Polymerizations from Mixtures of Epoxide, Lactone, Anhydride, and Carbon Dioxide. *Journal of the American Chemical Society* **2016**, *138*, 4120–4131.

- (24) Neilson, B. M.; Bielawski, C. W. Photoswitchable NHC-Promoted Ring-Opening Polymerizations. *Chemical Communications* **2013**, 49 (48), 5453–5455. <https://doi.org/10.1039/c3cc42424c>.
- (25) Ogawa, K. A.; Goetz, A. E.; Boydston, A. J. Metal-Free Ring-Opening Metathesis Polymerization. *Journal of the American Chemical Society* **2015**, 137 (4), 1400–1403. <https://doi.org/10.1021/ja512073m>.
- (26) Zhao, Y.; Zhu, S.; Liao, C.; Wang, Y.; Lam, J. W. Y.; Zhou, X.; Wang, X.; Xie, X.; Tang, B. Z. Cobalt-Mediated Switchable Catalysis for the One-Pot Synthesis of Cyclic Polymers. *Angewandte Chemie International Edition* **2021**, 1–7. <https://doi.org/10.1002/anie.202106285>.
- (27) Ihrig, S. P.; Eisenreich, F.; Hecht, S. Photoswitchable Polymerization Catalysis: State of the Art, Challenges, and Perspectives. *Chemical Communications* **2019**, 55 (30), 4290–4298. <https://doi.org/10.1039/c9cc01431d>.
- (28) Magenau, A. J. D.; Strandwitz, N. C.; Gennaro, A.; Matyjaszewski, K. Electrochemically Mediated Atom Transfer Radical Polymerization. *Science* **2011**, 332 (April), 81–83. <https://doi.org/10.4159/harvard.9780674333987.c22>.
- (29) Qi, M.; Dong, Q.; Wang, D.; Byers, J. A. Electrochemically Switchable Ring-Opening Polymerization of Lactide and Cyclohexene Oxide. *Journal of the American Chemical Society* **2018**, 140 (17), 5686–5690. <https://doi.org/10.1021/jacs.8b02171>.
- (30) Qi, M.; Zhang, H.; Dong, Q.; Li, J.; Musgrave, R. A.; Zhao, Y.; Dulock, N.; Wang, D.; Byers, J. A. Electrochemically Switchable Polymerization from Surface-Anchored Molecular Catalysts. *Chemical Science* **2021**. <https://doi.org/10.1039/d1sc02163j>.

- (31) Kernbichl, S.; Reiter, M.; Adams, F.; Vagin, S.; Rieger, B. CO₂-Controlled One-Pot Synthesis of AB, ABA Block, and Statistical Terpolymers from β -Butyrolactone, Epoxides, and CO₂. *Journal of the American Chemical Society* **2017**, *139*, 6787–6790.
- (32) Kernbichl, S.; Reiter, M.; Mock, J.; Rieger, B. Terpolymerization of β -Butyrolactone, Epoxides, and CO₂: Chemoselective CO₂-Switch and Its Impact on Kinetics and Material Properties. *Macromolecules* **2019**, *52* (21), 8476–8483. <https://doi.org/10.1021/acs.macromol.9b01777>.
- (33) Nuyken, O.; Pask, S. D. Ring-Opening Polymerization-An Introductory Review. *Polymers* **2013**, *5* (2), 361–403. <https://doi.org/10.3390/polym5020361>.
- (34) Stößer, T.; Sulley, G. S.; Gregory, G. L.; Williams, C. K. Easy Access to Oxygenated Block Polymers via Switchable Catalysis. *Nature Communications* **2019**, *10* (1), 1–9. <https://doi.org/10.1038/s41467-019-10481-w>.
- (35) Wang, Y.; Zhao, Y.; Zhu, S.; Zhou, X.; Xu, J.; Xie, X.; Poli, R. Switchable Polymerization Triggered by Fast and Quantitative Insertion of Carbon Monoxide into Cobalt–Oxygen Bonds. *Angewandte Chemie - International Edition* **2020**, *59* (15), 5988–5994. <https://doi.org/10.1002/anie.201914216>.
- (36) Pei, L.; Liu, F.; Liao, H.; Gao, J.; Zhong, L.; Gao, H.; Wu, Q. Synthesis of Polyethylenes with Controlled Branching with α -Diimine Nickel Catalysts and Revisiting Formation of Long-Chain Branching. *ACS Catalysis* **2018**, *8* (2), 1104–1113. <https://doi.org/10.1021/acscatal.7b03282>.
- (37) Mundil, R.; Wilson, L. E.; Schaarschmidt, D.; Císařová, I.; Merna, J.; Long, N. J. Redox-Switchable α -Diimine Palladium Catalysts for Control of Polyethylene Topology. *Polymer*

- 2019**, 179 (April). <https://doi.org/10.1016/j.polymer.2019.121619>.
- (38) Zhang, Y.; Jian, Z. Polar Additive Triggered Branching Switch and Block Polyolefin Topology in Living Ethylene Polymerization. *Macromolecules* **2021**, 54 (7), 3191–3196. <https://doi.org/10.1021/acs.macromol.1c00174>.
- (39) Delle Chiaie, K. R.; Biernesser, A. B.; Ortuño, M. A.; Dereli, B.; Iovan, D. A.; Wilding, M. J. T.; Li, B.; Cramer, C. J.; Byers, J. A.; Delle Chiaie, K. R.; et al. Block Copolymerization of Lactide and an Epoxide Facilitated by a Redox Switchable Iron-Based Catalyst. *Dalton Transactions* **2017**, 128 (38), 12971–12980. <https://doi.org/10.1039/c7dt03067c>.
- (40) Huang, M.; Gao, L.; Feng, J.; Huang, X.; Li, Z.; Huang, Z.; Wang, L. Cross-Linked Networks in Poly(Propylene Carbonate) by Incorporating (Maleic Anhydride/Cis-1,2,3,6-Tetrahydrophthalic Anhydride) Oligomer in CO₂/Propylene Oxide Copolymerization: Improving and Tailoring Thermal, Mechanical, and Dimensional Properties. *ACS Omega* **2020**, 5 (28), 17808–17817. <https://doi.org/10.1021/acsomega.0c02608>.
- (41) Deacy, A. C.; Gregory, G. L.; Sulley, G. S.; Chen, T. T. D.; Williams, C. K. Sequence Control from Mixtures: Switchable Polymerization Catalysis and Future Materials Applications. *Journal of the American Chemical Society* **2021**. <https://doi.org/10.1021/jacs.1c03250>.
- (42) Peeck, L. H.; Leuthäusser, S.; Plenio, H. Switched Stereocontrol in Grubbs - Hoveyda Complex Catalyzed ROMP Utilizing Proton-Switched NHC Ligands. *Organometallics* **2010**, 29 (19), 4339–4345. <https://doi.org/10.1021/om100628f>.
- (43) P'Pool, S. J.; Schanz, H. J. Reversible Inhibition/Activation of Olefin Metathesis: A Kinetic Investigation of ROMP and RCM Reactions with Grubbs' Catalyst. *Journal of the American Chemical Society* **2007**, 129 (46), 14200–14212. <https://doi.org/10.1021/ja071938w>.

- (44) Hyo Jae Yoon, Junpei Kuwabara, Jun-Hyun Kim, C. A. M. Allosteric Supramolecular Triple-Layer Catalysts. *Science* **2010**, *330* (October), 66–69.
- (45) Zhu, Y.; Radlauer, M. R.; Schneiderman, D. K.; Shaffer, M. S. P.; Hillmyer, M. A.; Williams, C. K. Multiblock Polyesters Demonstrating High Elasticity and Shape Memory Effects. *Macromolecules* **2018**, *51* (7), 2466–2475. <https://doi.org/10.1021/acs.macromol.7b02690>.
- (46) Li, C.; Dang, Y.-F.; Wang, B.; Pan, L.; Li, Y.-S. Constructing ABA- and ABCBA-Type Multiblock Copolyesters with Structural Diversity by Organocatalytic Self-Switchable Copolymerization. *Macromolecules* **2021**. <https://doi.org/10.1021/acs.macromol.1c00767>.
- (47) Yuan, Y.; Tam, M. F.; Simplaceanu, V.; Ho, C. A New Look at Hemoglobin Allostery. *Chem. Rev.* **2015**, *115* (4), 1702–1724. <https://doi.org/10.1021/cr500495x.A>.
- (48) Liu, S.; Bai, T.; Ni, K.; Chen, Y.; Zhao, J.; Ling, J.; Ye, X.; Zhang, G. Biased Lewis Pairs: A General Catalytic Approach to Ether-Ester Block Copolymers with Unlimited Ordering of Sequences. *Angewandte Chemie - International Edition* **2019**, *58* (43), 15478–15487. <https://doi.org/10.1002/anie.201908904>.
- (49) Luston, J., Manasek, Z. Copolymerization of Epoxides and Cyclic Anhydrides Catalyzed by Tertiary Amines in the Presence of Proton-Donating Compounds. *J. Macromol. Sci-Chem. A.* **1979**, *13* (6), 853–867.
- (50) Jeske, R. C.; DiCiccio, A. M.; Coates, G. W. Alternating Copolymerization of Epoxides and Cyclic Anhydrides: An Improved Route to Aliphatic Polyesters. *Journal of the American Chemical Society* **2007**, *129* (37), 11330–11331. <https://doi.org/10.1021/ja0737568>.

- (51) Jeske, R. C.; Rowley, J. M.; Coates, G. W. Pre-Rate-Determining Selectivity in the Terpolymerization of Epoxides, Cyclic Anhydrides, and CO₂: A One-Step Route to Diblock Copolymers. *Angewandte Chemie - International Edition* **2008**, *47* (32), 6041–6044. <https://doi.org/10.1002/anie.200801415>.
- (52) Duan, Z.; Wang, X.; Gao, Q.; Zhang, L.; Liu, B.; Kim, I. Highly Active Bifunctional Cobalt-Salen Complexes for the Synthesis of Poly(Ester-Block-Carbonate) Copolymer via Terpolymerization of Carbon Dioxide, Propylene Oxide, and Norbornene Anhydride Isomer: Roles of Anhydride Conformation Consideration. *Journal of Polymer Science, Part A: Polymer Chemistry* **2014**, *52* (6), 789–795. <https://doi.org/10.1002/pola.27057>.
- (53) Wang, Z.; Mu, Y. Chiral SalenCo(III) Complexes with Bulky Substituents as Catalysts for Stereoselective Alternating Copolymerization of Racemic Propylene Oxide with Carbon Dioxide and Succinic Anhydride. *Polymer Chemistry* **2021**, *12* (12), 1776–1786. <https://doi.org/10.1039/d0py01562h>.
- (54) Chidara, V. K.; Boopathi, S. K.; Hadjichristidis, N.; Gnanou, Y.; Feng, X. Triethylborane-Assisted Synthesis of Random and Block Poly(Ester-Carbonate)s through One-Pot Terpolymerization of Epoxides, CO₂, and Cyclic Anhydrides. *Macromolecules* **2021**, *54* (6), 2711–2719. <https://doi.org/10.1021/acs.macromol.0c02825>.
- (55) Zhang, J.; Wang, L.; Liu, S.; Kang, X.; Li, Z. A Lewis Pair as Organocatalyst for One-Pot Synthesis of Block Copolymers from a Mixture of Epoxide, Anhydride, and CO₂. *Macromolecules* **2021**, *54* (2), 763–772. <https://doi.org/10.1021/acs.macromol.0c02647>.
- (56) Plajer, A. J.; Williams, C. K. Heterotrimetallic Carbon Dioxide Copolymerization and Switchable Catalysts: Sodium Is the Key to High Activity and Unusual Selectivity.

- Angewandte Chemie - International Edition* **2021**, *60* (24), 13372–13379.
<https://doi.org/10.1002/anie.202101180>.
- (57) Zhou, Y.; Hu, C.; Zhang, T.; Xu, X.; Duan, R.; Luo, Y.; Sun, Z.; Pang, X.; Chen, X. One-Pot Synthesis of Diblock Polyesters by Catalytic Terpolymerization of Lactide, Epoxides, and Anhydrides. *Macromolecules* **2019**, *52* (9), 3462–3470.
<https://doi.org/10.1021/acs.macromol.9b00001>.
- (58) Zhu, S.; Wang, Y.; Ding, W.; Zhou, X.; Liao, Y.; Xie, X. Lewis Pair Catalyzed Highly Selective Polymerization for the One-Step Synthesis of A: ZCy(AB)XCyAz Pentablock Terpolymers. *Polymer Chemistry* **2020**, *11* (10), 1691–1695. <https://doi.org/10.1039/c9py01508f>.
- (59) Xia, X.; Suzuki, R.; Takojima, K.; Jiang, D. H.; Isono, T.; Satoh, T. Smart Access to Sequentially and Architecturally Controlled Block Polymers via a Simple Catalytic Polymerization System. *ACS Catalysis* **2021**, 5999–6009. <https://doi.org/10.1021/acscatal.1c00382>.
- (60) Su, Y. C.; Liu, W. L.; Li, C. Y.; Ko, B. T. Air-Stable Di-Nuclear Yttrium Complexes as Versatile Catalysts for Lactide Polymerization and Copolymerization of Epoxides with Carbon Dioxide or Phthalic Anhydride. *Polymer* **2019**, *167* (November 2018), 21–30.
<https://doi.org/10.1016/j.polymer.2019.01.060>.
- (61) Gregory, G. L.; Sulley, G. S.; Carrodegua, L. P.; Chen, T. T. D.; Santmarti, A.; Terrill, N. J.; Lee, K. Y.; Williams, C. K. Triblock Polyester Thermoplastic Elastomers with Semi-Aromatic Polymer End Blocks by Ring-Opening Copolymerization. *Chemical Science* **2020**, *11* (25), 6567–6581. <https://doi.org/10.1039/d0sc00463d>.
- (62) Stößer, T.; Williams, C. K. Selective Polymerization Catalysis from Monomer Mixtures: Using a Commercial Cr-Salen Catalyst To Access ABA Block Polyesters. *Angewandte Chemie*

- *International Edition* **2018**, *57* (21), 6337–6341.
<https://doi.org/10.1002/anie.201801400>.
- (63) Diment, W. T.; Stößer, T.; Kerr, R. W. F.; Phanopoulos, A.; Durr, C. B.; Williams, C. K. Ortho-Vanillin Derived Al(III) and Co(III) Catalyst Systems for Switchable Catalysis Using ϵ -Decalactone, Phthalic Anhydride and Cyclohexene Oxide. *Catalysis Science and Technology* **2021**, *11* (5), 1737–1745. <https://doi.org/10.1039/d0cy02164d>.
- (64) Yuntawattana, N.; Gregory, G. L.; Carrodegua, L. P.; Williams, C. K. Switchable Polymerization Catalysis Using a Tin(II) Catalyst and Commercial Monomers to Toughen Poly(L-Lactide). *ACS Macro Letters* **2021**, No. 11, 774–779. <https://doi.org/10.1021/acsmacrolett.1c00216>.
- (65) Stößer, T.; Mulryan, D.; Williams, C. K. Switch Catalysis To Deliver Multi-Block Polyesters from Mixtures of Propene Oxide, Lactide, and Phthalic Anhydride. *Angewandte Chemie - International Edition* **2018**, *57* (51), 16893–16897. <https://doi.org/10.1002/anie.201810245>.
- (66) Drobny, J. G. Styrenic Block Copolymers. In *Handbook of Thermoplastic Elastomers*; 2007; pp 161–177.
- (67) Guidotti, G.; Soccio, M.; Gazzano, M.; Fusaro, L.; Boccafocchi, F.; Munari, A.; Lotti, N. New Thermoplastic Elastomer Triblock Copolymer of PLLA for Cardiovascular Tissue Engineering: Annealing as Efficient Tool to Tailor the Solid-State Properties. *Polymer* **2021**, *213* (November 2020), 123336. <https://doi.org/10.1016/j.polymer.2020.123336>.
- (68) Macosko, C. W.; Guégan, P.; Khandpur, A. K.; Nakayama, A.; Marechal, P.; Inoue, T. Compatibilizers for Melt Blending: Premade Block Copolymers. *Macromolecules* **1996**, *29*

- (17), 5590–5598. <https://doi.org/10.1021/ma9602482>.
- (69) Xu, J.; Eagan, J. M.; Kim, S.; Pan, S.; Lee, B.; Klimovica, K.; Jin, K.; Lin, T.; Howard, M. J.; Ellison, C. J.; et al. Compatibilization of Isotactic Polypropylene (i PP) and High-Density Polyethylene (HDPE) with i PP – PE Multiblock Copolymers. **2018**. <https://doi.org/10.1021/acs.macromol.8b01907>.
- (70) Price, D. J.; Khuphe, M.; Davies, R. P. W.; McLaughlan, J. R.; Ingram, N.; Thornton, P. D. Poly(Amino Acid)-Polyester Graft Copolymer Nanoparticles for the Acid-Mediated Release of Doxorubicin. *Chemical Communications* **2017**, *53*, 8687–8690.
- (71) Raman, S. K.; Raja, R.; Arnold, P. L.; Davidson, M. G.; Williams, C. K. Waste Not, Want Not: CO₂ (Re)Cycling into Block Polymers. *Chemical Communications* **2019**, *55* (51), 7315–7318. <https://doi.org/10.1039/c9cc02459j>.
- (72) Zhao, J.; Pahovnik, D.; Gnanou, Y.; Hadjichristidis, N. A “Catalyst Switch” Strategy for the Sequential Metal-Free Polymerization of Epoxides and Cyclic Esters/Carbonate. *Macromolecules* **2014**, *47* (12), 3814–3822. <https://doi.org/10.1021/ma500830v>.
- (73) Gradišar, Š.; Žagar, E.; Pahovnik, D. Hybrid Block Copolymers of Polyesters/Polycarbonates and Polypeptides Synthesized via One-Pot Sequential Ring-Opening Polymerization. *Polymer Chemistry* **2018**, *9* (38), 4764–4771. <https://doi.org/10.1039/c8py00835c>.
- (74) Romain, D. C.; Williams, C. K. Chemoselective Polymerization Control: From Mixed-Monomer Feedstock to Copolymers. *Angewandte Chemie - International Edition* **2014**, *53* (6), 1607–1610. <https://doi.org/10.1002/anie.201309575>.
- (75) Paul, S.; Romain, C.; Shaw, J.; Williams, C. K. Sequence Selective Polymerization Catalysis: A New Route to ABA Block Copoly(Ester-b-Carbonate-b-Ester). *Macromolecules* **2015**, *48*

- (17), 6047–6056. <https://doi.org/10.1021/acs.macromol.5b01293>.
- (76) Hu, C.; Duan, R.; Yang, S.; Pang, X.; Chen, X. CO₂ Controlled Catalysis: Switchable Homopolymerization and Copolymerization. *Macromolecules* **2018**, *51* (12), 4699–4704. <https://doi.org/10.1021/acs.macromol.8b00696>.
- (77) Carrodeguas, L. P.; Chen, T. T. D.; Gregory, G. L.; Sulley, G. S.; Williams, C. K. High Elasticity, Chemically Recyclable, Thermoplastics from Bio-Based Monomers: Carbon Dioxide, Limonene Oxide and ϵ -Decalactone. *Green Chemistry* **2020**, 8298–8307. <https://doi.org/10.1039/d0gc02295k>.
- (78) Neumann, S.; Däbritz, S. B.; Fritze, S. E.; Leitner, L. C.; Anand, A.; Greiner, A.; Agarwal, S. Sustainable Block Copolymers of Poly(Limonene Carbonate). *Polymer Chemistry* **2021**, *12* (6), 903–910. <https://doi.org/10.1039/d0py01685c>.
- (79) Wu, G. P.; Darensbourg, D. J.; Lu, X. B. Tandem Metal-Coordination Copolymerization and Organocatalytic Ring-Opening Polymerization via Water to Synthesize Diblock Copolymers of Styrene Oxide/CO₂ and Lactide. *Journal of the American Chemical Society* **2012**, *134* (42), 17739–17745. <https://doi.org/10.1021/ja307976c>.
- (80) Darensbourg, D. J.; Wu, G. P. A One-Pot Synthesis of a Triblock Copolymer from Propylene Oxide/Carbon Dioxide and Lactide: Intermediacy of Polyol Initiators. *Angewandte Chemie - International Edition* **2013**, *52* (40), 10602–10606. <https://doi.org/10.1002/anie.201304778>.
- (81) Coulembier, O.; Moins, S.; Todd, R.; Dubois, P. External and Reversible CO₂ Regulation of Ring-Opening Polymerizations Based on a Primary Alcohol Propagating Species. *Macromolecules* **2014**, *47* (2), 486–491. <https://doi.org/10.1021/ma4024944>.

- (82) Li, M.; Zhang, P.; Chen, C. Light-Controlled Switchable Ring Opening Polymerization. *Macromolecules* **2019**, *52* (15), 5646–5651. <https://doi.org/10.1021/acs.macromol.9b00984>.
- (83) Eivgi, O.; Phatake, R. S.; Nechmad, N. B.; Lemcoff, N. G. Light-Activated Olefin Metathesis: Catalyst Development, Synthesis, and Applications. *Accounts of Chemical Research* **2020**, *53* (10), 2456–2471. <https://doi.org/10.1021/acs.accounts.0c00495>.
- (84) Osaki, M.; Takashima, Y.; Yamaguchi, H.; Harada, A. Switching of Polymerization Activity of Cinnamoyl- α -Cyclodextrin. *Organic and Biomolecular Chemistry* **2009**, *7* (8), 1646–1651. <https://doi.org/10.1039/b818241h>.
- (85) Dai, Z.; Cui, Y.; Chen, C.; Wu, J. Photoswitchable Ring-Opening Polymerization of Lactide Catalyzed by Azobenzene-Based Thiourea. *Chemical Communications* **2016**, *52* (57), 8826–8829. <https://doi.org/10.1039/c6cc04090j>.
- (86) Riffel, M. N.; Hern, Z. C.; Diaconescu, P. L. A Photoswitchable Organocatalyst Controls Trimethylene Carbonate and δ -Valerolactone Copolymerization. *Science Bulletin* **2018**, *63* (22), 1460–1461. <https://doi.org/10.1016/j.scib.2018.11.001>.
- (87) Eisenreich, F.; Kathan, M.; Dallmann, A.; Ihrig, S. P.; Schwaar, T.; Schmidt, B. M.; Hecht, S. A Photoswitchable Catalyst System for Remote-Controlled (Co)Polymerization in Situ. *Nature Catalysis* **2018**, *1* (7), 516–522. <https://doi.org/10.1038/s41929-018-0091-8>.
- (88) Fu, C.; Xu, J.; Boyer, C. Photoacid-Mediated Ring Opening Polymerization Driven by Visible Light. *Chemical Communications* **2016**, *52* (44), 7126–7129. <https://doi.org/10.1039/c6cc03084j>.
- (89) Teator, A. J.; Shao, H.; Lu, G.; Liu, P.; Bielawski, C. W. A Photoswitchable Olefin Metathesis

- Catalyst. *Organometallics* **2017**, *36* (2), 490–497.
<https://doi.org/10.1021/acs.organomet.6b00913>.
- (90) Eivgi, O.; Vaisman, A.; Nechmad, N. B.; Baranov, M.; Lemcoff, N. G. Latent Ruthenium Benzylidene Phosphite Complexes for Visible-Light-Induced Olefin Metathesis. *ACS Catalysis* **2020**, *10* (3), 2033–2038. <https://doi.org/10.1021/acscatal.9b05079>.
- (91) Wang, X.; Thevenon, A.; Brosmer, J. L.; Yu, I.; Khan, S. I.; Mehrkhodavandi, P.; Diaconescu, P. L. Redox Control of Group 4 Metal Ring-Opening Polymerization Activity toward ϵ -Lactide and ϵ -Caprolactone. *Journal of the American Chemical Society* **2014**, *136* (32), 11264–11267. <https://doi.org/10.1021/ja505883u>.
- (92) Delle Chiaie, K. R.; Yablon, L. M.; Biernesser, A. B.; Michalowski, G. R.; Sudyn, A. W.; Byers, J. A. Redox-Triggered Crosslinking of a Degradable Polymer. *Polymer Chemistry* **2016**, *7* (28), 4675–4681. <https://doi.org/10.1039/c6py00975a>.
- (93) Broderick, E. M.; Guo, N.; Vogel, C. S.; Xu, C.; Sutter, J.; Miller, J. T.; Meyer, K.; Mehrkhodavandi, P.; Diaconescu, P. L. Redox Control of a Ring-Opening Polymerization Catalyst. *Journal of the American Chemical Society* **2011**, *133* (24), 9278–9281. <https://doi.org/10.1021/ja2036089>.
- (94) Broderick, E. M.; Guo, N.; Wu, T.; Vogel, C. S.; Xu, C.; Sutter, J.; Miller, J. T.; Meyer, K.; Cantat, T.; Diaconescu, P. L. Redox Control of a Polymerization Catalyst by Changing the Oxidation State of the Metal Center. *Chemical Communications* **2011**, *47* (35), 9897–9899. <https://doi.org/10.1039/c1cc13117f>.
- (95) Biernesser, A. B.; Li, B.; Byers, J. A. Redox-Controlled Polymerization of Lactide Catalyzed by Bis(Imino)Pyridine Iron Bis(Alkoxide) Complexes. *Journal of the American Chemical*

- Society* **2013**, *135* (44), 16553–16560. <https://doi.org/10.1021/ja407920d>.
- (96) Biernesser, A. B.; Delle Chiaie, K. R.; Curley, J. B.; Byers, J. A. Block Copolymerization of Lactide and an Epoxide Facilitated by a Redox Switchable Iron-Based Catalyst. *Angewandte Chemie* **2016**, *128* (17), 5337–5340. <https://doi.org/10.1002/ange.201511793>.
- (97) Quan, S. M.; Wang, X.; Zhang, R.; Diaconescu, P. L. Redox Switchable Copolymerization of Cyclic Esters and Epoxides by a Zirconium Complex. *Macromolecules* **2016**, *49* (18), 6768–6778. <https://doi.org/10.1021/acs.macromol.6b00997>.
- (98) Wei, J.; Riffel, M. N.; Diaconescu, P. L. Redox Control of Aluminum Ring-Opening Polymerization: A Combined Experimental and DFT Investigation. *Macromolecules* **2017**, *50* (5), 1847–1861. <https://doi.org/10.1021/acs.macromol.6b02402>.
- (99) Abubekеров, M.; Vlček, V.; Wei, J.; Miehlich, M. E.; Quan, S. M.; Meyer, K.; Neuhauser, D.; Diaconescu, P. L. Exploring Oxidation State-Dependent Selectivity in Polymerization of Cyclic Esters and Carbonates with Zinc(II)Complexes. *iScience* **2018**, *7* (ii), 120–131. <https://doi.org/10.1016/j.isci.2018.08.020>.
- (100) Dai, R.; Lai, A.; Alexandrova, A. N.; Diaconescu, P. L. Geometry Change in a Series of Zirconium Compounds during Lactide Ring-Opening Polymerization. *Organometallics* **2018**, *37* (21), 4040–4047. <https://doi.org/10.1021/acs.organomet.8b00620>.
- (101) Wei, J.; Diaconescu, P. L. Redox-Switchable Ring-Opening Polymerization with Ferrocene Derivatives. *Accounts of Chemical Research* **2019**, *52* (2), 415–424. <https://doi.org/10.1021/acs.accounts.8b00523>.
- (102) Dai, R.; Diaconescu, P. L. Investigation of a Zirconium Compound for Redox Switchable Ring Opening Polymerization. *Dalton Transactions* **2019**, *48* (9), 2996–3002.

<https://doi.org/10.1039/c9dt00212j>.

- (103) Lai, A.; Hern, Z. C.; Diaconescu, P. L. Switchable Ring-Opening Polymerization by a Ferrocene Supported Aluminum Complex. *ChemCatChem* **2019**, *11* (16), 4210–4218. <https://doi.org/10.1002/cctc.201900747>.
- (104) Lai, A.; Clifton, J.; Diaconescu, P. L.; Fey, N. Computational Mapping of Redox-Switchable Metal Complexes Based on Ferrocene Derivatives. *Chemical Communications* **2019**, *55* (49), 7021–7024. <https://doi.org/10.1039/c9cc01977d>.
- (105) Deng, S.; Diaconescu, P. L. A Switchable Dimeric Yttrium Complex and Its Three Catalytic States in Ring Opening Polymerization. *Inorganic Chemistry Frontiers* **2021**, *8* (8), 2088–2096. <https://doi.org/10.1039/d0qi01479f>.
- (106) Savka, R.; Foro, S.; Gallei, M.; Rehahn, M.; Plenio, H. Oxidation-Triggered Ring-Opening Metathesis Polymerization. *Chemistry - A European Journal* **2013**, *19* (32), 10655–10662. <https://doi.org/10.1002/chem.201300868>.
- (107) Rosen, E. L.; Varnado, C. D.; Arumugam, K.; Bielawski, C. W. Metal-Centered Oxidations Facilitate the Removal of Ruthenium-Based Olefin Metathesis Catalysts. *Journal of Organometallic Chemistry* **2013**, *745–746*, 201–205. <https://doi.org/10.1016/j.jorganchem.2013.07.063>.
- (108) Varnado, C. D.; Rosen, E. L.; Collins, M. S.; Lynch, V. M.; Bielawski, C. W. Synthesis and Study of Olefin Metathesis Catalysts Supported by Redox-Switchable Diaminocarbene[3]Ferrocenophanes. *Dalton Transactions* **2013**, *42* (36), 13251–13264. <https://doi.org/10.1039/c3dt51278a>.
- (109) Abubekerov, M.; Shepard, S. M.; Diaconescu, P. L. Switchable Polymerization of

Norbornene Derivatives by a Ferrocene-Palladium(II) Heteroscorpionate Complex.
European Journal of Inorganic Chemistry **2016**, 2016 (15–16), 2634–2640.
<https://doi.org/10.1002/ejic.201501295>.

(110) Qi, M. Developing an Electrochemically Redox Switchable System for Polymer Synthesis,
2020.

(111) Chen, C. Redox-Controlled Polymerization and Copolymerization. *ACS Catalysis* **2018**, 8 (6),
5506–5514. <https://doi.org/10.1021/acscatal.8b01096>.

2.0 Chapter 2. Redox-switchable Polymerization by Chain-transfer (ReSPCT): A Versatile Method for the Copolymerization of Lactones, Epoxides and Carbon Dioxide

2.1 Introduction

Plastic waste is a growing problem as both production and consumption continue to grow exponentially.¹ A combination of strength, lightness and affordability have made plastics indispensable for modern society. While recycling is being pursued for single-use food and medical packaging, virgin polymer is still preferred due to polymer contamination leading to recycling¹ as well as hygienic and food safety issues.² Biodegradable plastics are a promising replacement for some of these single-use plastics.³⁻⁵ Common biodegradable polymers including poly(lactic acid), which occupies a large portion of the bioplastics production in global markets, including 18.7 % of the European bioplastic plastic market as of 2018.⁶ Poly(lactic acid) has achieved this market share due to the easily accessible monomer, lactide, which is in turn derived from starch and sugar sources including corn⁷ and sugar cane.⁷ Additionally, enantiopure poly(*L*-lactic acid) is a hard and strong plastic allowing it to be used for rigid packaging and disposable cutlery⁸. However, its low flexibility, brittleness and poor barrier properties make it undesirable for food packaging films.⁹ There are few examples for the direct modification of lactide^{10,11} and the synthesis of lactide derivatives generally relies on different feed stocks¹²⁻¹⁵ than sugar-derived lactic acid, changing the cost-benefits.

Poly(propylene carbonate), a biodegradable, aliphatic polycarbonate synthesized from propylene oxide and CO₂, possesses physical and mechanical properties that are

complementary to poly(*L*-lactic acid). It is an amorphous and flexible polymer with excellent barrier properties towards water and oxygen.^{16–18} Developments in epoxidation reactions have supported facile synthesis of epoxides from alkenes with a number of functional groups and with high enantioselectivity.^{19,20} The abundance of suitable natural and petrochemical olefin feedstocks²¹ simplifies further fine-tuning the thermal and mechanical properties of epoxide-derived polycarbonates through copolymerization^{22,23} while also offering opportunities to introduce reactive functional groups.²⁴

Although blends of the poly(propylene carbonate) and poly(lactic acid) have been produced, only partial compatibility^{25–27} was observed between the two polymers which can be enhanced with additives.^{28,29} Copolymers of poly(propylene carbonate) and poly(*L*-lactic acid) can be synthesized *in-situ* through the addition of anhydrides,^{30,31} epoxyacrylates²⁶ and peroxides³² or through transesterification of the two polymers.³³ Copolymers made *in-situ* have demonstrated benefits in both improving the toughness³³ and barrier properties²⁶ of poly(*L*-lactic acid), but lack well-defined structures. The mechanical properties of well-defined block copolymers of poly(*L*-lactic acid) and poly(propylene carbonate) are underexplored in comparison. The development of new strategies to produce well-defined copolymers of poly(propylene carbonate) and poly(*L*-lactic acid) could find uses as biodegradable elastomers, films or as compatibilizers for blending the homopolymers. Methods used for the copolymerization of lactide, CO₂ and propylene oxide could be applied to other lactones and epoxides as poly(*L*-lactic acid)'s crystallinity generally leads to poor blend compatibility, but copolymers are well known for their use as compatibilizers.³⁰

In the previous chapter, we mentioned various chemically-switchable or pressure-switchable methods for making copolymers of *L*-lactide, propylene oxide and CO₂. Darensbourg and coworkers used a bifunctional cobalt-salen complex **2.1** bearing a pendant ammonium group in conjunction with a bis(triphenylphosphine)iminium 2,4-di(nitro)phenolate (PPNDNP) cocatalyst (Scheme 2.1A).³⁴ First, propylene oxide-CO₂ ring-opening copolymerization (ROCOP) was used to form polycarbonate polyols. Then, when the CO₂ pressure was released, lactide, 1,8-diazabicyclo[5.4.0]undec-7-ene (DBU) and additional solvent were added to the solution. The polycarbonate polyols from the first step act as initiators for lactide polymerization. This method produced polymers with narrow dispersities ($M_w/M_n < 1.1$), but only α - ω -hydroxy-telechelic triblock copolymers with a BAB structure could be produced this way.

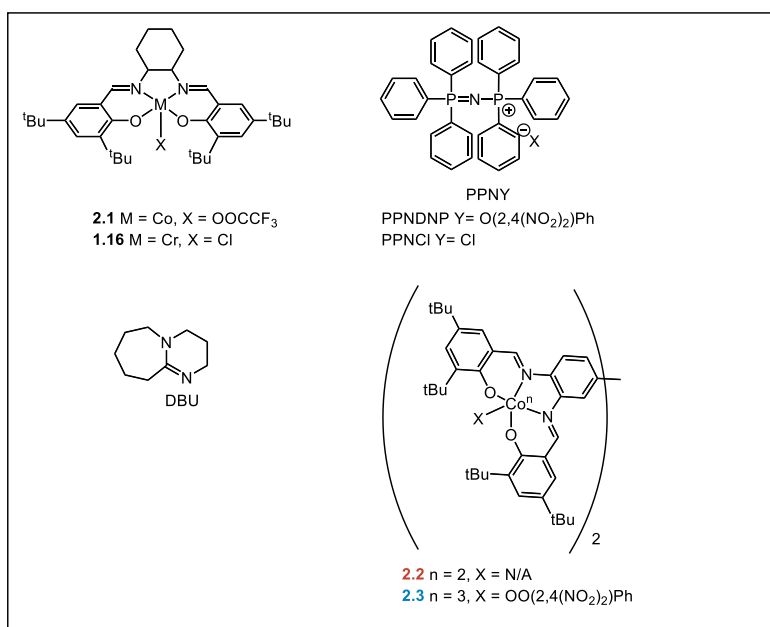
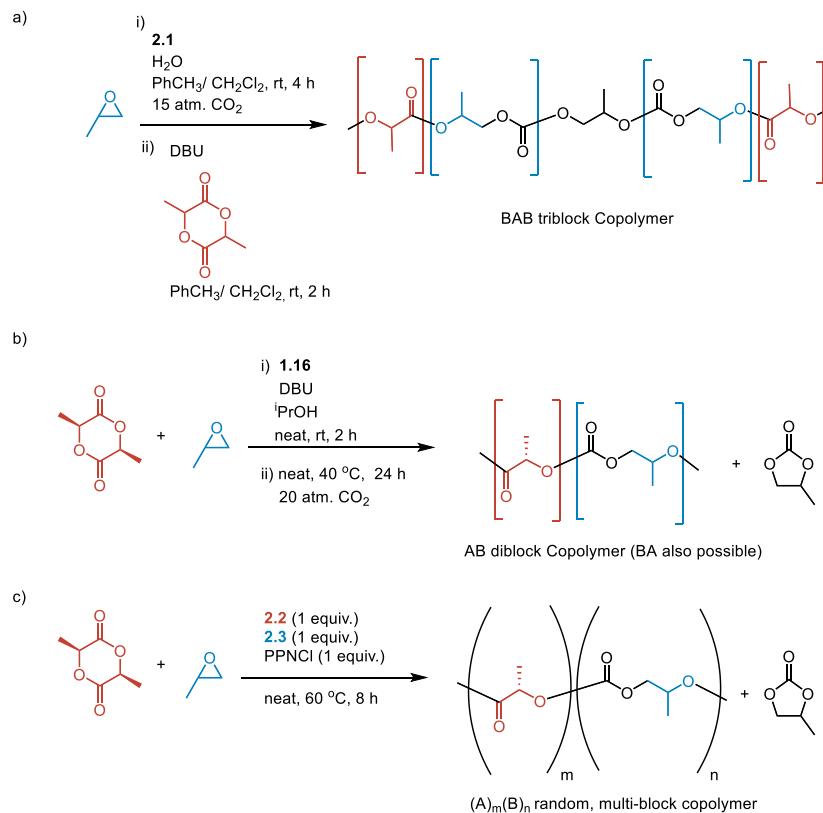
Chen and coworkers developed a pressure-switchable terpolymerization of *L*-lactide, propylene oxide and CO₂ through a chromium salen catalyst **1.16** and DBU cocatalyst (Scheme 2.1b).³⁵ Under high CO₂ pressure the catalysts were active for propylene oxide-CO₂ ROCOP while *L*-lactide ring-opening polymerization (ROP) was activated after CO₂ was removed. Under these conditions, diblock copolymers could be synthesized starting from either monomer. A drawback to this CO₂-controlled switching is that extensive purging with argon is needed to remove residual CO₂ in order to reactivate the catalyst for lactide ROP. Significant production of unwanted cyclic carbonate (35 % selectivity for propylene oxide) was also observed during epoxide-CO₂ copolymerization.

The Chen group were also able to demonstrate the simultaneous copolymerization of *L*-lactide, propylene oxide and CO₂ through a three component catalytic system consisting of a cobalt(II)-based dimer **2.2**, a cobalt(III)-based dimer **2.3** and PPNCI (Scheme 2.1c). The role of

each catalyst was systematically determined. **2.2** in conjunction with PPNCI was active, but slow for L-lactide ROP. **2.2** and PPNCI were unselective for polycarbonate formation during propylene oxide-CO₂ ROCOP. producing primarily cyclic carbonate. **2.3** in conjunction with PPNCI was active for *L*-lactide ROP and selective for polycarbonate production during propylene oxide-CO₂ ROCOP. Surprisingly, when **2.2**, **2.3** and PPNCI were all combined propylene oxide-CO₂ ROCOP proceeds significantly faster. Additionally, **2.3** and PPNCI were inactive for *L*-lactide ROP in the presence of CO₂, but upon the addition of **2.2** *L*-lactide ROP proceeded. When all three catalysts are together, both propylene oxide-CO₂ ROCOP and *L*-lactide ROP occur simultaneously producing random, multi-block copolymers of poly(lactic acid) and poly(propylene carbonate) of modest molecular weights (M_n= 3.8- 13.6 kDa) and narrow to broadened dispersities (M_w/M_n= 1.19- 1.47). Poly(lactic acid) rich copolymers possessed broader dispersities suggest lactide ROP was not as well controlled. Cyclic carbonate byproducts were also observed with 6-14 % selectivity.

Heterogeneous catalyst systems³⁶⁻³⁹ have been utilized for the simultaneous polymerization of lactide, propylene oxide and CO₂ to produce statistical and gradient

Scheme 2.1. Previous methods for the copolymerization of lactide, propylene oxide and CO₂ in one-pot. a) CO₂-switchable copolymerization of propylene oxide and CO₂ and then lactide by sequential addition of monomers. b) CO₂-switchable copolymerization of lactide then propylene oxide and CO₂. c) Statistical copolymerization of propylene oxide, CO₂ and lactide by a three component catalyst system.

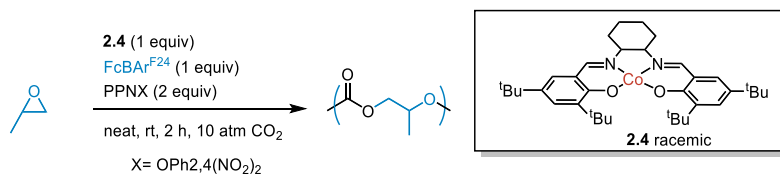


copolymers with high degrees of tunability in lactide incorporation in exchange for broad dispersities^{36,39} and/or unwanted polyether production.^{37,39} For other lactone and epoxide combinations, Williams^{40–43} and Rieger^{44,45} independently used single catalyst systems to synthesize various multi-block copolymers and even statistical copolymers at low CO₂ pressures with β -butyrolactone. However, reactions involving single catalysts are limited in monomer scope because that one catalyst has to be efficient for both ROP and ROCOP.

Our group has developed redox-switchable polymerization and copolymerizations of lactide and cyclohexene oxide,^{46–50} but the redox-switchable ROCOP of epoxides and CO₂ have not yet been reported in the literature. Typical methods for controlling ring-opening polymerizations with redox chemistry have primarily relied on the oxidation and reduction of iron with few exceptions.⁵¹ Cobalt salen catalysts have not been utilized for redox-switchable ring-opening polymerization despite the fact that cobalt(II) salen complexes **2.1** were shown to be easily oxidized by ferrocenium salts into cobalt(III) salen that are active for propylene oxide-CO₂ copolymerization in the presence of nucleophilic PPNX salts (Scheme 2.2).⁵²

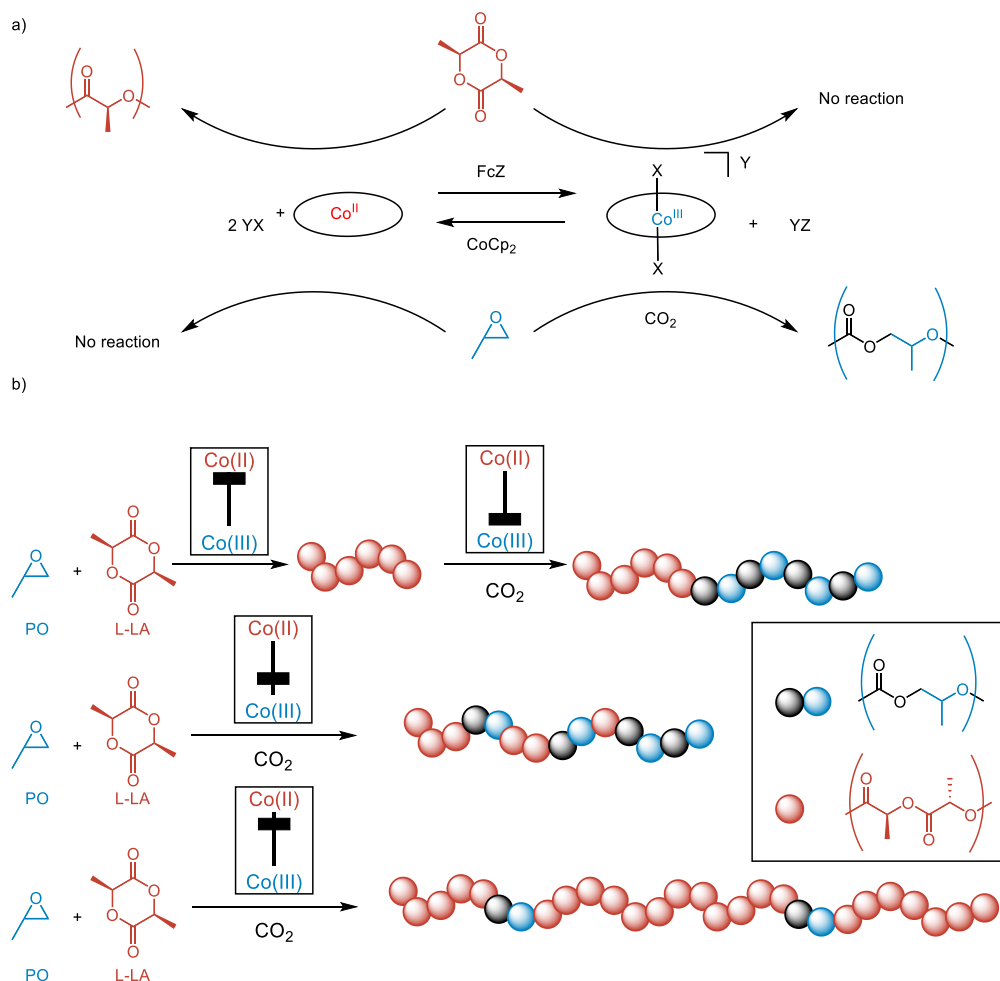
Cobalt(II) salen complexes lack nucleophilic ligands and are too electron rich for electrophilic monomer activation. We recognize the opportunity to pair a nucleophilic cocatalyst active for lactide ROP with cobalt(II) salen complexes to form a redox-switchable copolymerization catalyst (Scheme 2.3a). In this work, a cobalt(II) salen catalyst in conjunction

Scheme 2.2. Formation of active catalyst for propylene oxide-CO₂ ROCOP through *in-situ* oxidation of cobalt(II) catalyst **2.4** in the presence of a nucleophilic cocatalyst.



with a nucleophilic 2.2.2-cryptand-potassium alkoxide demonstrates the Redox-Switchable Polymerization by Chain Transfer (ReSPCT) of lactide, propylene oxide and CO₂ to synthesize blocky or statistical copolymers depending on the ratio of cobalt(II) to cobalt(III) (Scheme 2.3b). Oxidation and reduction of the cobalt-based catalyst drives chain transfer between the active catalysts for L-lactide ROP and propylene oxide-CO₂ ROCOP. Unlike previous systems developed for the synthesis of copoly(ester-carbonates) This system was highly tunable and presents a

Scheme 2.3. Accessing blocky and statistical copolymers of L-lactide, propylene oxide and CO₂ through redox-switchable polymerization by chain transfer (ReSPCT). A) Selectivity of catalysts for lactide ROP or propylene oxide-CO₂ ROCOP depending on oxidation state of the cobalt salen catalyst. b) Demonstration of how ReSPCT can be utilized to synthesize blocky and statistical copolymers of lactide, propylene oxide and CO₂. Sliders represent the relative ratio of cobalt(II)-based to cobalt(III)-based catalyst in the reaction mixture at any given point in the reaction with the top position being 100% cobalt (II) and the bottom representing 100% cobalt(III).



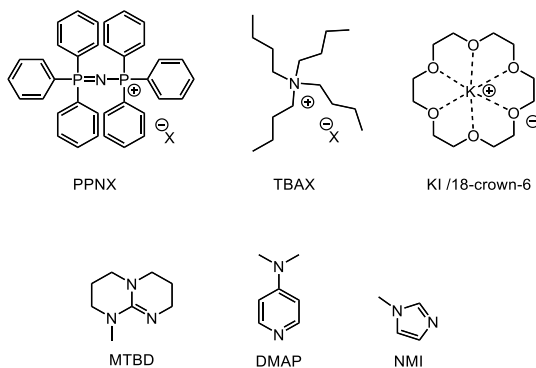
unique method for controlling reactions that could find uses outside of polymerization chemistry with other multi-catalyst reactions.

2.2 Initial Screening of Catalysts for *L*-lactide ROP

Cobalt-salen catalysts in tandem with a number of anionic salts and organobases have been efficient catalysts for the ROCOP of epoxides and CO₂, but not for *L*-lactide ROP (Scheme 2.4).^{53,54} However some of the cocatalysts had previously demonstrated living *L*-lactide ROP in the absence of cobalt(III) based catalysts.^{55–58} 18-crown-6 with potassium salts were particularly interesting to us because discrete potassium alkoxides had previously been combined with the 18-crown-6 for *L*-lactide ROP.⁵⁵ Metal alkoxides are common intermediates for both epoxide-CO₂ ROCOP and *L*-lactide ROP and thus provide an area where the two catalytic cycles could be bridged.

We hypothesized that redox-switchable polymerization would be possible for *L*-lactide, propylene oxide and CO₂ with a combination of 18-crown-6 potassium alkoxides and cobalt(II)

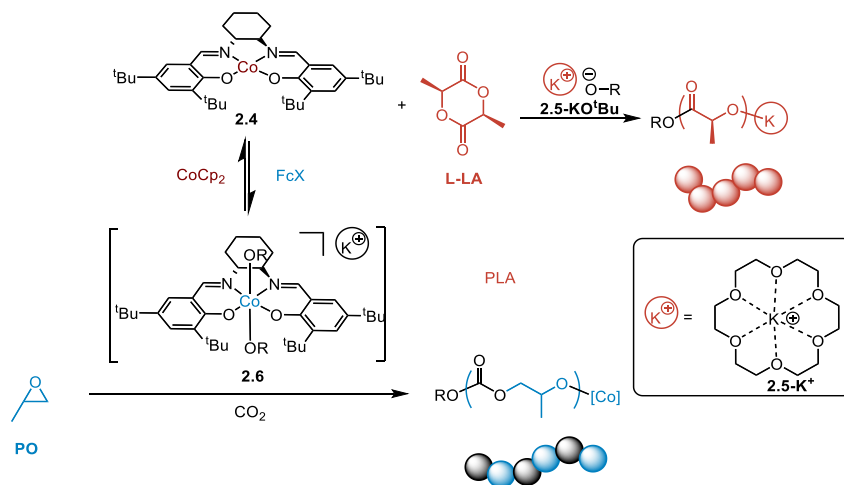
Scheme 2.4. Representative cocatalysts used for epoxide-CO₂ ROCOP with cobalt salen complexes.



salen complex **2.4** (Scheme 2.5). Under this design 18-crown-6 potassium tert-butoxide **2.5-KO^tBu** would carry out *L*-lactide ROP with electron-rich **2.4** acting as a spectator. **2.4** could be then be oxidized in the presence of **2.5-KO^tBu** to form an electron-deficient cobalt(III) salen cation that could bind up to two alkoxide anions to form **2.6**. 6-coordinate cobalt(III) alkoxides are believed to be the active species for epoxide-CO₂ ROCOP^{59,60} so we believed **2.6** would be active for propylene oxide-CO₂ ROCOP.

An advantage of this system in comparison to previous CO₂-switchable copolymerizations^{35,61} was that switching would be rapid, as has been observed with other redox-switchable copolymerizations,^{48,62-64} and unlike pressure-switchable systems which require rigorous degassing.^{35,40,43} Another potential benefit of redox-switchable copolymerizations was that non-stoichiometric additions of the redox reagents would lead to a mixed population of **2.4**, **2.5-KO^tBu** and **2.6** all being in solution which may allow for statistical copolymerization of the three monomers through chain-transfer amongst the active species.

Scheme 2.5. Original design for redox-switchable polymerization by chain-transfer (ReSPCT) for the copolymerization of *L*-lactide, propylene oxide and CO₂.



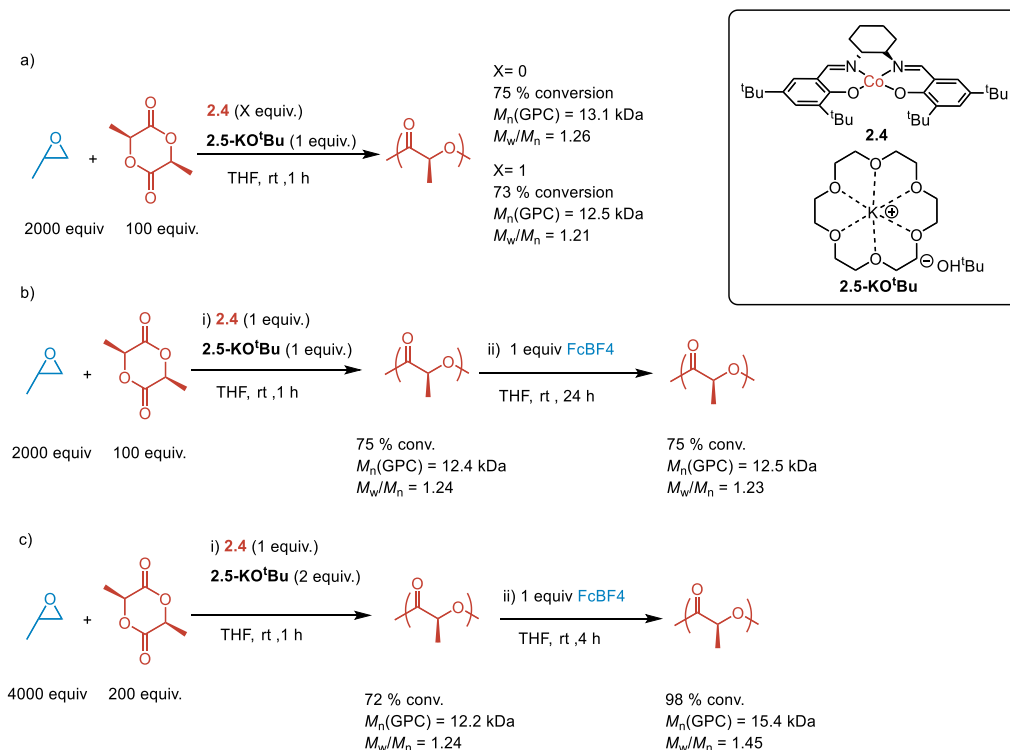
To test our catalyst design, we first examined if *L*-lactide ROP by $2.5\text{-KO}^t\text{Bu}$ would proceed cleanly in propylene oxide. The reaction reached 75 % conversion in 1 h with no formation of undesired polyether. We then wanted to know if the addition of **2.4** had any effect on *L*-lactide ROP (Scheme 2.6a). The presence of the cobalt(II) complex had no noticeable effect on lactide ROP. Next, we attempted the *in-situ* oxidation of **2.4** to form a cobalt (III) salen alkoxide complex, which we expected would be inactive for *L*-lactide ROP (Scheme 2.6b). Upon the addition of ferrocenium tetrafluoroborate (FcBF_4), the polymerization of *L*-lactide was halted and the solution went from red to brown. Over 4 hours the color reverted to red, which suggested the complex was decomposing to **2.4**, but further *L*-LA polymerization did not occur. Even 24 h after the addition of the oxidant, the polymer molecular weight and dispersity of the poly(lactic acid) did not change .

To form the desired cobalt(III) bis(alkoxide) complex **2.6**, a 2:1 ratio of $2.5\text{-KO}^t\text{Bu}$ to **2.4** would be needed as cobalt(III) salen complexes with only one nucleophile per metal center are known for requiring very high pressures of CO₂ (>50 atm) for propylene oxide-CO₂ ROCOP,^{53,65}

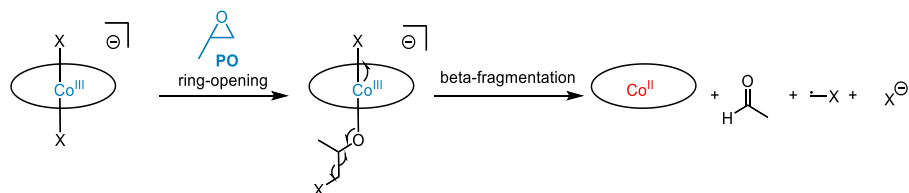
while cobalt(III) salen complexes with 2 or more nucleophiles per metal center are active at much lower pressures of CO₂ (5-20 atm).^{53,66} When we attempted the *in-situ* oxidation of **2.4** with 2 equivalents of **2.5-KO^tBu** the solution went from red to brown momentarily before reverting to red in seconds, which suggested the cobalt(III) complex was being reduced to **2.4**. *L*-lactide ROP continued and the dispersity of the poly(lactic acid) increased from $M_n/M_w = 1.24$ to $M_n/M_w = 1.45$, which suggested at least some alkoxides were remaining active while others were deactivated (Scheme 2.6c).

The spontaneous deactivation of cobalt alkoxides was not unprecedented in the literature as Rieger and coworkers the deactivation cobalt(III) porphyrin and salen catalysts to cobalt(II) complexes during propylene oxide-CO₂ ROCOP.⁶⁷ During the copolymerization, Rieger's team observed the production of acetaldehyde as well as the TOF decreasing as the

Scheme 2.6. a) Polymerization of *L*-lactide by 18-crown-6 potassium tert-butoxide with and without **2.4**. b) *In-situ* oxidation of **2.4** during *L*-lactide ROP. c) *In-situ* oxidation of **2.4** during *L*-lactide ROP.



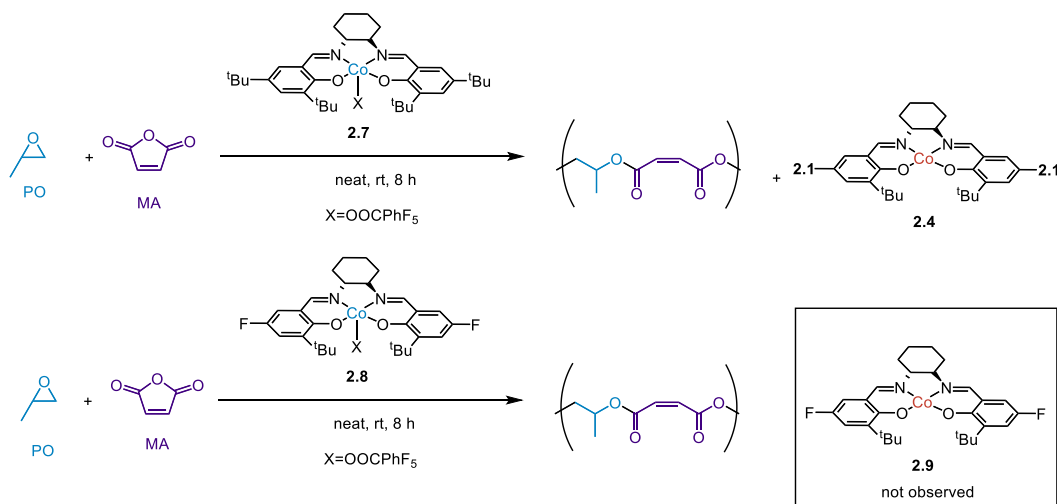
Scheme 2.7. Proposed mechanism for the deactivation of cobalt(III) catalysts during the ring-opening copolymerization of epoxides and carbon dioxide consistent with the detection of acetaldehyde.



reaction proceeded. An explanation consistent with these results is the beta fragmentation of cobalt alkoxides intermediates to cobalt(II) species, which is inactive for the copolymerization, acetaldehyde and carbon-centered radical (Scheme 2.8).

Coates and coworkers had also noted that during the cobalt(III) salen **2.7** catalyzed ROCOP of propylene oxide and maleic anhydride, the complex would decompose to the paramagnetic cobalt(II) complex **2.4**. This copolymerization also involves cobalt(III) alkoxide intermediates that could decompose to cobalt(II) species. The Coates groups tested a variety of ligand variants for ROCOP and only the substituting of a fluorine for the tert-butyl group at the 3 position lead to a long-lived complex. Cobalt(III) salen catalyst, **2.8**, did not produce any paramagnetic cobalt(II) species, **2.9**, during ROCOP (Scheme 2.8).⁶⁸ Lu and coworkers later also

Scheme 2.8. Cobalt(III) salen complex for epoxide-anhydride ROCOP. Fluorine-containing cobalt(III) salen complex **2.8** is resistant to autoreduction to inactive cobalt(II) species **2.9**.



demonstrated that **2.8** was competent for propylene oxide-CO₂ copolymerization in conjunction with PPNX salt cocatalysts.⁶⁹

We decided replace **2.4** with a complex based on **2.9** to improve catalyst stability during redox-switchable polymerizations. Cobalt(II) salen **2.9** was synthesized from the addition cobalt acetate and fluorinated salen ligand **2.10** under a nitrogen atmosphere and the compound was isolated as a dark red powder (Scheme 2.9). Both ¹H and ¹⁹F NMR spectra exhibited significant paramagnetic broadening which would be expected from a d⁷ cobalt(II) compound. An interesting feature of this complex's mass spectra in air was the formation of a stable dioxygen

Scheme 2.9. Synthesis of cobalt(II) salen-F complex **2.9**.

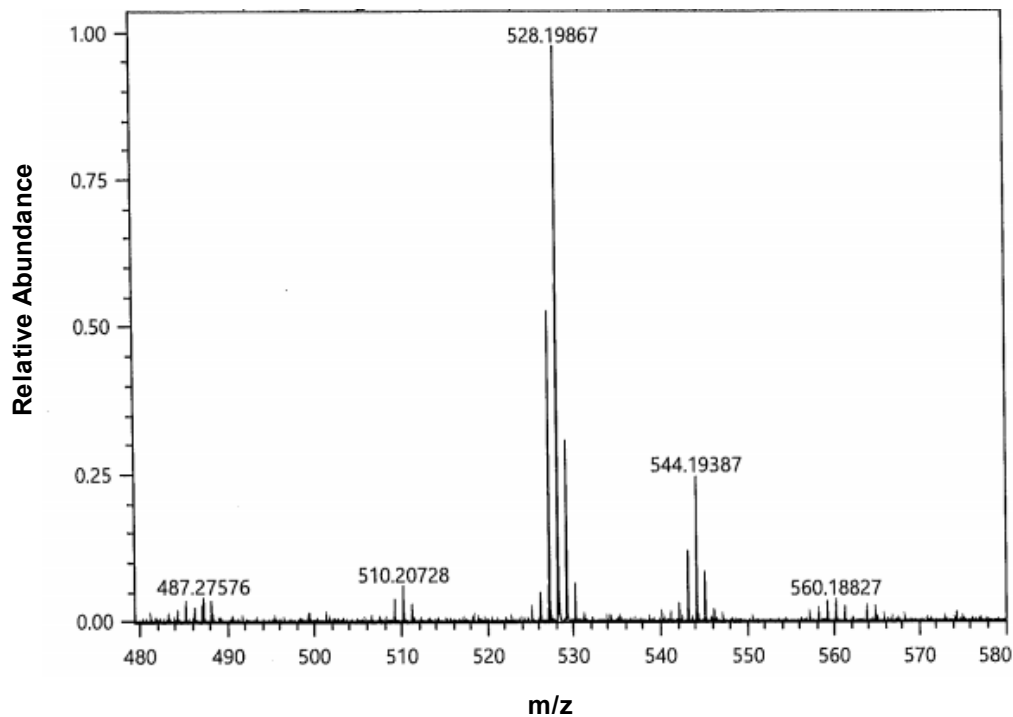
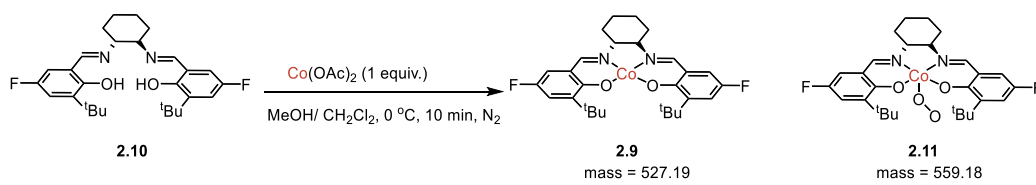
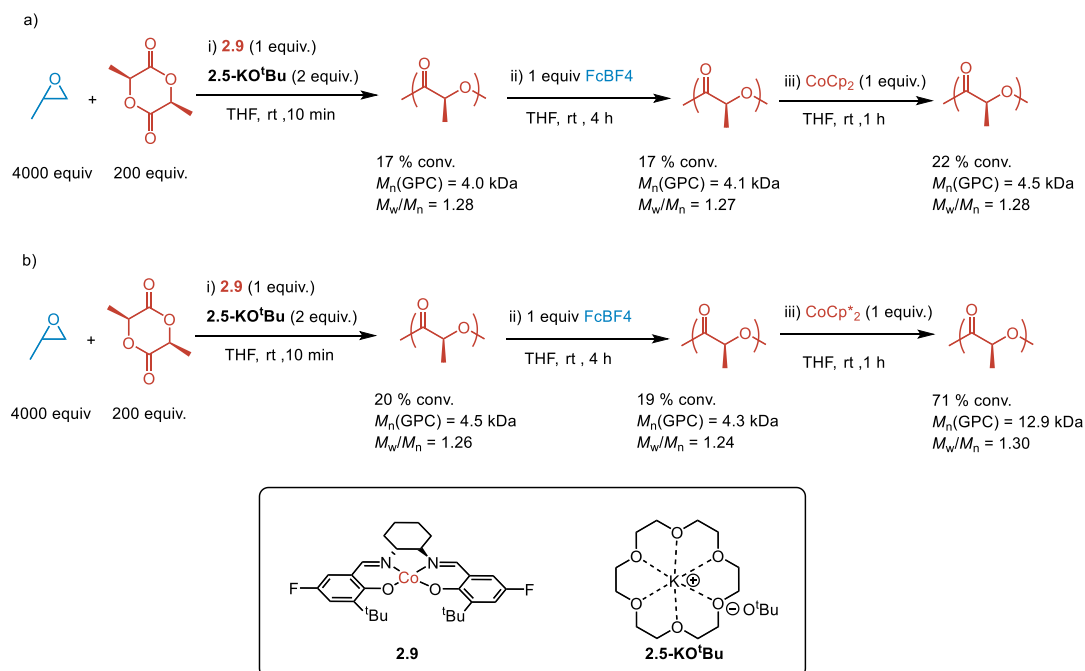


Figure 2.1. Mass spectra of cobalt(II) complex **2.9** and dioxygen adduct **2.11**.

adduct with a m/z of 560.19 (observed mass (560.19) = mass of cobalt(II)-based complex (527.19) + mass of O_2 (31.99) + mass of proton (1.01)) (Figure 2.1). This suggests the cobalt(II) complex was formed since it would have an unpaired electron in a d_{z^2} orbital that can form an adduct with dioxygen **2.11**. These oxygen adducts had been observed with similar cobalt(II) complexes.^{70,71} The solid was stable in air for months, but in organic solvents the compound will slowly oxidize to a brown, diamagnetic species that presumably was a cobalt(III) hydroxide.

Now with a new cobalt(II) complex **2.9**, we again attempted the *in-situ* redox-switching of *L*-lactide ROP. A mixture of **2.9** and **2.5-KO^tBu** was added to a solution of *L*-lactide and propylene oxide and allowed to stir at room temperature for ten minutes (Scheme 2.10a). $FcBF_4$ was added to the solution to oxidize the catalyst and after 4 h no additional lactide had polymerized suggesting a stable cobalt(III) complex had formed. We then added cobaltocene ($CoCp_2$) to reduce the cobalt(III) complex back to **2.9** and reactivate *L*-lactide ROP. The polymerization was active, but it was now much slower only reaching 22 % conversion an hour after the reduction step. We independently tested *L*-lactide polymerization in the presence of **2.9**, **2.5-KO^tBu** and $[CoCp_2][BF_4]$, the byproduct of catalyst reduction, and we observed a notable decrease in polymerization rate (45 % conversion in 24 h vs. 96 % conversion in 3 h). This slower polymerization rate was thought to be due to the cobaltocenium acting as a weak Lewis acid binding to the alkoxide. To test this hypothesis *L*-lactide polymerization was performed in the presence of decamethylcobaltocenium tetrafluoroborate ($[CoCp^*_2][BF_4]$), **2.9**

Scheme 2.10. Redox-switchable polymerization of *L*-lactide using FcBF_4 and a) cobaltocene (CoCp_2) or b) decamethylcobaltocene (CoCp^*_2).



and **2.5-KO^tBu** and the polymerization rate was only slightly slower than the reaction without an additive. (83 % conversion in 3 h). It is possible that factors besides Lewis acidity were affecting lactide polymerization including electrostatic interactions between the alkoxide and the cationic cobalt species. Regardless, we then demonstrated *L*-lactide ROP could proceed for 10 min to 20 % conversion, be deactivated upon the addition of FcBF_4 and reactivated 4 hours later after the addition of CoCp^*_2 (Scheme 2.10b). The polymerization then reached 71 % conversion in 1 hour while maintaining molecular weight control ($M_n = 12.9 \text{ kDa}$, $M_w/M_n = 1.30$).

2.3 Optimizing Homopolymerization Conditions

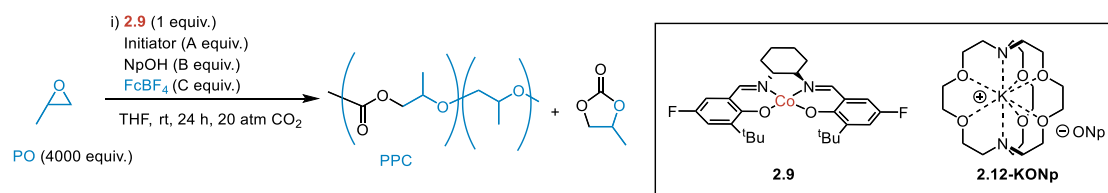
After finding a suitable catalyst system for redox-switchable *L*-lactide ROP, it was important to determine if the catalysts were compatible for propylene oxide-CO₂ ROCOP. **2.5-KO^tBu, 2.9** and FcBF₄ were pre-mixed in THF/propylene oxide and then loaded into a steel pressure bomb where it was exposed to 20 atm of CO₂. No polymer or cyclic carbonate was observed after 24 h (entry 1, Table 2.1). We decided to exchange tert-butoxide for a less, bulky initiator and attempted the copolymerization again with 18-crown-6/potassium neopentoxide **2.5-KONP**, and this time polymer was observed (entry 2, Table 2.2) along with 3.8 % consumption of propylene oxide. The reaction was selective for poly(propylene carbonate) (87 %) with only a small amount of cyclic propylene carbonate forming (3 %) and the remainder consisting of poly(propylene oxide). The observed molecular weight ($M_n = 17.4$ kDa) was more than double the theoretical molecular weight ($M_n = 7.8$ kDa) which indicates that not all of the initiator was active polymerization.

For further improvements in both reactivity and selectivity we looked into the history of cocatalyst development for epoxide-CO₂ ROCOP and noted the inverse relationship between how coordinating a cation was and the rate and selectivity of copolymerization.^{66,72} We wanted to maintain a similar structure as a 18-crown-6 for controlled lactide ROP, but also use a less coordinating cation, so 2.2.2 cryptand (**2.12**) was chosen. Cryptand salts had not previously been used for epoxide-CO₂ ROCOP, but there was precedent for 2.2.2-cryptand potassium salts in lactone ROP, which would be important for future compatibility experiments.⁷³ By combining **2.9, 2.12-KONp** and FcBF₄, a highly reactive complex for propylene oxide-CO₂ ROCOP was

formed (entry 3, Table 2.1). The reaction mixture became very viscous as 47.9 % of all the propylene oxide was consumed. The selectivity of the catalyst was improved with only 1 % propylene carbonate being formed and no polyether was detected. The molecular weight of the polymer ($M_n(\text{GPC}) = 722.9 \text{ kDa}$) was much larger than the theoretical molecular weight ($M_n(\text{theo}) = 195.3 \text{ kDa}$) which, again, suggested that not all of the initiators were active.

To improve initiation efficiency, we added exogenous neopentyl alcohol to the reaction to act as a chain transfer agent (entry 4, Table 2.1). This time the copolymerization reached high conversions (46.5 %) and the molecular weight was much closer to the theoretical molecular

Table 2.1. Copolymerization of propylene oxide and CO₂ by cobalt salen, **2.9**, with 2.2.2-cryptand potassium alkoxide cocatalysts, **2.12-KONp**.



Entry ^a	Init.	Equiv. Init.	Equiv. NpOH	Equiv. FcBF ₄	Conv. ^b (%)	Selectivity ^c PPC (%)	$M_n(\text{theo})$ ^d (kDa)	$M_n(\text{exp})$ ^e (kDa)	M_w/M_n ^e
1	2.5-KO ^t Bu	1.9	0	1	0	0	N/A	N/A	N/A
2	2.5-KONp	1.9	0	1	3.8	87	7.5	17.4	1.47
3	2.12-KONp	1.9	0	1	47.9	99	195.3	722.9	1.29
4	2.12-KONp	1.9	8	1	46.5	>99	19.2	18.3	1.07
5	2.12-KONp	1.9	8	0	3	0	N/A	N/A	N/A
6	2.12-KONp	0.95	8	1	0	N/A	N/A	N/A	N/A

^aReactions were set up by dissolving **2.9**, initiator, neopentanol, propylene oxide and the oxidant in 0.5 ml of THF at a [1]:[1.9]:[8]:[4000]:[1] ratio. Reactor was pressurized with 20 atm of CO₂ and allowed to stir at room temperature.

^bConversion was determined by the mass of the sample after solvent is removed/ mass of the polymer assuming 100 % conversion to polycarbonate or cyclic carbonate.

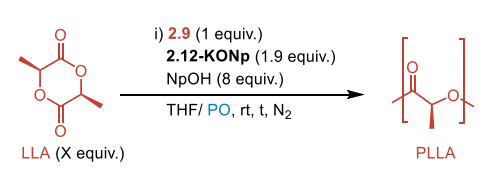
^cSelectivity for poly(propylene carbonate) vs. (cyclic carbonate) was determined by ¹H NMR by integrating the methine peak of poly(propylene carbonate) (5.01 ppm) vs. the methine peaks of the cyclic carbonate (4.86 ppm) and the methylene peaks of poly(propylene oxide) (3.54 ppm).

^dTheoretical molecular weight $M_n(\text{theo}) = (\text{conv.}_{\text{PPC}} * (\text{MW}_{\text{PO}} + \text{MW}_{\text{CO}_2}) * 4000 + \text{conv.}_{\text{PPO}} * (\text{MW}_{\text{PO}}) * 4000) / (\text{Initiator equiv.} + \text{NpOH equiv.})$.

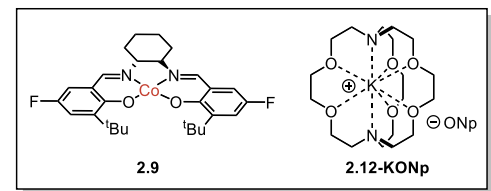
^eObtained from GPC (LS detector).

weight ($M_n(\text{GPC}) = 18.3 \text{ kDa}$, $M_n(\text{theo}) = 19.2 \text{ kDa}$). To determine if the corresponding cobalt(II) complex was active for propylene oxide- CO_2 ROCOP, the oxidant was omitted from the reaction (entry 5, Table 2.1). No poly(propylene carbonate) was observed and only a small amount of propylene carbonate was produced. When the initiator quantity was halved (entry 5, Table 2.1), there was no consumption of the propylene oxide, suggesting that the active species for catalysis was a cobalt(III) bis(alkoxide). Overall, 2.2.2-cryptand potassium alkoxides proved to

Table 2.2. Polymerization of *L*-lactide by 2.2.2 cryptand potassium neopentoxide **2.12-KONp** in the presence of cobalt(II) salen complex **2.9**.



LLA (X equiv.) $\xrightarrow[\text{THF/PO, rt, t, N}_2]{\text{i) 2.9 (1 equiv.)
2.12-KONp (1.9 equiv.)
NpOH (8 equiv.)}}$ PLLA



Entry ^a	LLA equiv	Time (h)	Conv. ^c (%)	$M_n(\text{theo})^d$ (kDa)	$M_n(\text{exp})^d$ (kDa)	M_w/M_n^d
1	200	0.5	64	1.9	2.0	1.09
2	400	3	94	5.5	7.7	1.17
3	1000	24	46	6.7	5.8	1.32
4 ^e	400	24	0	N/A	N/A	N/A

^aReactions were set up by dissolving **2.9**, initiator, neopentanol, and the oxidant in 0.5 ml of THF at a [1]:[1.9]:[8]:[4000]:[1] ratio. The catalyst solution is then added to *L*-Lactide in propylene oxide (1.0 ml). The mixture was allowed to stir at room temperature in a nitrogen-filled glovebox.

^bConversion was determined by ^1H NMR by comparing the lactide methine peak (5.0 ppm) to the methine peak of poly(lactic acid) (5.13 ppm).

^cTheoretical molecular weight $M_n(\text{theo}) = (\text{conv.} * \text{MW}_{\text{LLA}} * (\text{equiv. LLA})) / (\mathbf{2.12-KONp} \text{ equiv.} + \text{NpOH})$

^dObtained from GPC (RI detector).

^e1 equiv of FcBF_4 was added.

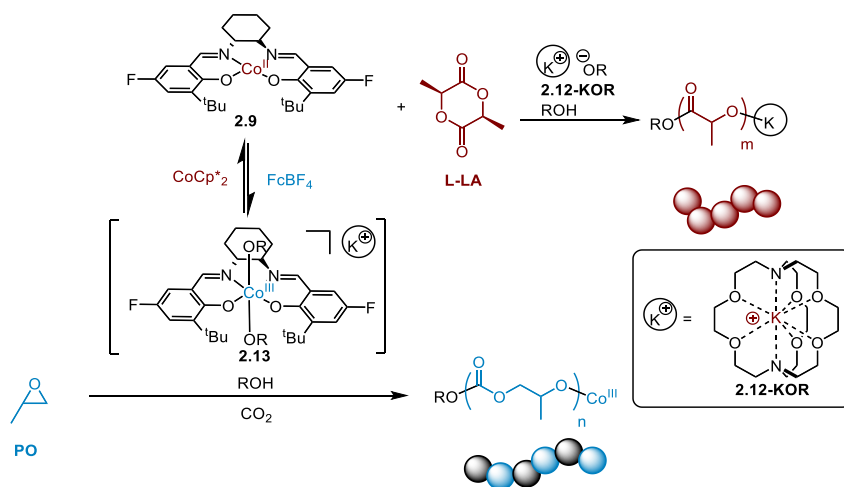
be suitable cocatalysts for propylene oxide-CO₂ ROCOP, so the remaining challenge would be to determine if this species was also proficient for redox-switchable *L*-lactide ROP.

The combination of **2.9**, **2.12-KONp** and neopentanol was active for *L*-lactide ROP reaching 64 % conversion in 0.5 h (entry 1, Table 2.2). The molecular weight of the resulting poly(*L*-lactic acid) matched the theoretical molecular weight ($M_n(\text{GPC}) = 2.0$ kDa, $M_n(\text{theo}) = 1.9$ kDa) and the dispersity was narrow ($M_w/M_n = 1.09$). When the *L*-lactide amount was increased to 400 equivalents the molecular weight still matched the theoretical molecular weight ($M_n(\text{GPC}) = 7.7$ kDa, $M_n(\text{theo}) = 5.5$ kDa). At 1000 equivalents of *L*-lactide the dispersity did begin to broaden ($M_w/M_n = 1.32$) which may be indicative of transesterification, but the molecular weight is still in line with the theoretical molecular weight ($M_n(\text{GPC}) = 5.8$ kDa, $M_n(\text{theo}) = 6.7$ kDa). To determine if the polymerization would still be redox-switchable we combined FcBF₄, **2.9**, **2.12-KONp** and neopentanol with *L*-lactide and after 24 h, no polymer was observed by ¹H NMR (entry 4, Table 2.2). From our experiments with *L*-lactide ROP we discovered that a combination of cobalt(II) salen complex **2.9** and **2.12-KONp** were suitable catalysts for the redox-switchable ROP of *L*-lactide.

2.4 Kinetics of *L*-lactide Ring-opening Polymerization and Propylene Oxide-CO₂ Ring-opening Copolymerization During Redox Switches

After optimizing the choice of catalysts and redox reagents, we were able to modify our design for ReSPCT copolymerization (Scheme 2.11). *L*-Lactide ROP by 2.2.2-cryptand potassium alkoxide **2.12-KOR** is active when cobalt catalyst **2.9** is in the cobalt(II) oxidation state. The addition of up to 1 equivalent of FcBF₄ induces cobalt oxidation leading to the cobalt(III) complex **2.13** which is the active species for propylene oxide-CO₂ ROCOP. The addition of 1 equivalent CoCp*₂ reduces the cobalt complex to **2.9** and liberates the alkoxide to bind to the potassium cryptand reforming **2.12-KOR**, the active species for *L*-lactide ROP. Non-stoichiometric additions of either the oxidant or reductant would lead to a mixed population of cobalt(II) and cobalt(III)-based species in solution.

Scheme 2.11. Modified design for redox-switchable polymerization by chain-transfer for the copolymerization of *L*-lactide, propylene oxide and CO₂.



We now wanted to investigate the kinetics for each polymerization before and after oxidation/reduction to determine if the respective polymerizations were redox-reversible. For the ROP of *L*-lactide, a mixture of **2.9**, **2.12-KONp** and neopentanol in THF was added to a solution of *L*-lactide, propylene oxide in a nitrogen-filled glovebox, and the reaction was sampled periodically over two hours (Figure 2.2). All samples were quenched with 4-nitrophenol to prevent further polymerization. The polymerization of *L*-lactide proceeded rapidly in the first 10 minutes while **2.9** was in the Co(II) oxidation state, but the addition of FcBF₄ immediately halted the polymerization and no further polymerization was observed for at least 1 h with little change in the molecular weight over this time (Figure 2.2.). *L*-lactide polymerization can be reactivated upon the addition of CoCp*₂. The molecular weight increases

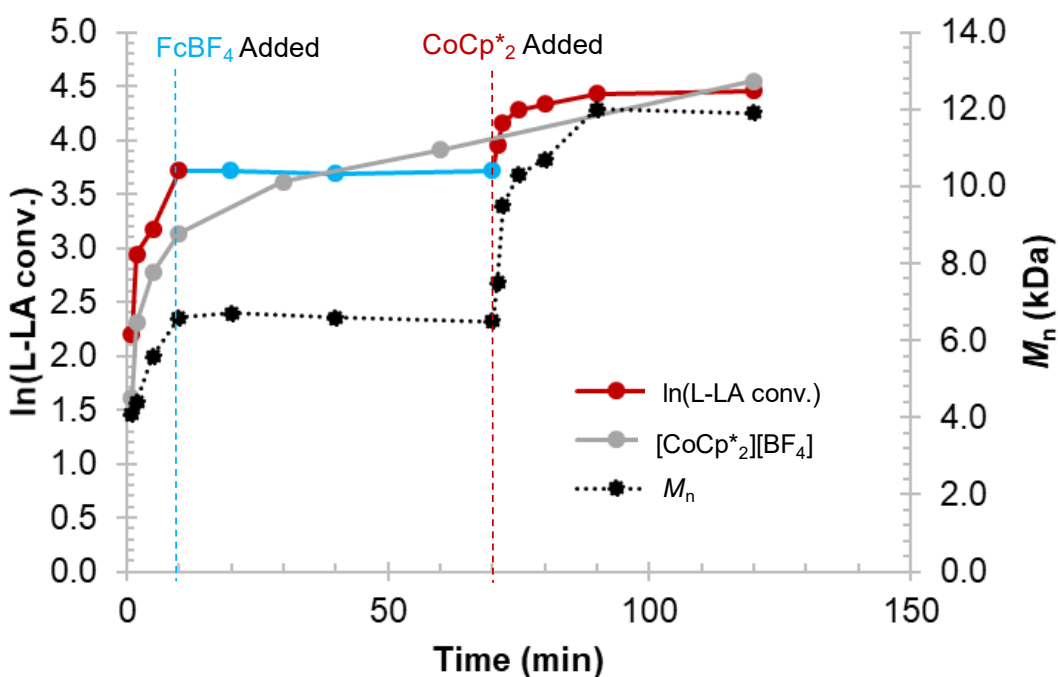


Figure 2.2. Redox-switchable polymerization of *L*-lactide by catalysts **2.9** and **2.12-KONp**. Red is the catalyst in the reduced cobalt(II) oxidation state while blue is in the oxidized cobalt(III) oxidation state. FcBF₄ is added at 10 min ($M_n(\text{GPC}) = 5.8$ kDa, $M_w/M_n = 1.20$), and CoCp*₂ at 70 min ($M_n(\text{GPC}) = 6.5$ kDa, $M_w/M_n = 1.24$). At the final time point ($M_n(\text{GPC}) = 11.9$ kDa, $M_w/M_n = 1.28$). A polymerization of *L*-lactide by **2.9** and **2.12-KONp** in the presence of 1 equivalent of [CoCp*₂][BF₄] without redox-switching was included for comparison.

only when the cobalt is reduced and the dispersity remains narrow throughout (1.1-1.3). We did note that the polymerization was faster upon the addition of the reductant which we attribute to evaporation of some of the propylene oxide cosolvent (boiling point = 34 °C) rather than any rate acceleration by the byproduct of catalyst reduction $[\text{CoCp}^*_2][\text{BF}_4]$. If solvent is evaporating during sampling of the reaction the catalyst concentration would increase as would the rate under non-zero order conditions. To test this hypothesis we performed a *L*-lactide ROP by **2.9** and **2.12-KONp** in the presence of $[\text{CoCp}^*_2][\text{BF}_4]$ (Figure 2.2). We observed slightly slower polymerization rates at earlier time points in agreement with previous experiments that had shown that $[\text{CoCp}^*_2][\text{BF}_4]$ slightly decreased overall lactide conversion in a given time period.

For propylene oxide- CO_2 ROCOP, a mixture of **2.9**, **2.12-KONp**, neopentanol and FcBF_4 in THF was added to propylene oxide in a steel pressure reactor at 20 atm CO_2 (Figure 2.3). The reaction was sampled periodically and each sample required the reactor to first be partially depressurized to a little over 1 atm CO_2 and then fully depressurized in the glovebox to avoid adding ambient water. Samples were taken while propylene oxide conversion was low, to keep the reaction from becoming viscous. Unlike lactide polymerization, the conversion of propylene oxide was linear while the cobalt is in the cobalt(III) oxidation state. This indicates the reaction is zero order in epoxide which is not uncommon for cobalt(III) salen catalyzed epoxide- CO_2 ROCOP.⁷⁴

Upon addition of CoCp^*_2 , no further propylene oxide conversion was observed. Curiously, almost all of the poly(propylene carbonate) was immediately converted to cyclic propylene carbonate. Under our proposed mechanism the reduction of the cobalt(III) catalyst

to a cobalt(II) complex would be accompanied by liberation of the alkoxides, which can then undergo the back-biting onto the polymer. Another explanation could be that the depressurization while the catalyst is in the cobalt(II) oxidation state removes the protective CO₂ that can convert the nucleophilic alkoxides into carbonate groups that may be less prone to back-biting reaction.

Upon oxidation of the cobalt(II) catalyst, more poly(propylene carbonate) was formed, but the polymerization was slower. The slower reaction rate was likely caused by competitive binding of propylene carbonate to the cobalt catalyst. The molecular weight of the poly(propylene carbonate) was too low to be measured by GPC chromatography. For *L*-lactide ROP and propylene oxide-CO₂ ROCOP, the catalyst pair of **2.9** and **2.12-KONp** were redox-switchable, but polymer back-biting is a challenge during propylene oxide-CO₂ ROCOP. Our

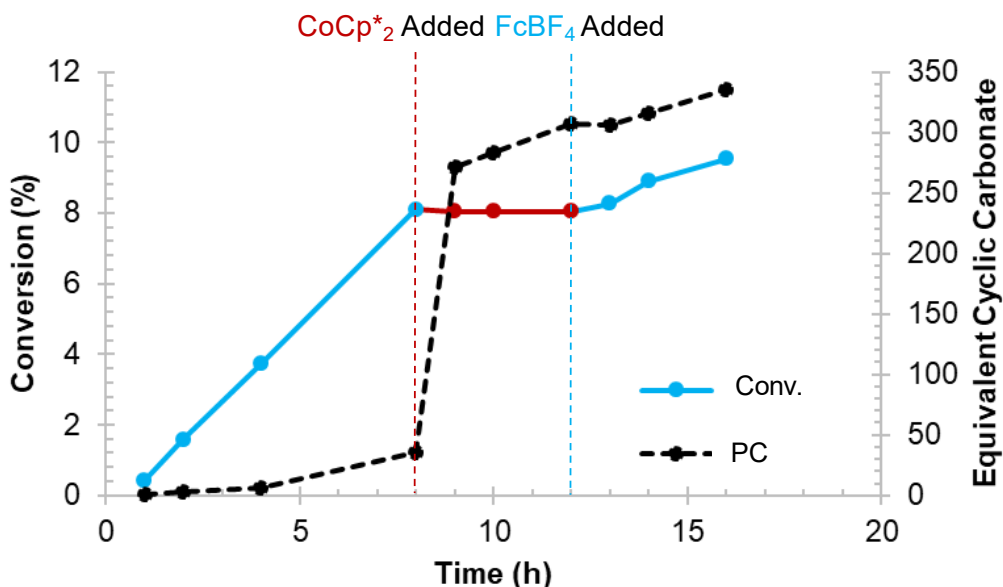


Figure 2.3. Redox-switchable polymerization of propylene oxide and CO₂ by catalyst **2.9**, **2.12-KONp** and FcBF₄. Red is the catalyst in the reduced cobalt(II) oxidation state while blue is in the oxidized cobalt(III) oxidation state. CoCp*₂ is added at 8 h and FcBF₄ at 12 h. Sampling required the reactor to be depressurized and pressurized.

hypothesis was that in the presence of *L*-lactide, *L*-lactide ROP would be more favorable than detrimental poly(propylene carbonate) back-biting.

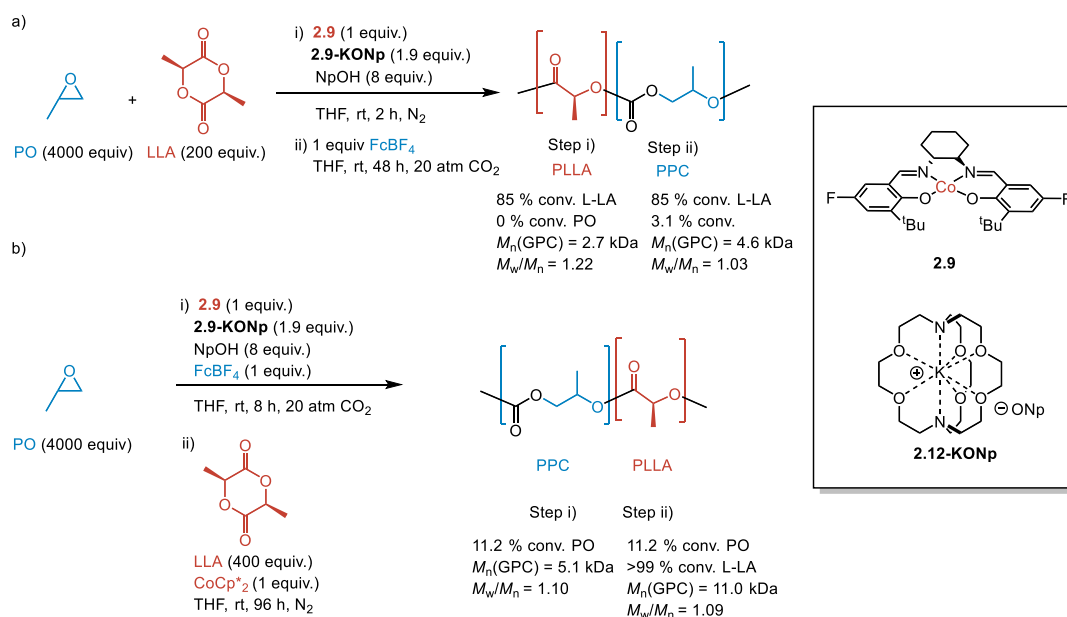
2.5 Sequential Copolymerization of *L*-Lactide, Propylene Oxide and CO₂ for Multi-block Copolymers

We had determined that the catalyst combination of **2.9** and **2.12-KONP** was active for *L*-lactide ROP when the cobalt catalyst was in the cobalt(II) oxidation state and inactive when the catalyst was in the cobalt(III) oxidation state. The complementary reactivity was observed for propylene oxide-CO₂ ROCOP, which was active in the cobalt(III) oxidation state and inactive in the cobalt(II) oxidation state. The orthogonality of each polymerization was promising for the copolymerization of *L*-lactide, propylene oxide and CO₂ as it should be possible to synthesize blocky copolymers through redox-switchable polymerization. To synthesize a diblock copolymer of poly(lactic acid) and poly(propylene carbonate) we added a mixture of **2.9**, **2.12-KONp** and neopentanol in THF to a solution of *L*-lactide in propylene oxide (Scheme 2.12a). After 2 h, 85 % of the *L*-lactide was consumed. We then added FcBF₄ to the solution and sealed the mixture in a steel pressure reactor. The reactor was pressurized with CO₂ and allowed to stir at room temperature for 48 h. The reaction was quenched with 10 % HCl in MeOH and the polymer was isolated. *L*-lactide appeared to significantly slow-down propylene oxide-CO₂ ROCOP as only 3.1 % of the propylene oxide was consumed. The molecular weight of the copolymers increases with each block (Figure 2.4) and only one diffusion peak is observed by Diffusion Ordered Spectroscopy (DOSY) NMR (Figure 2.5) which gave us confidence that a diblock poly(*L*-lactic

acid-*b*-propylene carbonate) was formed. It was surprising that homopolymer arising from chain transfer to water, was not observed for the poly(*L*-lactic acid) initiated poly(propylene carbonate). Poly(*L*-lactic-acid)'s hydrophobicity and crystallinity may have disfavored chain transfer to water instead of chain transfer to other growing polymer chains.⁶¹

After noting the successful copolymerization of the three monomers, starting from *L*-lactide, we then attempted to synthesize a diblock copolymer starting from propylene oxide-CO₂ ROCOP (Scheme 2.12b). Due to significantly slower rate of propylene oxide-CO₂ ROCOP was in the presence of *L*-lactide, we decided to sequentially add the monomers to produce a poly(carbonate-*b*-ester) copolymer. For the first block, a mixture of **2.9**, **2.12-KONp**, FcBF₄ and neopentanol in THF to propylene oxide in a steel pressure reactor. The reactor was pressurized

Scheme 2.12. Procedure for the ReSPCT copolymerization of *L*-lactide, propylene oxide and CO₂ for the synthesis of diblock copolymers. (a) Synthesis of poly(*L*-lactic acid-*b*-propylene carbonate). (b) Synthesis of poly(propylene carbonate-*b*-*L*-lactic acid).



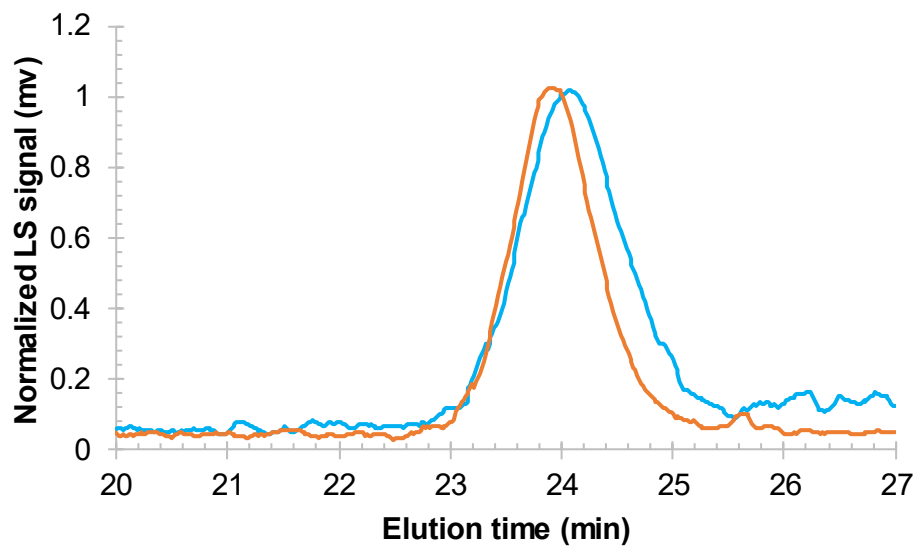


Figure 2.4. GPC chromatograms of poly(*L*-lactic acid) ($M_n(\text{GPC}) = 2.7 \text{ kDa}$, $M_w/M_n = 1.22$, blue) and poly(*L*-lactic acid-*b*-propylene carbonate) ($M_n(\text{GPC}) = 4.6 \text{ kDa}$, $M_w/M_n = 1.03$, orange) from Scheme 2.12A.

with 20 atm of CO_2 and allowed to stir at room temperature for 8 h. The CO_2 gas was first reduced to 1 atm and then fully released under an inert N_2 atmosphere in a glovebox to keep out atmospheric water. At 11.2 % conversion of propylene oxide, the reaction mixture was added to solid *L*-lactide and CoCp^*_2 to reduce the catalyst to the cobalt(II) oxidation state and initiate *L*-lactide ROP. The mixture was allowed to stir for another 8 h before being quenched with 10 % HCl in MeOH and then the volatiles were removed *in vacuo*. Unlike the redox-switchable copolymerization of propylene oxide and CO_2 , no cyclic propylene carbonate was produced after the addition of CoCp^*_2 . The *L*-lactide was also fully converted to poly(*L*-lactic acid) which demonstrated how the presence of *L*-Lactide prevented the back-biting reaction of poly(propylene carbonate) by liberated alkoxides. The GPC chromatograms of the polymer and

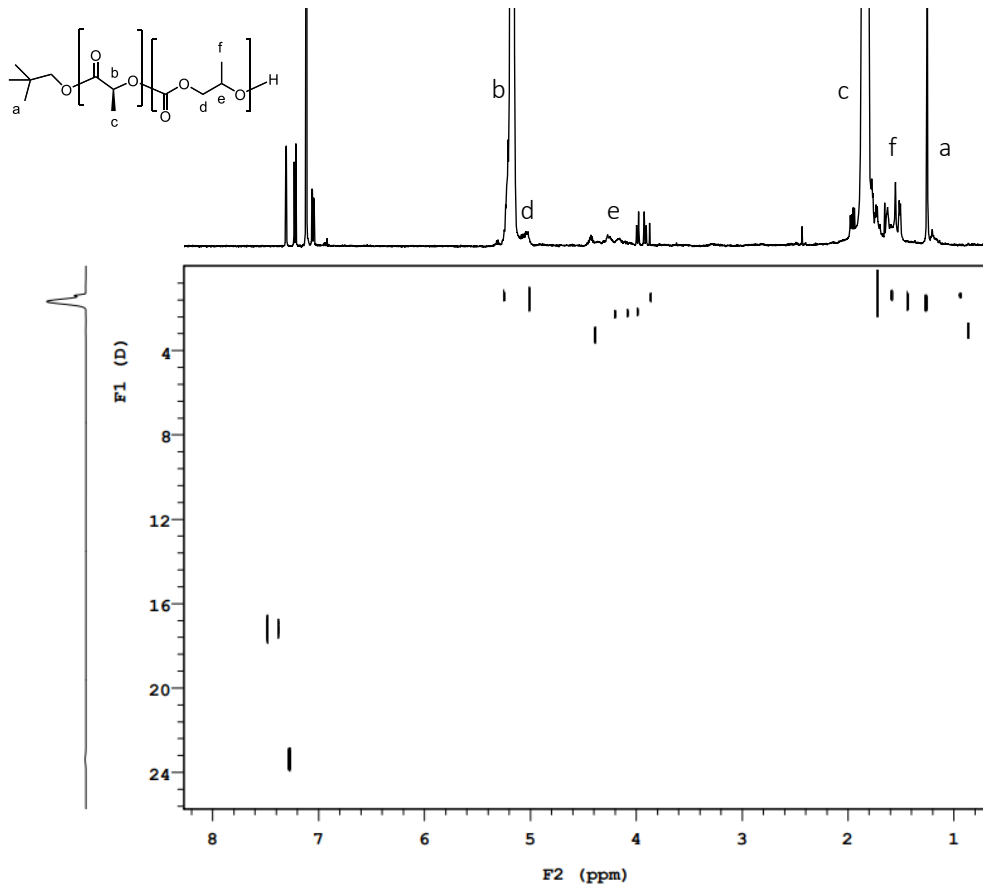


Figure 2.5. DOSY NMR of poly(*L*-lactic acid-*b*-propylene carbonate) from Scheme 2.12a.

copolymer were bimodal (Figure 2.6), which is not uncommon for propylene oxide-CO₂ ROCOP as even dry CO₂ is prone to trace water contamination.^{52,75} The DOSY spectrum also indicated two populations were present and both populations were copolymers Figure (2.7).

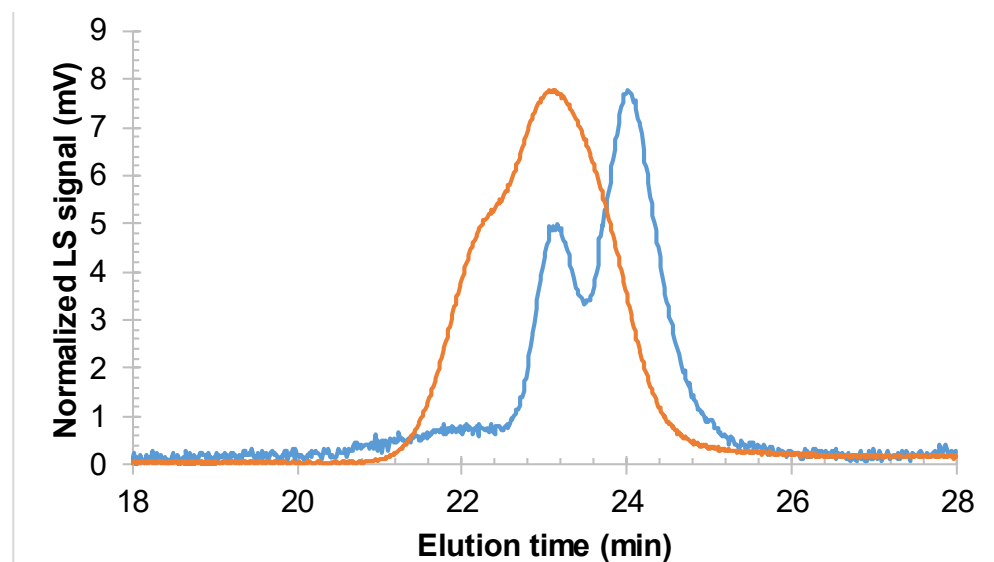


Figure 2.6. GPC chromatograms of poly(propylene carbonate) ($M_n(\text{GPC}) = 5.1 \text{ kDa}$, $M_w/M_n = 1.10$, blue), poly(propylene carbonate-*b*-*L*-lactic acid) ($M_n(\text{GPC}) = 11.0 \text{ kDa}$, $M_w/M_n = 1.09$, orange) from Scheme 2.12b. High molecular weight peak is likely caused by initiation with adventitious water.

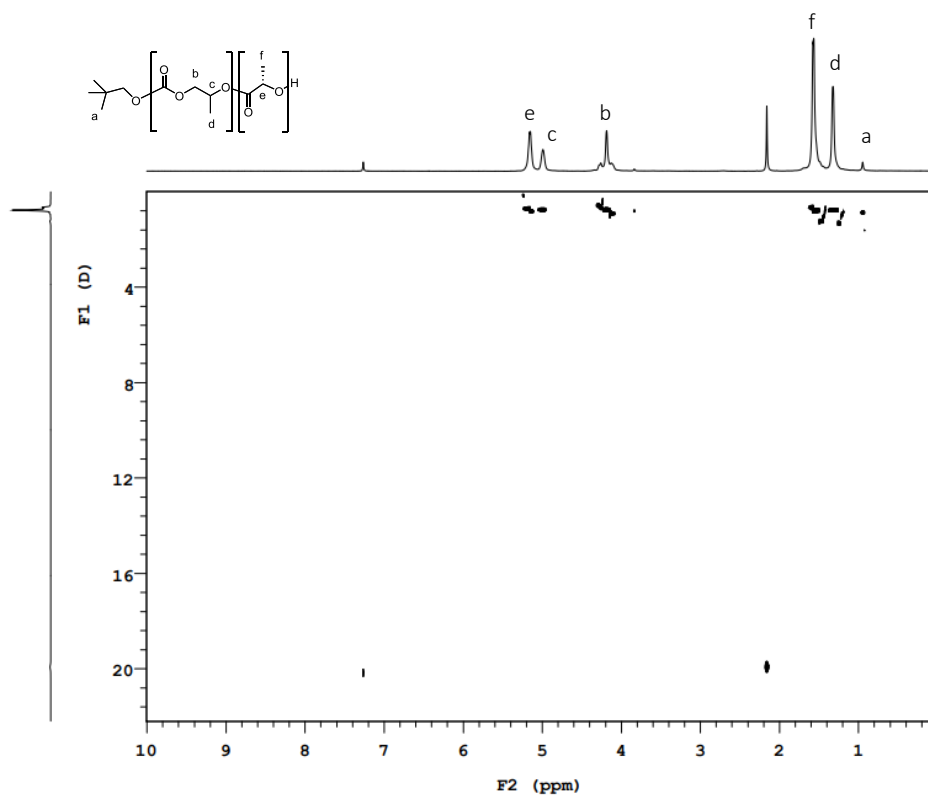
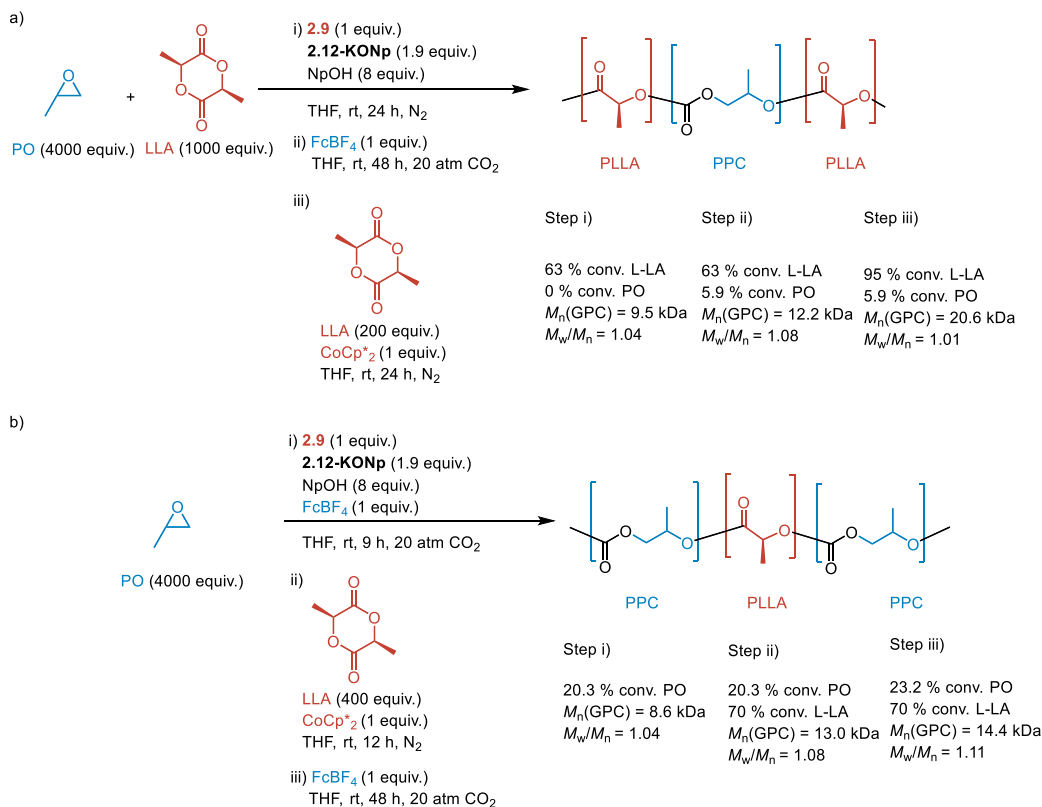


Figure 2.7. DOSY-NMR spectrum of poly(propylene carbonate-*b*-*L*-lactic acid) from Scheme 2.12b.

After successfully synthesizing diblock copolymers of poly(*L*-lactic acid) and poly(propylene carbonate) we wanted to determine if the system was robust enough to synthesize asymmetric triblock copolymers of poly(*L*-lactic acid) and poly(propylene carbonate). Previous switchable copolymerizations accesses symmetrical BAB triblock copolymers starting from diol initiators to make copolymers using one switch. ³⁴ This method will access asymmetric, ABA' triblock copolymers using two redox-switches. The method for synthesizing tri-block copolymers was essentially identical to the corresponding diblock procedure. For poly(*L*-lactic acid-*b*-propylene carbonate-*b*-*L*-lactic acid), the first poly(*L*-lactic acid) block was made with 1000 equivalents of lactide relative to **2.9**. After stirring for 24 h, the *L*-lactide reached 63 % conversion (Scheme 2.13a). The cobalt(II) complex was oxidized with FcBF₄, and

Scheme 2.13. Procedure for the ReSPCT copolymerization of *L*-lactide, propylene oxide and CO₂ for the synthesis of asymmetric, tri-block copolymers. (a) Synthesis of poly(*L*-lactic acid-*b*-propylene carbonate-*b*-*L*-lactic acid). (b) Synthesis of poly(propylene carbonate-*b*-*L*-lactic acid-*b*-propylene carbonate).



after 48 h under CO₂ pressure propylene oxide reached 5.9 % conversion. Finally, the CO₂ was removed and CoCp*₂ and another 200 equivalents of *L*-Lactide were added to the mixture. After 24 h, the final conversion for each monomer was 95 % for *L*-lactide and 5.9 % for propylene oxide. The copolymer has one diffusion peak by DOSY NMR (Figure 2.8) and the GPC chromatograms are unimodal (Figure 2.9). The elution time decreases going from a homopolymer to a diblock copolymer, but decreases going from a diblock to a triblock copolymer. Although molecular weight is generally inversely correlated with molecular weight it has been reported that block copolymers with strongly interacting blocks can lead to smaller hydrodynamic radii.⁷⁶ The use of a light scattering detector still allows for relatively accurate

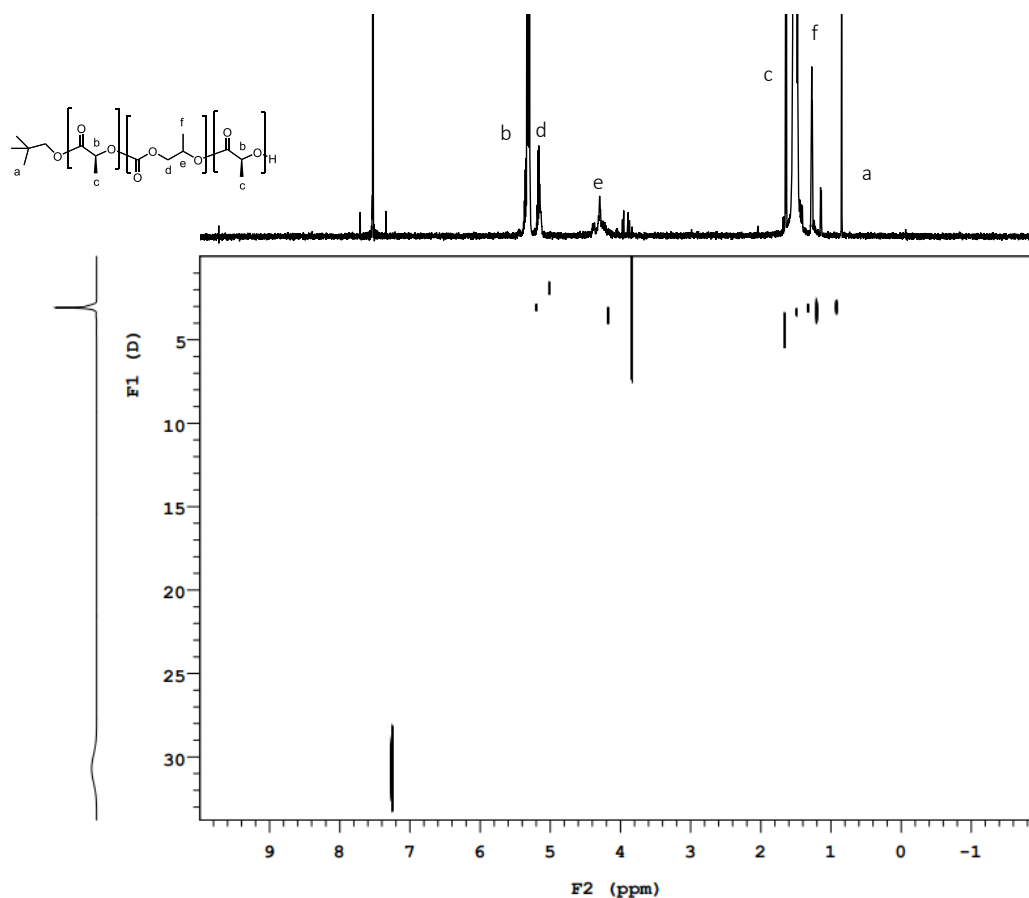


Figure 2.8. DOSY NMR of poly(*L*-lactic acid-*b*-propylene carbonate-*b*-*L*-lactic acid') from Scheme 2.13a.

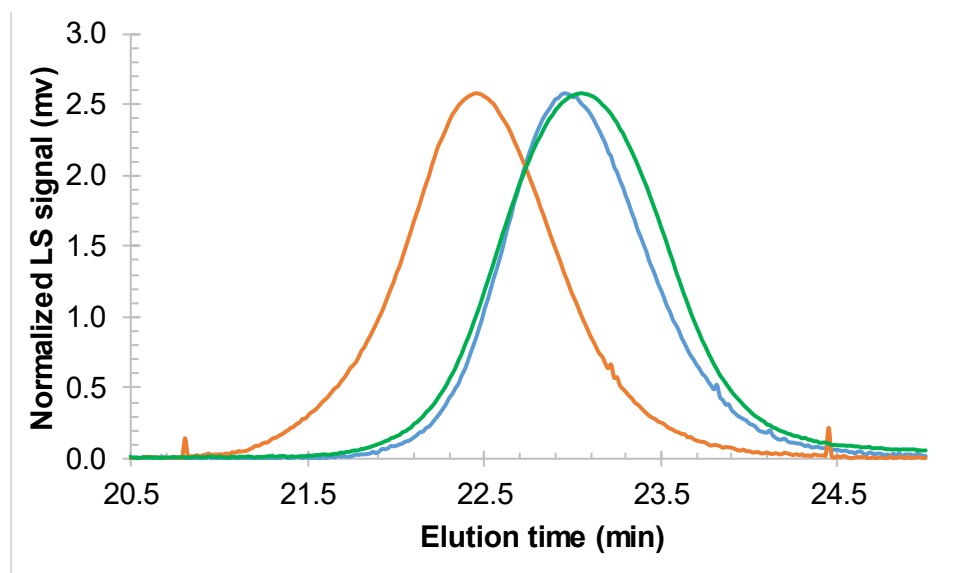


Figure 2.9 GPC chromatograms of poly(*L*-lactic acid) ($M_n(\text{GPC}) = 9.5$ kDa, $M_w/M_n = 1.04$, blue), poly(*L*-lactic acid-*b*-propylene carbonate) ($M_n(\text{GPC}) = 12.2$ kDa, $M_w/M_n = 1.08$, orange) and poly(*L*-lactic acid-*b*-propylene carbonate-*b*-*L*-lactic acid) ($M_n(\text{GPC}) = 20.6$ kDa, $M_w/M_n = 1.01$, green) from Scheme 2.14a.

molecular weight determinations for these types of copolymers. The two crystalline PLA blocks in the triblock copolymer may be experiencing these types of strong interactions that lead to longer elution times.

For poly(propylene carbonate-*b*-*L*-lactic acid-*b*-propylene carbonate) synthesis, the first polycarbonate block was synthesized without *L*-lactide in the reaction mixture. The solution was allowed to stir for 9 h under 20 atm of CO₂ reaching 20.3 % conversion of propylene oxide (Scheme 2.13b). The polyester midblock was synthesized by adding the reaction mixture to solid *L*-lactide (400 equiv. to **2.9**) and CoCp*₂ and then allowing the mixture to stir for 12 h under a nitrogen atmosphere (70 % conversion of *L*-lactide). Finally, FcBF₄ was added to oxidize the cobalt(II) complex and the reaction mixture was loaded into a steel pressure reactor and again pressurized with 20 atm of CO₂. After 48 h, the CO₂ pressure was released and the polymer was quenched with 10 % HCl in MeOH. The GPC chromatograms were bimodal and similar to the poly(carbonate-*b*-ester) the higher molecular weight polymer is likely from chain

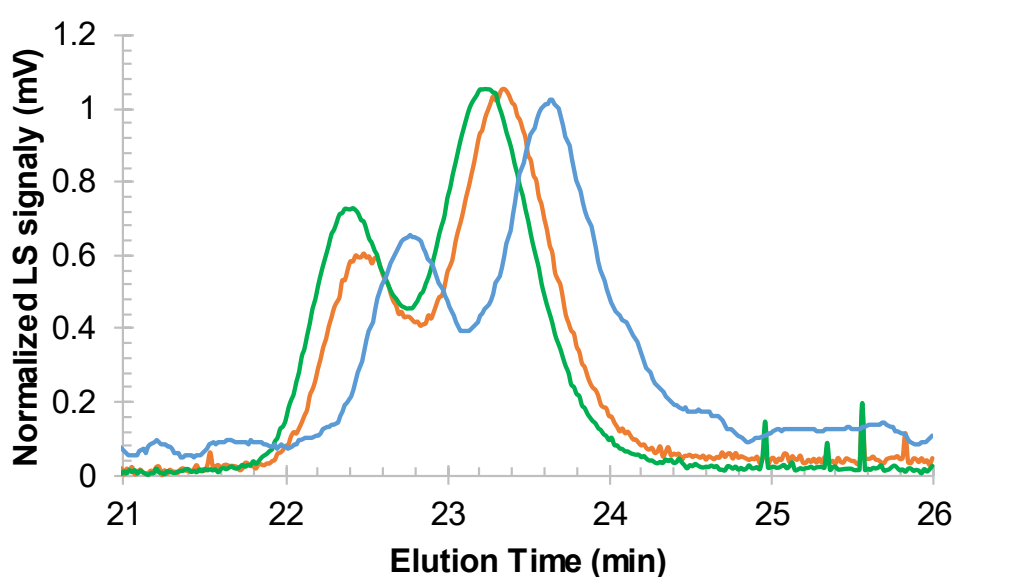


Figure 2.1 e), poly(propylene carbonate-*b*-*L*-lactic acid) ($M_n(\text{GPC}) = 13.0$ kDa, $M_w/M_n = 1.08$, orange) and poly(propylene carbonate-*b*-*L*-lactic acid-*b*-propylene carbonate') ($M_n(\text{GPC}) = 14.4$ kDa, $M_w/M_n = 1.11$, green) from Scheme 2.14b.

transfer to adventitious water (Figure 2.10) The elution time for the copolymers decreased after each block was added. The DOSY NMR had two peaks, which correspond to the smaller neopentanol-initiated triblock copolymer and a larger water-initiated telechelic pentablock copolymer respectively (Figure 2.11). Notably the neopentyl signal is only associated with the smaller, faster diffusing copolymer as expected.

To produce monomodal triblock polymers that start with a poly(propylene carbonate) blocks we decided to replace neopentanol with a diol as the chain transfer agent for polymerization. In this way any water initiated polymer will have the same structure as diol-initiated copolymers. (Scheme 2.14). We also elected to replace neopentoxide **2.12-KONp** initiator with the less nucleophilic **2.12-KO^tBu** in order to only produce telechelic copolymers. To synthesize the BAB copolymer A mixture of **2.9** and **2.12-KO^tBu** in THF was added to 1,8-octanediol (5 equiv. relative to **2.9**) and propylene oxide in a steel pressure reactor. The reactor

was pressurized with 20 atm of CO₂ and allowed to stir at room temperature for 24 h. The CO₂ was removed and only 13.7 % of the propylene oxide was consumed. The combination of 1.9 equivalents of **2.12-KO^tBu** and 5 equivalents of diol were not as reactive as 1.9 **2.12-KONp** and 8 equivalents of neopentanol (46.5 % propylene oxide conversion in 24 h) despite have the roughly equal numbers of primary alcohol initiators. This suggest the chain-transfer agent is involved in the rate determining step for ROCOP.

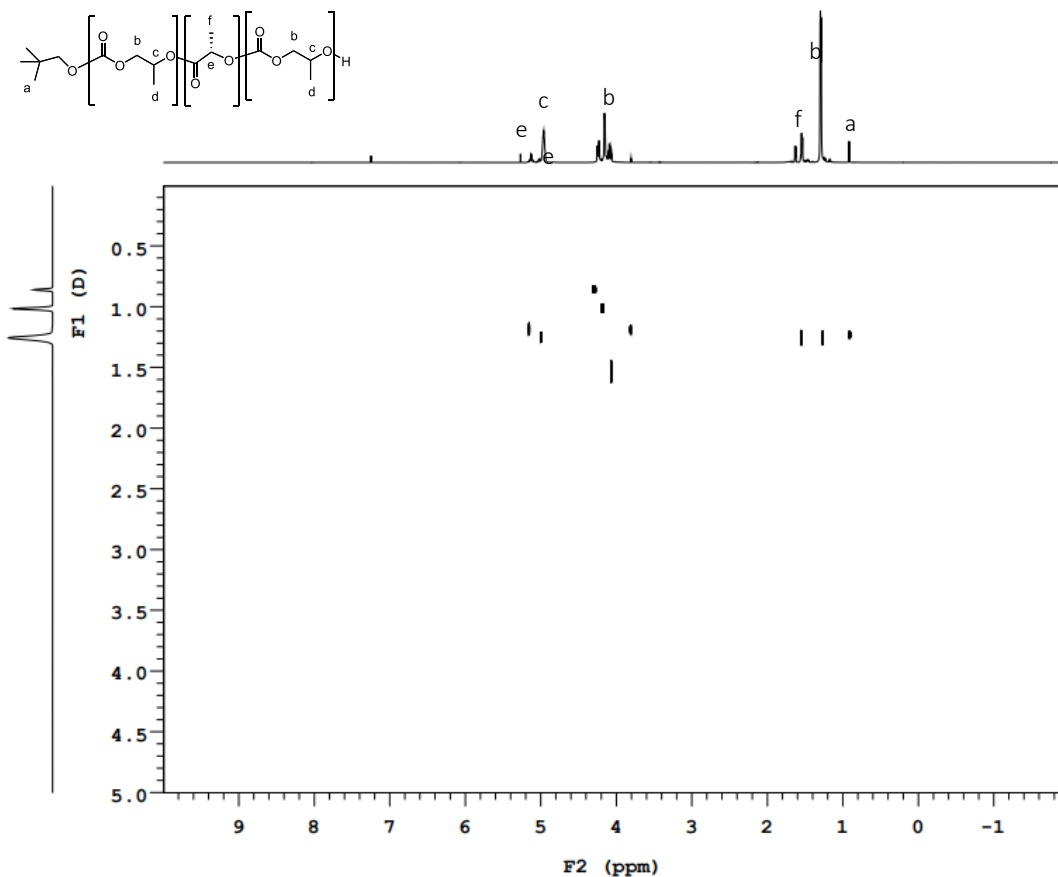
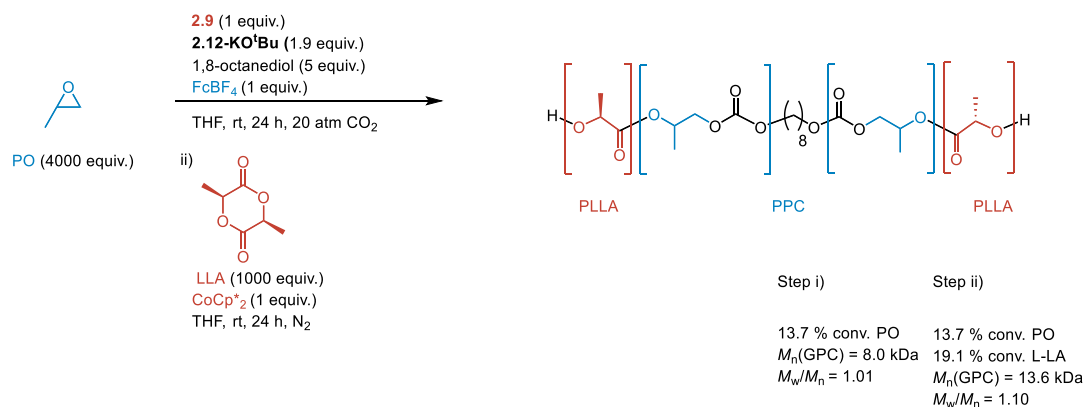


Figure 2.11. DOSY NMR of poly(propylene carbonate-*b*-L-lactic acid-*b*-propylene carbonate') from Scheme 2.13a.

To form the polyester blocks, the telechelic poly(carbonate) solution was added to *L*-lactide (1000 equivalents) and CoCp*₂ and allowed to stir at room temperature for 24 h under a N₂ atmosphere. The polymer was quenched and only 19 % of the *L*-lactide was consumed which was also relatively low. The molecular weight of both the polycarbonate ($M_n(\text{GPC}) = 8.0$ kDa, $M_n(\text{theo}) = 11.2$ kDa) and the telechelic copolymer ($M_n(\text{GPC}) = 16.7$ kDa, $M_n(\text{theo}) = 13.6$ kDa) were both significantly lower than the theoretical molecular weight. The lower molecular weight is likely due to chain transfer to water in the reaction. The GPC chromatograms were monomodal (Figure 2.12) and the DOSY NMR (Figure 2.13) had one large diffusion peak, with some minor peaks that may be tert-butoxide initiated copolymer. The combination of a diol with a non-nucleophilic base was successful for the synthesis of monomodal copolymers starting from polycarbonates.

Scheme 2.14. Procedures for the ReSPCT copolymerization of *L*-lactide, propylene oxide and CO₂ with 1,8-octanediol as an initiator.



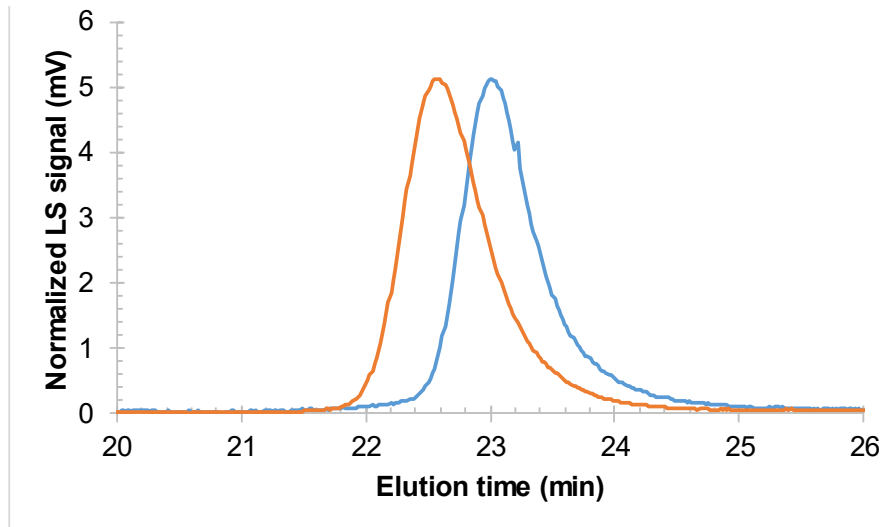


Figure 2.12. (top) GPC chromatograms of poly(propylene carbonate) ($M_n(\text{GPC}) = 8.0$ kDa, $M_w/M_n = 1.01$, blue) and poly(*L*-lactic acid-*b*-propylene carbonate-*b*-*L*-lactic acid) ($M_n(\text{GPC}) = 13.6$ kDa, $M_w/M_n = 1.10$, orange) from Scheme 2.14.

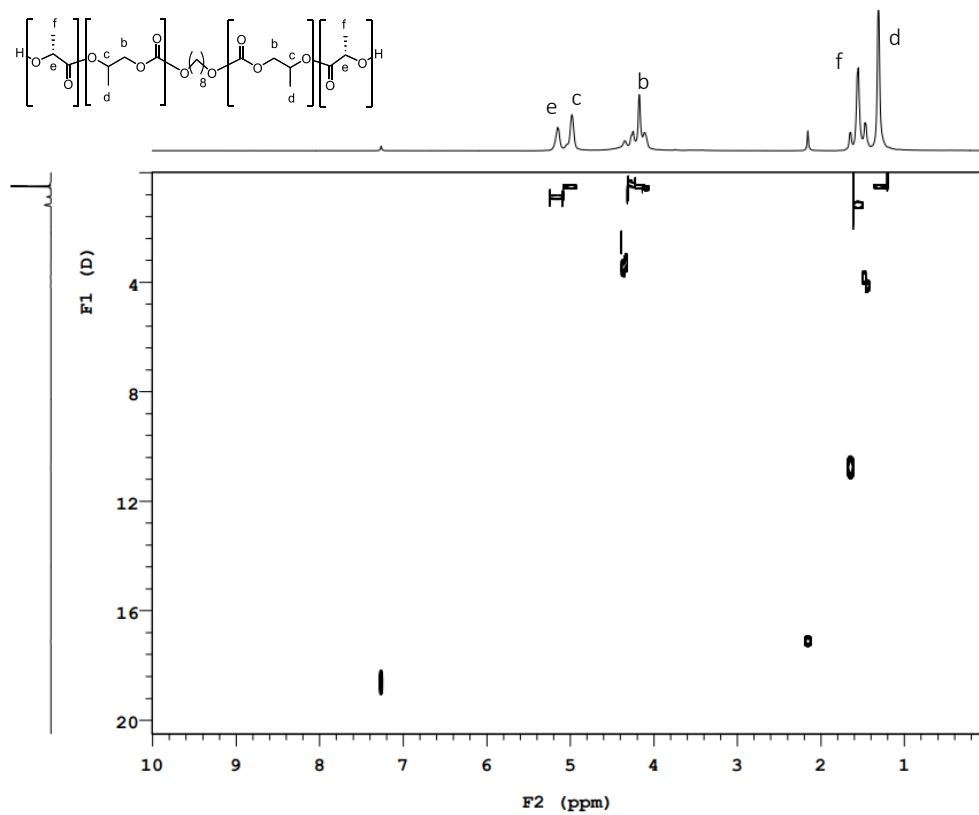
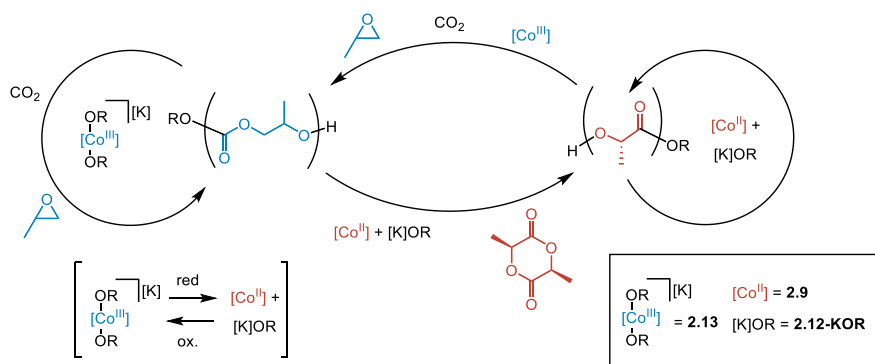


Figure 2.13. DOSY NMR spectrum of telechelic poly(*L*-lactic acid-*b*-propylene carbonate-*b*-*L*-lactic acid) from Scheme 2.14.

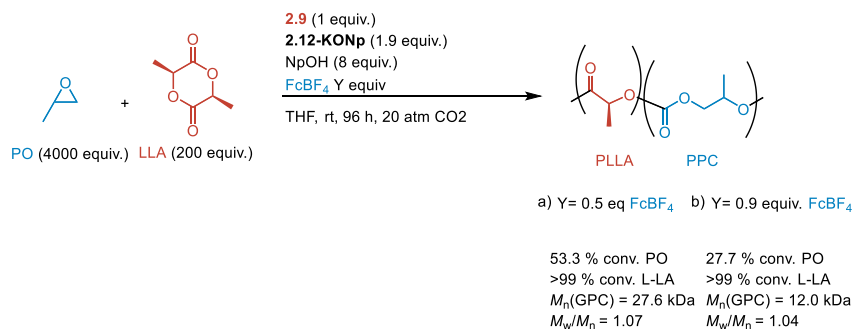
2.6 Synthesis of Statistical Copolymers of *L*-Lactide, Propylene Oxide and CO₂

A unique advantage of ReSPCT is the ability to adjust the relative ratios of poly(*L*-lactic acid) and poly(propylene carbonate) in copolymers through the partial oxidation/ reduction of the cobalt catalyst to create mixed populations of active catalysts (Scheme 2.15). In a mixed solution containing a cobalt(III)-based complex, a cobalt(II)-based complex and a 2.2.2-cryptand potassium alkoxide and a given alcohol initiator can undergo chain transfer to the active site for either *L*-Lactide ROP or propylene carbonate-CO₂ ROCOP. After insertion of one unit of either poly(propylene carbonate) or poly(*L*-lactic acid), a new alkoxide is formed and this macromolecular initiator can undergo further polymerization or undergo chain transfer with another alcohol. If the alcohol undergoes chain transfer to the cobalt(III) complex a unit of poly(propylene carbonate) will be added. An alcohol that undergoes chain transfer transfers to the 2.2.2-cryptand potassium alkoxide will add a unit of poly(*L*-lactic acid). When cobalt(II) concentrations are high, more 2.2.2-cryptand potassium alkoxide is free for *L*-lactide ROP and

Scheme 2.15. Statistical copolymerization of *L*-lactide, propylene oxide and CO₂ by mixed species of cobalt(II) and cobalt(III)-based salen complexes.



Scheme 2.16. Procedure for ReSPCT copolymerization of *L*-lactide, propylene oxide and CO₂ to synthesize statistical copolymers.



when cobalt(III) concentration is high more 2.2.2-cryptand potassium alkoxide is bound to the cobalt(III) complex for propylene oxide-CO₂ ROCOP.

We were able to adjust the incorporation of the two copolymers to synthesize copolymers with statistical regions (Scheme 2.16). To synthesize these statistical copolymers, we added a mixture of **2.9**, **2.12-KONp**, neopentanol and FcBF₄ (either 0.5 or 0.9 equivalents) in THF to a solution of *L*-lactide (200 equivalents to **2.9**) in propylene oxide. The mixture was sealed in a steel pressure reactor, pressurized with 20 atm of CO₂ and allowed to stir at room

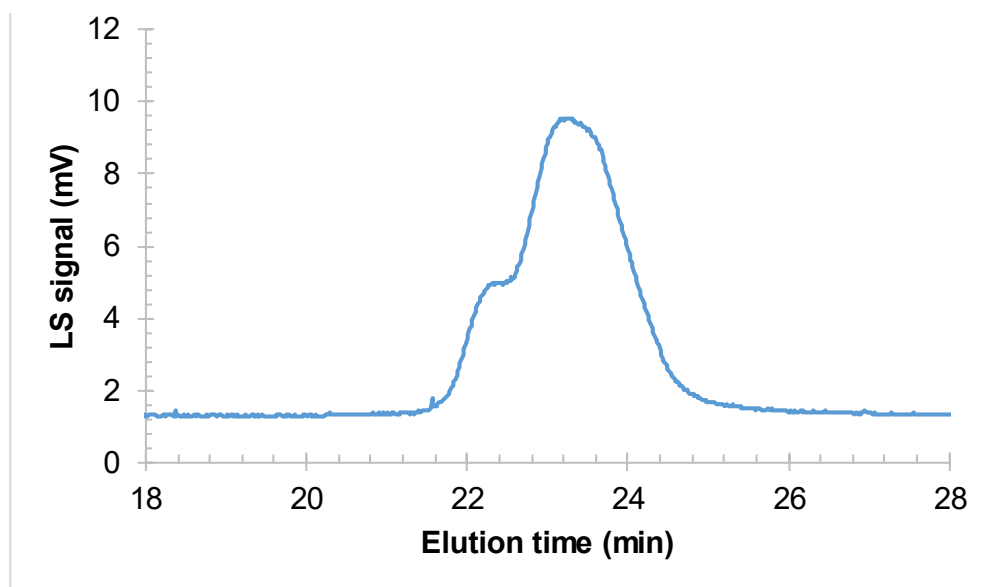


Figure 2.14. GPC chromatogram of poly(*L*-lactic acid-*s*-propylene carbonate) ($M_n(\text{GPC}) = 7.7$ kDa, $M_w/M_n = 1.07$) from Scheme 2.16a.

temperature for 96 h. The CO₂ was released and the reaction was quenched to leave behind poly(carbonate-*s*-ester) copolymer. All of the *L*-lactide was consumed for both reactions, but the total consumption of propylene oxide conversion was much lower for the sample with a 0.9 equivalents of FcBF₄ (53.3 %) compared to the sample with 0.5 equivalents of the oxidant (27.7 %). This is not surprising as the sample with more cobalt(III) in solution was more reactive for propylene oxide-CO₂ ROCOP. The GPC chromatograms revealed both copolymers possessed bimodal distributions (Figures 2.14 and 2.16) despite the presence of *L*-lactide during the copolymerization suggesting that water is acting as an initiator. This result supports our hypothesis that it is the hydrophobic and crystalline poly(*L*-lactic acid) chain that disfavors chain transfer reactions to water and not just a consequence of adding *L*-lactide to the

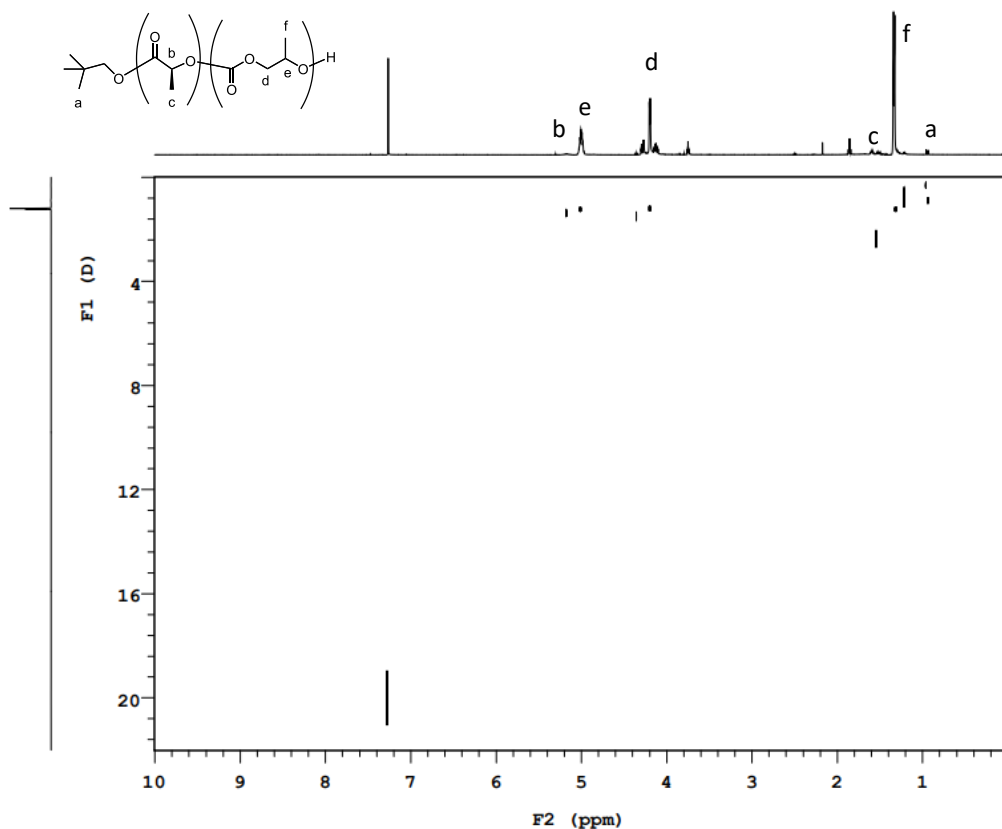


Figure 2.15. DOSY NMR spectrum of poly(*L*-lactic acid-*s*-propylene carbonate) from Scheme 2.16a.

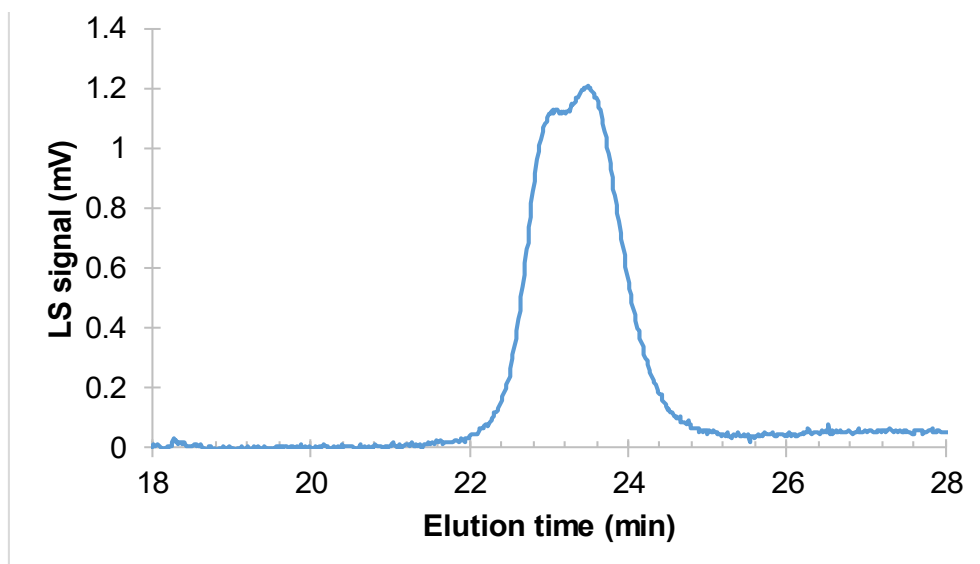


Figure 2.16. GPC chromatogram of poly(*L*-lactic acid-*s*-propylene carbonate) ($M_n(\text{GPC}) = 12.0$ kDa, $M_w/M_n = 1.04$) from Scheme 2.16b.

copolymerization mixture. The DOSY NMR spectra (Figures 2.15 and 2.17) for both copolymers revealed that the signals indicative of poly(*L*-lactic acid) the poly(propylene carbonate) diffuse together, further suggesting the formation of copolymers rather than separate homopolymers.

The ^1H NMR of the two copolymers synthesized with non-stoichiometric in amounts of oxidant gave some insight into the microstructure of the copolymers (Figure 2.18). For comparison we also included the ^1H NMR of poly(propylene carbonate-*b*-*L*-lactic acid) block copolymer synthesized with using ReSPCT. It is known that the methyl peak for poly(*L*-lactic acid) ($a = 1.55$ ppm in CDCl_3) inserted into a carbonate is shifted downfield ($a' = 1.60$ ppm).⁷⁷ The copolymer synthesized with a 0.9 equivalents of oxidant (a 9:1 concentration of cobalt(III) to cobalt(II) complexes) seemed to predominantly have poly(*L*-lactic acid) chains inserted into

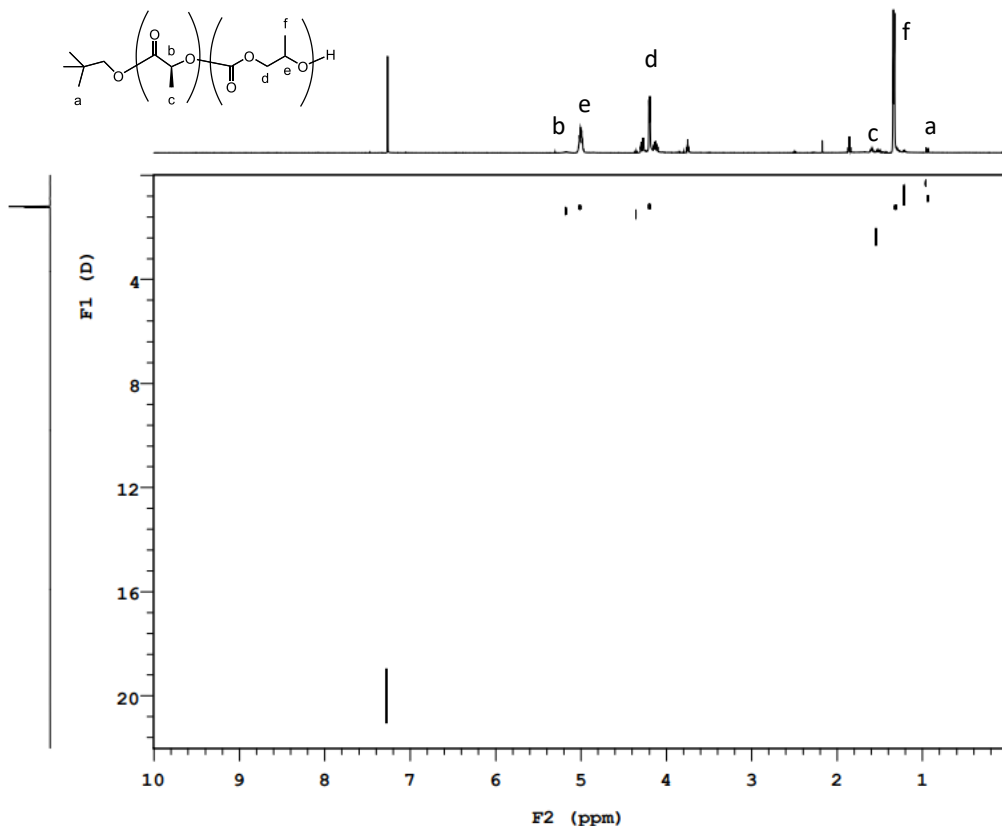


Figure 2.17. DOSY NMR spectrum of poly(*L*-lactic acid-*s*-propylene carbonate) from Scheme 2.16b.

CO₂ which suggests an alternating or random structure. The copolymer synthesized with a 0.5 equivalents of oxidant (a 1:1 concentration of cobalt(III) to cobalt(II) complexes) contained a mixture of poly(*L*-lactic acid) blocks and poly(*L*-lactic acid inserted into CO₂). This suggests the copolymer has either a random or gradient microstructure.

We also observed a difference in whether there was a neopentyl ester ($b = 0.91$ ppm) or carbonate end group ($b' = 0.95$ ppm) for each ratio of oxidants. With a 9:1 ratio of cobalt(III) to cobalt(II) equal amounts of neopentyl ester (from *L*-lactide insertion) and carbonate (from CO₂ insertion) were incorporated. With a 1:1 ratio of cobalt(III) to cobalt(II) only the neopentyl ester was observed. To achieve highly random copolymers an excess of cobalt(III) to cobalt(II)

was needed. For a quantitative analysis of the microstructure a different epoxide-lactone combination would be needed. The peaks of the diagnostic protons and carbons for poly(*L*-lactic acid) and poly(propylene carbonate) overlap in many regions by both the ^1H and ^{13}C NMR.^{33,77}

With our new understanding of the statistical copolymerization of *L*-lactide, propylene oxide and carbon dioxide we attempted to synthesize mixed copolymers containing blocky and statistical segments (Scheme 2.17). To synthesize poly(*L*-lactic acid-*b*-(*L*-lactic acid-*s*-propylene carbonate)-*b*-*L*-lactic acid) a mixture of **2.9**, **2.12-KONp** and neopentanol were added to *L*-

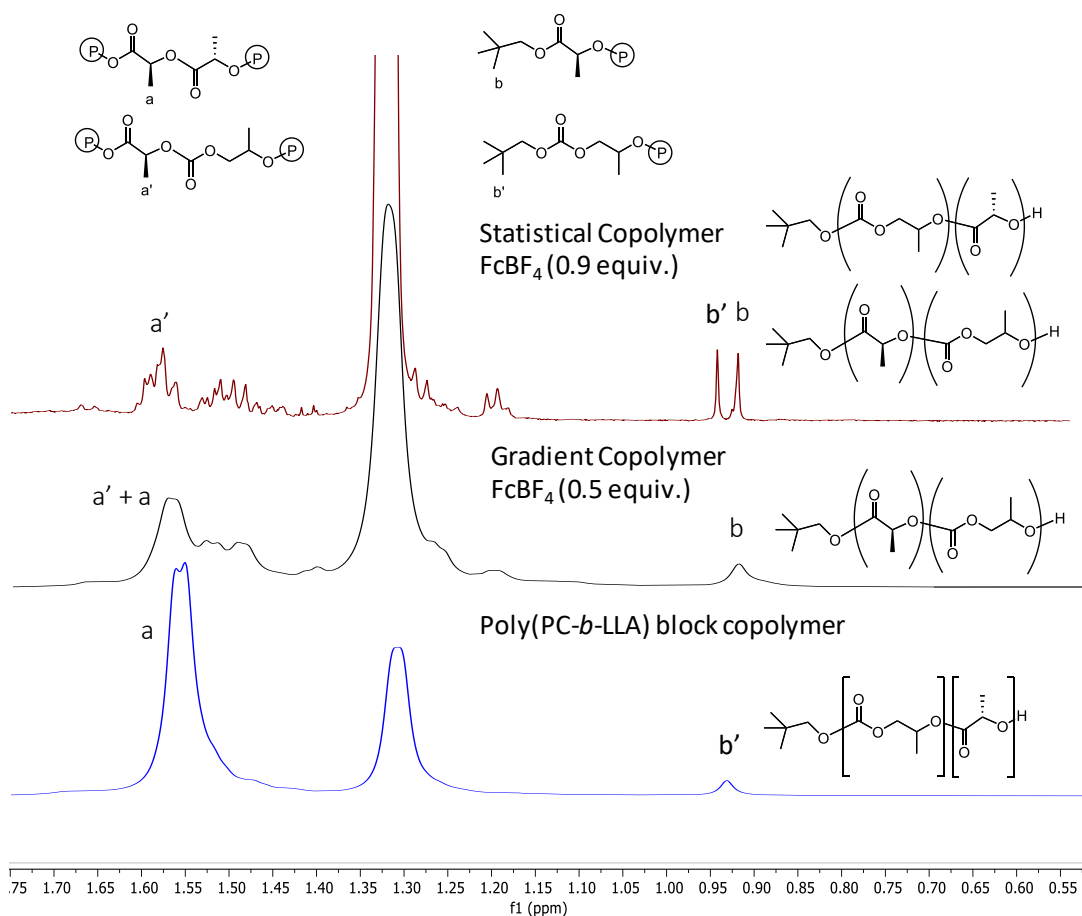
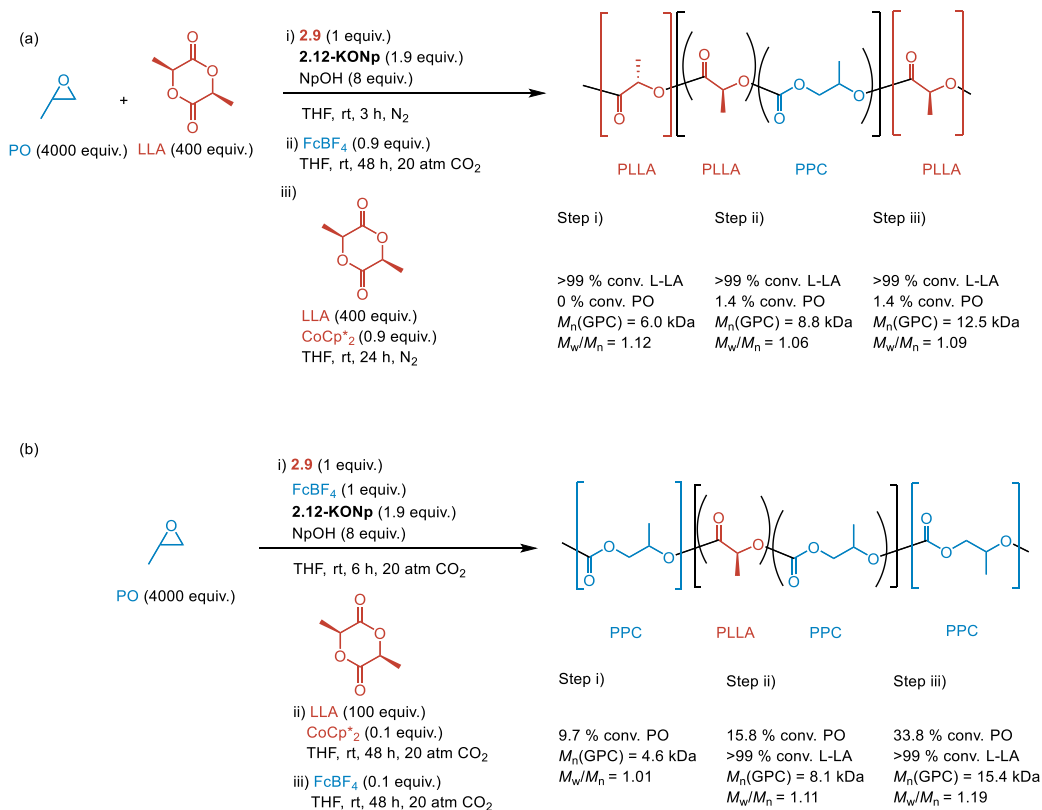


Figure 2.18. ^1H NMR Spectra of poly(*L*-lactic acid-*s*-propylene carbonate) from Scheme 2.16a (red), poly(*L*-lactic acid-*s*-propylene carbonate) from scheme 2.16b and poly(propylene carbonate-*b*-*L*-lactic acid) from Scheme 2.12b.

lactide in THF and allowed to stir at room temperature for 3 h (Scheme 2.17a). At 74 % conversion of *L*-lactide the mixture was oxidized with 0.9 equivalents of FcBF_4 and loaded into a steel pressure reactor. The reactor was pressurized with CO_2 and allowed to stir at room temperature for another 48 h. The reactor was depressurized (*L*-lactide = >99 % conversion, propylene oxide = 1.4 % conversion) and the reaction mixture was added to 0.9 equivalents of CoCp^*_2 and another *L*-lactide. After stirring for a final 24 h under N_2 , the reaction was quenched and a *L*-lactide (>99 %) and propylene oxide (1.4 %) conversion was determined by ^1H NMR. The GPC chromatograms were monomodal throughout the polymerization (Figure 2.19) and only one diffusion peak was observed in the DOSY NMR spectrum (Figure 2.20).

Scheme 2.17. Procedure for ReSPCT of *L*-lactide, propylene oxide and CO_2 to synthesize mixed-blocky and statistical copolymers. (a) Synthesis of poly(*L*-lactic acid-*b*-(*L*-lactic acid-*s*-propylene carbonate)-*b*-*L*-lactic acid). (b) Synthesis of poly(propylene carbonate-*b*-(*L*-lactic acid-*s*-propylene carbonate)-*b*-propylene carbonate).



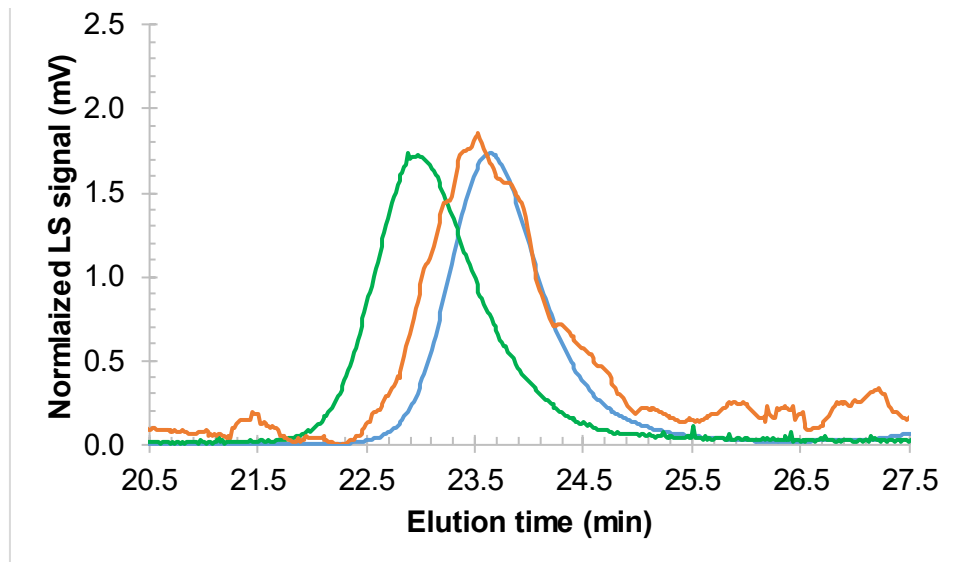


Figure 2.19. GPC Chromatogram of poly(*L*-lactic acid) ($M_n(\text{GPC})$ 6.0 kDa, $M_w/M_n = 1.12$, blue), poly(*L*-lactic acid-*b*-(*L*-lactic acid-*s*-propylene carbonate)) ($M_n(\text{GPC}) = 8.8$ kDa, $M_w/M_n = 1.06$, orange) and poly(*L*-lactic acid-*b*-(*L*-lactic acid-*s*-propylene carbonate)-*b*-*L*-lactic acid) ($M_n(\text{GPC}) = 12.5$ kDa, $M_w/M_n = 1.09$, green) from Scheme 2.17a.

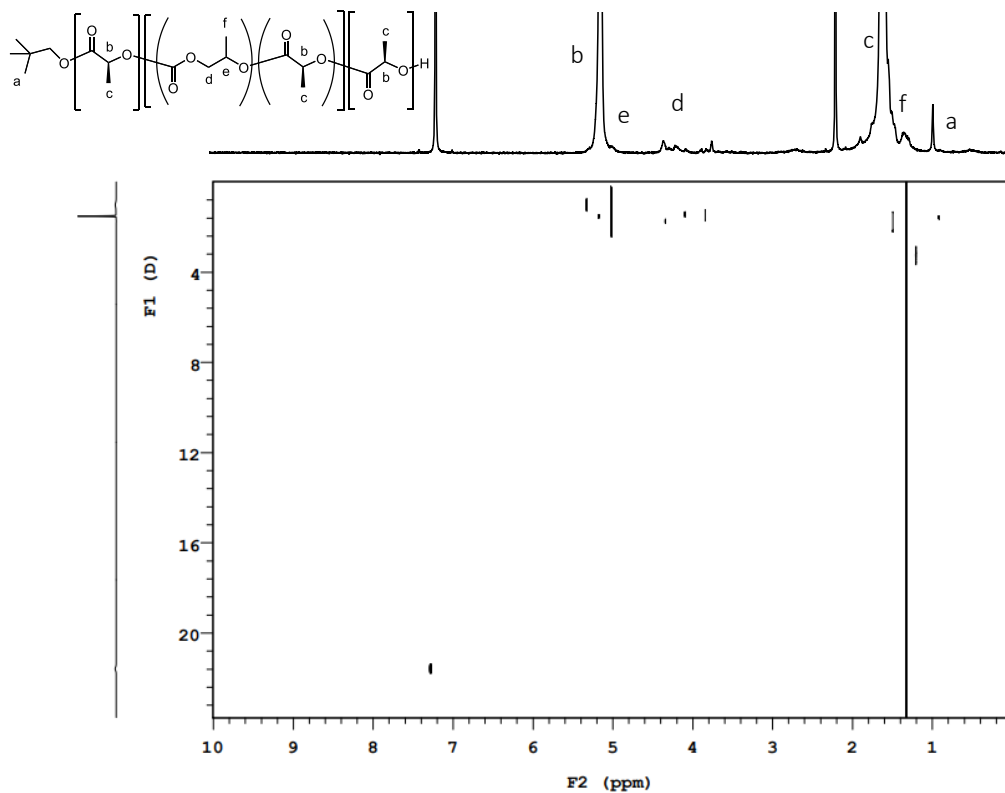


Figure 2.20. DOSY NMR spectrum of poly(*L*-lactic acid-*b*-(*L*-lactic acid-*s*-propylene carbonate)-*b*-*L*-lactic acid) from Scheme 2.17a.

To synthesize poly(propylene carbonate-*b*-(*L*-lactic acid-*s*-propylene carbonate)-*b*-propylene carbonate) a mixture of **2.9**, **2.12-KONp**, FcBF₄ (1 equivalent) and neopentanol in THF were added to propylene oxide and added to a steel pressure reactor (Scheme 2.17b). The reactor was charged with CO₂, and allowed to stir at room temperature for 6 h. The reactor was depressurized to determine propylene oxide conversion (9.7 %) and the reaction mixture was added to *L*-lactide (100 equivalents) and CoCP*₂ (0.1 equivalent). The mixture was again added to the pressure reactor and charged with CO₂. The GPC chromatograms were bimodal throughout the polymerization (Figure 2.21) and the poly(*L*-lactic acid) and poly(propylene carbonate) peaks diffused together by DOSY NMR (Figure 2.22) indicative of copolymer synthesis. Using ReSPCT copolymerization it was simple to synthesize copolymers with blocky

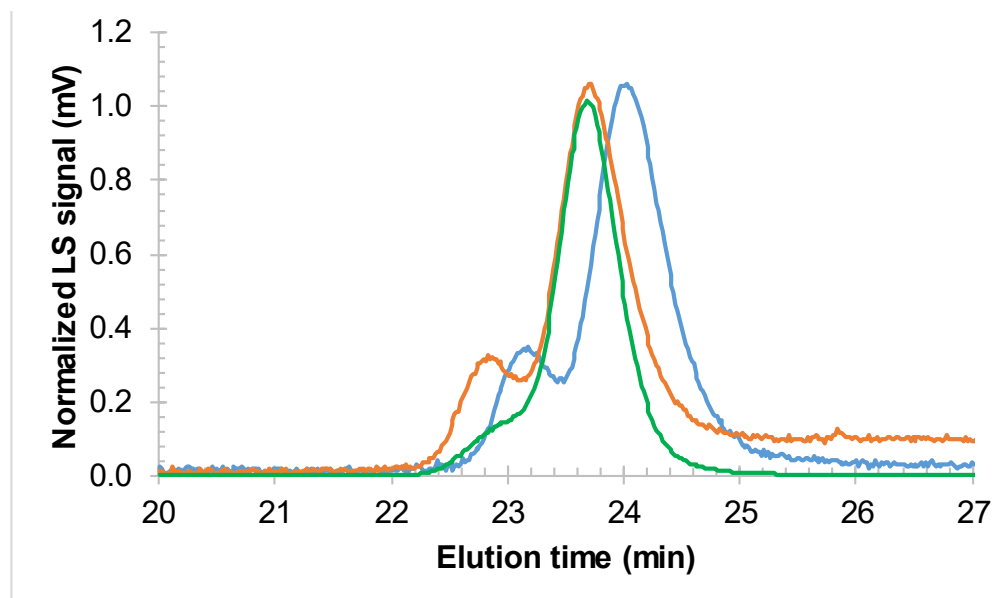


Figure 2.21. GPC Chromatogram of poly(propylene carbonate) ($M_n(\text{GPC}) = 4.6$ kDa, $M_w/M_n = 1.01$, blue), poly(propylene carbonate-*b*-(*L*-lactic acid-*s*-propylene carbonate)) ($M_n(\text{GPC}) = 8.1$ kDa, $M_w/M_n = 1.11$, orange) and poly(propylene carbonate-*b*-(*L*-lactic acid-*s*-propylene carbonate)-*b*-propylene carbonate) ($M_n(\text{GPC}) = 15.4$ kDa, $M_w/M_n = 1.19$, green) from Scheme 2.17b.

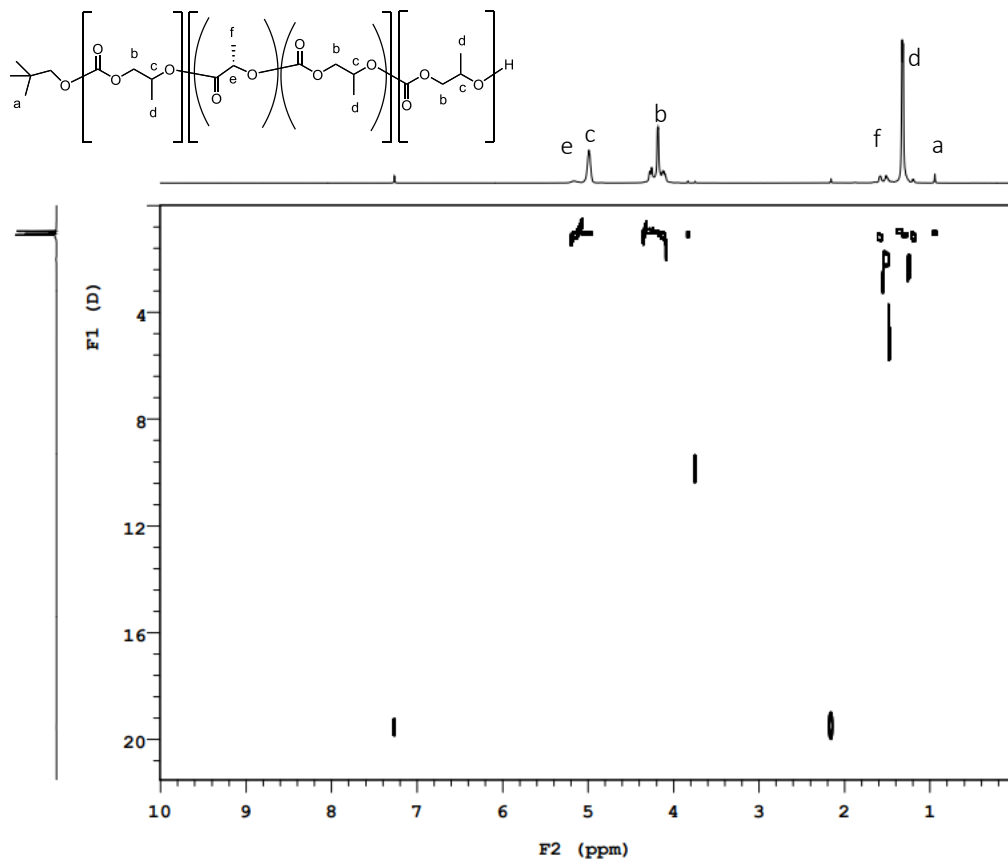


Figure 2.22. DOSY NMR spectrum of poly(propylene carbonate-*b*-(*L*-lactide-*s*-propylene carbonate)-*b*-propylene carbonate) from Scheme 2.17b.

and statistical segments from *L*-lactide, propylene oxide and CO₂. We hope this discovery allows for further study of the physical and mechanical properties of copolymers with intricate microstructures.

2.7 Conclusion

ReSPCT provides a versatile and tunable method for the synthesis of block of statistical copolymers of *L*-lactide, propylene oxide and CO₂. The addition of redox reagents to a mixture of cobalt-based catalysts and 2.2.2-cryptand alkoxides, allows for the predictable alteration of

the copolymer composition. The diverse range of biodegradable block and statistical copolymers of polyesters and polycarbonates that can be synthesized with this method could find uses in food packaging, biomedical implants and agricultural films. Future work will involve studying the ability for these block and statistical copolymers to act as compatibilizers for poly(*L*-lactic acid) and poly(propylene carbonate) and recording the thermal and mechanical properties of the resulting blends. Electrochemical redox-switching will also be pursued to simplify the act of switching between *L*-lactide ROP and epoxide-CO₂ ROCOP without depressurizing the reactor. Additionally, bifunctional catalysts containing both cryptand or crown ether moieties and cobalt salen will be synthesized to increase reaction rates and lower the minimum pressure needed for efficient copolymerization as has been demonstrated by other bifunctional cobalt salen catalysts.^{22,78}

2.8 Experimental

General Considerations: Propylene oxide was acquired from Acros Organics, dried over CaH₂ and distilled prior to polymerization. 18-crown-6 was purchased from Chemimpex, recrystallized from acetonitrile, and dried over P₂O₅ before use. 2.2.2-cryptand was acquired from Acros Organics and used as received. *L*-lactide was acquired from Natureworks, recrystallized in ethyl acetate then toluene and dried over P₂O₅. Tetrahydrofuran was dried over molecular sieves under an argon atmosphere. Cobalt(II) acetate tetrahydrate, cobaltocene and decamethylcobaltocene were purchased from Sigma Aldrich and used as received. Neopentyl alcohol was purchased from Sigma Aldrich and dried over alumina. 1,8-octanediol

was purchased from Alfa Aesar and dried over P₂O₅. Potassium tert-butoxide was purchased from Acros chemicals and sublimated under high vacuum and 250 °C before use. 99.8 % pure, “Bone dry” carbon dioxide was purchased from Airgas and further dried over activated manganese oxide and 3 Å° molecular sieves. (R,R)-N,N'-Bis(3-fluoro-5-tert-butylsalicylidene)-1,2-cyclohexanediamine (**2.10**) was synthesized according to literature procedures.⁶⁸ Ferrocenium tetrafluoroborate was synthesized according to literature procedures.⁷⁹ Potassium neopentoxide was synthesized according to literature procedures.⁸⁰ Tetrahydrofuran, diethyl ether, methanol and dichloromethane were obtained from Fisher Scientific. Tetrahydrofuran and diethyl ether were used after passage through a solvent purification system consisting of 3 Å° molecular sieves and manganese oxide under a blanket of argon and then degassed briefly by exposure to vacuum. Unless stated otherwise, all reactions were carried out in oven-dried glassware in a nitrogen-filled glove box or with standard Schlenk line techniques.⁸¹

GPC: All gel permeation chromatography (GPC) measurements were performed on an Agilent GPC220 in THF at 40 °C with three PL gel columns (10µm) in series and recorded with both a refractive index detector and a multi-angle, light-scattering detector at 15 and 90 degrees. Instrument was calibrated against 7 narrow molecular weight, polystyrene standards (GSK, 1,820,000- 3,180 g/mol).

Mass Spectrometry: High-resolution mass spectra were obtained at the using a JEOL AccuTOF DART.

IR: Infrared (IR) spectra were recorded on a Bruker attenuated total reflectance (ATR) infrared spectrometer.

Nuclear Magnetic Resonance: (NMR) spectra were recorded at ambient temperature on spectrometers with 500 and 600 MHz magnets for ^1H and DOSY NMR, 125 MHz for ^{13}C , 470 MHz for ^{19}F , Resonances for paramagnetic complexes are reported as chemical shift in ppm (peak with at half height, Hz).

Synthesis of [(R,R)-N,N'-Bis(3-fluoro-5-tert-butylsalicylidene)-1,2-cyclohexanediaminato(2-)]cobalt(II) (2.9) – Cobalt(II) acetate tetrahydrate (53 mg, 210 μmol) was added to an oven dried RB flask and dried at 80 °C on the Schleck line for 1 h. 5 ml of degassed MeOH was added to the cobalt to form a pink solution. The solution was chilled in an ice bath under flowing nitrogen. 2.10 (100 mg, 210 μmol) was dissolved in 2 ml of degassed CH_2Cl_2 and added to the cobalt solution. Mixture stirred for 10 min under nitrogen to form a bright red solid. Volatiles were removed in vacuo. Solid was washed with hexanes and filtered to leave a dark red solid. Yield (89 mg, 79%).

IR- 2950 cm^{-1} , 2867, 1595, 1524, 1432, 1320, 1252, 1200, 1174, 1050, 869 and 784 cm^{-1} .

Mass Spectra (DART) $\text{C}_{28}\text{H}_{35}\text{N}_2\text{O}_2\text{F}_2\text{Co}$ [H][Co(Salcy-F)]⁺ $m/z = 528.19867$ m/z calc= 528.19931 ^1H

NMR (CDCl_3 , 400 MHz): δ 13.68 (s, 1H), δ 8.3 (s, 1H), δ 7.3 (d, $J=2.5$, 1H), δ 6.97 (d, $J=2.5$, 1H), δ 3.32 (m, 1H), δ 2.0-1.8 (m, 2H), δ 1.8-1.65 (m, 1H), δ 1.45 (m, 1H), δ 1.41 (s, 9H), δ 1.24 (s, 9H)

ppm. ^{19}F NMR (CDCl_3 , 500 MHz): δ -126.7 (s)

Standard procedure for the polymerization of L-lactide

In a nitrogen-filled glove box, **2.9** (1.9 mg, 3.6 μmol) was weighed out into a glass vial with a teflon-coated stir bar. A stock solution of potassium neopentoxide (8.6 mg, 6.8 μmol) and 2.2.2-cryptand (25.6 mg, 6.8 μmol) was prepared in THF (2.0 ml). From the stock solution 0.2 ml was added to **2.9**. A stock solution of neopentanol (25.2 mg, 28.6 μmol) was prepared in

THF (1.0 ml). The stock solution (0.1 ml) was added to the glass vial. Solution was further diluted with an additional THF (0.2 ml). Mixture was added to *L*-lactide (103.0 mg, 715.6 μmol) dissolved in PO (1.0 ml). The solution stirred at room temperature for 0.5 h before being quenched with a solution of 10 % HCl in MeOH. Volatiles were removed *in vacuo*. Monomer conversion was measured by ^1H NMR comparing the methine proton on *L*-Lactide (q, 5.0 ppm) to the methine protons on the poly(*L*-lactic acid) (broad, 5.15 ppm). Polymer was dissolved in CH_2Cl_2 precipitated into cold MeOH. *L*-lactide conversion = 64 %. Yield = 52 mg, 78 %. SEC: M_n (GPC) = 2.0 kDa. $M_w/M_n = 1.09$

Sample procedure for the copolymerization of propylene oxide and carbon dioxide

In a nitrogen-filled glove box, **2.9** (1.9 mg, 3.6 μmol) was weighed out into a glass vial. A stock solution of potassium neopentoxide (8.6 mg, 6.8 μmol) and 2.2.2-cryptand (25.6 mg, 6.8 μmol) was prepared in THF (2.0 ml). From the stock solution (0.2 ml) was added to the glass vial. A stock solution of neopentanol (25.2 mg, 28.6 μmol) was prepared in THF (1.0 ml). The stock solution (0.1 ml) was added to the glass vial. Solution was further diluted with additional THF (0.2 ml). Propylene oxide (1.00 ml, 14.3 μmol) was added to the vial. Ferrocenium tetrafluoroborate (1.0 mg, 3.6 μmol) was added to the vial.

The solution was transferred to a glass-lined, steel bomb reactor containing with a Teflon stir bar. Reactor was sealed and pressurized with 20 atm of CO_2 . Reaction was allowed to stir at room temperature for 24 h. Reactor was depressurized slowly and reaction mixture was quenched with 10 % HCl in MeOH. Volatiles were removed *in vacuo* and further dried on a Schleck line overnight. Conversion was measured by comparing the mass of the polymer to the theoretical mass at full conversion. Monomer conversion was verified by ^1H NMR through

comparing the methyl groups on neopentyl ester end group (s, 0.95 ppm) to the methylene peaks of poly(propylene carbonate)(dd, 4.18 ppm). Polymer was dissolved in CH₂Cl₂ and precipitated in cold MeOH. Propylene oxide conversion = 46.5 %. Yield = 621 mg, 91 %. SEC: M_n (GPC) = 18.3 kDa. M_w/M_n = 1.07.

Procedure for the redox-switchable polymerization of L-lactide

In a nitrogen-filled glove box, **2.9** (1.9 mg, 3.6 μ mol) was weighed out into a glass vial with a teflon-coated stir bar. A stock solution of potassium neopentoxide (8.6 mg, 6.8 μ mol) and 2.2.2-cryptand (25.6 mg, 6.8 μ mol) was prepared in THF (2.0 ml). From the stock solution (0.2 ml) was added to the glass vial. A stock solution of neopentanol (25.2 mg, 28.6 μ mol) was prepared in THF (1.0 ml). The stock solution (0.1 ml) was added to the glass vial. Solution was further diluted with additional THF (0.2 ml). The mixture was added to L-lactide (514.9 mg, 14.30 μ mol) dissolved in PO (1.0 ml). The solution stirred at room temperature for 10 min with samples (0.075 ml) taken at 1, 2, 5 and 10 min before being quenched with 4-nitrophenol. After 10 min, ferrocenium tetrafluoroborate (0.8 mg, 3 μ mol) was added to the solution.

The solution stirred at room temperature for another 30 min with samples (0.075 ml) taken at 20, 40 and 70 min and quenched with 4-nitrophenol. The reaction mixture was added to decamethylcobaltocene (0.8 mg, 2 μ mol) and samples (0.075 ml) were taken at 71, 72, 75, 80, 90 and 120 min before being quenched with 4-nitrophenol. For all samples, volatiles were removed *in vacuo*. Monomer conversion was measured with ¹H NMR by comparing the methine proton on L-Lactide (q, 5.0 ppm) to the methine protons on the poly(L-lactic acid) (b, 5.15 ppm). Polymer was dissolved in CH₂Cl₂ precipitated into cold MeOH. Final L-Lactide conversion = 86 %, SEC: M_n (GPC) = 11.9 kDa M_w/M_n = 1.28).

Procedure for the redox-switchable copolymerization of propylene oxide and carbon dioxide

In a nitrogen-filled glove box, **2.9** (3.8 mg, 7.2 μmol) was weighed out into a glass vial. A stock solution of potassium neopentoxide (8.6 mg, 6.8 μmol) and 2.2.2-cryptand (25.6 mg, 6.8 μmol) was prepared in THF (2.0 ml). From the stock solution (0.4 ml) was added to the glass vial. A stock solution of neopentanol (25.2 mg, 28.6 μmol) was prepared in THF (1.0 ml). The stock solution (0.2 ml) was added to the glass vial. Solution was further diluted with additional THF (0.4 ml). Propylene oxide (1.00 ml, 14.3 μmol) was added to the vial. Ferrocenium tetrafluoroborate (2.0 mg, 7.2 μmol) was added to the vial.

The solution was transferred to a glass-lined, steel bomb reactor containing with a Teflon stir bar. Reactor was sealed and pressurized with 20 atm of CO_2 . Reaction was allowed to stir at room temperature for 8 h. For sampling, reactor was depressurized in the glovebox, a sample (0.15 ml) of the solution and reactor was pressurized with 20 atm of CO_2 . Samples were taken at 1, 2, 4 and 8 h and quenched with 10 % HCl in MeOH. After 8 h, decamethylcobaltocene (1.9 mg, 5.7 μmol) was added to the solution. Reactor was pressurized with CO_2 and samples (0.15 ml) were taken at 9, 10 and 12 h and quenched with 10 % HCl in MeOH. Reactor was depressurized inside the glovebox and ferrocenium tetrafluoroborate (1.3 mg, 4.6 μmol) was added to the reaction mixture and the reactor was sealed and pressurized for another 4 h. Samples (0.15 ml) were taken at 13, 14, and 16 h and quenched with 10 % HCl in MeOH. Volatiles were removed *in vacuo*. Monomer conversion was determined by ^1H NMR by comparing the methyl groups on neopentyl ester end group (0.95 ppm) to the methylene peaks of poly(propylene carbonate) (4.18 ppm) and the methylene peak of cyclic propylene carbonate (t, 4.56 ppm) Polymer was dissolved in CH_2Cl_2 and precipitated in cold MeOH.

Propylene oxide conversion = 9.5 %. Product was predominantly propylene carbonate (88 %) and the final oligomer molecular weight was too small to detect by size exclusion chromatography

Standard procedure for the block copolymerization of *L*-lactide then propylene oxide and CO₂

In a nitrogen-filled glove box, **2.9** (1.9 mg, 3.6 μmol) was weighed out into a glass vial with a teflon-coated stir bar. A stock solution of potassium neopentoxide (8.6 mg, 6.8 μmol) and 2.2.2-cryptand (25.6 mg, 6.8 μmol) was prepared in THF (2.0 ml). The stock solution (0.2 ml) was added to the vial. A stock solution of neopentanol (25.2 mg, 28.6 μmol) was prepared in THF (1.0 ml). The stock solution (0.1 ml) was added to the glass vial. Solution was further diluted with additional THF (0.2 ml). Mixture was added to *L*-lactide (103.0 mg, 715.6 μmol) dissolved in PO (1.0 ml). The solution stirred at room temperature for 2 h before 1/2 of the volume was taken for sampling (0.75 ml). Sample was quenched with a solution of 10 % HCl in MeOH. Volatiles were removed *in vacuo* and monomer conversion was measured by ¹H NMR by comparing the methine protons on the *L*-lactide (q, 5.00 ppm) to the methine proton on the poly(lactic acid) (b, 5.15 ppm). Polymer was dissolved in CH₂Cl₂ precipitated into cold MeOH. *L*-Lactide conversion = 85 %. Yield = 30.2 mg (69 %) SEC: $M_n(\text{GPC}) = 2.7 \text{ kDa}$ $M_w/M_n = 1.22$.

Ferrocenium tetrafluoroborate (0.5 mg, 2 μmol) was added to the remaining solution which was then transferred to a glass-lined, steel bomb reactor. Reactor was sealed and pressurized with 20 atm of CO₂. Reaction was allowed to stir at room temperature for 48 h. Reactor was depressurized slowly inside a glove box and the remaining solution was quenched with 10 % HCl in MeOH. Volatiles were removed *in vacuo* and further dried on a Schleck line overnight. Monomer conversion was measured by ¹H NMR by comparing the methine protons

on the *L*-lactide (q, 5.00 ppm) to the methine proton on the poly(lactic acid) (b, 5.15 ppm) and the methylene protons on poly(propylene carbonate) (b, 4.18 ppm). Polymer was dissolved in CH₂Cl₂ precipitated into cold MeOH. *L*-Lactide conversion = 85 %. Propylene oxide conversion (3.1 %) Yield = 52.5 mg (79 %) SEC: (M_n (GPC) = 4.6 kDa M_w/M_n = 1.03).

Standard procedure for the block copolymerization of propylene oxide and CO₂ then *L*-lactide

In a nitrogen-filled glove box, **2.9** (1.9 mg, 3.6 μmol) was weighed out into a glass vial. A stock solution of potassium neopentoxide (8.6 mg, 6.8 μmol) and 2.2.2-cryptand (25.6 mg, 6.8 μmol) was prepared in THF (2.0 ml). From the stock solution (0.2 ml) was added to the glass vial. A stock solution of neopentanol (25.2 mg, 28.6 μmol) was prepared in THF (1.0 ml). The stock solution (0.1 ml) was added to the glass vial. Solution was further diluted with additional THF (0.2 ml). Propylene oxide (1.00 ml, 14.3 μmol) was added to the vial. Ferrocenium tetrafluoroborate (1.0 mg, 3.6 μmol) was added to the vial.

The solution was transferred to a glass-lined, steel bomb reactor containing a Teflon stir bar. Reactor was sealed and pressurized with 20 atm of CO₂. Reaction was allowed to stir at room temperature for 8 h. The reactor was depressurized slowly in the glovebox and 1/2 of the reaction mixture was quenched with 10 % HCl in MeOH. Volatiles were removed *in vacuo*. Monomer conversion was determined by ¹H NMR by comparing the methyl groups on neopentyl ester end group (s, 0.95 ppm) to the methylene peaks of poly(propylene carbonate) (dd, 4.18 ppm). Polymer was dissolved in CH₂Cl₂ and precipitated in cold MeOH. Propylene oxide conversion = 11.2 %. Yield = mg, %. SEC: M_n (GPC) = 5.1 kDa. M_w/M_n = 1.10.

The remaining solution was added to decamethylcobaltocene (0.6 mg, 2 μmol) and *L*-lactide (103.0 mg, 715.6 μmol) in a glass vial allowed to stir at room temperature under

nitrogen for 8 h. The remaining solution was quenched with 10 % HCl in MeOH. Volatiles were removed *in vacuo*. Monomer conversion was measured with ^1H NMR by comparing the methine protons on the *L*-lactide (q, 5.00 ppm) to the methine proton on the poly(lactic acid) (b, 5.15 ppm) and the methylene protons on poly(propylene carbonate) (b, 4.18 ppm). Polymer was dissolved in CH_2Cl_2 precipitated into cold MeOH. *L*-lactide conversion = >99 %, Propylene oxide conversion = 11.2 %. Yield = 170 mg, 92 %. SEC: M_n (GPC) = 11.0 kDa. M_w/M_n = 1.09.

Standard procedure for the statistical copolymerization of *L*-lactide, propylene oxide and CO_2

In a nitrogen-filled glove box, **2.9** (1.9 mg, 3.6 μmol) was weighed out into a glass vial with a teflon-coated stir bar. A stock solution of potassium neopentoxide (8.6 mg, 6.8 μmol) and 2.2.2-cryptand (25.6 mg, 6.8 μmol) was prepared in THF (2.00 ml). The stock solution (0.20 ml) was added to the vial. A stock solution of neopentanol (25.2 mg, 28.6 μmol) was prepared in THF (1.00 ml). The stock solution (0.10 ml) was added to the glass vial. Solution was further diluted with additional THF (0.20 ml). Ferrocenium tetrafluoroborate (0.9 mg, 3 μmol) was added to the vial. Mixture was added to *L*-lactide (102.3 mg, 715.6 μmol) dissolved in propylene oxide (1.00 ml) and loaded into a glass-lined steel pressure reactor.

The reactor was pressurized with 20 atm of CO_2 . The solution stirred at room temperature for 96 h. Reactor was slowly depressurized and solution was quenched 10 % HCl in MeOH. Volatiles were removed *in vacuo* and monomer conversion was measured with ^1H NMR by comparing the methine protons on the *L*-lactide (q, 5.00 ppm) to the methine proton on the poly(lactic acid) (b, 5.15 ppm) and the methylene protons on poly(propylene carbonate) (b, 4.18 ppm). Polymer was dissolved in CH_2Cl_2 precipitated into cold MeOH. Propylene oxide

conversion (53.3 %) L-lactide conversion (>99 %) Yield = 749 mg, 85%. SEC: M_n (GPC) = 27.6 kDa.
 $M_w/M_n = 1.07$.

2.9 References

- (1) H. E. Mogens Lykketoft. *The New Plastics Economy Rethinking the Future of Plastics*; 2014.
- (2) Conn, R. E.; Kolstad, J. J.; Borzelleca, J. F.; Dixler, D. S.; Filer, L. J.; Ladu, B. N.; Pariza, M. W. Safety Assessment of Polylactide (PLA) for Use as a Food-Contact Polymer. *Food and Chemical Toxicology* **1995**, *33* (4), 273–283. [https://doi.org/10.1016/0278-6915\(94\)00145-E](https://doi.org/10.1016/0278-6915(94)00145-E).
- (3) Abioye, A. A.; Afolalu, S. A.; Yusuf, O. O.; Emetere, M. E.; Ongbali, S. O.; Arubayi, O. C.; Imade, K. I.; Olayinka, A. Enhancing the Production of Bioplastics for Sustainable Recycling and Biodegradation-Short Review. *IOP Conference Series: Materials Science and Engineering* **2021**, *1107* (1), 012180. <https://doi.org/10.1088/1757-899x/1107/1/012180>.
- (4) Nandakumar, A.; Chuah, J. A.; Sudesh, K. Bioplastics: A Boon or Bane? *Renewable and Sustainable Energy Reviews* **2021**, *147* (May), 111237. <https://doi.org/10.1016/j.rser.2021.111237>.
- (5) Di Bartolo, A.; Infurna, G.; Dintcheva, N. T. A Review of Bioplastics and Their Adoption in the Circular Economy. *Polymers* **2021**, *13* (8). <https://doi.org/10.3390/polym13081229>.
- (6) European Bioplastics. Bioplastics Market Development Update 2019. **2018**, 2019, 2018–2019.

- (7) McKeen, L. W. Plastics Used in Medical Devices. In *Handbook of Polymer Applications in Medicine and Medical Devices*; 2014; pp 21–53.
- (8) Lee, S. Y. Life Cycle Analysis: Comparing PLA Plastic Food Use Products on the Basis of Energy Consumption. *International Journal of Energy, Environment, and Economics* **2009**, *2* (February), 69–75.
- (9) Farah, S.; Anderson, D. G.; Langer, R. Physical and Mechanical Properties of PLA, and Their Functions in Widespread Applications — A Comprehensive Review. *Advanced Drug Delivery Reviews* **2016**, *107*, 367–392. <https://doi.org/10.1016/j.addr.2016.06.012>.
- (10) Fuoco, T.; Finne-Wistrand, A.; Pappalardo, D. A Route to Aliphatic Poly(Ester)s with Thiol Pendant Groups: From Monomer Design to Editable Porous Scaffolds. *Biomacromolecules* **2016**, *17* (4), 1383–1394. <https://doi.org/10.1021/acs.biomac.6b00005>.
- (11) Sinclair, F.; Shaver, M. P. Cross-Metathesis Functionalized Exo-Olefin Derivatives of Lactide. *Journal of Polymer Science, Part A: Polymer Chemistry* **2018**, *56* (7), 741–748. <https://doi.org/10.1002/pola.28947>.
- (12) Gerhardt, W. W.; Noga, D. E.; Hardcastle, K. I.; García, A. J.; Collard, D. M.; Weck, M. Functional Lactide Monomers: Methodology and Polymerization. *Biomacromolecules* **2006**, *7* (6), 1735–1742. <https://doi.org/10.1021/bm060024j>.
- (13) Bandelli, D.; Alex, J.; Helbing, C.; Ueberschaar, N.; Görls, H.; Bellstedt, P.; Weber, C.; Jandt, K. D.; Schubert, U. S. Poly(3-Ethylglycolide): A Well-Defined Polyester Matching the Hydrophilic Hydrophobic Balance of PLA. *Polymer Chemistry* **2019**, *10* (40), 5440–5451. <https://doi.org/10.1039/c9py00875f>.

- (14) Nishida, H.; Andou, Y.; Watanabe, K.; Arazoe, Y.; Ide, S.; Shirai, Y. Poly(Tetramethyl Glycolide) from Renewable Carbon, a Racemization-Free and Controlled Depolymerizable Polyester. *Macromolecules* **2011**, *44* (1), 12–13. <https://doi.org/10.1021/ma102289w>.
- (15) Jia, Z.; Jiang, J.; Zhang, X.; Cui, Y.; Chen, Z.; Pan, X.; Wu, J. Isotactic-Alternating, Heterotactic-Alternating, and ABAA-Type Sequence-Controlled Copolyester Syntheses via Highly Stereoselective and Regioselective Ring-Opening Polymerization of Cyclic Diesters. *Journal of the American Chemical Society* **2021**, *143* (11), 4421–4432. <https://doi.org/10.1021/jacs.1c00902>.
- (16) Sasanuma, Y.; Takahashi, Y. Structure-Property Relationships of Poly(Ethylene Carbonate) and Poly(Propylene Carbonate). *ACS Omega* **2017**, *2* (8), 4808–4819. <https://doi.org/10.1021/acsomega.7b00964>.
- (17) Luinstra, G. A. Poly(Propylene Carbonate), Old Copolymers of Propylene Oxide and Carbon Dioxide with New Interests: Catalysis and Material Properties. *Polymer Reviews* **2008**, *48* (1), 192–219. <https://doi.org/10.1080/15583720701834240>.
- (18) Luinstra, G. A.; Borchardt, E. Material Properties of Poly(Propylene Carbonates). **2011**, No. June 2011, 29–48. https://doi.org/10.1007/12_2011_126.
- (19) Mizuno, N.; Yamaguchi, K.; Kamata, K. Epoxidation of Olefins with Hydrogen Peroxide Catalyzed by Polyoxometalates. *Coordination Chemistry Reviews* **2005**, *249* (17-18 SPEC. ISS.), 1944–1956. <https://doi.org/10.1016/j.ccr.2004.11.019>.
- (20) De Faveri, G.; Ilyashenko, G.; Watkinson, M. Recent Advances in Catalytic Asymmetric Epoxidation Using the Environmentally Benign Oxidant Hydrogen Peroxide and Its Derivatives. *Chemical Society Reviews* **2011**, *40* (3), 1722–1760.

- <https://doi.org/10.1039/c0cs00077a>.
- (21) Poland, S. J.; Darensbourg, D. J. A Quest for Polycarbonates Provided: Via Sustainable Epoxide/CO₂ Copolymerization Processes. *Green Chemistry* **2017**, *19* (21), 4990–5011. <https://doi.org/10.1039/c7gc02560b>.
- (22) Li, H.; Niu, Y. Alternating Copolymerization of CO₂ with Propylene Oxide and Terpolymerization with Aliphatic Epoxides by Bifunctional Cobalt Salen Complex. *Polymer Journal* **2011**, *43* (2), 121–125. <https://doi.org/10.1038/pj.2010.112>.
- (23) Scharfenberg, M.; Hofmann, S.; Preis, J.; Hilf, J.; Frey, H. Rigid Hyperbranched Polycarbonate Polyols from CO₂ and Cyclohexene-Based Epoxides. *Macromolecules* **2017**, *50* (16), 6088–6097. <https://doi.org/10.1021/acs.macromol.7b01276>.
- (24) Scharfenberg, M.; Hilf, J.; Frey, H. Functional Polycarbonates from Carbon Dioxide and Tailored Epoxide Monomers: Degradable Materials and Their Application Potential. *Advanced Functional Materials* **2018**, *28* (10), 1–16. <https://doi.org/10.1002/adfm.201704302>.
- (25) Ma, X.; Jiugao, Y.; Wang, N. Compatibility Characterization of Poly(Lactic Acid)/Poly(Propylene Carbonate) Blends. *Journal of Polymer Science, Part B: Polymer Physics* **2006**, *44* (1), 94–101. <https://doi.org/10.1002/polb.20669>.
- (26) Sun, Q.; Mekonnen, T.; Misra, M.; Mohanty, A. K. Novel Biodegradable Cast Film from Carbon Dioxide Based Copolymer and Poly(Lactic Acid). *Journal of Polymers and the Environment* **2016**, *24* (1), 23–36. <https://doi.org/10.1007/s10924-015-0743-6>.
- (27) Li, Y.; Yu, Y. C.; Han, C. Y.; Wang, X. H.; Huang, D. X. Sustainable Blends of Poly(Propylene Carbonate) and Stereocomplex Polylactide with Enhanced Rheological Properties and

- Heat Resistance. *Chinese Journal of Polymer Science (English Edition)* **2020**, *38* (11), 1267–1275. <https://doi.org/10.1007/s10118-020-2408-8>.
- (28) Dong, X.; Liu, L.; Wang, Y.; Li, T.; Wu, Z.; Yuan, H.; Ma, P.; Shi, D.; Chen, M.; Dong, W. The Compatibilization of Poly (Propylene Carbonate)/Poly (Lactic Acid) Blends in Presence of Core-Shell Starch Nanoparticles. *Carbohydrate Polymers* **2021**, *254* (October 2020), 117321. <https://doi.org/10.1016/j.carbpol.2020.117321>.
- (29) Hao, Y. ping; Yang, H. li; Zhang, G. bao; Zhang, H. liang; Gao, G.; Dong, L. song. Rheological, Thermal and Mechanical Properties of Biodegradable Poly(Propylene Carbonate)/Polylactide/Poly(1,2-Propylene Glycol Adipate) Blown Films. *Chinese Journal of Polymer Science (English Edition)* **2015**, *33* (12), 1702–1712. <https://doi.org/10.1007/s10118-015-1714-z>.
- (30) Galloway, J. A.; Jeon, H. K.; Bell, J. R.; MacOsko, C. W. Block Copolymer Compatibilization of Cocontinuous Polymer Blends. *Polymer* **2005**, *46* (1), 183–191. <https://doi.org/10.1016/j.polymer.2004.10.061>.
- (31) Zhou, L.; Zhao, G.; Jiang, W. Effects of Catalytic Transesterification and Composition on the Toughness of Poly(Lactic Acid)/Poly(Propylene Carbonate) Blends. *Industrial and Engineering Chemistry Research* **2016**, *55* (19), 5565–5573. <https://doi.org/10.1021/acs.iecr.6b00315>.
- (32) Qin, S. X.; Yu, C. X.; Chen, X. Y.; Zhou, H. P.; Zhao, L. F. Fully Biodegradable Poly(Lactic Acid)/Poly(Propylene Carbonate) Shape Memory Materials with Low Recovery Temperature Based on in Situ Compatibilization by Dicumyl Peroxide. *Chinese Journal of Polymer Science (English Edition)* **2018**, *36* (6), 783–790. <https://doi.org/10.1007/s10118->

018-2065-3.

- (33) Wang, Z.; Zhang, M.; Liu, Z.; Zhang, S.; Cao, Z.; Yang, W.; Yang, M. Compatibilization of the Poly(Lactic Acid)/Poly(Propylene Carbonate) Blends through in Situ Formation of Poly(Lactic Acid)-b-Poly(Propylene Carbonate) Copolymer. *Journal of Applied Polymer Science* **2018**, *135* (11), 1–15. <https://doi.org/10.1002/app.46009>.
- (34) Darensbourg, D. J.; Wu, G. P. A One-Pot Synthesis of a Triblock Copolymer from Propylene Oxide/Carbon Dioxide and Lactide: Intermediacy of Polyol Initiators. *Angewandte Chemie - International Edition* **2013**, *52* (40), 10602–10606. <https://doi.org/10.1002/anie.201304778>.
- (35) Hu, C.; Duan, R.; Yang, S.; Pang, X.; Chen, X. CO₂ Controlled Catalysis: Switchable Homopolymerization and Copolymerization. *Macromolecules* **2018**, *51* (12), 4699–4704. <https://doi.org/10.1021/acs.macromol.8b00696>.
- (36) Gu, L.; Qin, Y.; Gao, Y.; Wang, X.; Wang, F. One-Pot Terpolymerization of CO₂, Propylene Oxide and Lactide Using Rare-Earth Ternary Catalyst. *Chinese Journal of Chemistry* **2012**, *30* (9), 2121–2125. <https://doi.org/10.1002/cjoc.201200636>.
- (37) Tang, L.; Luo, W.; Xiao, M.; Wang, S.; Meng, Y. One-Pot Synthesis of Terpolymers with Long l-Lactide Rich Sequence Derived from Propylene Oxide, CO₂, and l-Lactide Catalyzed by Zinc Adipate. *Journal of Polymer Science, Part A: Polymer Chemistry* **2015**, *53* (14), 1734–1741. <https://doi.org/10.1002/pola.27617>.
- (38) Liu, N.; Gu, C.; Chen, M.; Zhang, J.; Yang, W.; Zhan, A.; Zhang, K.; Lin, Q.; Zhu, L. Terpolymerizations of CO₂, Propylene Oxide and DL-Lactide Catalyzed by Zn-Fe DMC Catalysts with Quaternary Ammonium Salts. *ChemistrySelect* **2020**, *5* (8), 2388–2394.

<https://doi.org/10.1002/slct.201904461>.

- (39) Li, X.; Duan, R. L.; Hu, C. Y.; Pang, X.; Deng, M. X. Copolymerization of Lactide, Epoxides and Carbon Dioxide: A Highly Efficient Heterogeneous Ternary Catalyst System. *Polymer Chemistry* **2021**, *12* (11), 1700–1706. <https://doi.org/10.1039/d0py01592j>.
- (40) Sulley, G. S.; Gregory, G. L.; Chen, T. T. D.; Peña Carrodeguas, L.; Trott, G.; Santmarti, A.; Lee, K. Y.; Terrill, N. J.; Williams, C. K. Switchable Catalysis Improves the Properties of CO₂-Derived Polymers: Poly(Cyclohexene Carbonate- b-ε-Decalactone- b-Cyclohexene Carbonate) Adhesives, Elastomers, and Toughened Plastics. *Journal of the American Chemical Society* **2020**, *142* (9), 4367–4378. <https://doi.org/10.1021/jacs.9b13106>.
- (41) Romain, C.; Zhu, Y.; Dingwall, P.; Paul, S.; Rzepa, H. S.; Buchard, A.; Williams, C. K. Chemoselective Polymerizations from Mixtures of Epoxide, Lactone, Anhydride, and Carbon Dioxide. *Journal of the American Chemical Society* **2016**, *138*, 4120–4131.
- (42) Chen, T. T. D.; Zhu, Y.; Williams, C. K. Pentablock Copolymer from Tetracomponent Monomer Mixture Using a Switchable Dizinc Catalyst. *Macromolecules* **2018**, *51* (14), 5346–5351. <https://doi.org/10.1021/acs.macromol.8b01224>.
- (43) Paul, S.; Zhu, Y.; Romain, C.; Brooks, R.; Saini, P. K.; Williams, C. K. Ring-Opening Copolymerization (ROCOP): Synthesis and Properties of Polyesters and Polycarbonates. *Chemical Communications* **2015**, *51* (30), 6459–6479. <https://doi.org/10.1039/c4cc10113h>.
- (44) Kernbichl, S.; Reiter, M.; Adams, F.; Vagin, S.; Rieger, B. CO₂-Controlled One-Pot Synthesis of AB, ABA Block, and Statistical Terpolymers from β-Butyrolactone, Epoxides, and CO₂. *Journal of the American Chemical Society* **2017**, *139*, 6787–6790.

- (45) Kernbichl, S.; Reiter, M.; Mock, J.; Rieger, B. Terpolymerization of β -Butyrolactone, Epoxides, and CO₂: Chemoselective CO₂-Switch and Its Impact on Kinetics and Material Properties. *Macromolecules* **2019**, *52* (21), 8476–8483.
<https://doi.org/10.1021/acs.macromol.9b01777>.
- (46) Qi, M.; Dong, Q.; Wang, D.; Byers, J. A. Electrochemically Switchable Ring-Opening Polymerization of Lactide and Cyclohexene Oxide. *Journal of the American Chemical Society* **2018**, *140* (17), 5686–5690. <https://doi.org/10.1021/jacs.8b02171>.
- (47) Qi, M.; Zhang, H.; Dong, Q.; Li, J.; Musgrave, R. A.; Zhao, Y.; Dulock, N.; Wang, D.; Byers, J. A. Electrochemically Switchable Polymerization from Surface-Anchored Molecular Catalysts. *Chemical Science* **2021**. <https://doi.org/10.1039/d1sc02163j>.
- (48) Delle Chiaie, K. R.; Yablon, L. M.; Biernesser, A. B.; Michalowski, G. R.; Sudyn, A. W.; Byers, J. A. Redox-Triggered Crosslinking of a Degradable Polymer. *Polymer Chemistry* **2016**, *7* (28), 4675–4681. <https://doi.org/10.1039/c6py00975a>.
- (49) Biernesser, A. B.; Li, B.; Byers, J. A. Redox-Controlled Polymerization of Lactide Catalyzed by Bis(Imino)Pyridine Iron Bis(Alkoxide) Complexes. *Journal of the American Chemical Society* **2013**, *135* (44), 16553–16560. <https://doi.org/10.1021/ja407920d>.
- (50) Biernesser, A. B.; Delle Chiaie, K. R.; Curley, J. B.; Byers, J. A. Block Copolymerization of Lactide and an Epoxide Facilitated by a Redox Switchable Iron-Based Catalyst. *Angewandte Chemie* **2016**, *128* (17), 5337–5340.
<https://doi.org/10.1002/ange.201511793>.
- (51) Broderick, E. M.; Guo, N.; Wu, T.; Vogel, C. S.; Xu, C.; Sutter, J.; Miller, J. T.; Meyer, K.; Cantat, T.; Diaconescu, P. L. Redox Control of a Polymerization Catalyst by Changing the

- Oxidation State of the Metal Center. *Chemical Communications* **2011**, 47 (35), 9897–9899. <https://doi.org/10.1039/c1cc13117f>.
- (52) Hatazawa, M.; Nakabayashi, K.; Ohkoshi, S. ichi; Nozaki, K. In Situ Generation of Coll–Salen Complexes for Copolymerization of Propylene Oxide and CO₂. *Chemistry - A European Journal* **2016**, 22 (38), 13677–13681. <https://doi.org/10.1002/chem.201602546>.
- (53) Cohen, C. T.; Chu, T.; Coates, G. W. Cobalt Catalysts for the Alternating Copolymerization of Propylene Oxide and Carbon Dioxide: Combining High Activity and Selectivity. *Journal of the American Chemical Society* **2005**, 127 (31), 10869–10878. <https://doi.org/10.1021/ja051744l>.
- (54) S, S.; Min, J. K.; Seong, J. E.; Na, S. J.; Lee, B. Y. A Highly Active and Recyclable Catalytic System for CO₂/Propylene Oxide Copolymerization. *Angewandte Chemie - International Edition* **2008**, 47 (38), 7306–7309. <https://doi.org/10.1002/anie.200801852>.
- (55) Sipos, L., Zsuga, M., Kelen, T. Living Ring-Opening Polymerization of L,L-Lactide Initiated with Potassium t-Butoxide and Its 18-Crown-6 Complex. *Polymer Bulletin* **1992**, 27 (5), 495–502.
- (56) Sipos, L.; Dunda, T.; Zsuga, M. The Role of Complex Formation in the Anionic Polymerization of L-Lactide. *Polymer Bulletin* **1997**, 38, 609–612.
- (57) Wu, B. B.; Tian, L. L.; Wang, Z. X. Ring-Opening Polymerization of Rac-Lactide Catalyzed by Crown Ether Complexes of Sodium and Potassium Iminophenoxides. *RSC Advances* **2017**, 7 (39), 24055–24063. <https://doi.org/10.1039/c7ra03394j>.
- (58) Fernández-Millán, M.; Ortega, P.; Cuenca, T.; Cano, J.; Mosquera, M. E. G. Alkali-Metal

- Compounds with Bio-Based Ligands as Catalysts for Ioselective Lactide Polymerization: Influence of the Catalyst Aggregation on the Polymerization Control. *Organometallics* **2020**, *39* (12), 2278–2286. <https://doi.org/10.1021/acs.organomet.0c00237>.
- (59) Darensbourg, D. J. Making Plastics from Carbon Dioxide: Salen Metal Complexes as Catalysts for the Production of Polycarbonates from Epoxides and CO₂. *Chemical Reviews* **2007**, *107* (6), 2388–2410. <https://doi.org/10.1021/cr068363q>.
- (60) Offermans, W. K.; Bizzarri, C.; Leitner, W.; Müller, T. E. Surprisingly Facile CO₂ Insertion into Cobalt Alkoxide Bonds: Theoretical Investigation. *Beilstein Journal of Organic Chemistry* **2015**, *11*, 1340–1351. <https://doi.org/10.3762/bjoc.11.144>.
- (61) Darensbourg, D. J.; Wu, G. P. A One-Pot Synthesis of a Triblock Copolymer from Propylene Oxide/Carbon Dioxide and Lactide: Intermediacy of Polyol Initiators. *Angewandte Chemie - International Edition* **2013**, *52* (40), 10602–10606. <https://doi.org/10.1002/anie.201304778>.
- (62) Delle Chiaie, K. R.; Biernesser, A. B.; Ortuño, M. A.; Dereli, B.; Iovan, D. A.; Wilding, M. J. T.; Li, B.; Cramer, C. J.; Byers, J. A.; Delle Chiaie, K. R.; et al. Block Copolymerization of Lactide and an Epoxide Facilitated by a Redox Switchable Iron-Based Catalyst. *Dalton Transactions* **2017**, *128* (38), 12971–12980. <https://doi.org/10.1039/c7dt03067c>.
- (63) Wang, X.; Thevenon, A.; Brosmer, J. L.; Yu, I.; Khan, S. I.; Mehrkhodavandi, P.; Diaconescu, P. L. Redox Control of Group 4 Metal Ring-Opening Polymerization Activity toward L-Lactide and ϵ -Caprolactone. *Journal of the American Chemical Society* **2014**, *136* (32), 11264–11267. <https://doi.org/10.1021/ja505883u>.
- (64) Lowe, M. Y.; Shu, S.; Quan, S. M.; Diaconescu, P. L. Investigation of Redox Switchable

- Titanium and Zirconium Catalysts for the Ring Opening Polymerization of Cyclic Esters and Epoxides. *Inorganic Chemistry Frontiers* **2017**, *4* (11), 1798–1805.
<https://doi.org/10.1039/c7qi00227k>.
- (65) Qin, Z.; Thomas, C. M.; Lee, S.; Coates, G. W. Cobalt-Based Complexes for the Copolymerization of Propylene Oxide and CO₂: Active and Selective Catalysts for Polycarbonate Synthesis. *Angewandte Chemie - International Edition* **2003**, *42* (44), 5484–5487. <https://doi.org/10.1002/anie.200352605>.
- (66) Lu, X. B.; Shi, L.; Wang, Y. M.; Zhang, R.; Zhang, Y. J.; Peng, X. J.; Zhang, Z. C.; Li, B. Design of Highly Active Binary Catalyst Systems for CO₂/Epoxide Copolymerization: Polymer Selectivity, Enantioselectivity, and Stereochemistry Control. *Journal of the American Chemical Society* **2006**, *128* (5), 1664–1674. <https://doi.org/10.1021/ja056383o>.
- (67) Xia, W.; Salmeia, K. A.; Vagin, S. I.; Rieger, B. Concerning the Deactivation of Cobalt(III)-Based Porphyrin and Salen Catalysts in Epoxide/CO₂ Copolymerization. *Chemistry - A European Journal* **2015**, *21* (11), 4384–4390. <https://doi.org/10.1002/chem.201406258>.
- (68) Diccio, A. M.; Longo, J. M.; Rodríguez-Calero, G. G.; Coates, G. W. Development of Highly Active and Regioselective Catalysts for the Copolymerization of Epoxides with Cyclic Anhydrides: An Unanticipated Effect of Electronic Variation. *Journal of the American Chemical Society* **2016**, *138* (22), 7107–7113.
<https://doi.org/10.1021/jacs.6b03113>.
- (69) Jiang, Y. J.; Ren, W. M.; Liu, Y.; Lu, X. B. Synthesis of Polycarbonate Block Terpolymers Using Robust Cobalt Catalyst Systems. *Chinese Journal of Polymer Science (English Edition)* **2019**, *37* (12), 1200–1204. <https://doi.org/10.1007/s10118-019-2270-8>.

- (70) Floriani, C.; Calderazzo, F. Oxygen Adducts of Schiff's Base Complexes Of. *J. Chem. Soc. (A)* **1969**, No. 946, 946–953.
- (71) Adduct, M. D.; Huie, B. E. N. T.; Kurilla, M. G.; Ealick, S. E. Oxygen-Carrying Cobalt Complexes. 10. Structures of N,N'-Ethylenebis(3-Tert-Butylsaliylideniminato)Cobalt(II) and Its Monomeric Dioxygen Adduct. *Inorg. Chem.* **1980**, *19* (2), 340–344.
- (72) Cohen, C. T.; Coates, G. W. Alternating Copolymerization of Propylene Oxide and Carbon Dioxide with Highly Efficient and Selective (Salen)Co(III) Catalysts: Effect of Ligand and Cocatalyst Variation. *Journal of Polymer Science: Part A: Polymer Chemistry* **2006**, *44*, 5182–5191. <https://doi.org/10.1002/pola>.
- (73) Jedlinski, Z.; Kowalczyk, M.; Glówkowski, W.; Grobelny, J.; Szwarc, M. Novel Polymerization of β -Butyrolactone Initiated by Potassium Naphthalenide in the Presence of a Crown Ether or a Cryptand. *Macromolecules* **1991**, *24* (2), 349–352. <https://doi.org/10.1021/ma00002a002>.
- (74) Ren, W. M.; Liu, Z. W.; Wen, Y. Q.; Zhang, R.; Lu, X. B. Mechanistic Aspects of the Copolymerization of CO₂ with Epoxides Using a Thermally Stable Single-Site Cobalt(III) Catalyst. *Journal of the American Chemical Society* **2009**, *131* (32), 11509–11518. <https://doi.org/10.1021/ja9033999>.
- (75) Jia, M.; Hadjichristidis, N.; Gnanou, Y.; Feng, X. Monomodal Ultrahigh-Molar-Mass Polycarbonate Homopolymers and Diblock Copolymers by Anionic Copolymerization of Epoxides with CO₂. *ACS Macro Letters* **2019**, *8* (12), 1594–1598. <https://doi.org/10.1021/acsmacrolett.9b00854>.
- (76) Philipps, K.; Junkers, T.; Michels, J. J. The Block Copolymer Shuffle in Size Exclusion

- Chromatography: The Intrinsic Problem with Using Elugrams to Determine Chain Extension Success. *Polymer Chemistry* **2021**, *12* (17), 2522–2531.
<https://doi.org/10.1039/d1py00210d>.
- (77) Li, X.; Hu, C.; Pang, X.; Duan, R.; Chen, X. One-Pot Copolymerization of Epoxides/Carbon Dioxide and Lactide Using a Ternary Catalyst System. *Catalysis Science and Technology* **2018**, *8* (24), 6452–6457. <https://doi.org/10.1039/c8cy01856a>.
- (78) Ren, W. M.; Zhang, X.; Liu, Y.; Li, J. F.; Wang, H.; Lu, X. B. Highly Active, Bifunctional Co(III)-Salen Catalyst for Alternating Copolymerization of CO₂ with Cyclohexene Oxide and Terpolymerization with Aliphatic Epoxides. *Macromolecules* **2010**, *43* (3), 1396–1402. <https://doi.org/10.1021/ma902321g>.
- (79) Deb, M.; Hazra, S.; Dolui, P.; Elias, A. J. Ferrocenium Promoted Oxidation of Benzyl Amines to Imines Using Water as the Solvent and Air as the Oxidant. *ACS Sustainable Chemistry and Engineering* **2019**, *7* (1), 479–486.
<https://doi.org/10.1021/acssuschemeng.8b03966>.
- (80) Hanawalt, E. M.; Farkas, J.; Richey, H. G. Organomagnesates from Reactions of Dialkylmagnesium Compounds with Alkali-Metal Alkoxides, Potassium Hydride, and Other Salts. *Organometallics* **2004**, *23* (3), 416–422.
<https://doi.org/10.1021/om030544k>.
- (81) Berger, B. J.; Bercaw, J. E. Vacuum Line Techniques for Handling Air-Sensitive Organometallic Compounds. In *Experimental Organometallic Chemistry*; 1987; pp 79-115.

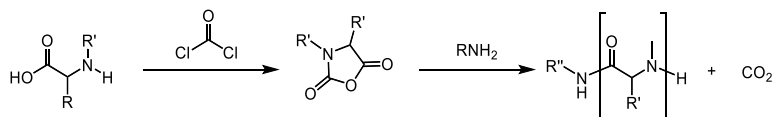
3.0 Chapter 3. Redox-switchable, *N*-carboxyanhydride Polymerization and Applications for Copolymerization

3.1 Introduction

When it comes to materials that are both lightweight and strong¹⁻³ with high thermal stability⁴, polyamides have little competition. Industrial polyamides are predominantly formed through step growth polymerizations from diamine and diacid⁵ starting materials. These polyamides find uses as textiles and fibers as well as engineering materials.^{1,5,6} Biodegradable polyamides from amino acids have an even greater diversity of functions as not only fibers⁷ and structural materials⁸, but also as gels,⁹ catalysts¹⁰ and drugs¹¹ due to their precise ordering^{12,13} and variety of functionalized side chains. While nature routinely polymerizes amino acids using enzymes, large, synthetic poly(amino acid)s are typically derived from *N*-carboxyanhydride (NCA) ring-opening polymerization (ROP).¹⁴

NCAs can be easily synthesized from the addition of amino acids to phosgene or a phosgene derivative (Scheme 3.1). The chain-growth polymerization of NCAs are most commonly achieved using primary amine initiators (referred to here as the simple amine method) in highly polar solvents like dimethylformamide.^{15,16} The polymerization is driven by the loss of CO₂ and the simple amine method typically produces polyamides with good control over molecular weight, but it often requires multiple days to reach full conversion at ambient conditions. There has been extensive progress to increase the rate of amine-initiated reactions, which include

Scheme 3.1. Synthesis of NCAs from amino acids and the polymerization of NCAs through the simple amine method.

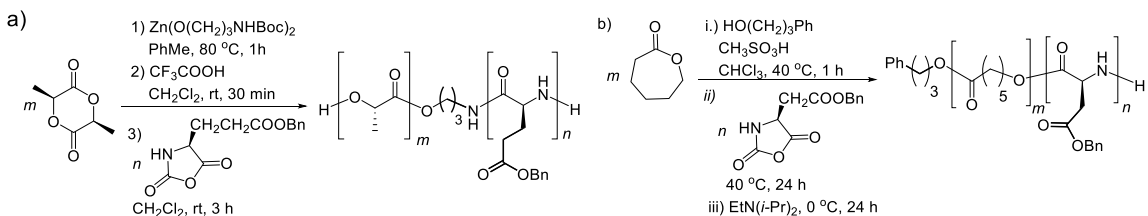


removing CO₂,^{17–20} using polyamine initiators,^{21–23} halogenated solvents,^{24,25} using biphasic systems with poly(ethylene glycol)-amine initiators,^{26,27} , strong bases^{28,29} as well as organocatalysts including N-heterocyclic carbenes^{30,31} and crown ethers.³² Metal-based catalysts for NCA polymerization have been shown to function as Lewis acids for amines or other nucleophilic initiators^{33–35}, bases to deprotonate-NCA NH bonds^{36–38} or precursors to form 5-member-ring metallocycles as the catalytic species.^{14,39–41} Despite the abundance of initiators and catalysts known to polymerize NCAs, there are few reports where NCAs undergo copolymerization with other cyclic monomers (e.g., lactones, epoxides, cyclic carbonates, etc.).^{42–45} The copolymers resulting from such reactions are attractive because they add the mechanical properties of the polyamides to commodity polymers,^{46–48} demonstrate improved biocompatibility and degradability,^{49,50} and/or undergo phase separation to make polymer micelles that are useful in drug delivery applications.^{51–53}

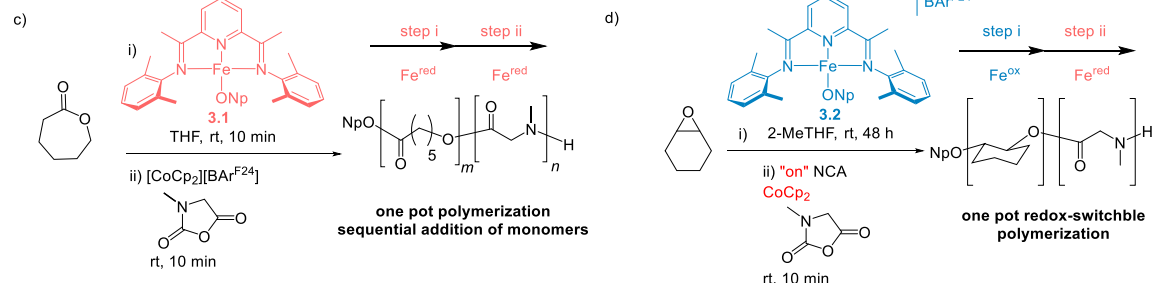
Most reported syntheses of polyamide block copolymers involve macromolecular initiators with amine end groups for the simple amine method of NCA polymerization.^{47,54–56} These macromolecular initiators can be virtually any class of polymer as long as post-polymerization functionalization or deprotection sequence produces a primary or secondary amine. This strategy allows for copolymers of olefins^{57,58}, polyethers,^{46,52,55,59} polyesters^{47,54–56} among others⁶⁰ to be synthesized, but the functionalization and deprotection steps can be difficult to carry out quantitatively and often require multiple purification steps. For example, Meyrueix and coworkers synthesized copolymers of *L*-lactide and γ -benzyl-*L*-glutamate-NCA by first polymerizing lactide through a zinc alkoxide catalyst containing a bifunctional initiator with an alcohol and a tert-butyl carbamate (BOC) protected amine moiety (Scheme 3.2a).⁵⁴ The resulting end group functionalized poly(*L*-lactic acid) was then isolated and purified before the BOC group was removed through the addition of trifluoroacetic acid. The polymer was then

Scheme 3.2. Previous methods to produce copolymers of polyamides and other polymers: (a) End group deprotection of a macroinitiator. (b) Sequential addition of strong acids and bases. Methods reported in this work using iron-based catalysts: (c) Sequential addition of monomers using; and (d) Redox-switchable copolymerization.

Previous work



This work



purified an additional time before being used as a macroinitiator for γ -benzyl-*L*-glutamate-NCA polymerization to synthesize the final copolymer. Each purification step required for copolymer synthesis adds to the cost and difficulty of developing these desirable materials.

There are only a few reports that describe the one-pot synthesis of block copolymers containing polyamides derived from NCAs and another monomer that can engage in ring-opening polymerization.⁴²⁻⁴⁵ Pahovnik and coworkers reported a general method that relies on single insertion of an NCA monomer to polyester or polycarbonate macroinitiators under acidic conditions followed by careful addition of base to initiate-NCA polymerization (Scheme 3.2b).⁴⁴ While this method provided access to poly(ester-*b*-amide) and poly(carbonate-*b*-amide) block copolymers, the multistage reactions took several days for completion. The Guo group demonstrated that tin octanoate can be used for the copolymerization of the *N*-substituted, sarcosine *N*-carboxyanhydride and ϵ -caprolactone.^{42,43} While the polymerization of sarcosine-NCA is rapid at room temperature under active nitrogen flow the subsequent polymerization of the lactone requires elevated temperatures (110 °C) to produce the desired poly(amide-*b*-ester). Herein, we describe a complementary approach that uses iron(II) bis(imino)pyridine-based catalysts, to carry out the efficient polymerization of NCAs. We also produce block copolymers either through sequential addition of monomers (for polyester copolymers, Scheme 3.2c) or through redox-switchable polymerization reactions (for polyether copolymers, Scheme 3.2d). The catalysis is efficient and proceeds in one pot, providing convenient access to useful polypeptide copolymers that incorporate other functional monomers.

3.2 Polymerization of *N*-Carboxyanhydrides by Redox-switchable Iron Bis(imino)pyridine Alkoxide Complexes

An emerging area in synthetic, polymer chemistry is switchable polymerization reactions,^{61,62} which rely on the application of an external stimulus to alter the reactivity of a polymerization reaction *in situ*. The switch can be used to alter polymer composition and/or architecture. As mentioned in chapter 1, a variety of stimuli have been used for switchable polymerizations with redox-switchable polymerization being notable for the diversity of application. Redox-switchable polymerizations have been demonstrated to produce block copolymers,^{63–66} to control polyolefin branching,^{67,68} trigger crosslinking reactions,⁶⁹ and create patterned surfaces.⁷⁰

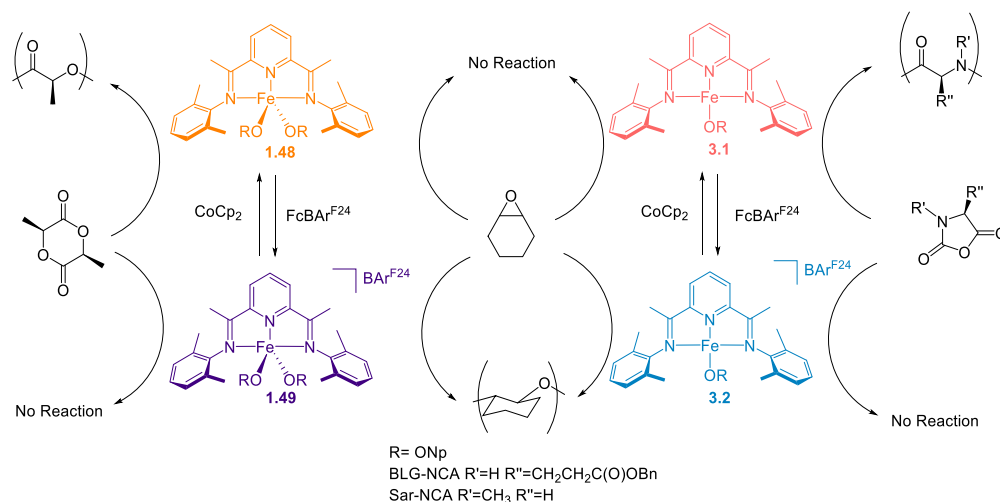
Over the past few years, we have been investigating a family of iron-based catalysts that have redox-switchable characteristics for the polymerization of lactide and epoxides (left, Scheme 3.3).^{64,66,70–73} We have leveraged this reactivity to control the monomer sequence in block copolymers starting from mixtures of monomers^{64,66} to develop redox-triggered crosslinking reactions,⁶⁹ and for patterning in surface-initiated polymerization reactions.⁷⁰ Recently, we have also developed an electrochemical method that can be used instead of chemical redox reagents to control the polymerization reactions.^{66,70} Although redox-switchable polymerization catalysts are known for cyclic olefins,^{74,75} lactones including lactide,^{71,76} and epoxides,^{64,65} they have not been demonstrated for the switchable polymerization of NCAs. We anticipated that the versatility of the bis(imino)pyridine iron complexes for ring opening polymerization reactions

could be exploited to create a redox-switchable catalytic system that would also be amenable for the production of block copolymers containing polyamides (right, Scheme 3.3).

We have previously reported the synthesis of iron bis(imino)pyridine complexes **1.48** and **1.49**^{64,71} as well as $(^{2,6}\text{MeBIP})\text{FeOCH}_2\text{C}(\text{CH}_3)_3$, **3.1**,^{72,73} which led to a family of complexes that differed by charge, formal oxidation state, and coordination number (Scheme 3.3). Access to a cationic iron complex **3.2** would provide a second possible catalyst combination (*i.e.*, **3.1** and **3.2**) that could be used for redox switching. We expected that this combination would demonstrate different reactivity for NCA polymerization compared to the original redox-switchable catalytic system (*i.e.*, **1.48** and **1.49**). Fortunately, complex **3.2** could be easily accessed by oxidizing neutral iron complex **3.1** with ferrocenium tetrakis[(3,5-bis(trifluoromethyl)phenyl)borate ($\text{FcBAr}^{\text{F24}}$), which proceeded cleanly as evidenced by ^1H , ^{11}B and ^{19}F NMR spectroscopy.

To understand what catalyst features are best for NCA polymerization, the activities of **1.48**, **1.49**, **3.1** and **3.2** were evaluated for the polymerization of γ -benzyl-*L*-glutamate-NCA (Table

Scheme 3.3. Iron bis(iminopyridine) alkoxide complexes used in redox-switchable copolymerizations of (left) lactide and cyclohexene oxide and (right) N-carboxyanhydride (NCAs) and cyclohexene oxide.



3.1). These studies revealed that neutral, iron complexes **1.48** and **3.1** were almost identical in overall conversion reaching 50% and 48 % conversion in 48 h (entries 3 and 6, Table 3.1). Full conversion of the monomer was not observed under these conditions. Due to how quickly the polymerization rate decays (Figure 3.1) without a significant broadening of dispersity we hypothesized the reduced activity is due to product inhibition rather than catalyst decomposition. The product inhibition would result from the coordination of the product, poly(γ -benzyl-*L*-glutamate), which contains nucleophilic amide groups that can compete with the monomer for coordination to the catalyst.

In order to get a better sense for the relative activities of **1.48** and **3.1** without complications from product inhibition, each catalyst precursor was evaluated by monitoring reactions at lower conversions (Figure 3.1). These experiments revealed that complex **1.48** and complex **3.1** have very similar reactivity with **3.1** being slightly more active than **1.48**. This trend is likely a consequence of **3.1** containing the more electron-rich metal center compared to **1.48** (formally Fe(I) vs. Fe(II), respectively), which is consistent with NCAs being more commonly polymerized with base initiators^{14,15} rather than acid catalysts.^{44,77} In contrast to **1.48** and **3.1**, cationic iron complexes **1.49** and **3.2** were much less active for γ -benzyl-*L*-glutamate-NCA polymerization. Reactions catalyzed by **1.49** were slow, leading to only 10 % conversion after 48 h with a broad molecular weight distribution and significant tailing towards higher molecular weights (entry 7, Table 3.1), while complex **3.2** did not react with γ -benzyl-*L*-glutamate-NCA even after extended reaction times (entry 8, Table 3.1). Metal catalyzed coordination-insertion ROP generally involves both electrophilic activation at the metal center and the nucleophilicity of the initiator.⁷⁸ Our results imply that although the nucleophilicity of the electron rich metal

complexes is most important for efficient NCA polymerization, the difference in reactivity between more electrophilic **1.49** and less electrophilic **3.2** suggests that the electrophilic activation can be sufficient for some NCA polymerization. **3.2** is neither sufficiently electron rich nor sufficient electrophilic for NCA ROP. Thus, the overall reactivity of the family of complexes towards NCA polymerization is **3.1** > **1.48** >> **1.49** >> **3.2**.

While studying the reactivity trends we also noted that poly(γ -benzyl-L-glutamate), obtained from reactions with catalysts **1.48** and **3.1**, possessed low dispersities. The molecular weight was much closer the theoretical molecular weight for polymer produced by catalyst **1.48** in comparison to **3.1**. We admit that the molecular weight measurements may not be as accurate as possible as the molecular weights were determined by size-exclusion chromatography equipped with a refractive index detector relative to polystyrene standards in polar

Table 3.1. Polymerization of γ -benzyl-L-glutamate N-carboxyanhydride (BLG-NCA) by various iron bis(iminopyridine) alkoxide complexes.^a

BLG-NCA (100 equiv.) $\xrightarrow[\text{THF, rt, t}]{\text{Catalyst (1 equiv.)}}$ Polymer

entry	[Fe]	time (h)	conversion (%) ^b	$M_n(\text{theo})$ (kDa)	$M_n(\text{exp})^d$ (kDa)	M_w/M_n ^e
1	1.48	1	6	0.7 ^c	N/A	N/A
2	1.48	24	36	3.9 ^c	3.7	1.15
3	1.48	48	50	5.0 ^c	4.8	1.20
4	3.1	1	11	2.4 ^d	3.3	1.19
5	3.1	24	38	8.3 ^d	4.6	1.18
6	3.1	48	48	10.5 ^d	5.0	1.22
7	1.49	48	10	1.0 ^c	22.4	2.36
8	3.2	48	0	N/A	N/A	N/A

^a Reactions were carried out at room temperature in THF using 1:100 catalyst:BLG-NCA at [0.35 M] relative to monomer. ^b Conversion determined by ¹H NMR. ^c Theoretical molecular weight $M_n(\text{theo}) = \text{conversion} * (\text{MW}_{\text{BLG-NCA}} - \text{MW}_{\text{CO}_2}) * 100 / 2$. ^d Theoretical molecular weight $M_n(\text{theo}) = \text{conversion} * (\text{MW}_{\text{BLG-NCA}} - \text{MW}_{\text{CO}_2}) * 100$. ^e Determined by size-exclusion chromatography relative to polystyrene standards using an RI detector.

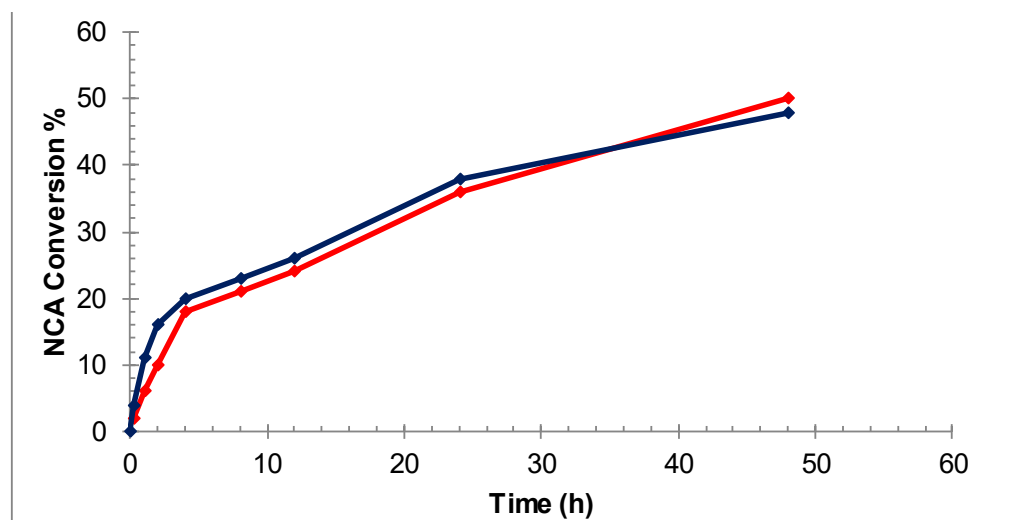


Figure 3.1. The conversion of γ -benzyl-L-glutamate-NCA vs. time for complexes **1.48** (red) and **3.1** (blue). Reactions were set up with a 1:100 equivalents [Catalyst]:[NCA] in THF.

dimethylformamide (DMF). The presence of hydrogen bond donors on poly(γ -benzyl-L-glutamate) may lead to a significantly different reorganization in DMF compared to polystyrene. The alkoxide initiators were not incorporated into any poly(γ -benzyl-L-glutamate) sample which precluded the use of ^1H NMR as an independent verification of molecular weight. We were instead able to measure the poly(γ -benzyl-L-glutamate) produced by catalyst **3.1** by matrix-assisted laser desorption/ionization (MALDI) mass spectrometry (Figure 3.2). The center of the peaks ($m = 4.684$ kDa) is greater than the close to the molecular weight measured by GPC ($M_n = 3.3$ kDa, $M_w/M_n = 1.19$) which indicates that the GPC measurement slightly undervalues the real molecular weight of the polymer. The molecular weight from the MALDI is significantly larger than the theoretical molecular weight ($M_n(\text{theo}) = 2.4$ kDa) which could suggest inefficient initiation. The MALDI spectrum was also informative for the absence of an end group derived from the alkoxide initiator, instead the end group matches the mass of deprotonated NCA. These

findings would help us propose a mechanism for this reaction which we will further delve into later this chapter.

3.3 Redox-switchable Polymerization of NCAs, the Unexpected Effect of Lewis Acid Additives and the Subsequent Mechanistic Investigation

For an effective redox-switchable polymerization, orthogonal reactivity is desired between two oxidation states of a catalyst to prevent side-reactions. We only observed

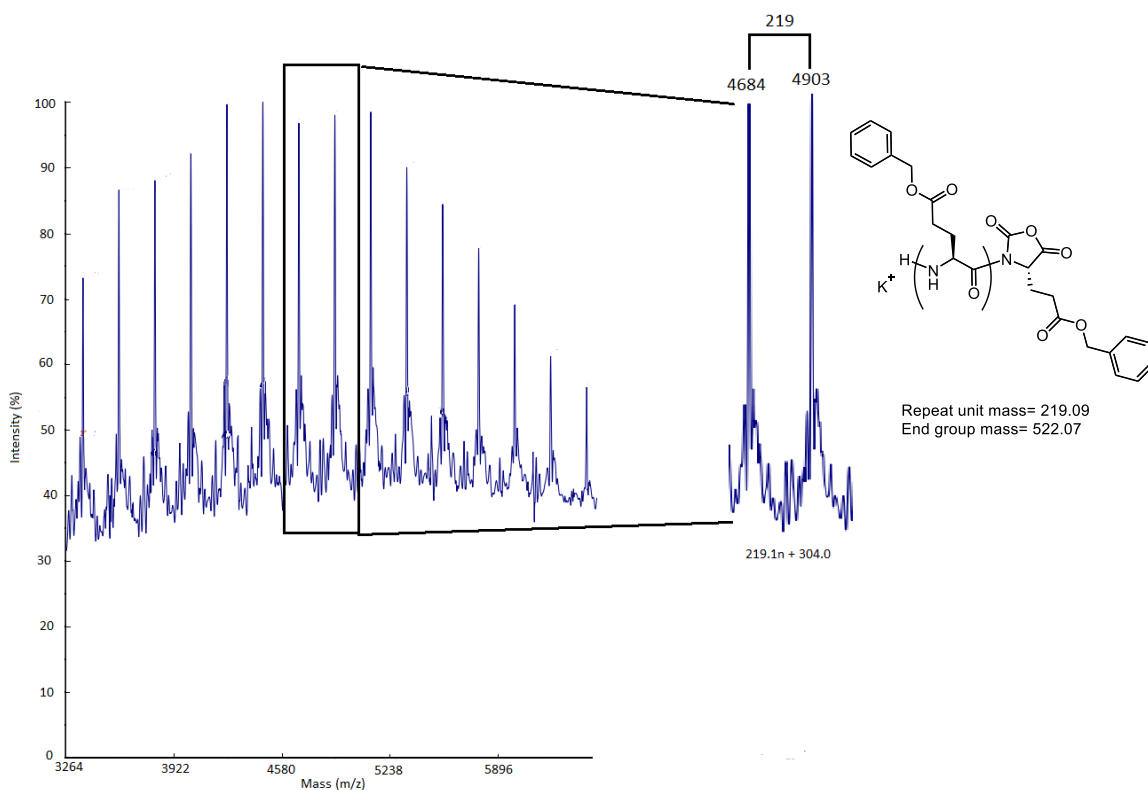


Figure 3.2. MALDI mass spectrum of poly(γ -benzyl-L-glutamate) polymerized by **3.1** from Table 3.1, entry 4. $M_n(\text{theo}) = 2.4$ kDa, $M_n(\text{GPC}) = 3.3$ kDa, $M_w/M_n = 1.19$.

orthogonal reactivity for **3.1** and **3.2** towards the polymerization of γ -benzyl-*L*-glutamate-NCA. To this end, redox-switching through the iterative addition of chemical redox reagents was pursued (Figure 3.3). Addition of FcBAR^{F24} to γ -benzyl-*L*-glutamate-NCA polymerization reactions catalyzed by **3.1** led to an immediate color change from pale blue green to golden brown, which was indicative of catalyst oxidation. Concurrent with catalyst oxidation, no further γ -benzyl-*L*-glutamate-NCA polymerization was observed as expected. Furthermore, no change in molecular weight or molecular weight distribution was observed even after stirring for an additional four hours. The addition of cobaltocene (CoCp₂) reduced the catalyst and led to consumption of the γ -benzyl-*L*-glutamate-NCA monomer, which was more rapid than observed initially. Moreover, the catalyst was no longer limited to low conversion and instead reached an ultimate conversion of 99% four hours after adding CoCp₂ (Figure 3.3). Despite the significant increase in reaction rate, molecular weight distributions remained narrow ($M_w/M_n = 1.13$), suggesting a single active catalyst.

The dramatic increase in polymerization activity observed after the catalyst underwent oxidation and reduction in redox-switchable polymerization reactions warranted further investigation. The reactivity of the redox reagents (i.e. FcBAR^{F24} and CoCp₂) and the byproducts from the redox reactions (i.e. Fc and [CoCp₂][BAR^{F24}]) revealed that only CoCp₂ was active for γ -benzyl-*L*-glutamate-NCA polymerization in the absence of **3.1** (Table 3.2). The polymerization initiated by CoCp₂ alone was rapid, reached completion in less than 10 minutes. Unlike the redox-switchable polymerization reaction, however, significantly higher molecular weight polymer was obtained ($M_n = 73.8$ kDa), and the polymer had a broad molecular weight distribution ($M_w/M_n = 2.38$). Cobaltocene initiated polymerizations were more reminiscent of strong base, potassium

tert-butoxide, initiated polymerization ($M_n = 25.8$ kDa, $M_w/M_n = 3.31$) (entry 3, Table 3.2) which may suggest a common anionic amide is being generated, but further investigation outside the scope of this work would be required. The improved molecular weight control along with the rapid color change (occurring in seconds) observed during the redox-switchable polymerization reaction led us to conclude that electron transfer from CoCp_2 to the catalyst was faster than direct polymerization of γ -benzyl-*L*-glutamate-NCA with CoCp_2 . Consequently, we concluded that the iron-based catalyst is necessary for the controlled, redox-switchable polymerization.

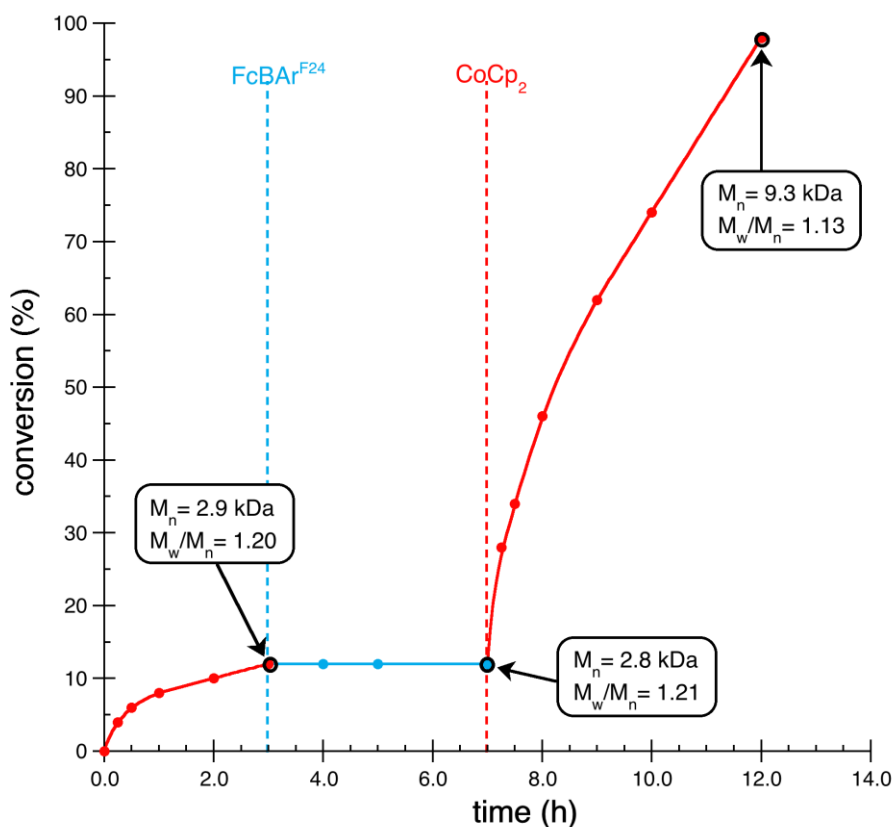


Figure 3.3. Redox-switchable polymerization of γ -benzyl-*L*-glutamate-NCA by complex **3.1** in THF at room temperature. Oxidation and reduction of the catalyst are represented with dotted lines and are enacted with the addition of $\text{FcBAR}^{\text{F}24}$ and CoCp_2 , respectively. The red and blue data points indicate when the catalyst is in the reduced and oxidized oxidation states, respectively. Number averaged molecular weights (M_n) and molecular weight distributions (M_w/M_n) for the indicated data points were determined by GPC relative to polystyrene standards.

We then explored the interactions between the various redox reagents had on γ -benzyl-*L*-glutamate-NCA polymerization by **3.1**. When **3.1** was oxidized to **3.2** *in-situ* the resulting complex was inactive as expected, (entry 7, Table 3.2). Ferrocene had little to no influence on the polymerization (entry 8, Table 3.2) which was similar to the results from **3.1** alone (entry 6, Table 3.2). Both CoCp_2 and $[\text{CoCp}_2][\text{BAR}^{\text{F}24}]$ lead to significant enhancements in polymerization rates (entries 9 and 10, Table 3.2) which given the demonstrated reactivity of free cobaltocene with NCAs is likely to be the result of a common cobaltocenium species being formed for both

Table 3.2. Polymerization of γ -benzyl-*L*-glutamate-NCA (BLG-NCA) by iron bis(iminopyridine) alkoxide complex, **3.1**, with additives.^a

entry	Catalyst	additive	time (h)	Conv. ^b (%)	$M_n(\text{theo})^c$ (kDa)	$M_n(\text{exp})^d$ (kDa)	M_w/M_n^d
1	N/A	FcBAR ^{F24}	48	0	N/A	N/A	N/A
2	N/A	CoCp ₂	0.17	>99	21.9	73.8	2.38
3	N/A	KO ^t Bu	0.17	>99	21.9	25.8	3.31
4	N/A	Fc	48	0	N/A	N/A	N/A
5	N/A	$[\text{CoCp}_2][\text{BAR}^{\text{F}24}]$	48	0	N/A	N/A	N/A
6	3.1	N/A	24	38	8.3	4.6	1.18
7	3.1	FcBAR ^{F24}	48	0	N/A	N/A	N/A
8	3.1	Fc	24	37	8.1	5.3	1.32
9	3.1	CoCp ₂	24	96	21.0	11.1	1.27
10	3.1	$[\text{CoCp}_2][\text{BAR}^{\text{F}24}]$	8	99	21.5	13.0	1.32
11	3.1	$[\text{CoCp}_2][\text{PF}_6]$	8	99	21.5	14.1	1.30
12	3.1	$[\text{CoCp}_2][\text{BAR}^{\text{F}24}]$	24	92	5.7	1.7	1.70
13	3.1	B(C ₆ F ₅) ₃	24	0	N/A	N/A	N/A
14	3.1	Sc(OTf) ₃	24	0	N/A	N/A	N/A
15	3.1	AlCl ₃	24	0	N/A	N/A	N/A
16	3.1	ZnCl ₂	24	0	N/A	N/A	N/A
17	3.1	Zr(Cp) ₂ Cl ₂	24	12	2.6	N/A	N/A
18	3.1	BPh ₃	24	10	2.2	N/A	N/A
19	3.1	Zn(^{4,4t} -bubpy)Cl ₂	24	70	15.3	13.1	1.27

^a Reactions were carried out at room temperature in THF using [1]: [1]: [100], [catalyst]: [additive]: [monomers] with a monomer concentration of [0.35 M]. ^b Conversion determined by ¹H NMR. ^c Theoretical molecular weight $M_n(\text{theo}) = \text{conversion} * (\text{MW}_{\text{BLG-NCA}} - \text{MW}_{\text{CO}_2}) * 100$. ^d Determined by size-exclusion chromatography relative to polystyrene standards using an RI detector.

polymerizations. The narrow dispersity would then be due to the presence of the iron complex moderating the reactivity of the amide species.

The mechanism of rate enhancement by cobaltocenium was unknown so we investigated the influence of both the counteranion as well as the sterics of the cobaltocenium cation. Exchanging $[\text{CoCp}_2][\text{BAr}^{\text{F24}}]$ for $[\text{CoCp}_2][\text{PF}_6]$ had a minor influence on overall conversion with both reactions reaching >90 % conversion in 8 h (entry 11, Table 3.2), suggesting that the anion has little effect on the reaction rate. In contrast, when the sterically more encumbered and more electron rich decamethylcobaltocenium tetrakis[3,5-bis(trifluoromethyl)phenyl]borate ($[\text{CoCp}^*]_2[\text{BAr}^{\text{F24}}]$) was used as an additive, no noticeable rate enhancement was observed (entry 12, Table 3.2). These findings lead us to believe $[\text{CoCp}_2][\text{BAr}^{\text{F24}}]$ is functioning as a Lewis acid binding to the more basic amide-like NCA carbonyls and activating the monomer while leaving

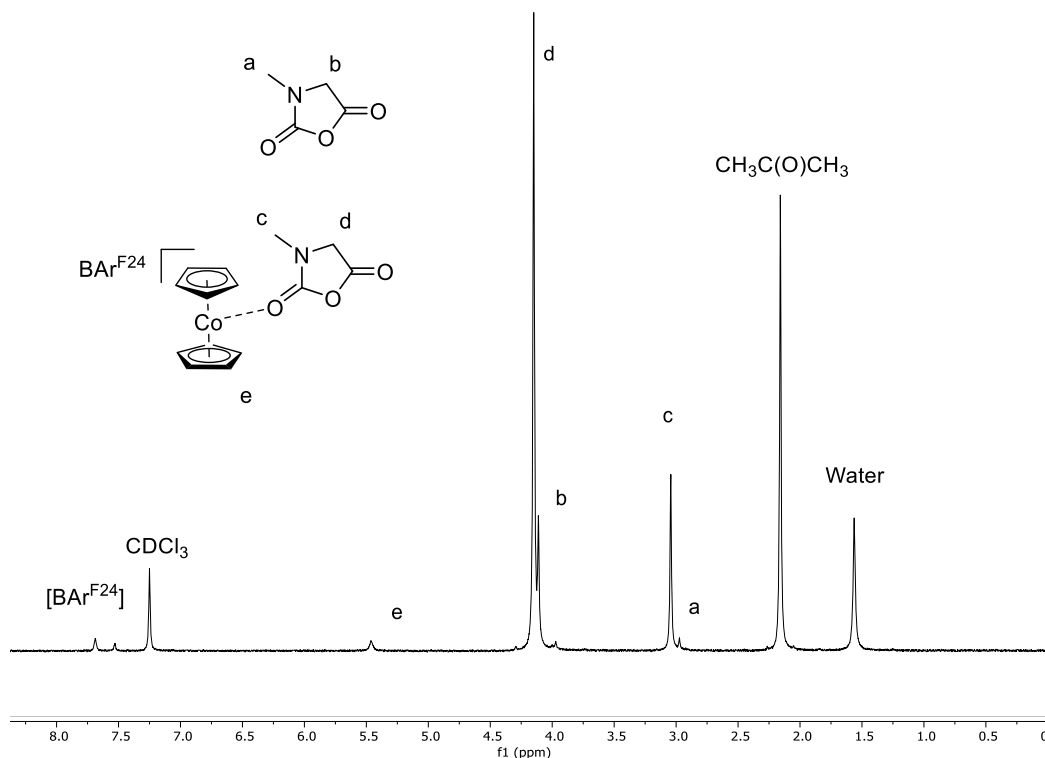


Figure 3.4. 600 MHz, ^1H NMR spectrum of 1:1 sarcosine-NCA: $[\text{CoCp}_2][\text{BAr}^{\text{F24}}]$ in CDCl_3 .

the ester-like carbonyl open to bind to the catalyst. It is also possible that the Lewis acid is binding to polyamide carbonyls on the growing chain to prevent binding to the catalyst which would inhibit binding of the monomer. We were able to observe through ^1H NMR spectroscopy the interaction between $[\text{CoCp}_2][\text{BAR}^{\text{F}24}]$ and the simple NCA (Figure 3.4). The peaks on the NCA are shifted slightly downfield suggesting electron density is moving from the NCA into the weak Lewis acid. The interaction between the Lewis acid and monomer supports our hypothesis that the species could be activating the monomer, but at this moment we cannot rule out interactions between the Lewis acid and the growing polymer chain.

We then investigated other Lewis acids to compare their influence on polymerization rates. Strong Lewis acids and sterically open metal salts all completely shut down NCA polymerization and turned the solution from red to colorless, indicative of complex decomposition (entries 13-16, Table 3.2). Weak Lewis acids (BPh_3) and more sterically congested Lewis acids ($\text{Zr}(\text{Cp})_2\text{Cl}_2$) both had negative effects on polymerization rate but did not kill the catalyst or turn the solution colorless (entries 17 and 18, Table 3.2). Only the unconventional Lewis acid, $\text{Zn}^{(4,4\text{tbu})\text{Bpy}}\text{Cl}_2$, improved the polymerization rate (70 % in 24 h) suggesting there must be a balance between Lewis acidity and steric bulk to achieve cooperative catalysis.

We next explored how $[\text{CoCp}_2][\text{BAR}^{\text{F}24}]$ affected the redox-switchable polymerization of γ -benzyl-*L*-glutamate-NCA (Figure 3.3). When a reaction starting with a mixture γ -benzyl-*L*-glutamate-NCA and $[\text{CoCp}_2][\text{BAR}^{\text{F}24}]$ was exposed to the iron complex **3.1**, we observed a rapid polymerization before oxidation and after reduction, which is consistent with the rate enhancements observed previously in the presence of the cobaltocenium cocatalyst (Figure 3.5). Notably, additional equivalents of $[\text{CoCp}_2][\text{BAR}^{\text{F}24}]$ formed from the redox switching process did

not influence the polymerization rates significantly. While γ -benzyl-*L*-glutamate-NCA polymerization reactions catalyzed by **3.1** demonstrated narrow molecular weight distributions ($M_w/M_n < 1.35$), molecular weights remained lower than expected and did not increase significantly with conversion. It is known that basic or bulky additives will initiate-NCA polymerization by deprotonating NCA monomers,^{14,28,79,80} but these polymerization reactions generally produce polymer with high molecular weights and/or broader molecular weight distributions (i.e., $M_w/M_n = 2-5$) than what was observed when **3.1** was used as the catalyst. Therefore, instead of an anionic polymerization mechanism initiated by **3.1**, we favor a

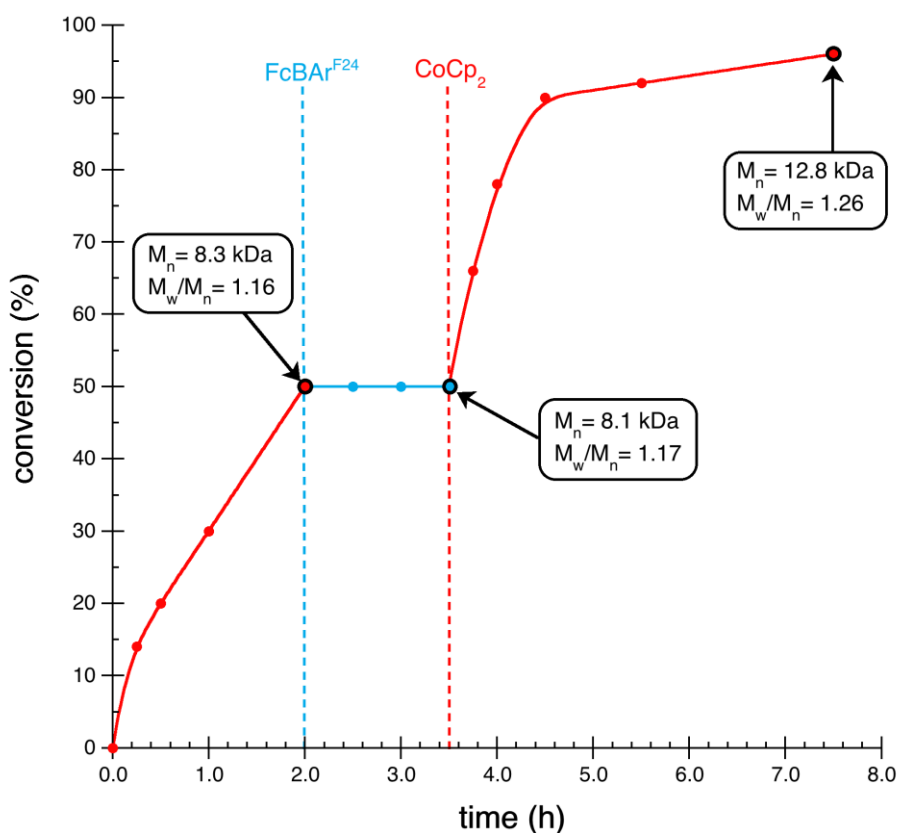
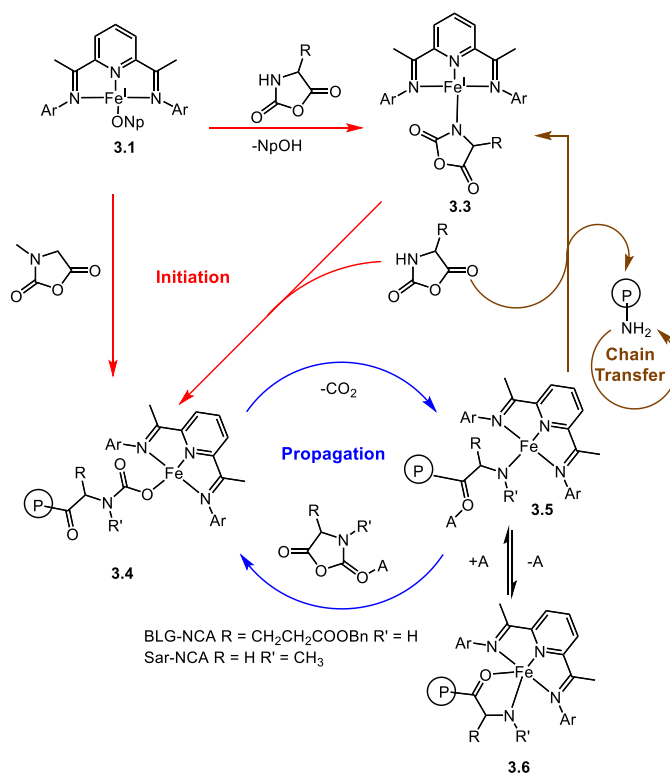


Figure 3.5. Redox-switchable polymerization of γ -benzyl-*L*-glutamate-NCA by complex **3.1** in THF at room temperature. Oxidation and reduction of the catalyst are represented with dotted lines and are enacted with the addition of $\text{FcBAR}^{\text{F24}}$ and CoCp_2 , respectively. The red and blue data points indicate when the catalyst is in the reduced and oxidized oxidation states, respectively. M_n and M_w/M_n for the indicated data points were determined by GPC.

coordination-insertion mechanism initiated by deprotonation of the γ -benzyl-*L*-glutamate-NCA monomer (Scheme 3.4). Deprotonation of γ -benzyl-*L*-glutamate-NCA by **3.1** leads to complex **3.3**, which can then insert into a second γ -benzyl-*L*-glutamate-NCA monomer to produce iron carbamate complex **3.4**. Decarboxylation produces iron amide complex **3.5**, which can propagate polymerization by inserting into γ -benzyl-*L*-glutamate-NCA to regenerate complex **3.4**. Instead of inserting an NCA monomer, **3.5** can also deprotonate γ -benzyl-*L*-glutamate-NCA to liberate a growing polymer chain (i.e., *P*-NH₂) and regenerating iron complex **3.3** that can then reenter the catalytic cycle. This mechanism may serve as a termination event, but chain transfer can also occur if iron amide complex **3.5** undergoes degenerative exchange with the free amine. Such mechanisms are common in many ring-opening polymerization reactions that proceed by a

Scheme 3.4. Proposed coordination-insertion mechanism for γ -benzyl-*L*-glutamate-NCA (BLG-NCA) or and sarcosine-NCA (Sar-NCA) polymerization catalyzed by **3.1** and co-catalyzed by a Lewis acid co-catalyst (A). The Lewis acidic co-catalyst could serve two functions: to activate the NCA monomer for insertion and/or to prevent product inhibition by inhibiting polyamide binding to the catalyst.



coordination-insertion mechanism.⁸¹ Chain transfer to the monomer may explain why the dispersity of the polymer increases over time as more initiators are formed. At this time cannot rule out the dispersity increasing due to back-biting along the growing polymer chain although no evidence for this side reaction was observed by MALDI (Figure 3.2) at lower conversions.

The role of the Lewis acid additive can be explained if a coordination-insertion mechanism is operative (Scheme 3.4). The Lewis acid may bind to the NCA to activate it for insertion from the basic iron alkoxide **3.1** or iron amide intermediates **3.3** or **3.5**. Another likely role for the Lewis acid co-catalyst is to prevent product inhibition. After insertion of an NCA monomer and decarboxylation to form intermediate **3.5**, the amide carbonyl from the newly formed peptide is ideally situated to form a five-membered ring chelate with iron to form complex **3.6**. If formed, **3.6** would inhibit polymerization by preventing the next NCA monomer from binding to the catalyst. However, in the presence of a Lewis acidic co-catalyst, the amide carbonyl can interact with the Lewis acid instead of the iron center, thereby freeing up the metal for subsequent NCA enchainment.

In order to determine if the Lewis acid effect is also observed for the simple amine method of NCA polymerization, a solution of dimethyl amine in THF was added as the initiator for γ -benzyl-*L*-glutamate-NCA with and without the presence of $[\text{CoCp}_2][\text{BAr}^{\text{F}24}]$. A significant retardation in polymerization rates was observed when $[\text{CoCp}_2][\text{BAr}^{\text{F}24}]$ was present in contrast to the rate enhancement seen when $[\text{CoCp}_2][\text{BAr}^{\text{F}24}]$ was combined with **3.1**. Rather than bind preferentially to the monomer, the Lewis acid is likely binding to the more basic amine initiator slowing down the polymerization rate. These experiments further demonstrate that the polymerization mechanism involving the iron-based catalyst **3.1** differs significantly from the

simple amine method.

To test whether deprotonation of γ -benzyl-*L*-glutamate-NCA is solely responsible for absence of initiator end groups in the final polymer, **3.1** was evaluated as catalysts for sarcosine-NCA polymerization (Table 3.3). Unlike γ -benzyl-*L*-glutamate-NCA, sarcosine-NCA does not contain an acidic N–H proton, which would preclude formation of complex **3.3** being formed as well as the chain transfer mechanism pathway proposed in Scheme 3.4. In the absence of [CoCp₂][BAr^{F24}], complex **3.1** was very active for the polymerization of sarcosine-NCA. The reaction reached 70 % conversion in only 10 minutes at room temperature; further conversion was not seen at extended reaction times (entry 1, Table 3.3). Little change was seen when reaction continued to run for 4 h, but prolonged stirring for 24 h led to the molecular weight decreasing and dispersity increasing (entries 2 and 3, Table 3.3). The lower molecular weight and increased dispersity is likely due to backbiting reactions, which may prevail at high conversions. The polymerization once again displayed narrow molecular weight distributions and molecular weights were close to the theoretical molecular weights. Moreover, molecular weights changed with catalyst loading, which is typical for polymerizations that proceed with good molecular weight control (entries 4-6, Table 3.3).

Unlike polymer obtained from γ -benzyl-*L*-glutamate-NCA polymerizations, end group analysis of the polymer obtained from Sarcosine-NCA by ¹H NMR and the MALDI mass spectra all revealed the presence of an ester end group additionally the molecular weight calculated by ¹H NMR end group analysis agrees with the molecular weight determined by GPC. Cyclic oligomers were also detected in the MALDI spectrum. These observations are consistent with the mechanistic hypothesis shown in Scheme 3.4. Without the ability to deprotonate the NCA

monomer, initiation of sarcosine-NCA occurs from insertion of the alkoxide into the NCA monomer. Moreover, sarcosine-NCA propagation proceeds without chain transfer leading to molecular weights that agree with theoretical molecular weights as the catalyst loading is altered.

Similarly to γ -benzyl-L-glutamate-NCA polymerization reactions, sarcosine-NCA polymerization reactions catalyzed by **3.1** could reach full conversion without loss in molecular weight control when $[\text{CoCp}_2][\text{BAR}^{\text{F}24}]$ was added to the reaction (entry 7, Table 2). Moreover, the oxidized complex **3.2** was completely inactive for sarcosine-NCA polymerization (entry 8, Table 2). Overall, these results demonstrated that **3.1** was an excellent catalyst for N-substituted NCA polymerization reactions, especially in the presence of the Lewis acidic additive $[\text{CoCp}_2][\text{BAR}^{\text{F}24}]$, and the catalyst also demonstrated great potential to be used in a redox-switchable system.

Table 3.3. Polymerization of sarcosine-NCA by iron bis(iminopyridine complexes **3.1** and **3.2**.^a

Sar-NCA (100 equiv.)

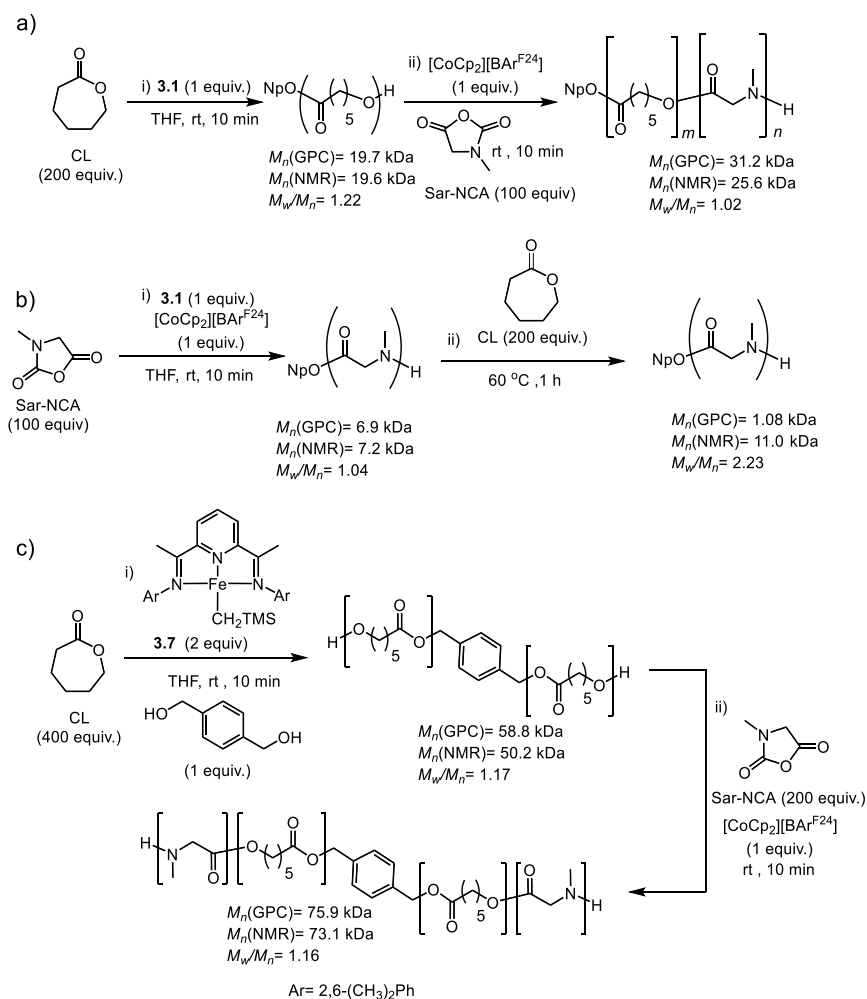
Entry	Catalyst	Catalyst equiv.	Conversion (%) ^b	$M_n(\text{theo})$ (kDa) ^c	$M_n(\text{exp})$ (kDa) ^d	M_w/M_n ^d
1	3.1	1	70	5.0	5.0	1.15
2 ^e	3.1	1	71	5.0	5.8	1.06
3 ^f	3.1	1	70	5.0	3.7	1.48
4	3.1	2	65	2.5	3.0	1.35
5	3.1	0.5	67	9.5	9.6	1.05
6	3.1	0.025	71	19.9	20.3	1.03
7 ^g	3.1	1	>99	7.1	7.1	1.06
8	3.2	1	0	N/A	N/A	N/A

^a Reactions were carried out for 10 min in THF using catalyst at [0.35 M] relative to monomer. ^b Conversion was determined by ¹H NMR and mass of precipitated polymer. ^c Theoretical molecular weight $M_n(\text{theo}) = \text{conversion} * (\text{MW}_{\text{Sar-NCA}} - \text{MW}_{\text{CO}_2}) * 100$. ^d Determined by GPC versus polystyrene standards. ^e Reaction ran for 4 hours. ^f Reaction ran for 24 hours. ^g $[\text{CoCp}_2][\text{FcBAR}^{\text{F}24}]$ (1 mol%) was also added to the reaction.

3.4 Copolymerization of Caprolactone and Sarcosine-NCA

The combination of **3.1** and $[\text{CoCp}_2][\text{BAr}^{\text{F}24}]$ was established to be an effective catalyst for the polymerization of sarcosine-NCA. Additionally, we had determined that the alkoxide initiator was incorporated as an ester end group in the polymer which would be needed for copolymerization with lactones. We decided to leverage the exceptional activity of **3.1** for ϵ -caprolactone polymerization^{72,73} to form copolymers between sarcosine-NCA and ϵ -

Scheme 3.5 a) Diblock copolymerization of ϵ -caprolactone (CL) then sarcosine-NCA (Sar-NCA) by **3.1** and $[\text{CoCp}_2][\text{BAr}^{\text{F}24}]$ through sequential addition of monomers. b) Attempted copolymerization of sarcosine-NCA then ϵ -caprolactone, but only poly(sarcosine) was observed. (c) Telechelic, triblock copolymerization of ϵ -caprolactone then sarcosine-NCA by **3.7** and $[\text{CoCp}_2][\text{BAr}^{\text{F}24}]$ through sequential addition of monomers.



caprolactone (Scheme 3.5). As expected, exposing **3.1** to ϵ -caprolactone followed by $[\text{CoCp}_2][\text{BAR}^{\text{F}24}]$ and sarcosine-NCA led to the production of copoly(ester-*b*-amide) block copolymers (Scheme 3.5a). The polymer obtained was of moderately high molecular weight and narrow molecular weight distribution ($M_n = 31.2$ kDa, $M_w/M_n = 1.08$) (Figure 3.6), and the block copolymer microstructure was verified using DOSY spectroscopy (Figure 3.7).

Encouraged by these results the opposite order of monomer addition was explored next. Unfortunately, the polymer produced from sarcosine-NCA polymerization catalyzed by **3.1** and $[\text{CoCp}_2][\text{BAR}^{\text{F}24}]$ ($M_n = 6.9$ kDa, $M_w/M_n = 1.04$) was not capable of initiating ϵ -caprolactone ROP (Scheme 3.5b). We attempted to drive the reaction by increasing the temperatures up to 60 °C and prolonged reaction times. The inactivity towards ϵ -caprolactone was particularly surprising considering the exceptional activity that **3.1** had for the ROP of ϵ -caprolactone.^{72,73} We hypothesize that the decreased reactivity of ϵ -caprolactone after sarcosine-NCA polymerization is likely due to the ability for the polyamide carbonyls to chelate to the iron catalyst (e.g.,

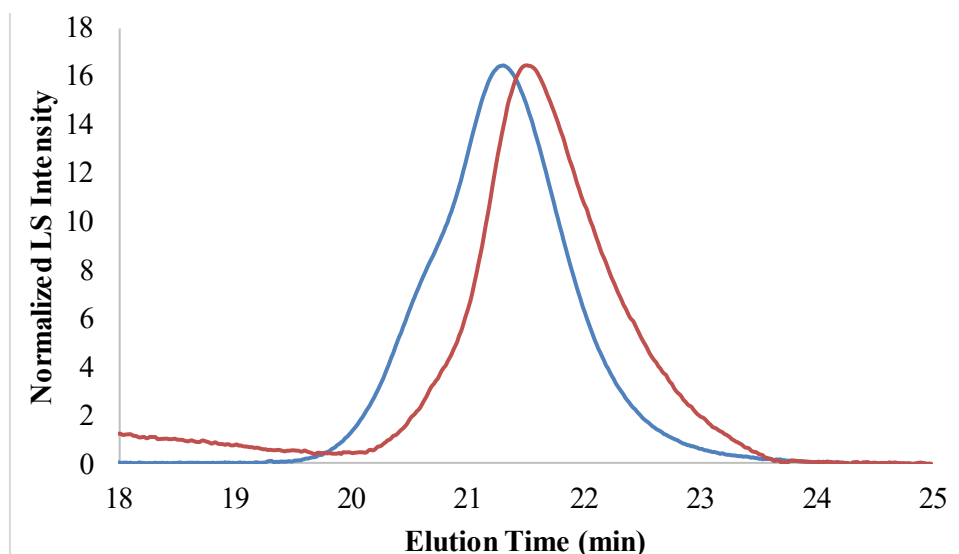


Figure 3.6. GPC chromatogram of poly(ϵ -caprolactone) ($M_n(\text{GPC}) = 31.2$ kDa, $M_w/M_n = 1.08$, blue) and poly(ϵ -caprolactone-*b*-sarcosine) ($M_n(\text{GPC}) = 31.2$ kDa, $M_w/M_n = 1.08$, red) from Scheme 3.5A. Measurement taken in THF at 40 °C and recorded by a LS detector.

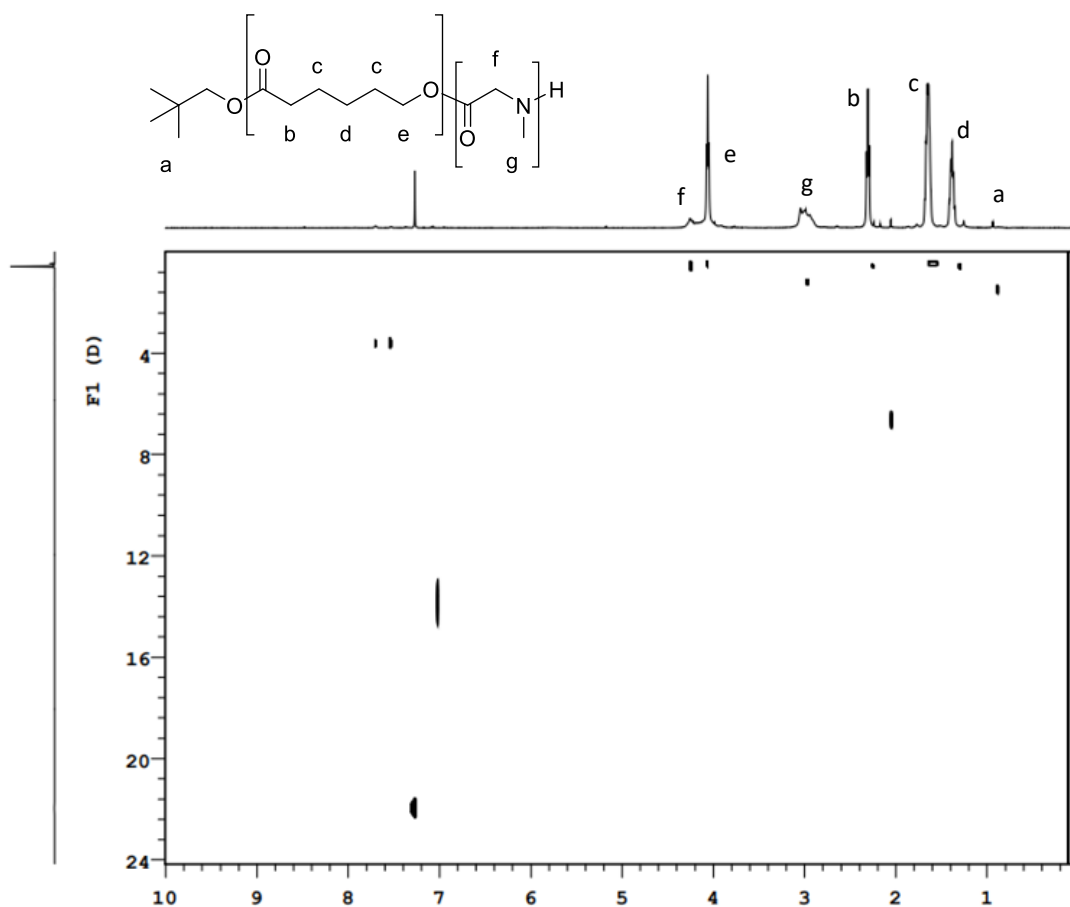


Figure 3.7. 600 MHz, DOSY NMR spectra of poly(ϵ -caprolactone-*b*-sarcosine) from Scheme 3.5A in CDCl_3 .

intermediate **3.6**, Scheme 3.4), which can be sufficiently overcome with the addition of $[\text{CoCp}_2][\text{BAR}^{\text{F}24}]$ for NCA monomers but not for the less nucleophilic ϵ -caprolactone monomer.

Despite this limitation, A-B-A poly(amide-*b*-ester-*b*-amide) triblock copolymers were accessible using a telechelic polymerization approach (Scheme 3.5c). The addition of diol initiator 1,4-benzenedimethanol to bis(imino)pyridine iron alkyl precursor **3.7** generated an alkoxide catalyst *in-situ*, which was suitable for ϵ -caprolactone polymerization. The molecular weight of the polyester produced was close to the theoretical amount at >99 % conversion as determined by GPC and NMR ($M_n(\text{exp, GPC}) = 58.8$ kDa; $M_n(\text{exp, NMR}) = 50.2$ kDa; $M_n(\text{theo}) = 50.2$ kDa) and

the molecular weight distribution was narrow ($M_w/M_n = 1.17$) (Scheme 3.5c). The addition of $[\text{CoCp}_2][\text{BAR}^{\text{F}24}]$ and sarcosine-NCA led to efficient conversion of the NCA monomer and production of the A-B-A poly(amide-*b*-ester-*b*-amide) triblock copolymer. Monomodal molecular weight distributions of the resulting copolymers were observed by GPC along with a clear increase in molecular weight, supporting chain elongation at all molecular weights. ($M_n(\text{GPC}) = 75.9 \text{ kg/mol}$, $M_w/M_n = 1.16$) (Figure 3.8), which was supported by ^1H NMR and DOSY spectroscopy. (Figure 3.9).

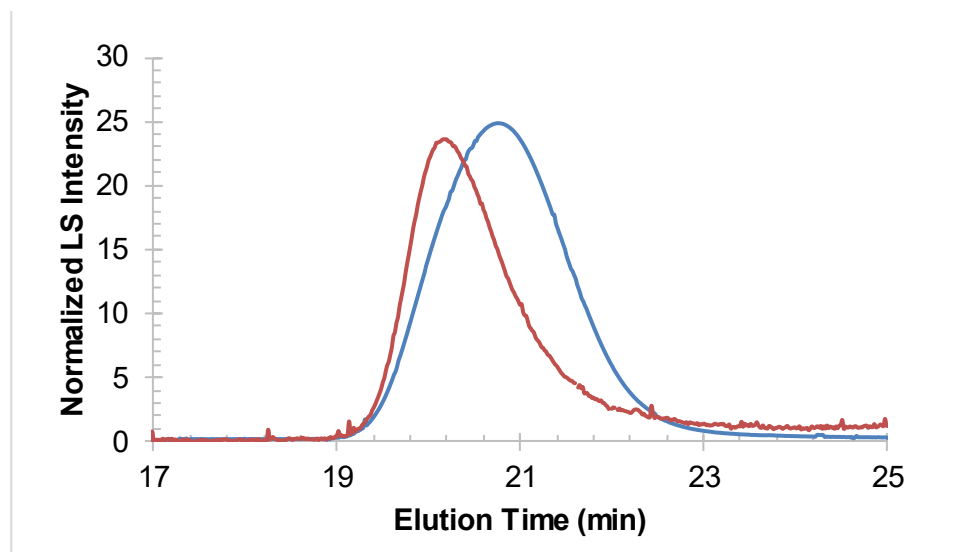


Figure 3.8. GPC chromatogram from the telechelic copolymerization poly(ϵ -caprolactone) (blue, $M_n = 58.8 \text{ kDa}$, $M_w/M_n = 1.17$) and poly(sarcosine-*b*- ϵ -caprolactone-*b*-sarcosine) (red, $M_n = 75.9 \text{ kDa}$, $M_w/M_n = 1.16$) from Scheme 3.5c.

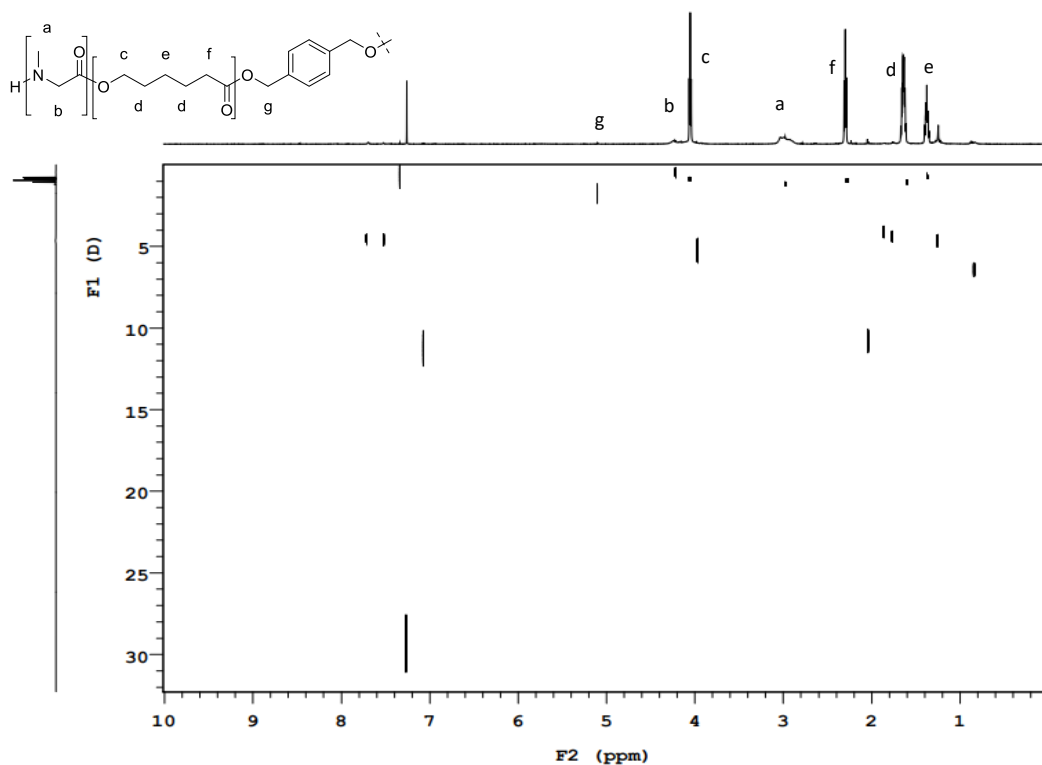


Figure 3.9. 600 MHz, ^1H DOSY NMR spectra of poly(sarcosine-*b*- ϵ -caprolactone-*b*-sarcosine) from Scheme 4c in CDCl_3 .

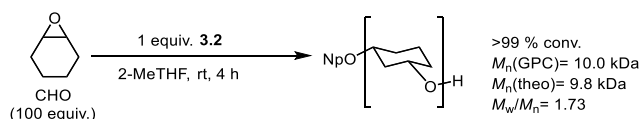
3.5 Copolymerization of Sarcosine-NCA and Cyclohexene Oxide

To expand the number of monomers our catalyst could copolymerize with sarcosine-NCA we looked at monomers that would be suitable for a redox-switchable polymerization. Our group had previously demonstrated that the cationic, formally iron (III) complex **1.49** was active for epoxide polymerization,⁶⁴ which neutral, formally iron(II) complex **1.48** is inactive towards.⁷² The complementary reactivity observed between the **1.48** and **1.49** inspired the development of a redox-switchable polymerization reaction between lactide and epoxides that led to the

production of block copolymers either from sequential addition of monomers or from a pool of both monomers.⁶⁴ We believed that we could achieve a similar redox-switchable reaction for NCAs and epoxides using **3.1** and **3.2**. We had already demonstrated that **3.1** was inactive for epoxide ROP similar to **1.48**.⁷² Considering **3.2** and **1.49** were both cationic iron complexes, it was expected that **3.2** would also be active for epoxide ROP. Validation of this expectation would then make the redox-switchable copolymerization of epoxides with NCAs possible by leveraging the redox-switchable activity of **3.1** for NCA ROP and epoxide ROP.

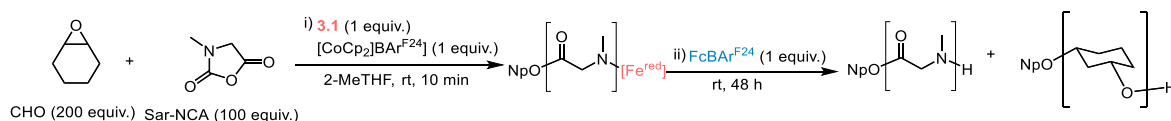
As anticipated, catalyst **3.2** was very active for cyclohexene oxide ROP. In the presence of THF both THF and cyclohexene oxide were consumed so to simplify analysis we decided to replace the solvent with bulkier 2-methyltetrahydrofuran (2-MeTHF) which was not consumed during cyclohexene oxide ROP (Scheme 3.5). As was the case with **1.49**, cyclohexene oxide polymerization catalyzed by **3.2** did not demonstrate living characteristics, producing more disperse polymers ($M_w/M_n = 1.73$), but with molecular weights close to the theoretical molecular weights (e.g., $M_n(\text{exp}) = 10.0 \text{ kg/mol}$, $M_n(\text{theo}) = 9.8 \text{ kg/mol}$, $M_w/M_n = 1.73$ at 1% catalyst loading and 98% conversion). While quantitative rate measurements were complicated by differences in solvents for catalyst compatibility (CH_2Cl_2 for **1.49** and 2-MeTHF for **3.2**), **3.2** was less efficient as a catalyst for cyclohexene oxide polymerization when qualitatively compared to **1.49**,⁶⁴ with polymerizations reaching high conversions in hours with **3.2** as opposed to minutes with **1.49**.

Scheme 3.6. Polymerization of cyclohexene oxide (CHO) by **3.2**.



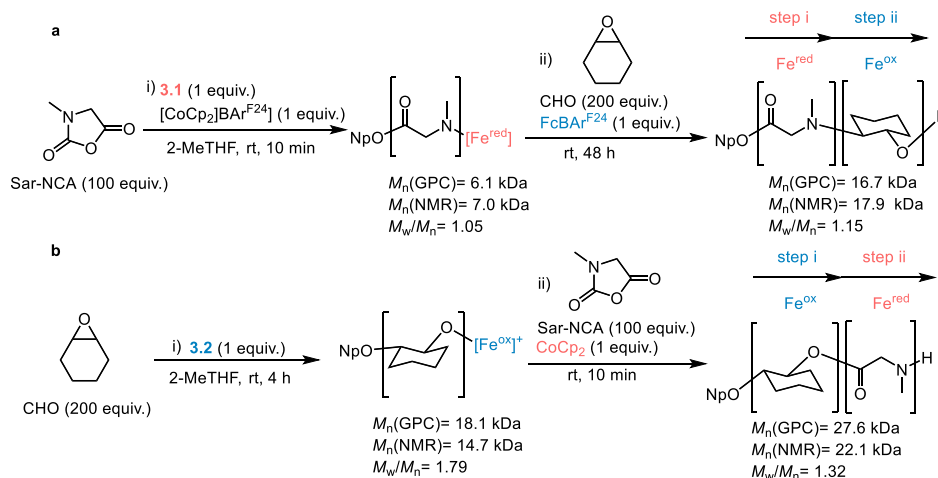
Encouraged by the reactivity of **3.1** and **3.2** towards sarcosine-NCA and cyclohexene oxide, respectively, copolymerization reactions were next attempted wherein the chemoselectivity of the catalyst was altered through the addition of redox reagents *in situ*. When a mixture of sarcosine-NCA and cyclohexene oxide was exposed to **3.1** and $[\text{CoCp}_2][\text{BAR}^{\text{F24}}]$, clean conversion of sarcosine-NCA was observed with no conversion of cyclohexene oxide. Addition of $\text{FcBAR}^{\text{F24}}$ to the reaction led to the polymerization of cyclohexene oxide, which was consistent with the redox switching experiments for cyclohexene oxide. However, precipitation of the polymer in hexanes resulted in the isolation of separate homopolymers, specifically poly(sarcosine) in the precipitate and soluble poly(cyclohexene oxide). We expected the homopolymer formation was a product of the reaction of $\text{FcBAR}^{\text{F24}}$ and cyclohexene oxide as had been observed by others during redox-switchable copolymerizations.⁸² To prevent this side reaction we explored the sequential addition of monomers/reagents for copolymerization to ensure the redox reagents were quenched before monomer addition. (Scheme 3.6a). The polymerization of sarcosine-NCA proceeded when exposed to **3.1** and $[\text{CoCp}_2][\text{BAR}^{\text{F24}}]$. GPC analysis of the poly(sarcosine) revealed a monomodal molecular weight distribution although there was some low molecular weight tailing, which may be a side effect of the lower solubility of sarcosine-NCA in 2-MeTHF compared to THF. When $\text{FcBAR}^{\text{F24}}$ was added to the reaction, a rapid color change occurred, consistent with the oxidation of the iron complex. Cyclohexene oxide was then added, and full conversion to polymer was observed.

Scheme 3.7. Attempted synthesis of polyether-polyamide diblock copolymers using a **3.1/3.2** catalyzed redox-switchable polymerization in a solution of mixed monomers.



Unlike the reaction initiated with both monomers initially present, the product obtained from sequential addition of monomers and redox reagents lead to a copolymer with a monomodal molecular weight distribution by GPC (Scheme 3.7a). Unfortunately separate GPCs had to be used to measure the poly(sarcosine) copolymer and the subsequent poly(sarcosine-*b*-cyclohexene oxide) copolymer due to solvent and column incompatibility so the two elution times could not be directly compared. Regardless, ^1H and DOSY NMR spectroscopies were also consistent with the formation of a poly(amide-*b*-ether) block copolymer. These results suggest that the polyether product formed in the procedure starting from mixture of monomers likely arises from competitive reaction of cyclohexene oxide with $\text{FcBAR}^{\text{F}24}$ instead of electron transfer between $\text{FcBAR}^{\text{F}24}$ and the iron-based complex. To complete the evaluation of **3.1**- $[\text{CoCp}_2][\text{BAR}^{\text{F}24}]/\mathbf{3.2}$ as a redox-switchable polymerization system for the production of block copolymers that contain amides and ethers, the polymerization of cyclohexene oxide followed by Sarcosine-NCA was pursued (Scheme 3.7b). As was the case with the switch between **3.1** and **3.2**, sequential addition of CoCp_2 to a cyclohexene oxide polymerization catalyzed by **3.2** followed

Scheme 3.8. Synthesis of polyether-polyamide diblock copolymers using a **3.1/3.2** catalyzed redox-switchable polymerization a) Poly(sarcosine-*b*-cyclohexene oxide) and b) poly(cyclohexene oxide-*b*-sarcosine) synthesis required the sequential addition of redox reagents and monomers.



by sarcosine-NCA led to the production of a poly(ether-*b*-amide) block copolymer without significant production of polyether or polyamide byproducts. Formation of the block copolymer was confirmed by ^1H and DOSY NMR spectroscopies and molecular weight analysis by GPC revealed monomodal molecular weight distributions, but it does not appear that high molecular weight polyether is retained in the copolymer NMR (Figure 3.10). Either chain extension is incomplete or any polyether rich copolymers are lost as the polymer is isolated during the purification step. Poly(cyclohexene oxide) could be easily precipitated into methanol, but the copolymers were soluble in methanol, so instead they had to be purified through precipitation into cold acetone.

Redox-switchable polymerization also allowed us to access triblock copolymers of sarcosine-NCA and cyclohexene oxide. The poly(ether-*b*-amide-*b*-ether') triblock copolymer was synthesized by first polymerizing cyclohexene oxide using **3.2** as the catalyst (Scheme 3.7b). Subsequent addition of CoCp_2 and sarcosine-NCA resulted in the formation of the diblock copolymer poly(cyclohexene oxide-*b*-sarcosine). Finally, the addition of $\text{FcBAR}^{\text{F}24}$ to this reaction

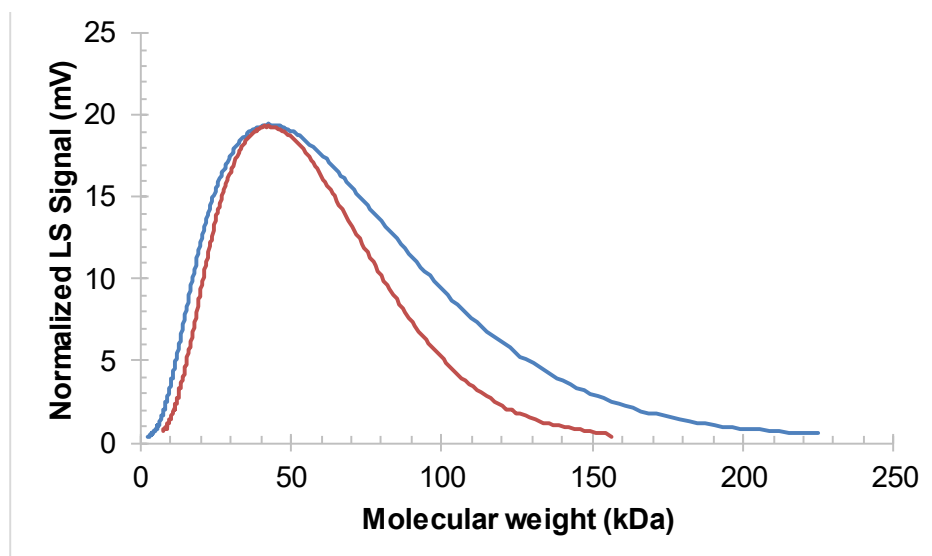


Figure 3.10. GPC chromatogram from the copolymerization of CHO (blue, $M_n = 18.1$ kDa, $M_w/M_n = 1.79$) then sarcosine-NCA (red, $M_n = 22.1$ kDa, $M_w/M_n = 1.32$) from Scheme 3.7B.

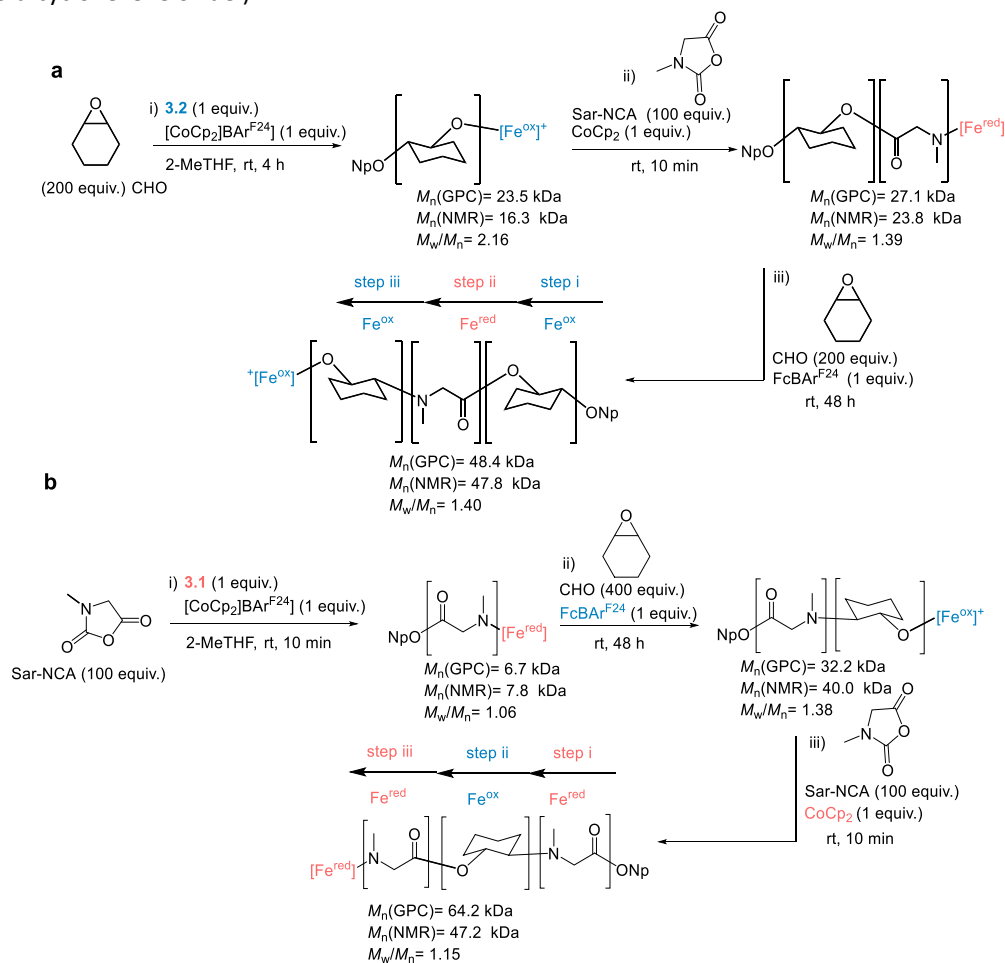
followed by additional cyclohexene oxide led to the triblock copolymer poly(cyclohexene oxide-*b*-sarcosine-*b*-cyclohexene oxide') (Scheme 3.8a).

The formation of both triblock copolymers was supported with ^1H and DOSY NMR. The GPC spectra (Figure 3.11, top) remained monomodal throughout either copolymerization reaction, but it is notable that the high molecular weight tail fraction of the pure poly(cyclohexene oxide) was not retained in the diblock copolymer, which could be due to the precipitation step not being efficient for collecting polyether-rich copolymers. Poly(cyclohexene oxide) was collected by precipitation into methanol, but methanol made a poor solvent for copolymer precipitation, each copolymer was instead precipitated into cold acetone because both homopolymers are poorly soluble in cold acetone. The ^1H NMR of the supernatant for all copolymer precipitations contained both polyether and polyamide resonances, suggesting the precipitation could be causing fractionation of the copolymer by order of relative solubility. If this is occurring it could also be possible that any diol impurities in the cyclohexene oxide could be producing high molecular weight, telechelic copolymer that are may be more soluble than the copolymers produced in one direction and therefore any high molecular weight fraction of the copolymer would not be carried on into the GPC chromatogram.

The complementary poly(amide-*b*-ether-*b*-amide') A-B-A' triblock copolymer was formed through sequential addition of monomers and oxidants/reductants. To synthesize this block copolymer, **3** and $[\text{CoCp}_2][\text{BAr}^{\text{F}24}]$ were used to polymerize Sarcosine-NCA (Scheme 3.7b). Upon addition of $\text{FcBAr}^{\text{F}24}$, the metal complex containing a poly(sarcosine) chain was oxidized and the addition of cyclohexene oxide led to formation of the diblock copolymer poly(sarcosine-*b*-cyclohexene oxide). Addition of CoCp_2 followed by an additional Sarcosine-NCA resulted in the

formation of the triblock copolymer poly(sarcosine-*b*-cyclohexene oxide-*b*-sarcosine') (Scheme 3.7a). Analysis of the diblock and triblock copolymers by GPC revealed uniform chain extension and monomodal molecular weight distributions (Figure 3.11, bottom). The molecular weight determined by GPC increases significantly after the addition of sarcosine-NCA (32.2 kDa to 64.2 kDa) while the molecular weight determined by end group analysis using ^1H NMR increases less significantly (40.0 kDa to 47.2 kDa) and better matches the theoretical molecular weight. The

Scheme 3.9. Synthesis of polyether-polyamide triblock copolymers using a **3.1/3.2** catalyzed redox-switchable polymerization. (a) Poly(sarcosine-*b*-cyclohexene oxide-*b*-sarcosine) and (b) poly(cyclohexene oxide-*b*-sarcosine-*b*-cyclohexene oxide').



discrepancy in the molecular weights determined by NMR and GPC may be caused by some aggregation of the poly(sarcosine)-rich copolymer in THF, leading to higher than expected molecular weight measurements by GPC. The formation of the triblock copolymers was supported with ^1H and DOSY NMR.

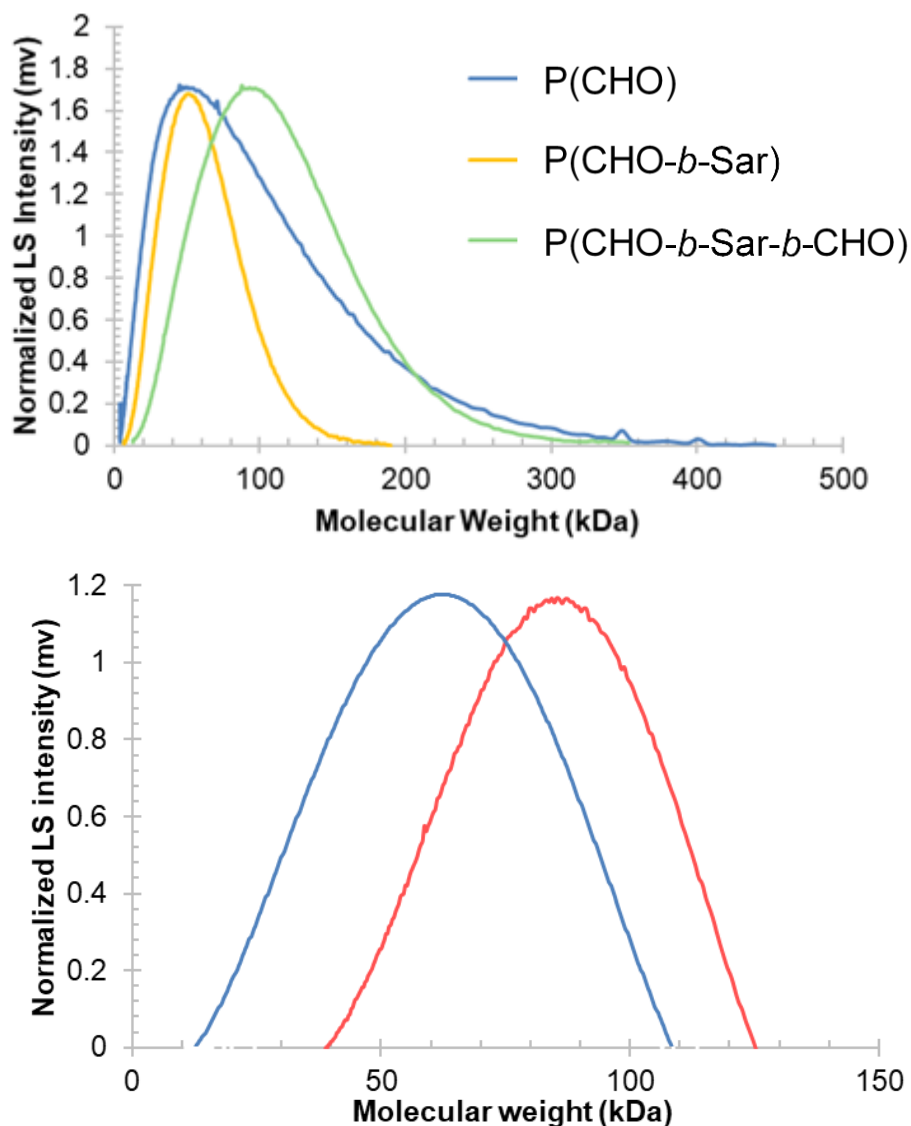


Figure 3.11. (Top) GPC chromatogram of triblock copolymers of cyclohexene oxide (CHO) and sarcosine-NCA (Sar-NCA). Poly(cyclohexene oxide) ($M_n = 17.6$ kDa, $M_w/M_n = 2.16$, blue), poly(cyclohexene oxide-*b*-sarcosine) ($M_n = 27.9$ kDa, $M_w/M_n = 1.39$, orange) and poly(cyclohexene oxide-*b*-sarcosine-*b*-cyclohexene oxide') ($M_n = 48.4$ kDa, $M_w/M_n = 1.40$, green) from Scheme 3.8A. (Bottom) GPC chromatogram of poly(sarcosine-*b*-cyclohexene oxide) ($M_n = 32.2$ kDa, $M_w/M_n = 1.38$, blue) and poly(sarcosine-*b*-cyclohexene oxide-*b*-sarcosine') ($M_n = 62.2$ kDa, $M_w/M_n = 1.15$, red) from Scheme 3.8B.

3.6 Conclusion

The low valent iron complex **3.1** was found to be an efficient catalysts for NCA ROP, especially when used in combination with a mild Lewis acid, such as [CoCp₂][BAR^{F24}]. Unlike most NCA polymerization reactions, the mechanism for NCA polymerization with **3.1** is likely a coordination-insertion mechanism that benefits from cooperative interactions with a Lewis acid cocatalyst. The similar intermediates that this mechanism shared with the proposed mechanism for lactone polymerization catalyzed by **3.1**⁴⁴ enabled these complexes to be used as catalysts for the uncommonly reported, one-pot, copolymerization reactions between sarcosine-NCA and ϵ -caprolactone. With the appropriate order of addition and choice of initiator, diblock and triblock copolymers that incorporate sarcosine-NCA and ϵ -caprolactone could be obtained.

Moreover, complex **3.1** could be reversibly oxidized during the polymerizations with one electron redox reagents, which resulted in the first example of a redox-switchable polymerization of NCAs. This reactivity was combined with orthogonal reactivity of the oxidized complex **3.2** for cyclohexene oxide polymerization to produce poly(amide-*b*-ether) block copolymers, the composition of which could be altered through *in situ* addition of chemical oxidants and reductants. Future improvements to the system will include adoption of the electrochemical redox switching system we recently reported to address redox reagent incompatibility, and further monomer and catalyst engineering targeting a broader set of NCA monomers for incorporation into copolymerization reactions. The success of these efforts is expected to lead to the synthesis of new polymeric materials with useful and tunable properties that would benefit a wide variety of applications from new thermoplastic materials to drug delivery devices.

3.7 Experimental

General Considerations: Cyclohexene oxide and 2-methyltetrahydrofuran were dried over CaH₂ and distilled prior to polymerization. Tetrahydrofuran was dried over 3 Å molecular sieves and activated manganese oxide under an argon atmosphere. Complexes **1.48**, **1.49** and **3.1** and **3.7** were synthesized as described previously.^{71,72} Amino acids γ -benzyl-L-glutamate-NCA and sarcosine were purchased from Acros Organics and used as received. Triphosgene was purchased from Chem-Impex International Inc. and used as received. Tetrabutylammonium hexafluorophosphate was purchased from Oakwood Chemicals and dried over P₂O₅ *in vacuo*. γ -benzyl-L-glutamic acid was obtained from Sigma Aldrich and used as obtained. Sarcosine was obtained from Sigma Aldrich and dried over P₂O₅ *in vacuo*. Monomers γ -benzyl-L-glutamate *N*-carboxyanhydride⁴⁴ and sarcosine *N*-carboxyanhydride⁵³, were synthesized according to literature procedures. FcBAR^{F24} was synthesized according to literature procedures.⁸³ Unless stated otherwise, all reactions were carried out in oven-dried glassware in a nitrogen-filled glove box or with standard Schlenk line techniques.⁸⁴ Solvents were used after passage through a solvent purification system consisting of molecular sieves and activated manganese oxide under a blanket of argon and then degassed briefly by exposure to vacuum.

Evan's Method: Magnetic moments were determined by Evan's method^{85,86} in THF by means of a procedure published by Gibson and coworkers.⁸⁷

SEC: Due to solubility concerns, polymers size-exclusion chromatography (SEC) by permeation chromatography (GPC) was performed on two separate instruments. For polyesters, polyethers and all copolymers an Agilent GPC220 in THF at 40 °C with three PL gel columns (10 μ m) in series

and recorded with both a refractive index detector and a multi-angle, light-scattering detector at 15 and 90 degrees. Instrument was calibrated against 7 narrow molecular weight, polystyrene standards (GSK, 1,820,000- 3,180 g/mol). For polyamide homopolymers a Tosoh EcoSEC instrument HLC-8320GPC with a refractive index (RI) detector and three Tosoh TSKgel Alpha M columns (7.8mmID × 300 mm, resin type: methacrylate, particle size:13 µm, pore size: mixed bed). These columns were maintained at 50 °C for all analyses. All samples were eluted by DMF + 0.01% LiBr at a flow rate of 0.6 mL/min. Calibration was performed using polystyrene standards (ReadyCal Kit, Sigma-Aldrich#81434). Samples were passed through 0.20 µm nylon filters before being injected into the SEC system. Unfortunately, this instrument was not equipped with a light-scattering detector so we elected not to use the instrument for measuring the copolymers of polyamides with polyesters or polyethers.

Mass Spectrometry: Matrix-assisted, laser desorption/ ionization time of flight (MALDI-TOF) mass spectrometry was conducted on either a Bruker Autoflex LRF Speed or a Voyager DE STR mass spectrometer. Poly(sarcosine) samples were prepared by either dissolving 1 mg /ml of polymer in CHCl₃ with a matrix consisting of 10 mg/ ml trans-2-[3-(4-tert-Butylphenyl)-2-methyl-2-propenylidene]malononitrile as the matrix. Spectra were collected using a 1:10 ratio of polymer solution to matrix solution. Poly(γ-benzyl-L-glutamate) samples were prepared by dissolving 1 mg/ ml in THF with a matrix consisting of α-Cyano-4-hydroxycinnamic acid and silver iodide and potassium iodide as cation sources. Samples were run at a 1:10:1 ratio of polymer to matrix to total cation source.

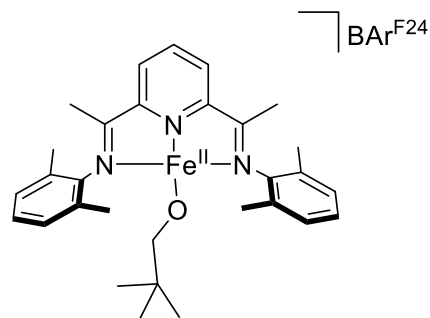
Nuclear Magnetic Resonance: (NMR) spectra were recorded at ambient temperature on spectrometers operating at 500 or 600 MHz for ¹H and DOSY NMR, 125 MHz for ¹³C, 128 MHz for

^{11}B , 470 MHz for ^{19}F . Resonances for paramagnetic complexes are reported as chemical shift in ppm (peak with at half height, Hz).

IR: Infrared (IR) spectra were recorded on a Bruker, attenuated total reflectance (ATR) infrared spectrometer.

Synthesis of iron bis(2,6-dimethylphenyl)-2,6-bis(imino)pyridine neopentoxide][tetrakis(3,5-trifluoromethylphenyl)]borate], **3.2**

In a nitrogen-filled glove box, complex **3.1** (50.0 mg, 97.6 μmol) was measured into a 20 ml glass vial. A solution of ferrocenium tetrakis[3,5-bis(trifluoromethyl)phenyl]borate (102.4 mg, 97.6 μmol) in tetrahydrofuran (5 ml) was added to the vial and stirred at room temperature for 30 min turning the



solution dark blue. Volatiles were removed *in vacuo* to leave a blue, oily solid. Oil was washed with pentane to remove ferrocene. Oil was dried to leave a blue solid. Yield (134 mg, quantitative).

^1H NMR (δ in CD_2Cl_2 , 600 MHz, ppm, broad singlets): 66.56, 63.37, 28.84, 0.86, -6.62, -16.24, -42.07, -209.09 ^{11}B NMR (δ in CD_2Cl_2 , 600 MHz, ppm): -5.95, ^{19}F NMR (δ in CD_2Cl_2 , 600 MHz, ppm): δ -62.38. IR (neat, cm^{-1}) 3012, 2966, 1588, 1468, 1349, 1275, 1121, 1044, 982, 951, 921, 885, 882, 774, 735 and 685.

Standard Procedure for the polymerization of *N*-carboxyanhydrides by iron bis(imino)pyridine complexes

In a nitrogen-filled glove box, γ -benzyl-*L*-glutamate *N*-carboxyanhydride (100 mg, 380.0 μmol) was dissolved in tetrahydrofuran (0.85 ml) in a glass vial. Iron Complex **3.1** (2.0 mg, 3.8

μmol) was dissolved in 0.25 ml of THF. The two solutions were combined and stirred at room temperature. Aliquots were removed periodically and terminated with benzoic acid. Solvent was removed *in vacuo* and conversion was determined for γ -benzyl-*L*-glutamate-NCA by ^1H NMR in CDCl_3 by comparing the benzyl methylene protons on the NCA and polymer to the methine protons on the monomer. The poly(γ -benzyl-*L*-glutamate) was then dissolved in chloroform and precipitated into diethyl ether and dried to leave a light tan solid. Due to the overlap of monomer and polymer signals for sarcosine-NCA by both ^1H NMR and IR in THF, conversion was determined by dissolving the polymer in chloroform and precipitating the mixture in diethyl ether. Polymer was dried *in vacuo* and the mass obtained was compared to the expected mass at 100 % conversion. This was supported by the ratio of methyl groups on the neopentyl ester to the methylene protons in the precipitated polymer.

Sample procedure for the redox-switchable polymerization of γ -benzyl-*L*-glutamate-NCA

In a nitrogen-filled glove box, γ -benzyl-*L*-glutamate *N*-carboxyanhydride (500 mg, 1.90 mmol) was dissolved in tetrahydrofuran (4.0 ml) in a glass vial. Complex **3.1** (9.7 mg, 18.9 μmol) was dissolved in THF (1.0 ml). The two solutions were combined at room temperature and allowed to stir. Aliquots (0.36 ml) were taken at 0.25, 0.50, 1.0, 2.0 and 3.0 h and terminated with benzoic acid. Ferrocenium tetrakis[3,5-bis(trifluoromethyl)phenyl]borate (12.8 mg, 12.2 μmol) was added to the remaining solution turning it blue. Aliquots (0.36 ml) were taken after an additional 1.0, 2.0 and 4.0 h and terminated with benzoic acid. Cobaltocene (1.5 mg, 8.2 μmol) was added to the remaining solution turning it yellow-green. Aliquots (0.36 ml) were taken after an additional 0.25, 0.50, 1.0, 2.0, 3.0 and 5.0 h and then quenched with benzoic acid. Solvent was removed *in vacuo* and conversion was determined by ^1H NMR in CDCl_3 by the benzyl peaks

in the monomer and polymer against the methine protons of the monomer. Polymer was collected by precipitating the polymer from dichloromethane into diethyl ether until all monomer is removed. $^1\text{H NMR}$ (δ in CDCl_3 , 500 MHz, ppm) δ = 1.78-2.68 broad ($2\text{H} \times n$ ($-\text{CH}_2\text{CH}_2\text{C}(\text{O})\text{O}-$) $_n$), 3.85-4.05 broad ($2\text{H} \times n$ ($-\text{CH}_2\text{CH}_2\text{C}(\text{O})\text{O}-$) $_n$), 4.45-4.69 broad ($2\text{H} \times n$ ($-\text{NHCH}(\text{R})\text{C}(\text{O})\text{O}-$) $_n$), 4.90-5.27 broad ($2\text{H} \times n$ ($-\text{C}(\text{O})\text{OCH}_2\text{C}_6\text{H}_5$) $_n$), 7.06- 7.43 ($5\text{H} \times n$ ($-\text{C}(\text{O})\text{OCH}_2\text{C}_6\text{H}_5$) $_n$), and 8.15- 8.39 broad ($1\text{H} \times n$ ($-\text{NHCH}(\text{R})\text{C}(\text{O})-$).

Sample procedure for the redox-switchable polymerization of γ -benzyl-*L*-glutamate-NCA with $[\text{CoCp}_2][\text{BAR}^{\text{F}24}]$

In a nitrogen-filled glove box, γ -benzyl-*L*-glutamate *N*-carboxyanhydride (300 mg, 1.14 mmol) was dissolved in tetrahydrofuran (2.5 ml) in a glass vial. Complex **3.1** (5.8 mg, 11.4 μmol) was dissolved in THF (0.5 ml). The two solutions were combined at room temperature and allowed to stir. Aliquots (0.25 ml) were taken at 0.25, 0.5, 1.0, and 2.0 h and terminated with benzoic acid. Ferrocenium tetrakis[3,5-bis(trifluoromethyl)phenyl]borate (7.9 mg, 7.5 μmol) was added to the remaining solution. Aliquots (0.25 ml) were taken after an additional 0.5, 1.0 and 1.5 h and terminated with benzoic acid. Cobaltocene (0.9 mg, 4.8 μmol) was added to the remaining solution. Aliquots (0.25 ml) were taken after an additional 0.25, 0.50, 1.0, 2.0 and 5.0 h and then quenched with benzoic acid. Solvent was removed *in vacuo* and conversion was determined by $^1\text{H NMR}$ in CDCl_3 by the benzyl peaks in the monomer and polymer against the methine protons of the monomer. Polymer was collected by precipitating the polymer from dichloromethane into diethyl ether until all monomer is removed. $^1\text{H NMR}$ (δ in CDCl_3 , 500 MHz, ppm) δ = 1.76-2.70 broad ($2\text{H} \times n$ ($-\text{CH}_2\text{CH}_2\text{C}(\text{O})\text{O}-$) $_n$), 3.83-4.07 broad ($2\text{H} \times n$ ($-\text{CH}_2\text{CH}_2\text{C}(\text{O})\text{O}-$) $_n$),

4.47-4.72 broad (2H x n (-NHCH(R)C(O)O-)_n), 4.85- 5.30 broad (2H x n (-C(O)OCH₂C₆H₅)_n), 7.04-7.46 (5H x n (-C(O)OCH₂C₆H₅)_n), and 8.10- 8.50 broad (1H x n (-NHCH(R)C(O)-).

Standard Procedure for the polymerization of γ -benzyl-L-glutamate-NCA by iron complexes with various additives

In a nitrogen-filled glove box, γ -benzyl-L-glutamate *N*-carboxyanhydride (100.0 mg, 380.0 μ mol) was dissolved in tetrahydrofuran (0.60 ml) in a glass vial. Complex **3.1** (2.0 mg, 3.8 μ mol) and cobaltocenium tetrakis[3,5-bis(trifluoromethyl)phenyl]borate (4.0 mg, 3.8 μ mol) were dissolved in THF (0.25 ml) and added to the monomer. The two solutions were combined and stirred at room temperature for 8 hours. Aliquots were removed periodically and terminated with benzoic acid. Solvent was removed *in vacuo* and conversion was determined for γ -benzyl-L-glutamate *N*-carboxyanhydride by ¹H NMR in CDCl₃ by comparing the benzyl methylene protons on the NCA and polymer to the methine protons on the monomer. The poly(γ -benzyl-L-glutamate) was then dissolved in chloroform and precipitated into diethyl ether and dried to leave a light tan solid.

Procedure for the polymerization of ϵ -caprolactone

In a nitrogen-filled glove box, ϵ -c (100 mg, 876 μ mol) was dissolved in tetrahydrofuran (1.5 ml) in a glass vial. Complex **3.1** (2.20 mg, 4.39 μ mol) was dissolved in tetrahydrofuran (1.0 ml) and allowed to stir for 5 min. The two solutions were then combined at room temperature and allowed to stir for 10 min. Sample was quenched by moist air. Solvent was removed *in vacuo* and conversion was determined by ¹H NMR in CDCl₃ by integrating the methylene protons alpha to the carbonyl on the polymer to the methylene protons alpha to the carbonyl on the monomer.

Polymer was collected by precipitation into methanol. Polymer was further dried *in vacuo* to leave a pale yellow solid (91 mg, 91 %). Conversion ϵ -caprolactone >99 %

SEC (THF): $M_n = 22.0$ kDa, $M_w/M_n = 1.20$ $^1\text{H NMR} = (\delta \text{ in } \text{CDCl}_3, 500 \text{ MHz, ppm})$ 0.94 s (9H) 1.32-1.43 bs (2H x 2n (-CH₂CH₂CH₂₋)_n), 1.52-1.70 bs (4H x 4n (-CH₂CH₂CH₂₋)_n), 2.23- 2.36 bs (2H x 2n (-C(O)CH₂CH₂₋)_n) and 3.93- 4.15s (2H x 2n (-CH₂CH₂O-) _n).

Procedure for the sequential copolymerization of ϵ -caprolactone and sarcosine-NCA

In a nitrogen-filled glove box, ϵ -caprolactone (99.0 mg, 867 μmol) and 1,3,5-trimethoxybenzene (10.2 mg, 60.7 μmol) were dissolved in tetrahydrofuran (1.5 ml) in a glass vial. Complex **3** (9.9 mg, 8.69 μmol) was dissolved in tetrahydrofuran (1.0 ml). The two solutions were combined and stirred at room temperature. 1/5th of the solution was taken as a sample after 10 minutes. Sample was quenched by moist air. Volatiles were removed *in vacuo* and conversion was determined by $^1\text{H NMR}$ in CDCl_3 by integrating the methylene protons on each block of the polymer versus the methylene protons of the monomer. Polymer was precipitated into methanol (44 mg, 89 %) Conversion ϵ -caprolactone >99 % SEC (THF): $M_n = 19.7$ kDa, $M_w/M_n = 1.22$ $^1\text{H NMR} = (\delta \text{ in } \text{CDCl}_3, 500 \text{ MHz, ppm})$

For the next block, cobaltocenium tetrakis[3,5-bis(trifluoromethyl)phenyl]borate (4.10 mg, 3.90 μmol) was added to the solution. Sarcosine N-carboxyanhydride (45 mg, 390 μmol) was then added to the solution and allowed to stir at room temperature. After 1 h, excess benzoic acid was added to terminate the reaction. Solvent was removed *in vacuo* and conversion was determined by $^1\text{H NMR}$ in CDCl_3 by integrating the methylene protons alpha to the carbonyl for poly(caprolactone) to the methylene protons on ϵ -caprolactone and the methine protons on poly(sarcosine) compared to the methine protons of sarcosine *N*-carboxyanhydride. Polymer was

collected by precipitating the polymer into diethyl ether. Polymer was further dried *in vacuo* to leave a yellowish-brown solid (53 mg, 82 %) NMR spectra compared to results in the literature.^{42,43} Conversion ϵ -caprolactone >99 %, Conversion Sarcosine-NCA >99 % SEC (THF): $M_n = 31.2$ kDa, $M_w/M_n = 1.02$ $^1\text{H NMR} = (\delta$ in CDCl_3 , 500 MHz, ppm) 0.77-0.99 s (9H, $\text{C}(\text{CH}_3)_3\text{CH}_2\text{O}-$) 1.31-1.41 (2H x 2n ($-\text{CH}_2\text{CH}_2\text{CH}_2-$)_n), 1.56-1.71 bs (4H x 4n ($-\text{CH}_2\text{CH}_2\text{CH}_2-$)_n), 2.23- 2.35 bs (2H x 2n ($-\text{C}(\text{O})\text{CH}_2\text{CH}_2-$)_n), 2.85- 3.11 bs (3H x 3n ($-\text{C}(\text{O})\text{CH}_2\text{N}(\text{CH}_3)-$)_m), 3.85- 4.31 bs (2H x 2n ($-\text{C}(\text{O})\text{CH}_2\text{N}(\text{CH}_3)-$)_m), 3.95- 4.11 bs (2H x 2n ($-\text{CH}_2\text{CH}_2\text{O}-$)_n), and 3.93- 4.12 bs (2H x 2n ($-\text{CH}_2\text{CH}_2\text{O}-$)_n).

Procedure for the telechelic polymerization of ϵ -caprolactone

In a nitrogen-filled glove box, ϵ -caprolactone (50.0 mg, 438 μmol) was dissolved in tetrahydrofuran (1.0 ml) in a glass vial. Complex **3.7** (2.25 mg, 4.39 μmol) and 1,4-benzenedimethanol (0.30 mg, 2.2 mmol) were dissolved in tetrahydrofuran (1.5 ml) and allowed to stir for 5 min. The two solutions were then combined at room temperature and allowed to stir for 10 min. The solution was quenched in moist air. Solvent was removed *in vacuo* and conversion was determined by $^1\text{H NMR}$ in CDCl_3 by integrating the methylene protons alpha to the carbonyl on the polymer to the methylene protons alpha to the carbonyl on the monomer. Polymer was collected by precipitation into diethyl ether. Polymer was further dried *in vacuo* to leave a light, tan solid (45 mg, 85 %). Conversion ϵ -caprolactone >99 %. SEC (THF): $M_n = 21.0$ kDa, $M_w/M_n = 1.04$. $^1\text{H NMR} = (\delta$ in CDCl_3 , 500 MHz, ppm) 1.32-1.42 bs (2H x 2n ($-\text{CH}_2\text{CH}_2\text{CH}_2-$)_{2n}), 1.52-1.70 bs (4H x 4n ($-\text{CH}_2\text{CH}_2\text{CH}_2-$)_{2n}), 2.23- 2.36 bs (2H x 2n ($-\text{C}(\text{O})\text{CH}_2\text{CH}_2-$)_{2n}), 3.93- 4.15 bs (2H x 2n ($-\text{CH}_2\text{CH}_2\text{O}-$)_{2n}), 5.10 s (4 H $-\text{OCH}_2\text{C}_6\text{H}_4\text{CH}_2\text{O}-$) and 7.34 s (4 H $-\text{OCH}_2\text{C}_6\text{H}_4\text{CH}_2\text{O}-$).

Procedure for the sequential, telechelic copolymerization of ϵ -caprolactone and Sarcosine-NCA

In a nitrogen-filled glove box, ϵ -caprolactone (100.0 mg, 876 μmol) was dissolved in tetrahydrofuran (1.5 ml) in a glass vial. Complex **3.7** (2.30 mg, 4.5 μmol) and 1,4-benzenedimethanol (0.30 mg, 2.2 μmol) were dissolved in tetrahydrofuran (1.0 ml) and allowed to stir for 5 min. The two solutions were then combined at room temperature and allowed to stir for 10 min. 1/2 of the solution was taken as a sample after 10 minutes. Sample was quenched by moist air. Volatiles were removed *in vacuo* and conversion was determined by ^1H NMR in CDCl_3 by integrating the methylene protons alpha to the carbonyl for poly(caprolactone) to the methylene protons on ϵ -caprolactone. Polymer was collected after precipitation in cold methanol and drying *in vacuo* (40 mg, 87 %). Conversion ϵ -caprolactone 95 %. SEC (THF): $M_n = 58.8$ kDa, $M_w/M_n = 1.17$. ^1H NMR= (δ in CDCl_3 , 500 MHz) 1.34-1.43 (2H x 2n (-CH₂CH₂CH₂-)_{2n}), 1.52-1.70 (4H x 4n (-CH₂CH₂CH₂-)_{2n}), 2.28- 2.36 (2H x 2n (-C(O)CH₂CH₂-)_{2n}), 4.03-4.09 (2H x 2n (-CH₂CH₂O-)_{2n}), 5.10 (4 H -OCH₂C₆H₄CH₂O-) and 7.34 (4 H -OCH₂C₆H₄CH₂O-).

For the next block, cobaltocenium tetrakis[3,5-bis(trifluoromethyl)phenyl]borate (2.3 mg, 2.2 μmol) was added to the remaining solution. Sarcosine N-carboxyanhydride (25.2 mg, 219 μmol) was then added to the solution and stirred at room temperature. After 30 min, excess benzoic acid was added to terminate the reaction. Solvent was removed *in vacuo* and conversion was determined by ^1H NMR in CDCl_3 by integrating the methylene protons alpha to the carbonyl for poly(caprolactone) to the methylene protons on ϵ -caprolactone and the methine protons on poly(sarcosine) compared to the methine protons of sarcosine *N*-carboxyanhydride. Polymer was collected by precipitating the polymer into diethyl ether. Polymer was further dried *in vacuo* to

leave a yellowish-brown solid (41 mg, 63 %). NMR spectra compared to results in the literature.^{42,43} Conversion ϵ -caprolactone 95 %, Conversion sarcosine-NCA >99 % SEC (THF): M_n = 75.9 kDa, M_w/M_n = 1.16. ^1H NMR= (δ in CDCl_3 , 600 MHz, ppm) 1.32-1.43 bs (2H x 2n (- $\text{CH}_2\text{CH}_2\text{CH}_2$ -)_{2n}), 1.57-1.70 bs (4H x 4n (- $\text{CH}_2\text{CH}_2\text{CH}_2$ -)_{2n}), 2.25- 2.34 bs (2H x 2n (-C(O) CH_2CH_2 -)_{2n}), 2.83-3.10 bs (3H x 2m (-N(CH_3)-)_{2m}), 3.85- 4.32 bs (2H x 2n (-N(CH_3) $\text{CH}_2\text{C}(\text{O})$ -)_{2m}), 4.03- 4.08 bs (2H x 2n (- $\text{CH}_2\text{CH}_2\text{O}$ -)_{2n}), 3.85- 4.32 bs (2H x 2n (-N(CH_3) $\text{CH}_2\text{C}(\text{O})$ -)_{2n}), 5.10 s (4 H - $\text{OCH}_2\text{C}_6\text{H}_4\text{CH}_2\text{O}$ -) and 7.34 s (4 H - $\text{OCH}_2\text{C}_6\text{H}_4\text{CH}_2\text{O}$ -).

Standard procedure for the polymerization of cyclohexene oxide

In a nitrogen-filled glove box, cyclohexene oxide (50.0 mg, 509 μmol) was dissolved in 2-methyltetrahydrofuran (1.00 ml). Complex **3.2** (7.0 mg, 5.1 μmol) was dissolved in 2-methyltetrahydrofuran (0.45 ml). The two solutions were combined at room temperature and stirred for 1 hour. Sample was quenched in air and conversion was determined by ^1H NMR in CDCl_3 by integrating the methine proton of the polymer versus the methine proton on the monomer. Volatiles were removed *in vacuo* and conversion was further verified by the remaining mass of the polymer. Polymer was precipitated into cold methanol to leave an oily solid. (46 mg, 92 %) SEC (THF): M_n = 10.0 kDa, M_w/M_n = 1.73. ^1H NMR= (δ in CDCl_3 , 500 MHz, ppm) 0.88-0.94 s (9H (-C(CH_3)_{3CH₂O-)), 1.06-2.10 bs (8H x n (-CH(C_4H_8)CHO-)_n), and 3.01-3.72 bs (2H x n (-CH(C_4H_8)CHO-)_n).}

Procedure for the sequential copolymerization of cyclohexene oxide and sarcosine-NCA

In a nitrogen-filled glove box, cyclohexene oxide (85.2 mg, 869 μmol) was dissolved in 2-methyltetrahydrofuran (0.75 ml) in a glass vial. Complex **3.2** (6.0 mg, 4.4 μmol) was dissolved in 2-methyltetrahydrofuran (0.5 ml). The two solutions were combined and stirred at room

temperature. 1/2 of the solution was taken after 4 hours and quenched with benzoic acid. Volatiles were removed *in vacuo* and conversion was determined by ^1H NMR in CDCl_3 by integrating the methine proton of the polymer versus the methine proton on the monomer. Remaining monomer was removed *in vacuo* and polymer was precipitated into methanol (27 mg, 78 %). Cyclohexene oxide conversion 81 %. SEC (THF): $M_n = 18.1$ kDa, $M_w/M_n = 1.79$. ^1H NMR= (δ in CDCl_3 , 500 MHz, ppm) 0.88-0.93 s (9H (-C(CH₃)₃CH₂O-)), 1.07-2.11bs (8H x n (-CH(C₄H₈)CHO-)_n), and 3.04-3.66 bs (2H x n (-CH(C₄H₈)CHO-)_n).

For the next block, cobaltocene (0.41 mg, 2.1 μmol) was added to the remaining solution. Sarcosine-NCA (25 mg, 220 μmol) was then added to the solution. The solution was allowed to stir at room temperature for another 10 min before being quenched with benzoic acid. Volatiles were removed *in vacuo* and conversion was determined by ^1H NMR in CDCl_3 by integrating the methine proton on each block of the polymer versus the methine protons on their respective monomers. The copolymer was collected by precipitation into cold hexanes. Polymer was then dried *in vacuo* to leave a yellowish-brown solid (37 mg, 72 %). Conversion cyclohexene oxide 81 %, Conversion Sarcosine-NCA >99 % SEC (THF): $M_n = 17.5$ kDa, $M_w/M_n = 2.16$. ^1H NMR= (δ in CDCl_3 , 600 MHz, ppm) 0.85-0.91 s (9H (-C(CH₃)₃CH₂O-)), 0.98-2.45 bs (8H x n (-CH(C₄H₈)CHO-)_n), 2.76-3.17 bs (3H x m (-C(O)CH₂N(CH₃)-)_m), 2.76-3.70 bs (2H x n (-CH(C₄H₈)CHO-)_n) and 3.85-4.45 bs (2H x m (-C(O)CH₂N(CH₃)-)_m). ^{13}C NMR= (δ in CDCl_3 , 100 MHz, ppm) 19.41- 21.31, 21.38- 24.34, 25.33- 27.13, 27.98- 32.00, 32.80- 34.58. 69.28- 70. 74, 72.88- 74.93 and 165.43- 170.33.

Procedure for the sequential copolymerization of sarcosine-NCA and cyclohexene oxide

In a nitrogen filled glove box, sarcosine *N*-carboxyanhydride (50 mg, 434 μmol) and were dissolved in 2-methyltetrahydrofuran (2.0 ml) in a glass vial. Complex **3.1** (2.2 mg, 4.3 μmol) was

dissolved in 2-methyltetrahydrofuran (0.5 ml). The two solutions were combined. Cobaltocenium tetrakis[3,5-bis(trifluoromethyl)phenyl]borate (4.5 mg, 4.3 μmol) was then added to the solution and the solution was allowed to stir at room temperature for 10 min. 1/2 of the solution was taken and quenched with benzoic acid. Volatiles were removed *in vacuo* and conversion was determined by ^1H NMR in CDCl_3 by integrating the methine proton on the polymer versus the methine proton on the monomers. Polymer was precipitated in diethyl ether and dried *in vacuo*, to leave a light brown solid (13 mg, 86 %). Conversion sarcosine-NCA >99 % SEC (DMF/LiBr): $M_n = 6.1$ kDa, $M_w/M_n = 1.05$. ^1H NMR= (δ in CDCl_3 , 500 MHz, ppm) 0.85-0.96 s (9H (-C(CH₃)₃CH₂O-)), 2.85-3.15 bs (3H x m (-C(O)CH₂N(CH₃)-)_m), and 3.87-4.34 bs (2H x m (-C(O)CH₂N(CH₃)-)_m).

For the next block ferrocenium tetrakis[3,5-bis(trifluoromethyl)phenyl]borate (2.3 mg, 2.2 μmol) was added to the remaining solution followed by cyclohexene oxide (42.6 mg, 434 μmol) and allowed to stir for an additional 48 h. The sample was then quenched with benzoic acid. Volatiles were removed *in vacuo* and conversion was determined by ^1H NMR in CDCl_3 by integrating the methine proton on each block of the polymer versus the methine proton on the respective monomers. Polymer was collected by precipitation into cold hexanes and dried *in vacuo* to leave a yellowish-brown solid (32 mg, 77 %). Conversion cyclohexene oxide 60 %, Conversion sarcosine-NCA >99 % SEC (THF) $M_n = 16.7$ kDa, $M_w/M_n = 1.15$. ^1H NMR= (δ in CDCl_3 , 600 MHz, ppm) 0.91-0.95 s (9H (-C(CH₃)₃CH₂O-)), 1.03-2.08 bs (8H x n (-CH(C₄H₈)CHO-)_n), 2.78-3.15 bs (3H x m (-C(O)CH₂N(CH₃)-)_m), 2.80-3.70 bs (2H x n (-CH(C₄H₈)CHO-)_n) and 3.79-4.39 bs (2H x m (-C(O)CH₂N(CH₃)-)_m). ^{13}C NMR= (δ in CDCl_3 , 125 MHz, ppm) 19.47-21.74, 21.89- 25.24, 25.56-26.89, 28.60- 34.53, 34.58-34.96, 49.27- 52.13, 69.01- 70.57 and 167.68- 169.82.

Procedure for the sequential copolymerization of cyclohexene oxide, Sarcosine-NCA then cyclohexene oxide

In a nitrogen-filled glove box, **4** (5.9 mg, 12 μmol) was dissolved in 2-methyltetrahydrofuran (0.5 ml) in a glass vial. To this was added cyclohexene oxide (85.3 mg, 869 μmol) was dissolved in 2-methyltetrahydrofuran (0.50 ml). The two solutions were combined and stirred at room temperature for 4 h. 1/3rd of the sample was taken and quenched in air. Volatiles were removed *in vacuo* and conversion was determined by ^1H NMR in CDCl_3 by integrating the methine proton on the polymer versus the methine proton on the respective monomers. The polymer sample was collected by precipitation into methanol (18 mg, 75 %). Conversion cyclohexene oxide 84 %. SEC (THF): $M_n = 23.5$ kDa, $M_w/M_n = 1.58$. ^1H NMR= (δ in CDCl_3 , 500 MHz, ppm) 0.86-0.92 s (9H (-OCH₂(CH₃)₃), 1.05-2.06 bs (8H x m (-OCH(C₄H₈)CH-)m) and 3.02-3.63 bs (2H x m (-OCH(C₄H₈)CH-)m).

For the next block, sarcosine *N*-carboxyanhydride (33.3 mg, 289 μmol) was dissolved in 2-methyltetrahydrofuran (1.5 ml) and added to the solution. Cobaltocene (0.55 mg, 2.9 μmol) in 2-methyltetrahydrofuran (0.1 ml) was added to the solution right afterward. The solution was allowed to stir at room temperature for 15 min before another 1/3^{re} of the solution was taken and terminated with a slight excess of benzoic acid. Volatiles were removed *in vacuo* and conversion was determined by ^1H NMR in CDCl_3 by integrating the methine proton on each block of the polymer versus the methine proton on the respective monomers. The polymer sample was collected by precipitation into cold acetone (29 mg, 84 %). Conversion Sarcosine-NCA >99 % Conversion cyclohexene oxide 84 %. SEC (THF): $M_n = 32.2$ kDa. $M_w/M_n = 1.38$. ^1H NMR= (δ in CDCl_3 ,

500 MHz, ppm) 0.77-0.93 bs (9H (-OCH₂(CH₃)₃), 1.02-2.13 bs (8H x m (-OCH(C₄H₈)CH-) _m), 2.84-3.13 bs (3H x n (-N(CH₃)CH₂C(O)-) _n), 3.14-3.70 bs (2H x m (-OCH(C₄H₈)CH-) _m) and 3.84-4.40 bs (2H x n (-N(CH₃)CH₂C(O)-) _n).

For the final block, ferrocenium tetrakis[3,5-bis(trifluoromethyl)phenyl]borate (1.5 mg, 1.4 μmol) was added to the solution. Cyclohexene oxide (28.4 mg, 289 μmol) was added to the solution right afterwards and the solution stirred at room temperature for a final 24 h. The sample was then quenched with a slight excess of benzoic acid. Volatiles were removed *in vacuo* and conversion was determined by ¹H NMR in CDCl₃ by integrating the methine proton on each block of the polymer versus the methine proton on the respective monomers. The polymer sample was collected by precipitation into cold acetone. Polymer was further dried *in vacuo* to leave a yellowish-brown solid (29 mg, 61 %). Conversion Sarcosine-NCA >99 % Conversion cyclohexene oxide 65 %. SEC (THF): $M_n = 48.4$ kDa. $M_w/M_n = 1.40$. ¹H NMR= (δ in CDCl₃, 500 MHz, ppm) 0.79-0.93 bs (9H (-OCH₂(CH₃)₃), 1.01-2.08 bs (8H x m (-OCH(C₄H₈)CH-) _m), 2.84-3.15 bs (3H x n (-N(CH₃)CH₂C(O)-) _n), 3.15-3.65 bs (2H x m (-OCH(C₄H₈)CH-) _m) and 3.84-4.40 bs (2H x n (-N(CH₃)CH₂C(O)-) _n). ¹³C NMR= (δ in CDCl₃, 125 MHz, ppm) 19.7, 20.2- 20.9 m, 22.0- 23.0, 23.0-23.9, 25.9- 26.2, 26.3- 27.0, 28.2- 31.6, 33.0- 33.5, 33.6- 34.2, 35.2- 36.3, 48.8- 51.5, 68.7, 69.4-70.5, 71.1, 77.6- 82.0, 167.9.

Procedure for the sequential copolymerization of sarcosine-NCA, cyclohexene oxide then sarcosine-NCA

In a nitrogen-filled glove box, sarcosine *N*-carboxyanhydride (50.0 mg, 435 μmol) was dissolved in 2-methyltetrahydrofuran (2.0 ml). Complex **3.1** (2.2 mg, 4.3 μmol) was dissolved in 2-methyltetrahydrofuran (0.5 ml) in a glass vial and added to the monomer solution.

Cobaltocenium tetrakis[3,5-bis(trifluoromethyl)phenyl]borate (4.5 mg, 4.3 μmol) was then added to the mixture and allowed to stir at room temperature for 10 min. 1/4th of the sample was taken and quenched with a slight excess of benzoic acid. Volatiles were removed *in vacuo* and conversion was determined by ¹H NMR in CDCl₃ by integrating the methine proton on the polymer versus the methine proton on the monomers. Polymer was precipitated into diethyl ether (9.4 mg, 91 %). Conversion Sarcosine-NCA >99 % SEC (DMF/LiBr): $M_n = 6.7$ kDa, $M_w/M_n = 1.06$. ¹H NMR= (δ in CDCl₃, 500 MHz, ppm) 0.89-0.97 s (9H (-OCH₂(CH₃)₃), 2.85-3.16 bs (3H x n (-N(CH₃)CH₂C(O)-)_n) and 3.90-4.32 bs (2H x n (-N(CH₃)CH₂C(O)-)_n).

For the next block, ferrocenium tetrakis[3,5-bis(trifluoromethyl)phenyl]borate (3.4 mg, 3.2 μmol) was added to the solution. Cyclohexene oxide (127.9 mg, 1.300 mmol) was added to the solution immediately afterwards and the solution stirred at room temperature for a 48 h. Another 1/3rd of the solution was taken for sampling and quenched with a slight excess of benzoic acid. Volatiles were removed *in vacuo* and conversion was determined by ¹H NMR in CDCl₃ by integrating the methine proton on each block of the polymer versus the methine proton on the respective monomers. The polymer sample was collected by precipitation into cold acetone (30 mg, 48 %). Conversion cyclohexene oxide 92 %, Conversion sarcosine-NCA >99 %. SEC (THF): $M_n = 46.3$ kDa, $M_w/M_n = 1.36$. ¹H NMR= (δ in CDCl₃, 500 MHz, ppm) 0.78-0.94 bs (9H (-OCH₂(CH₃)₃), 1.02-2.11 bs (8H x m (-OCH(C₄H₈)CH-)_m), 2.88-3.15 bs (3H x n (-N(CH₃)CH₂C(O)-)_n), 3.15-3.66 bs (2H x m (-OCH(C₄H₈)CH-)_m) and 3.70-4.41 bs (2H x n (-N(CH₃)CH₂C(O)-)_n).

For the final block, sarcosine *N*-carboxyanhydride (25.0 mg, 217 μmol) was dissolved in 2-methyltetrahydrofuran (0.9 ml) and added to the solution. Cobaltocene (0.41 mg, 2.1 μmol) was added to the solution immediately afterwards. The solution was allowed to stir at room

temperature for 10 min before being quenched with a slight excess of benzoic acid. Volatiles were removed *in vacuo* and conversion was determined by ^1H NMR in CDCl_3 by integrating the methine proton on each block of the polymer versus the methine proton on the respective monomers. The polymer sample was collected by precipitation into diethyl ether. The polymer sample was collected by precipitation into cold acetone. Polymer was further dried in *vacuo* to leave a yellowish-brown solid (54 mg, 73 %). Conversion cyclohexene oxide 92 %, Conversion Sarcosine-NCA >99 % SEC (THF): $M_n = 64.2$ kDa, $M_w/M_n = 1.15$. ^1H NMR= (δ in CDCl_3 , 500 MHz, ppm) 0.79-0.94 bs (9H (-OCH₂(CH₃)₃), 1.05-2.22 bs (8H x m (-OCH(C₄H₈)CH-)m), 2.89-3.13 bs (3H x n (-N(CH₃)CH₂C(O)-)n), 3.09-3.65 bs (2H x m (-OCH(C₄H₈)CH-)m) and 3.84-4.38 bs (2H x n (-N(CH₃)CH₂C(O)-)n). ^{13}C NMR= (δ in CDCl_3 , 125 MHz, ppm) 22.4, 22.7- 23.7, 24.7- 25.6, 25.6- 26.5, 28.6, 28.9- 29.6, 30.3- 34.3, 36.4, 37.3- 39.2, 51.2- 54.0, 71.7- 73.0, 73.7, 75.2- 85.0, 137.4, 169.7- 172.6.

3.8 References

- (1) García, J. M.; García, F. C.; Serna, F.; de la Peña, J. L. High-Performance Aromatic Polyamides. *Progress in Polymer Science (Oxford)* **2010**, *35*, 623–686.
- (2) Song, L.; Zhu, T.; Yuan, L.; Zhou, J.; Zhang, Y.; Wang, Z.; Tang, C. Ultra-Strong Long-Chain Polyamide Elastomers with Programmable Supramolecular Interactions and Oriented Crystalline Microstructures. *Nature Communications* **2019**, *10* (1), 1–8.
<https://doi.org/10.1038/s41467-019-09218-6>.
- (3) Shakiba, M.; Rezvani Ghomi, E.; Khosravi, F.; Jouybar, S.; Bigham, A.; Zare, M.; Abdouss, M.; Moaref, R.; Ramakrishna, S. Nylon—A Material Introduction and Overview for Biomedical Applications. *Polymers for Advanced Technologies* **2021**, *32* (9), 3368–3383.
<https://doi.org/10.1002/pat.5372>.
- (4) Trigo-López, M.; Sanjuán, A. M.; Mendía, A.; Muñoz, A.; García, F. C.; García, J. M. Heteroaromatic Polyamides with Improved Thermal and Mechanical Properties. *Polymers* **2020**, *12* (8). <https://doi.org/10.3390/polym12081793>.
- (5) Marchildon, K. Polyamides - Still Strong after Seventy Years. *Macromolecular Reaction Engineering* **2011**, *5*, 22–54.
- (6) *Nylon 6 & 66 Market Analysis By Product (Nylon 6, Nylon 66) By Application (Automotive, Electrical & Electronic, Engineering Plastic, Textiles, Others), By Region, And Segment Forecasts, 2018 - 2025*; 2017.
- (7) Rippon, J. A.; Christoe, J. R.; Denning, R. J.; Evans, D. J.; Huson, M. G.; Lamb, P. R.; Millington, K. R.; Pierlot, A. P. *Wool: Structure, Properties, and Processing*; 2016.

<https://doi.org/10.1002/0471440264.pst402.pub2>.

- (8) Qiu, W.; Patil, A.; Hu, F.; Liu, X. Y. Hierarchical Structure of Silk Materials Versus Mechanical Performance and Mesoscopic Engineering Principles. *Small* **2019**, *15* (51), 1–45. <https://doi.org/10.1002/sml.201903948>.
- (9) Bromberg, L. E.; Ron, E. S. Temperature-Responsive Gels and Thermogelling Polymer Matrices for Protein and Peptide Delivery. *Advanced Drug Deliv* **1998**, *31* (2), 197–221.
- (10) Wu, S.; Snajdrova, R.; Moore, J. C.; Baldenius, K.; Bornscheuer, U. T. Biocatalysis: Enzymatic Synthesis for Industrial Applications. *Angewandte Chemie - International Edition* **2021**, *60* (1), 88–119. <https://doi.org/10.1002/anie.202006648>.
- (11) Lee, A. C. L.; Harris, J. L.; Khanna, K. K.; Hong, J. H. A Comprehensive Review on Current Advances in Peptide Drug Development and Design. *International Journal of Molecular Sciences* **2019**, *20* (10), 1–21. <https://doi.org/10.3390/ijms20102383>.
- (12) Van Beek, J. D.; Hesst, S.; Vollrath, F.; Meier, B. H. The Molecular Structure of Spider Dragline Silk: Folding and Orientation of the Protein Backbone. *Proceedings of the National Academy of Sciences of the United States of America* **2002**, *99* (16), 10266–10271. <https://doi.org/10.1073/pnas.152162299>.
- (13) Agarwal, P. K. Enzymes: An Integrated View of Structure, Dynamics and Function. *Microbial Cell Factories* **2006**, *5*, 1–12. <https://doi.org/10.1186/1475-2859-5-2>.
- (14) Deming, T. J. *UCLA Synthesis and Self-Assembly of Well Defined Block Copolypeptides Via*; 2013; Vol. 262. <https://doi.org/10.1007/12>.
- (15) González-Henríquez, C. M.; Sarabia-Vallejos, M. A.; Rodríguez-Hernández, J. Strategies to Fabricate Polypeptide-Based Structures via Ring-Opening Polymerization of N-

- Carboxyanhydrides. *Polymers* **2017**, *9* (11). <https://doi.org/10.3390/polym9110551>.
- (16) Rasines Mazo, A.; Allison-Logan, S.; Karimi, F.; Chan, N. J. A.; Qiu, W.; Duan, W.; O'Brien-Simpson, N. M.; Qiao, G. G. Ring Opening Polymerization of α -Amino Acids: Advances in Synthesis, Architecture and Applications of Polypeptides and Their Hybrids. *Chemical Society Reviews* **2020**, *49* (14), 4737–4834. <https://doi.org/10.1039/c9cs00738e>.
- (17) Habraken, G. J. M.; Wilsens, K. H. R. M.; Koning, C. E.; Heise, A. Optimization of N-Carboxyanhydride (NCA) Polymerization by Variation of Reaction Temperature and Pressure. *Polymer Chemistry* **2011**, *2* (6), 1322–1330. <https://doi.org/10.1039/c1py00079a>.
- (18) Fan, J.; Zou, J.; He, X.; Zhang, F.; Zhang, S.; Raymond, J. E.; Wooley, K. L. Tunable Mechano-Responsive Organogels by Ring-Opening Copolymerizations of N-Carboxyanhydrides. *Chemical Science* **2013**, *5*, 141–150.
- (19) Zou, J.; Fan, J.; He, X.; Zhang, S.; Wang, H.; Wooley, K. L. A Facile Glovebox-Free Strategy to Significantly Accelerate the Syntheses of Well-Defined Polypeptides by N-Carboxyanhydride (NCA) Ring-Opening Polymerizations. *Macromolecules* **2013**, *46*, 4223–4226.
- (20) Pickel, D. L.; Politakos, N.; Avgeropoulos, A.; Messman, J. M. A Mechanistic Study of α -(Amino Acid)-n-Carboxyanhydride Polymerization: Comparing Initiation and Termination Events in High-Vacuum and Traditional Polymerization Techniques. *Macromolecules* **2009**, *42* (20), 7781–7788. <https://doi.org/10.1021/ma901340y>.
- (21) Zhao, W.; Gnanou, Y.; Hadjichristidis, N. Fast and Living Ring-Opening Polymerization of α -Amino Acid N-Carboxyanhydrides Triggered by an “Alliance” of Primary and Secondary

- Amines at Room Temperature. *Biomacromolecules* **2015**, *16* (4), 1352–1357.
<https://doi.org/10.1021/acs.biomac.5b00134>.
- (22) Zhao, W.; Gnanou, Y.; Hadjichristidis, N. From Competition to Cooperation: A Highly Efficient Strategy towards Well-Defined (Co)Polypeptides. *Chemical Communications* **2015**, *51*, 3663–3666.
- (23) Chen, C.; Fu, H.; Baumgartner, R.; Song, Z.; Lin, Y.; Cheng, J. Proximity-Induced Cooperative Polymerization in “Hinged” Helical Polypeptides. *Journal of the American Chemical Society* **2019**, *141*, 8680–8683.
- (24) Song, Z.; Fu, H.; Baumgartner, R.; Zhu, L.; Shih, K. C.; Xia, Y.; Zheng, X.; Yin, L.; Chipot, C.; Lin, Y.; et al. Enzyme-Mimetic Self-Catalyzed Polymerization of Polypeptide Helices. *Nature Communications* **2019**, *10*, 1–7.
- (25) Lv, S.; Kim, H.; Song, Z.; Feng, L.; Yang, Y.; Baumgartner, R.; Tseng, K. Y.; Dillon, S. J.; Leal, C.; Yin, L.; et al. Unimolecular Polypeptide Micelles via Ultrafast Polymerization of N-Carboxyanhydrides. *Journal of the American Chemical Society* **2020**, *142* (19), 8570–8574.
<https://doi.org/10.1021/jacs.0c01173>.
- (26) Wang, X.; Song, Z.; Tan, Z.; Zhu, L.; Xue, T.; Lv, S.; Fu, Z.; Zheng, X.; Ren, J.; Cheng, J. Facile Synthesis of Helical Multiblock Copolypeptides: Minimal Side Reactions with Accelerated Polymerization of N-Carboxyanhydrides. *ACS Macro Letters* **2019**, *8*, 1517–1521.
<https://doi.org/10.1021/acsmacrolett.9b00784>.
- (27) Grazon, C.; Salas-Ambrosio, P.; Ibarboure, E.; Buol, A.; Garanger, E.; Grinstaff, M. W.; Lecommandoux, S.; Bonduelle, C. Aqueous Ring-Opening Polymerization-Induced Self-Assembly (ROPISA) of N-Carboxyanhydrides. *Angewandte Chemie - International Edition*

- 2020**, *59*, 622–626.
- (28) Wu, Y.; Zhang, D.; Ma, P.; Zhou, R.; Hua, L.; Liu, R. Lithium Hexamethyldisilazide Initiated Superfast Ring Opening Polymerization of Alpha-Amino Acid N-Carboxyanhydrides. *Nature Communications* **2018**, *9*, 1–10.
- (29) Wu, Y. M.; Zhang, W. W.; Zhou, R. Y.; Chen, Q.; Xie, C. Y.; Xiang, H. X.; Sun, B.; Zhu, M. F.; Liu, R. H. Facile Synthesis of High Molecular Weight Polypeptides via Fast and Moisture Insensitive Polymerization of α -Amino Acid N-Carboxyanhydrides. *Chinese Journal of Polymer Science (English Edition)* **2020**, *38* (10), 1131–1140.
<https://doi.org/10.1007/s10118-020-2471-1>.
- (30) Li, G.; Donghui, Z. Cyclic Poly(α -Peptoid)s and Their Block Copolymers from N-Heterocyclic Carbene-Mediated Ring-Opening Polymerizations of N-Substituted N-Carboxylanhydrides. *Journal of the American Chemical Society* **2009**, *131*, 18072–18074.
- (31) Zhang, H.; Nie, Y.; Zhi, X.; Du, H.; Yang, J. Controlled Ring-Opening Polymerization of α -Amino Acid N-Carboxy-Anhydride by Frustrated Amine/Borane Lewis Pairs. *Chemical Communications* **2017**, *53* (37), 5155–5158. <https://doi.org/10.1039/c7cc01440f>.
- (32) Xia, Y.; Song, Z.; Tan, Z.; Xue, T.; Wei, S.; Zhu, L.; Yang, Y.; Fu, H.; Jiang, Y.; Lin, Y.; et al. Accelerated Polymerization of N-Carboxyanhydrides Catalyzed by Crown Ether. *Nature Communications* **2021**, *12* (1). <https://doi.org/10.1038/s41467-020-20724-w>.
- (33) Deming, T. J. Transition Metal-Amine Initiators for Preparation of Well-Defined Poly(γ -Benzyl L-Glutamate). *Journal of the American Chemical Society* **1997**, *119*, 2759–2760.
- (34) Raman, S. K.; Brulé, E.; Tschan, M. J. L.; Thomas, C. M. Tandem Catalysis: A New Approach to Polypeptides and Cyclic Carbonates. *Chemical Communications* **2014**, *50*

- (89), 13773–13776. <https://doi.org/10.1039/c4cc05730a>.
- (35) Nie, Y.; Zhi, X.; Du, H.; Yang, J. Zn(OAc)₂-Catalyzing Ring-Opening Polymerization of N-Carboxyanhydrides for the Synthesis of Well-Defined Polypeptides. *Molecules* **2018**, *23* (4). <https://doi.org/10.3390/molecules23040760>.
- (36) Peng, H.; Ling, J.; Shen, Z. Ring Opening Polymerization of α -Amino Acid N-Carboxyanhydrides Catalyzed by Rare Earth Catalysts: Polymerization Characteristics and Mechanism. *Journal of Polymer Science, Part A: Polymer Chemistry* **2012**, *50* (6), 1076–1085. <https://doi.org/10.1002/pola.25848>.
- (37) Peng, H.; Ling, J.; Zhu, Y.; You, L.; Shen, Z. Polymerization of α -Amino Acid N-Carboxyanhydrides Catalyzed by Rare Earth Tris(Borohydride) Complexes: Mechanism and Hydroxy-Endcapped Polypeptides. *Journal of Polymer Science, Part A: Polymer Chemistry* **2012**, *50* (15), 3016–3029. <https://doi.org/10.1002/pola.26077>.
- (38) Ling, J.; Peng, H.; Shen, Z. Deprotonation Reaction of α -Amino Acid N-Carboxyanhydride at 4-CH Position by Yttrium Tris[Bis(Trimethylsilyl)Amide]. *Journal of Polymer Science, Part A: Polymer Chemistry* **2012**, *50* (18), 3743–3749. <https://doi.org/10.1002/pola.26156>.
- (39) Deming, T. J. Facile Synthesis of Block Copolypeptides of Defined Architecture. *Nature* **1997**, *390*, 386–389.
- (40) Deming, T. J. Cobalt and Iron Initiators for the Controlled Polymerization of α -Amino Acid-N-Carboxyanhydrides. *Macromolecules* **1999**, *32* (13), 4500–4502. <https://doi.org/10.1021/ma9902899>.
- (41) Deming, T. J.; Curtin, S. A. Chain Initiation Efficiency in Cobalt- and Nickel-Mediated

- Polypeptide Synthesis. *Journal of the American Chemical Society* **2000**, *122* (24), 5710–5717. <https://doi.org/10.1021/ja994281q>.
- (42) Cui, S.; Wang, X.; Li, Z.; Zhang, Q.; Wu, W.; Liu, J.; Wu, H.; Chen, C.; Guo, K. One-Pot Glovebox-Free Synthesis, Characterization, and Self-Assembly of Novel Amphiphilic Poly(Sarcosine-*b*-Caprolactone) Diblock Copolymers. *Macromolecular Rapid Communications* **2014**, *35*, 1954–1959.
- (43) Cui, S.; Pan, X.; Gebru, H.; Wang, X.; Liu, J.; Liu, J.; Li, Z.; Guo, K. Amphiphilic Star-Shaped Poly(Sarcosine)-Block-Poly(ϵ -Caprolactone) Diblock Copolymers: One-Pot Synthesis, Characterization, and Solution Properties. *Journal of Materials Chemistry B* **2017**, *5*, 679–690.
- (44) Gradišar, Š.; Žagar, E.; Pahovnik, D. Hybrid Block Copolymers of Polyesters/Polycarbonates and Polypeptides Synthesized via One-Pot Sequential Ring-Opening Polymerization. *Polymer Chemistry* **2018**, *9* (38), 4764–4771. <https://doi.org/10.1039/c8py00835c>.
- (45) Schmid, T. E.; Robert, C.; Richard, V.; Raman, S. K.; Guérineau, V.; Thomas, C. M. Aluminum-Catalyzed One-Pot Synthesis of Polyester-*b*-Polypeptide Block Copolymers by Ring-Opening Polymerization. *Macromolecular Chemistry and Physics* **2019**, *220* (14), 1–4. <https://doi.org/10.1002/macp.201900040>.
- (46) Deng, C.; Rong, G.; Tian, H.; Tang, Z.; Chen, X.; Jing, X. Synthesis and Characterization of Poly(Ethylene Glycol)-*b*-Poly(L-Lactide)-*b*-Poly(L-Glutamic Acid) Triblock Copolymer. *Polymer* **2005**, *46* (3), 653–659. <https://doi.org/10.1016/j.polymer.2004.11.100>.
- (47) Planellas, M.; Puiggali, J. Synthesis and Properties of Poly(L-Lactide)-*b*-Poly(L-

- Phenylalanine) Hybrid Copolymers. *International Journal of Molecular Sciences* **2014**, *15*, 13247–13266.
- (48) Guo, A. R.; Yang, W. X.; Yang, F.; Yu, R.; Wu, Y. X. Well-Defined Poly(γ -Benzyl- L - Glutamate)- g -Polytetrahydrofuran: Synthesis, Characterization, and Properties. *Macromolecules* **2014**, *47*, 5450–5461.
- (49) Duan, L. J.; Kim, M. J.; Jung, J. H.; Chung, D. J.; Kim, J. Synthesis of Poly(L,L-Lactic Acid-Co-Lysine) and Its Cell Compatibility Evaluation as Coating Material on Metal. *Macromolecular Research* **2010**, *18*, 806–811.
- (50) Price, D. J.; Khuphe, M.; Davies, R. P. W.; McLaughlan, J. R.; Ingram, N.; Thornton, P. D. Poly(Amino Acid)-Polyester Graft Copolymer Nanoparticles for the Acid-Mediated Release of Doxorubicin. *Chemical Communications* **2017**, *53*, 8687–8690.
- (51) Dorresteyn, R.; Ragg, R.; Rago, G.; Billecke, N.; Bonn, M.; Parekh, S. H.; Battagliarin, G.; Peneva, K.; Wagner, M.; Klapper, M.; et al. Biocompatible Polylactide- Block - Polypeptide- Block -Polylactide Nanocarrier. **2013**, 8–13.
- (52) Sill, K. N.; Sullivan, B.; Carie, A.; Edward Semple, J. Synthesis and Characterization of Micelle-Forming PEG-Poly(Amino Acid) Copolymers with Iron-Hydroxamate Cross-Linkable Blocks for Encapsulation and Release of Hydrophobic Drugs. *Biomacromolecules* **2017**, *18*, 1874–1884.
- (53) Birke, A.; Ling, J.; Barz, M. Polysarcosine-Containing Copolymers: Synthesis, Characterization, Self-Assembly, and Applications. *Progress in Polymer Science* **2018**, *81*, 163–208.
- (54) Caillol, S.; Lecommandoux, S.; Mingotaud, A. F.; Schappacher, M.; Soum, A.; Bryson, N.;

- Meyrueix, R. Synthesis and Self-Assembly Properties of Peptide-Polylactide Block Copolymers. *Macromolecules* **2003**, *36*, 1118–1124.
- (55) Peng, H.; Xiao, Y.; Mao, X.; Chen, L.; Crawford, R.; Whittaker, A. K. Amphiphilic Triblock Copolymers of Methoxy-Poly(Ethylene Glycol)-b-Poly(L-Lactide)-b-Poly(L-Lysine) for Enhancement of Osteoblast Attachment and Growth. *Biomacromolecules* **2009**, *10*, 95–104.
- (56) Tinajero-Díaz, E.; Martínez de Ilarduya, A.; Muñoz-Guerra, S. Synthesis and Properties of Diblock Copolymers of ω -Pentadecalactone and α -Amino Acids. *European Polymer Journal* **2019**, *116*, 169–179.
- (57) Dimitrov, I.; Schlaad, H. Synthesis of Nearly Monodisperse Polystyrene-Polypeptide Block Copolymers via Polymerisation of N-Carboxyanhydrides. *Chemical Communications* **2003**, *3* (23), 2944–2945. <https://doi.org/10.1039/b308990h>.
- (58) Radchenko, A. V.; Grange, J.; Vax, A.; Jean-Baptiste-Dit-Dominique, F.; Matmour, R.; Grelier, S.; Peruch, F. Facile Synthesis of 1,4-: Cis -Polyisoprene-Polypeptide Hybrids with Different Architectures. *Polymer Chemistry* **2019**, *10* (19), 2456–2468. <https://doi.org/10.1039/c9py00241c>.
- (59) Floudas, G.; Papadopoulos, P.; Klok, H. A.; Vandermeulen, G. W. M.; Rodriguez-Hernandez, J. Hierarchical Self-Assembly of Poly(γ -Benzyl-L-Glutamate)-Poly(Ethylene Glycol)-Poly(γ -Benzyl-L-Glutamate) Rod-Coil-Rod Triblock Copolymers. *Macromolecules* **2003**, *36* (10), 3673–3683. <https://doi.org/10.1021/ma025918k>.
- (60) Meyer, M.; Schlaad, H.; March, R. V.; Re, V.; Recci, M.; March, V. Poly (2-Isopropyl-2-Oxazoline) - Poly (L -Glutamate) Block Copolymers through Ammonium-Mediated NCA

- Polymerization. **2006**, 3967–3970.
- (61) Teator, A. J.; Lastovickova, D. N.; Bielawski, C. W. Switchable Polymerization Catalysts. *Chemical Reviews* **2016**, *116*, 1969–1992.
- (62) Chen, C. Redox-Controlled Polymerization and Copolymerization. *ACS Catalysis* **2018**, *8* (6), 5506–5514. <https://doi.org/10.1021/acscatal.8b01096>.
- (63) Wang, X.; Thevenon, A.; Brosmer, J. L.; Yu, I.; Khan, S. I.; Mehrkhodavandi, P.; Diaconescu, P. L. Redox Control of Group 4 Metal Ring-Opening Polymerization Activity toward ϵ -Lactide and ϵ -Caprolactone. *Journal of the American Chemical Society* **2014**, *136* (32), 11264–11267. <https://doi.org/10.1021/ja505883u>.
- (64) Biernesser, A. B.; Delle Chiaie, K. R.; Curley, J. B.; Byers, J. A. Block Copolymerization of Lactide and an Epoxide Facilitated by a Redox Switchable Iron-Based Catalyst. *Angewandte Chemie* **2016**, *128* (17), 5337–5340. <https://doi.org/10.1002/ange.201511793>.
- (65) Quan, S. M.; Wang, X.; Zhang, R.; Diaconescu, P. L. Redox Switchable Copolymerization of Cyclic Esters and Epoxides by a Zirconium Complex. *Macromolecules* **2016**, *49* (18), 6768–6778. <https://doi.org/10.1021/acs.macromol.6b00997>.
- (66) Qi, M.; Dong, Q.; Wang, D.; Byers, J. A. Electrochemically Switchable Ring-Opening Polymerization of Lactide and Cyclohexene Oxide. *Journal of the American Chemical Society* **2018**, *140* (17), 5686–5690. <https://doi.org/10.1021/jacs.8b02171>.
- (67) Zhao, M.; Chen, C. Accessing Multiple Catalytically Active States in Redox-Controlled Olefin Polymerization. *ACS Catalysis* **2017**, *7* (11), 7490–7494. <https://doi.org/10.1021/acscatal.7b02564>.

- (68) Mundil, R.; Wilson, L. E.; Schaarschmidt, D.; Císařová, I.; Merna, J.; Long, N. J. Redox-Switchable α -Diimine Palladium Catalysts for Control of Polyethylene Topology. *Polymer* **2019**, *179* (April). <https://doi.org/10.1016/j.polymer.2019.121619>.
- (69) Delle Chiaie, K. R.; Yablon, L. M.; Biernesser, A. B.; Michalowski, G. R.; Sudyn, A. W.; Byers, J. A. Redox-Triggered Crosslinking of a Degradable Polymer. *Polymer Chemistry* **2016**, *7* (28), 4675–4681. <https://doi.org/10.1039/c6py00975a>.
- (70) Qi, M.; Zhang, H.; Dong, Q.; Li, J.; Musgrave, R. A.; Zhao, Y.; Dulock, N.; Wang, D.; Byers, J. A. Electrochemically Switchable Polymerization from Surface-Anchored Molecular Catalysts. *Chemical Science* **2021**. <https://doi.org/10.1039/d1sc02163j>.
- (71) Biernesser, A. B.; Li, B.; Byers, J. A. Redox-Controlled Polymerization of Lactide Catalyzed by Bis(Imino)Pyridine Iron Bis(Alkoxide) Complexes. *Journal of the American Chemical Society* **2013**, *135* (44), 16553–16560. <https://doi.org/10.1021/ja407920d>.
- (72) Delle Chiaie, K. R.; Biernesser, A. B.; Ortuño, M. A.; Dereli, B.; Iovan, D. A.; Wilding, M. J. T.; Li, B.; Cramer, C. J.; Byers, J. A. The Role of Ligand Redox Non-Innocence in Ring-Opening Polymerization Reactions Catalysed by Bis(Imino)Pyridine Iron Alkoxide Complexes. *Dalton Transactions* **2017**, *46* (38), 12971–12980. <https://doi.org/10.1039/c7dt03067c>.
- (73) Ortuño, M. A.; Dereli, B.; Chiaie, K. R. D.; Biernesser, A. B.; Qi, M.; Byers, J. A.; Cramer, C. J. The Role of Alkoxide Initiator, Spin State, and Oxidation State in Ring-Opening Polymerization of ϵ -Caprolactone Catalyzed by Iron Bis(Imino)Pyridine Complexes. *Inorganic Chemistry* **2018**, *57*, 2064–2071.
- (74) Varnado, C. D.; Rosen, E. L.; Collins, M. S.; Lynch, V. M.; Bielawski, C. W. Synthesis and

- Study of Olefin Metathesis Catalysts Supported by Redox-Switchable Diaminocarbene[3]Ferrocenophanes. *Dalton Transactions* **2013**, 42 (36), 13251–13264. <https://doi.org/10.1039/c3dt51278a>.
- (75) Abubekеров, M.; Shepard, S. M.; Diaconescu, P. L. Switchable Polymerization of Norbornene Derivatives by a Ferrocene-Palladium(II) Heteroscorpionate Complex. *European Journal of Inorganic Chemistry* **2016**, 2016 (15–16), 2634–2640. <https://doi.org/10.1002/ejic.201501295>.
- (76) Broderick, E. M.; Guo, N.; Wu, T.; Vogel, C. S.; Xu, C.; Sutter, J.; Miller, J. T.; Meyer, K.; Cantat, T.; Diaconescu, P. L. Redox Control of a Polymerization Catalyst by Changing the Oxidation State of the Metal Center. *Chemical Communications* **2011**, 47 (35), 9897–9899. <https://doi.org/10.1039/c1cc13117f>.
- (77) Gradišar, Š.; Žagar, E.; Pahovnik, D. Ring-Opening Polymerization of N-Carboxyanhydrides Initiated by a Hydroxyl Group. *ACS Macro Letters* **2017**, 6 (6), 637–640. <https://doi.org/10.1021/acsmacrolett.7b00379>.
- (78) Nifant'ev, I.; Ivchenko, P. Coordination Ring-Opening Polymerization of Cyclic Esters: A Critical Overview of DFT Modeling and Visualization of the Reaction Mechanisms. *Molecules* **2019**, 24 (22). <https://doi.org/10.3390/molecules24224117>.
- (79) Kricheldorf, H. R.; Lossow, C. Von; Schwarz, G. Tertiary Amine Catalyzed Polymerizations of α -Amino Acid N-Carboxyanhydrides: The Role of Cyclization. *Journal of Polymer Science: Part A: Polymer Chemistry* **2006**, 44 (May), 4680–4695. <https://doi.org/10.1002/pola.21553>.
- (80) Goodman, M.; Arnon, U. The Mechanism of Strong-Base-Initiated Polymerization of N-

- Carboxyanhydrides. *Journal of the American Chemical Society* **1964**, *86* (16), 3384–3390.
<https://doi.org/10.1021/ja01070a035>.
- (81) Inoue, S. Immortal Polymerization: The Outset, Development, and Application. *J. Polym. Sci. Part A: Polym. Chem.* **2000**, *38*, 2861–2871.
- (82) Lowe, M. Y.; Shu, S.; Quan, S. M.; Diaconescu, P. L. Investigation of Redox Switchable Titanium and Zirconium Catalysts for the Ring Opening Polymerization of Cyclic Esters and Epoxides. *Inorganic Chemistry Frontiers* **2017**, *4* (11), 1798–1805.
<https://doi.org/10.1039/c7qi00227k>.
- (83) Le Bras, J.; Jiao, H.; Meyer, W. E.; Hampel, F.; Gladysz, J. . Synthesis, Crystal Structure, and Reactions of the 17-Valence-Electron Rhenium Methyl Complex [(H5-C5Me5)Re(NO)(P(4-C6H4CH3)3)(CH3)]⁺ B(3,5-C6H3(CF3)2)4⁻: Experimental and Computational Bonding Comparisons with 18-Electron Methyl and Methylidene Complexes. *Journal of Organometallic Chemistry* **2000**, *616*, 54–66.
- (84) Berger, B. J.; Bercaw, J. E. Vacuum Line Techniques for Handling Air-Sensitive Organometallic Compounds. In *Experimental Organometallic Chemistry*; 1987; pp 79-115.
- (85) Evans, D. F. The Determination of the Paramagnetic Susceptibility of Substances in Solution by Nuclear Magnetic Resonance. *J. Chem. Soc.* **1959**, 2003–2005.
- (86) Schubert, E. M. Utilizing the Evans Method with a Superconducting NMR Spectrometer in the Undergraduate Laboratory. *Journal of Chemical Education* **1992**, *69*, 62.
- (87) Britovsek, G. J. P.; Gibson, V. C.; Spitzmesser, S. K.; Tellmann, K. P.; White, A. J. P.; Williams, D. J. Cationic 2,6-Bis(Imino)Pyridine Iron and Cobalt Complexes: Synthesis, Structures, Ethylene Polymerisation and Ethylene/Polar Monomer Co-Polymerisation

Studies. *Journal of the Chemical Society, Dalton Transactions* **2002**, No. 6, 1159–1171.

<https://doi.org/10.1039/b106614p>.

4.0 Chapter 4: Redox-switchable, *N*-carboxyanhydride Polymerization from Surface-anchored Catalysts

4.1 Introduction

Solid surfaces are routinely modified with polymers to change a wide-range of properties including corrosion resistance,^{1,2} antifouling,^{3,4} wettability,⁵ substrate affinity,^{6,7} environmental protection^{8,9} among many other changes that are valuable for coatings or sensors. While conventional coatings rely on the deposition of polymers onto fibrous, particulate or flat substrates, these coatings are prone to damage, cracking and dissolution.¹⁰ A wide range of polymers from polyolefins,^{11–15} to polyesters^{16–18} to polyethers^{16,19} have been chemically bonded to surfaces to form protective coatings that are more robust than their deposited counterparts.¹⁰ Polyamides derived from amino acids are particularly appealing due to the wide variety of accessible functional groups, higher-order structures and biocompatibility.²⁰

Polyamides are commonly bound to surfaces using either grafting to²¹ or grafting from strategies.^{22,23} With the grafting to approach, a premade polymer with a reactive functional group is chemically bound to the surface. A grafting from approach uses an anchored initiator to grow the polymer directly from the surface. The former strategy has the benefit of being useful for making well-defined polymer surfaces, but this approach tends to have low grafting densities²¹ and often requires intermediate purification steps. The grafting from approach in contrast leads to less well-defined polymers and is more vulnerable to trace impurities,²⁰ but

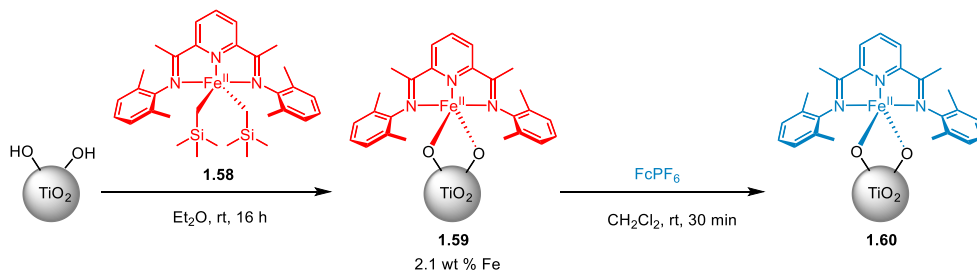
very high grafting densities have been reported.¹¹ Both strategies have been demonstrated for polyamides²⁴ with the latter being well represented in the literature^{20,25–28} due to the ease of amino acid-derived, *N*-carboxyanhydride (NCA) polymerization from amine-initiators on surfaces. Polyamide surfaces have been grown on silica,^{29,30} magnetic nanoparticles²⁷ and polymeric surfaces^{31,32} using NCAs. It is relatively facile to synthesize polyamide films on surfaces containing one or two NCA blocks, but there are no examples of complex structures with three or more polymer blocks that have been made using this method. The inability to access these complex morphologies is a consequence of the difficulties controlling or determining the structures of surface initiated polymers.

As mentioned in earlier chapters, redox-switchable polymerization³³ is an effective method for controlling catalyst activity *in-situ* through either chemical^{34–40} or electrochemical^{16,41,42} means. In the previous chapter I demonstrated redox-switchable polymerization of NCAs with catalyst **3.1** so here we are investigating methods to anchor analogous catalysts to surfaces for NCA polymerization. We expect that a redox-switchable surface bound catalyst that would allow for the synthesis of well-defined multi-block copolymers. Here we demonstrate the synthesis of iron complexes anchored onto 25 nm powder (P25) TiO₂ nanoparticle surfaces and investigate how the redox properties of these Fe(I)-TiO₂ and Fe(II)⁺-TiO₂ exhibit the same on/off behavior as the homogenous counterparts. With this fine control over catalyst activity, this system could prove to be valuable in designing highly tunable and customizable surfaces through surface patterning as well as designing methods for producing and cleaving sequence specific-block copolymers.

4.2 Synthesis of Iron on Titania Nanoparticles and their Activity for NCA Polymerization

In the previous chapter, iron(I) bis(imino)pyridine alkoxide catalyst **3.1** was shown to be a suitable, redox-switchable catalyst for *N*-carboxyanhydride polymerization. To synthesize an analogous surface bound species, onto electrochemically accessible surfaces we turned to previous successes in our group for immobilizing iron bis(imino)pyridine dialkyl complexes **1.58** to UV treated P25 TiO₂ nanoparticles (Scheme 4.1).¹⁶ This strategy relied on reacting the abundant, acidic hydroxyl groups on the titania surface⁴³ with the basic, iron bis(imino)pyridine alkyl **1.58** to generate iron(II) oxide groups on the semiconductor surface **1.59**. Surface-bound Iron(II) oxide species on TiO₂ nanoparticles **1.59** could still be chemically oxidized to formally Iron(III) oxide **1.60** while remaining anchored to the solid surface. The Mössbauer spectrum of spectrum of **1.59** had revealed that only 81 % of the surface bound catalyst is consistent with a neutral iron(II) species similar to an iron(II) species with the remaining 19% corresponding to a formally iron (III) species. The formally iron (III) species was theorized to arise from electron transfer from the TiO₂ to the iron. Similarly, **1.60** was not predominantly a formally iron(III) complex, but also exhibited features of a neutral iron(II) species. Regardless the reactivities of

Scheme 4.1. The anchoring of redox-active, iron(II) bis(imino)pyridine alkyl complex **1.58** onto TiO₂ nanoparticles and the oxidation of these solid-supported iron complexes.



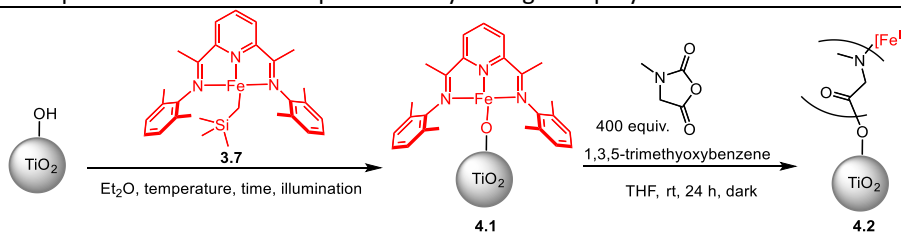
1.59 and **1.60** were sufficiently different in reactivity to allow for some control over the growth of polymers on the surface.

It was expected that iron(I) bis(imino)pyridine alkyl complex **3.7** would behave similarly to **1.58** and efficiently form an anchored iron complex on TiO₂. However, because TiO₂ is known to be a photocatalyst⁴⁴ we were concerned that the more electron rich iron(I) bis(imino)pyridine complexes would be even more prone to TiO₂ induced oxidation. Additionally, previous protonolysis reactions between **3.7** and aliphatic alcohols were most successful at low temperatures due to the low thermal stability of **3.7**.³⁹ In an abundance of caution, the anchoring of **3.7** onto TiO₂ nanoparticles was first attempted at -35 °C in the dark for 1 hour (entry 1, Table 4.1). The formerly white TiO₂ nanoparticles became dark in color similar to previously synthesized iron(I) bis(imino)pyridine alkoxides,^{39,45} suggesting that the anchored iron(I) complex **4.1** was present. The iron loading was measured to be only 0.25 wt % by Inductively Coupled Plasma Optical Emission Spectroscopy (ICP-OES). This was much lower than what had been measured previously for **1.59** (2.1 %) which is surprising as each iron(I) complex only requires one hydroxyl group on the surface, but each iron(II) complex requires 2 nearby hydroxyl group for anchoring, so the maximum loading of iron(I) complexes should be higher. To increase iron loading we increased the anchoring time from 1 to 4 hours which only led to a small increasing iron loading to 0.29 wt. %. (entry 2, Table 4.1). Performing the anchoring at room temperature (entry 3, Table 4.1) or in light (entry 4, Table 4.1) to better resemble the conditions for iron(II) anchoring (Scheme 4.1), but neither factor had any influence on the overall iron loading.

Despite the consistency of the iron loading between each batch of nanoparticles, there were significant differences when each batch of nanoparticles were tested for sarcosine-NCA ROP. The most reactive catalyst was anchored at low temperatures for 1 h in the dark (Table 4.1, entry 1). It must also be noted that the 56 % conversion only refers to polymer on the surface, as there was also a large amount of polymer in the supernatant, likely from back-biting reactions, that has a broad peak that overlaps with the monomer by ^1H NMR. The free polyamide in the supernatant was collected by precipitation into diethyl ether. The sample with the longest anchoring time only reached 29 % conversion in 48 h, despite having the highest iron loading. (Table 4.1, entry 2, Table 4.1). The disparity in activity is indicative that not all of the iron deposited on the surface is active for polymerization. Even more striking was the inactivity for the samples anchored at room temperature (Table 4.1, entry 3) or in light (Table 4.1, entry 4) that were much less efficient at sarcosine-NCA ROP (0 % conversion and 5 % conversion, respectively in 48 h) The low reactivity could be caused by catalyst decomposition or oxidation during the anchoring step. We attempted to determine if these differences were could be identified through Mössbauer spectroscopy, but the iron loading was too low to obtain a strong signal.

To examine the polymer on the surface we utilized a procedure developed to by our group to cleave polymer bound to the surface by either titanium carboxylates or titanium alkoxides (Scheme 4.2).¹⁶ Surface bound poly(lactic acid) **1.61** and surface bound poly(cyclohexene oxide) **1.62** had previously been cleaved after treatment with methyl iodide. The resulting polymers were both capped with methyl end groups evidence of nucleophilic attack of methyl iodide titanium carboxylates/ alkoxides. Sarcosine-NCA initiated by iron(I) oxide complex **4.1** should also have a titanium carboxylate end group so we believed methyl iodide would be able to cleave the polyamide from the surface. First, iron polyamide complex

Table 4.1. Parameters tested for anchoring iron bis(imino)pyridine complexes onto TiO₂ nanoparticles and the subsequent activity during NCA polymerization.



Entry ^a	Time (h)	Temp. (°C)	Illuminated ^b	Iron Loading wt (%) ^c	NCA Conv. (%) ^{de}
1	1	-35 to 25	No	0.25	56 ^f
2	4	-35 to 25	No	0.29	29
3	1	25	No	0.25	0
4	1	-35 to 25	Yes	0.25	5

^aAnchoring was conducted with 0.48 mM of **3.E** in Et₂O while stirring at 1000 rpm. ^bAmbient, white

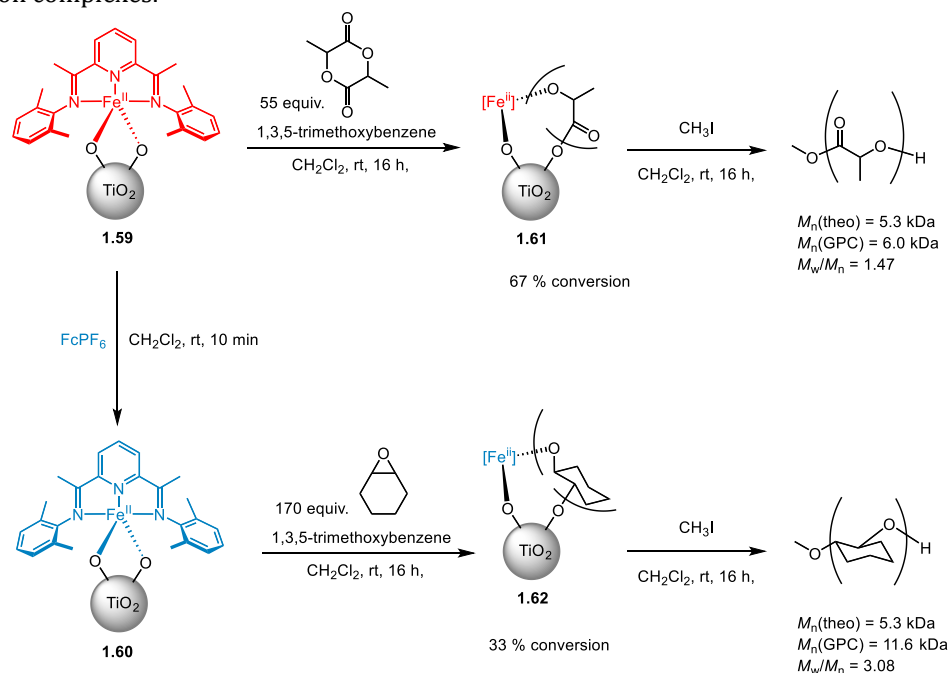
fluorescent lights. ^cMeasured by ICP-OES after dissolving iron on TiO₂ particles in dilute nitric acid.

^dPolymerization allowed to take place with 0.18 mM sarcosine-NCA and 0.45 μM [CoCp₂][BAr^{F24}] at

25 °C in THF for 48 h. ^eConversion was measured by ¹H NMR from the ratio of internal standard to

NCA-monomer. ^fPoly(sarcosine) is observed in the supernatant by ¹H NMR

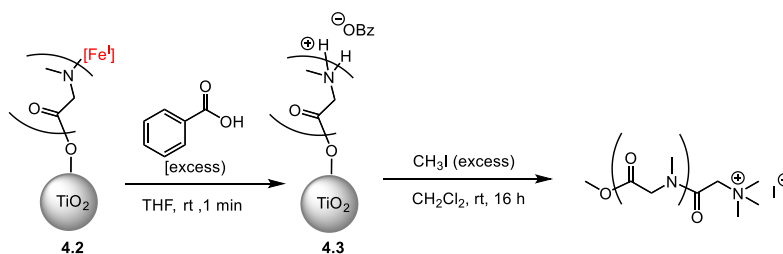
Scheme 4.2. Polymerization of *rac*-lactide or cyclohexene oxide off of titanium nanoparticles by surface anchored iron complexes.



4.2 was first quenched with benzoic acid to prevent side reactions with the reactive amine end group forming polyamide coated TiO_2 **4.3** (Scheme 4.2). **4.3** was then treated with methyl iodide to cleave the polymer and the polymer was precipitated from dichloromethane into diethyl ether.

The poly(sarcosine) collected the supernatant and the poly(sarcosine) cleaved from the surface (entry 1, Table 4.1) were both measured by GPC chromatography (Figure 4.1). The two chromatograms overlap very closely, with both spectra primarily consisting of oligomers although the polymer in the supernatant ($M_n = 2.5 \text{ kDa}$, $M_w/M_n = 1.58$) has less low molecular weight tailing than the cleave polymer ($M_n = 2.2 \text{ kDa}$, $M_w/M_n = 1.78$). Both polymers are significantly smaller than the theoretical molecular weight ($M_n = 15.9 \text{ kDa}$) which could be indicative of chain transfer to free hydroxide groups on the TiO_2 surface. Chain transfer to alcohol initiators has not been observed for the molecular iron(I) complex **3.1** during sarcosine-

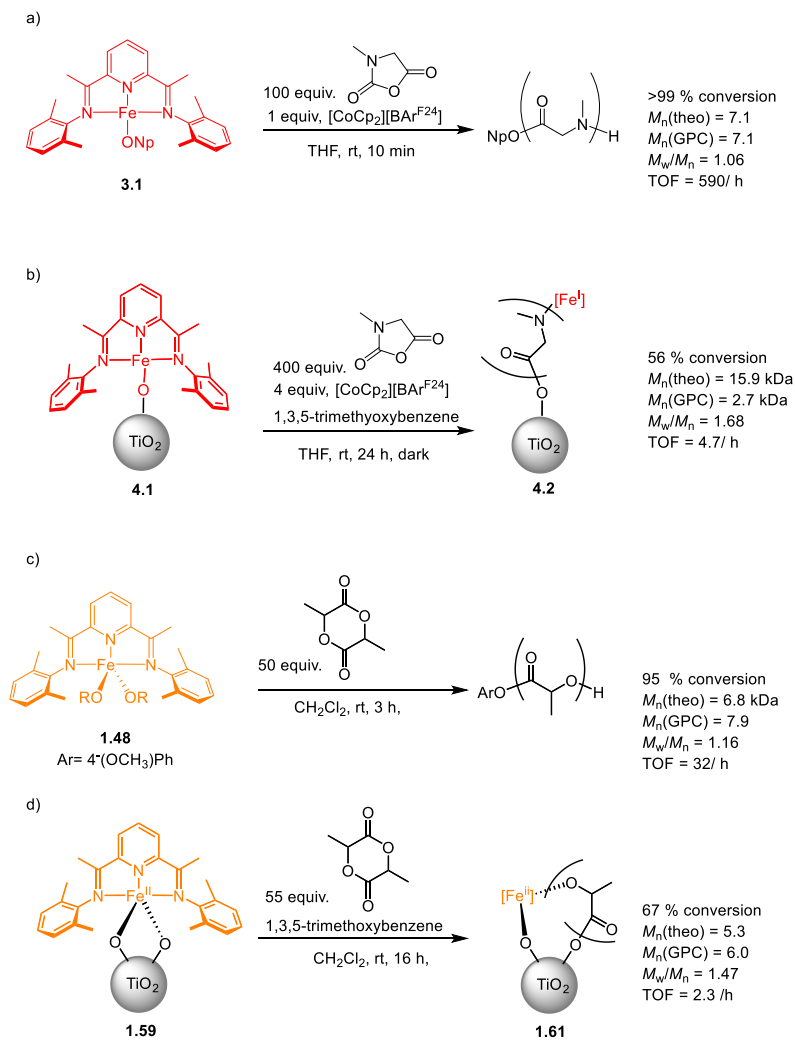
Scheme 4.3. Cleavage of poly(sarcosine) from TiO₂ nanoparticles by treatment with methyl iodide.



NCA polymerization, however the homogenous polymerization of sarcosine-NCA is extremely rapid reaching full conversion in 10 min (Scheme 4.4a). while the same reaction is considerably slower on the TiO₂ nanoparticle (Scheme 4.4b) which may make chain transfer more favorable than propagation.

The homogenous polymerization displays living characteristics with a narrow dispersity ($M_w/M_n = 1.06$) in comparison to the broad dispersity observed from polymer cleaved off of the TiO₂ ($M_w/M_n = 1.78$). The difference in dispersity between *rac*-lactide polymerization initiated by molecular iron(II) catalyst **1.48** ($M_w/M_n = 1.16$) (Scheme 4.4c) and heterogeneous iron(II) catalyst **1.59** ($M_w/M_n = 1.47$) (Scheme 4.4d) is less stark in comparison. The turnover frequency (TOF) of the heterogeneous polymerization of *rac*-lactide (TOF = 32/h) and sarcosine-NCA (TOF = 4.7/h) are both significantly slower than their homogenous counterparts (TOF = 2.3/h

Scheme 4.4. Comparison of molecular and surface bound catalysts for ROP a) Polymerization of sarcosine-NCA by molecular catalyst **3.1**. b) polymerization of sarcosine-NCA by surface-bound catalyst **4.1**. c) Polymerization of *rac*-lactide by molecular catalyst **1.48**. d) polymerization of *rac*-lactide by surface-bound catalyst **1.59**.



and TOF = 560/h, respectively). Sarcosine-NCA polymerization is affected more negatively with the heterogeneous catalyst **4.1** only 0.84 % the TOF as its homogenous counterpart **3.1**.

Further comparison of relative reaction rates with identical monomers would be valuable for determining whether the monomer or the catalyst binding mode has a greater influence on the difference in TOF between homogenous and surface-bound catalysts.

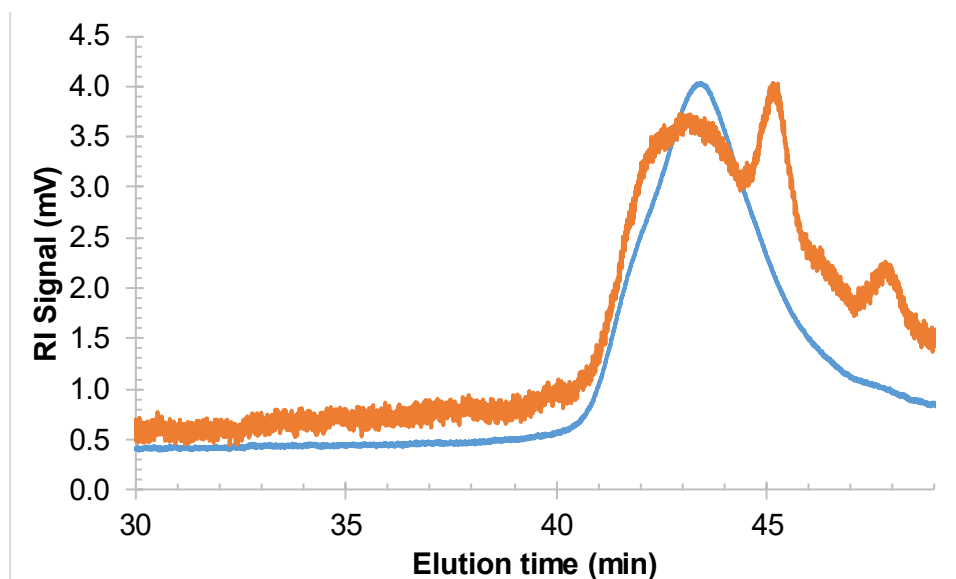
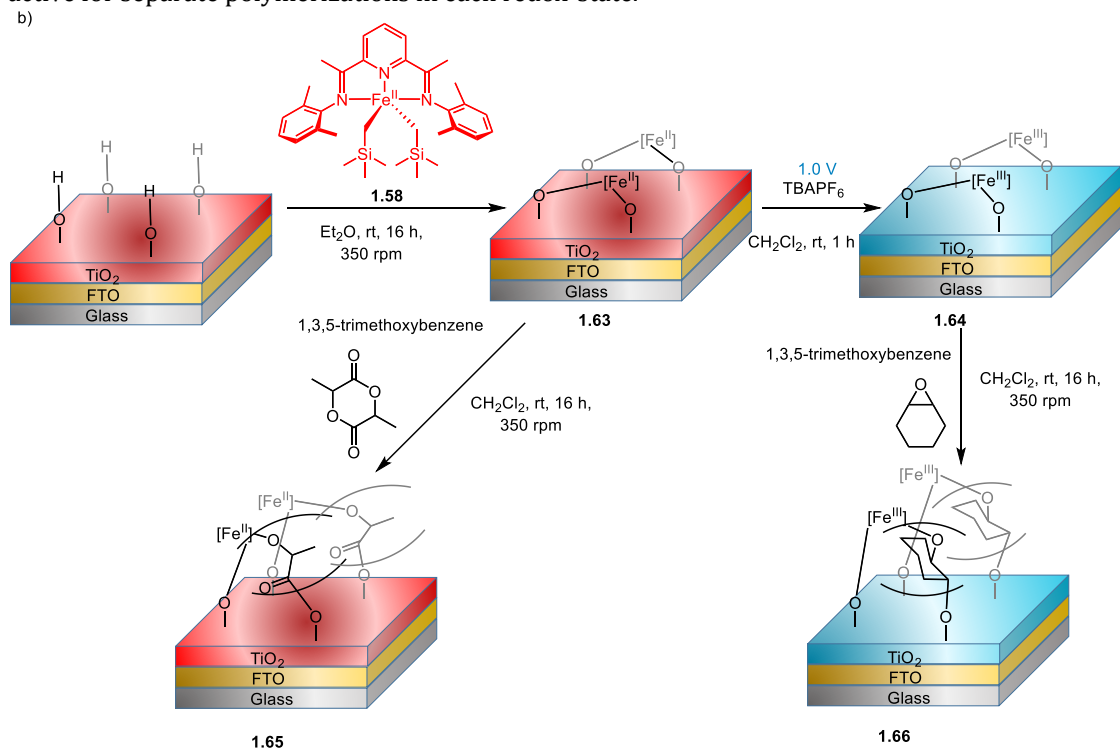


Figure 4.1. GPC chromatograms of poly(sarcosine) ($M_n = 2.5$ kDa, $M_w/M_n = 1.58$) in the supernatant (blue) and poly(sarcosine) ($M_n = 2.2$ kDa, $M_w/M_n = 1.78$) cleaved from TiO_2 nanoparticles (orange) for entry 1, Table 4.1.

4.3 Anchoring Iron Complexes onto Electrode Surfaces and Their Activity for Sarcosine-NCA Polymerization

While catalysts on TiO_2 nanoparticles are useful for testing the reactivity of a surface bound catalyst due to their high surface area, for electrochemically-switchable polymerization we needed to anchor our complex onto an electrode. Our group had previously anchored iron(II) bis(iminopyridine) complexes onto P25 TiO_2 nanoparticles as the active material and fluorine-doped tin oxide as the conductive substrate. (Scheme 4.5).¹⁶ The iron(II) oxide species

Scheme 4.5. The anchoring of redox-active, iron(II) bis(imino)pyridine alkyl complex **1.58** onto layered surfaces consisting of TiO₂ nanoparticles on a layer of FTO on glass slides. Complex was active for separate polymerizations in each redox-state.



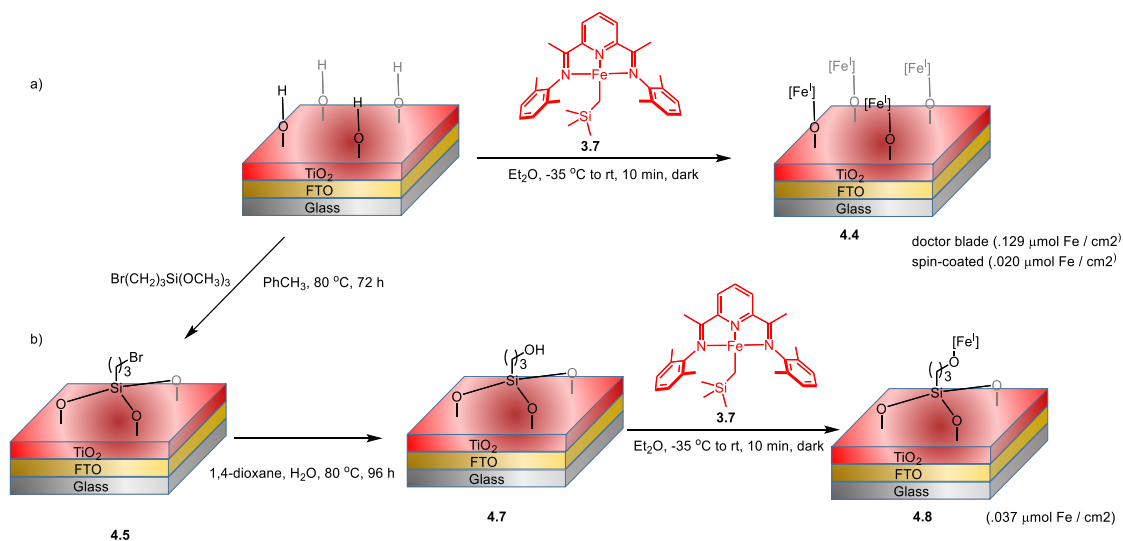
could be oxidized to the formally iron(III) oxide species **1.64**. **1.63** was active for lactide ROP while the oxidized species **1.64** was active for cyclohexene oxide ROP, which is consistent with the reactivity of the corresponding iron complexes **1.59** and **1.60** on TiO₂ nanoparticles. The Cyclic Voltammetry (CV) traces of **1.63** displayed a consistent peak separation of 200 mV even as scan rate was altered from 20 mV/s to 400 mV/s. The constant peak separation indicated the complex was not diffusing away from the surface, while the 200 mV peak separation was attributed to the mesoporous TiO₂ layer behaving as a capacitor.

We decided to screen a variety of electrodes for anchored iron(I) complexes to determine how structure related to polymerization activity. P25 TiO₂-FTO electrodes were one of the electrodes we chose because of our group's experience with anchoring iron complexes on these surfaces.¹⁶ In order to determine how the thickness of the electrode surface influences

both iron loading and the peak separation, we decided to synthesize P25 TiO₂-FTO electrodes using two methods, doctor blade and spin-coating.⁴⁶ For the doctor blade method a 0.3 mg/ ml slurry of the P25 TiO₂ in ethanol/ acetic acid was pasted onto the FTO-glass electrode and made uniform using a doctor blade to wipe off the excess slurry. The electrodes were annealed at 450 °C for 30 min and then exposed to UV irradiation for 30 min to increase the hydroxyl content on the surface.⁴⁷ The assembly of the spin-coated electrodes also began with a 0.3 mg/ ml slurry of the P25 TiO₂ in ethanol/ acetic acid that is pasted onto the FTO-glass slides. The electrodes were placed in a spin coater and spun at 500 rpm for 10 s and then 2000 rpm for 45 s. This electrode was also annealed at 450 °C for 30 min followed by 30 min of UV irradiation. The two electrodes were compared by optical profilometry and the average thickness of the doctor blade electrodes 17.8 μm while the spin-coated electrode was thinner measuring only 1.5 μm. P25 TiO₂-FTO electrodes were exposed to **3.7** in diethyl ether in the dark at -35 °C for ten minutes (Scheme 4.6a). After ten minutes both the doctor blade and the spin-coated TiO₂ electrodes turned dark blue. After ten minutes excess **3.6** was washed with THF to leave behind the TiO₂-anchored iron(I) electrode **4.4**. Each electrode was measured by ICP-OES to quantify the iron loading. The doctor blade electrode contained 0.129 μmol/ cm² (entry 1, Table 4.2) while the spin-coated electrode had an even lower loading of 0.020 μmol/ cm² (entry 3, Table 4.2). The catalyst loading at these short anchoring times is roughly proportional to the difference in surface thickness between the two electrode.

Besides these heterogenous hydroxy initiators, we also wanted to investigate surfaces with well-defined initiators and for this reason we synthesized two types of hydroxyl-functionalized self-assembled monolayers. A silyl SAM was grown on a spin-coated P25 TiO₂-FTO electrode by refluxing the the electrode and 3-bromopropyl trimethoxysilane in toluene for 3 days to synthesize a bromine-containing SAM on TiO₂ **4.6** (Scheme 4.6b). Excess silane was removed by rinsing the electrode with toluene, methanol and isopropanol. The bromo-functionalized SAM was dried under vacuum at 80 °C. **4.6** was then soaked in 1,4-dioxane and water at 80 °C for 4 days to make the hydroxyl-functionalized SAM on TiO₂ **4.7**. **4.7** was dried at 80 °C under vacuum overnight before the anchoring experiment. **3.7** was anchored to **4.7** diethyl ether in the dark at -35 °C for ten minutes. The SAM on TiO₂- anchored iron (I) electrode **4.8** was washed with THF and the iron loading was measured as 0.037 μmol/ cm² which is almost double the loading on the spin-coated TiO₂ electrode **4.6**. The maximum loading of the

Scheme 4.6. Synthesis of electrode and anchoring of iron bis(imino)pyridine alkyl complexes onto electrode surfaces. a) Anchoring iron bis(imino)pyridine complexes onto P25 TiO₂-FTO electrodes. b) Synthesis of hydroxyl functionalized self-assembled monolayers (SAM) onto P25 TiO₂-FTO electrodes. Anchoring iron complexes onto the TiO₂ SAM.



SAM should be lower than the spin-coated electrode because 3 hydroxyl groups on the TiO₂ surface are needed to form the SAM layer. This experiment reveals that iron(I) alky **3.7** is not reacting with every hydroxyl group on the surface during the anchoring step.

We compared all iron(I)-anchored electrodes for sarcosine-NCA polymerization in presence of the cocatalyst [CoCp₂][BAr^{F24}] (Table 4.2) All surfaces tested were active for polymerization, but there were noticeable difference in polymerization activity. The anchored doctor blade P25 TiO₂ electrode **4.4** reached 11 % conversion in 24 h which is a turnover number of 180 relatives to iron. Another doctor blade P25 TiO₂ electrode was prepared by anchoring **3.7** for 1 h instead of 10 min which lead to a higher iron loading (0.210 μmol/ cm²) (entry 2, Table 4.2). When this electrode was tested for sarcosine-NCA polymerization 29 % of the monomer was consumed, and the TON (290) was slightly higher. When the doctor blade electrodes were compared to the spin-coated electrode P25 TiO₂ **4.4**, the latter had much higher TON (3200) (entry 3, Table 4.2). The disparity in TON could be caused by more iron on the thicker, doctor blade electrode being inactive or inaccessible to the monomer. We decided to test an even thinner spin-coated electrode containing the iron(I) catalyst and this electrode had a very high TON of 10,400 (entry 4, Table 4.1). Unfortunately, this high reactivity comes at the cost of a very low iron content on the surface (0.005 μmol Fe/ cm²) that would be challenging for further catalyst characterization. We were pleased to note that the iron(I) complex on the SAMs on P25 TiO₂ **4.8** reached a TON of 4100 (entry 5, Table 4.2).

We observed free polyamide in the supernatant for entries 1, 4 and 5, Table 4.2) which could be occurring from poly(sarcosine) back-biting. The cause of this polymer in the supernatant is currently unknown and answering that question is an objective for future investigations. Unfortunately, by ^1H NMR, poly(sarcosine) overlaps with the sarcosine-NCA making it difficult to determine overall conversion of the NCA. Due to this limitation, it is

Table 4.2. Sarcosine-NCA polymerization activity of iron(I)-based complexes anchored on electrodes.

Entry	Electrode Coating Method	Electrode Surface Area (cm ²)	Iron Loading ($\mu\text{mol Fe/cm}^2$) ^a	Sar-NCA Conv. on surface ^b (%)	Sar-NCA TON on surface ^a
1	Doctor blade P25 TiO ₂	2.1	0.129	11 ^f	180
2	Doctor Blade P25 TiO ₂ ^d	2.1	0.210	29	290
3	Spin-coated P25 TiO ₂	3.0	0.020	44	3,200
4	Spin-coated P25 TiO ₂ ^e	3.0	0.005	36 ^f	10,400
5	SAM on P25 TiO ₂	2.1	0.037	35 ^f	4,100

^aElectrodes were anchored for 10 min in [0.35 M] **3.7** in Et₂O at -35 °C in the dark. For polymerizations, anchored electrodes were added to 434 μmol of sarcosine-NCA with 4.3 μmol of [CoCp₂][BAR^{F24}] in 10 ml of THF at room temperature in the dark with a stir rate of 1000 rpm. 1,3,5-trimethoxybenzene was added as an internal standard to measure conversion.

^bMeasured by ^1H NMR relative to internal standard.

^cSar-NCA TON = (Conv._{sarcosine-NCA} * mol sarcosine-NCA) / (Electrode surface areas * Iron loading)

^dElectrode was anchored for 1 hour.

^eSpin-coated electrode was synthesized with 0.1 mg TiO₂/ml EtOH/AcOH

^fPoly(sarcosine) present in the supernatant.

difficult to assess which electrode surfaces are the most active, but the spin-coated electrodes and the SAMs on TiO₂ appear to be promising candidate for surface polymerizations of NCAs.

4.4 Redox Behavior of Anchored Iron Complexes on Electrode Surfaces

To enable future redox-switchable polymerizations, we investigated the redox behavior of the surface bound catalysts and compared them to those of **3.1** in solution. When we examined **3.1** by cyclic voltammetry the oxidation and reduction events were not reversible indicating catalyst decomposition (Figure 4.2). However, redox events became quasi or even fully reversible when short chains of ϵ -caprolactone or γ -benzyl-*L*-glutamate-NCA were grown off of the iron catalyst (Scheme 4.4). The addition of ϵ -caprolactone lead to a significant change

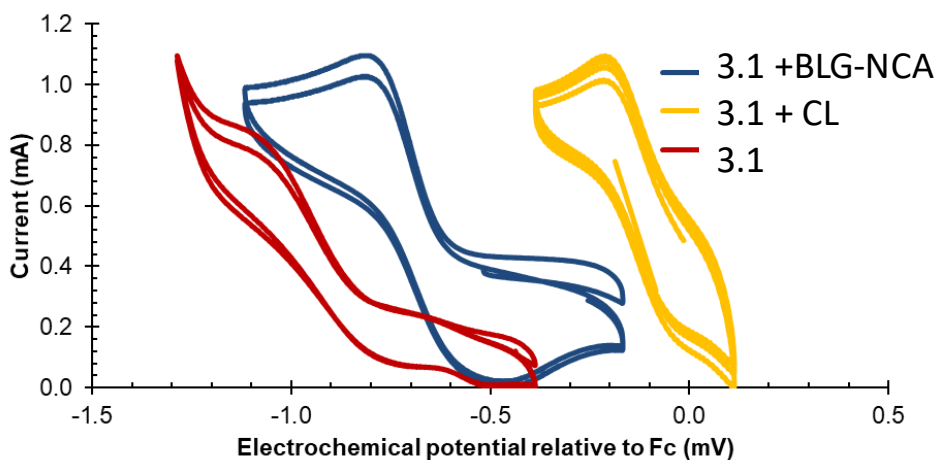
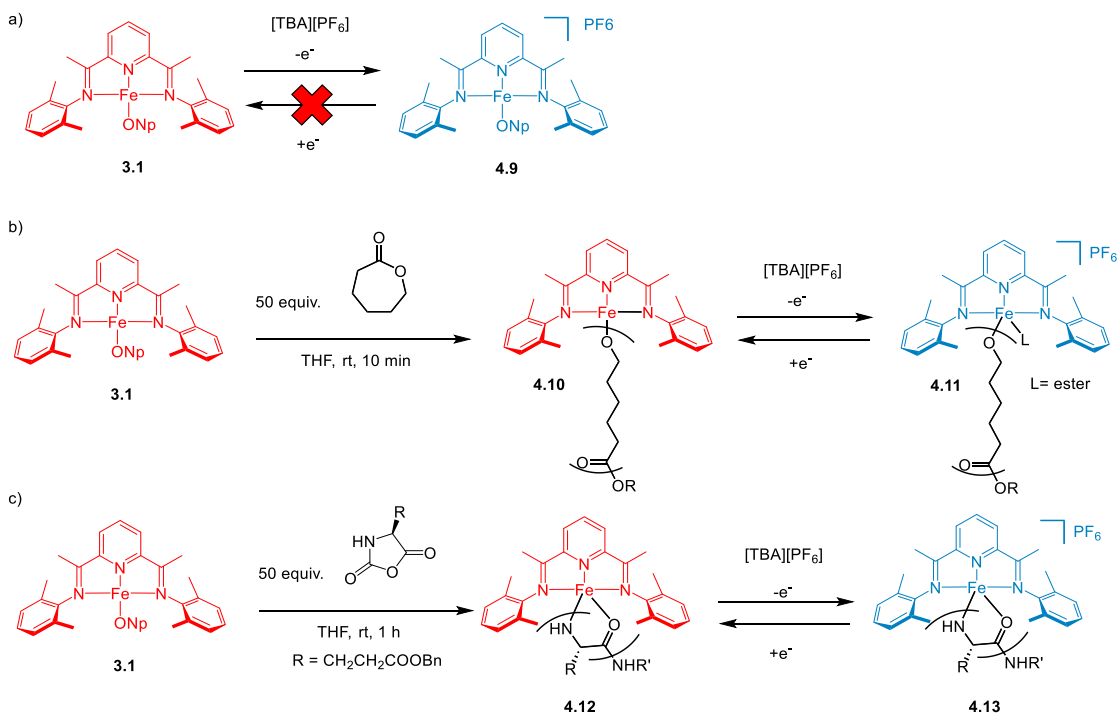


Figure 4.2. CV of [24.4 mM]: [0.49 mM] **3.1**: monomer in 0.1 M TBAPF₆ in THF, scan rate = 20 mV/s. Electrochemical potential is measured relative to ferrocene. The iron (I) complex **3.1** without any monomer (red) is not redox-reversible. The addition of ϵ -caprolactone (CL) (yellow) is quasi-reversible electrochemically. The mixture of **3.1** and γ -benzyl-*L*-glutamate-NCA (BLG-NCA) is fully reversible.

in the reduction potential of the complex (-0.85 mV to -0.10 mV) and the redox event becomes quasi-reversible. The addition of an γ -benzyl-*L*-glutamate-NCA led to a smaller shift in redox potential (-0.85 mV to -0.68 mV), but the complex is now fully reversible for oxidation and reduction. We believe this shift is due to coordination from the ester or amide groups on the respective polymers, stabilizing the low-valent iron catalyst during the redox reactions (Scheme 4.7).

During catalyst oxidation a low-valent iron cation is produced which could be stabilized by Lewis basic donors. For the polyester, while it is unlikely for an intramolecular nine-member ring chelate between the iron center and the poly(ϵ -caprolactone) chain, intermolecular ester groups on nearby metal catalysts could coordinate to the iron center **4.11**. For the polyamide, we envisioned a stable five-coordinate chelate complex **4.13** could form. **4.13** would then be

Scheme 4.7. Stability of iron(I)-based complex **3.1** (a) before polymerization (b) after ϵ -caprolactone polymerization (c) after γ -benzyl-*L*-glutamate-NCA polymerization.



more reversible because the coordination of Lewis basic groups to the iron catalyst is more favorable.

We observed similar behavior with P25 TiO₂ anchored, iron complex **4.4** in response to electrochemical stimulus. **4.4** can be oxidized to **4.14** (Scheme 4.8a), but without a polymer chain on the complex the anchored complexes will decompose during catalyst reduction (Figure 4.3). **4.4** can be stabilized by allowing sarcosine-NCA to first polymerize for 0.5- 4 hours forming **4.15** (Scheme 4.8b). After the polymerization, the CV of the anchored iron(I) complex is reversible, presumably due to the formation of a stable-5 member-ring chelate **4.16** (Scheme 4.8b). The redox potential for the anchored complex is slightly more reducing than the homogenous complex (-0.85 mV vs. -0.75 mV) and it is sufficiently separated from the oxidation

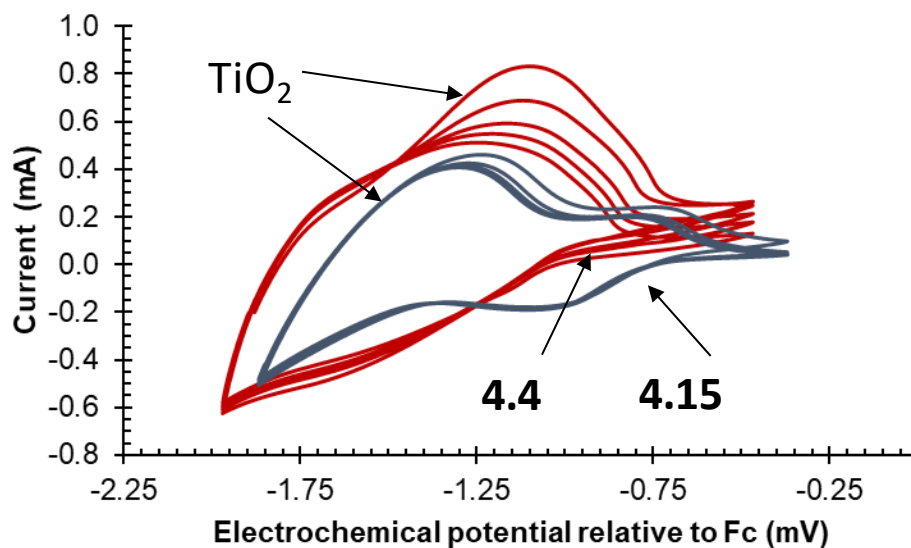
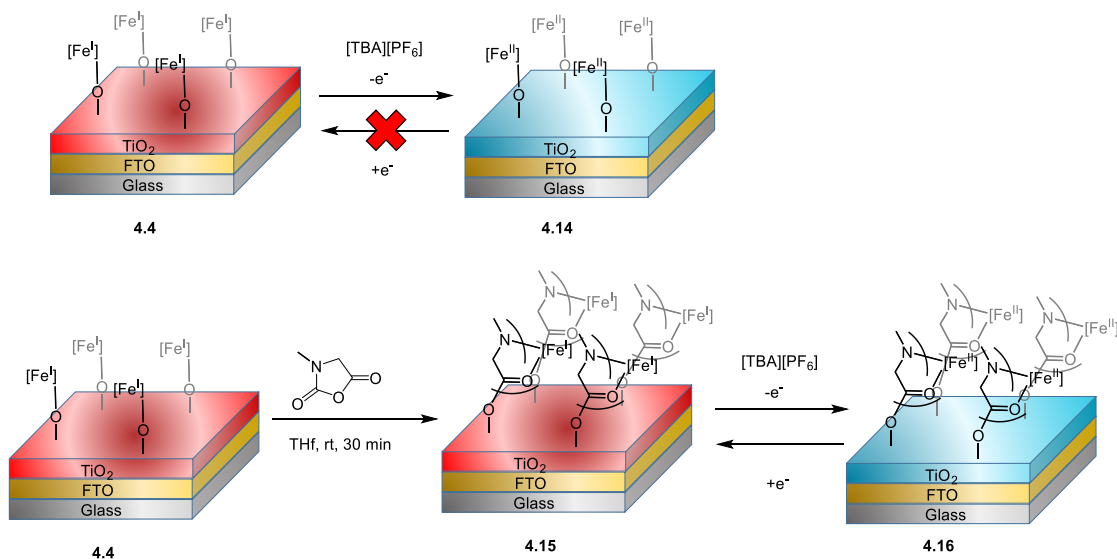


Figure 4.3. CVs of anchored complex **4.4** (ref) and complex **4.4** after polymerizing sarcosine-NCA **4.15** (blue) in 0.1 M TBAPF₆ in THF, scan rate = 50 mV/s. The large feature from (1.35-1.15 mv) is the reduction of the TiO₂ substrate.

Scheme 4.8. (a) Stability of iron(I)-based complex **4.4** under cyclic voltammetry (b) Stability of iron(I)-based complex **4.4** under cyclic voltammetry after polymerizing sarcosine-NCA.



peak for the TiO₂ peak to be distinguishable. A notable feature in the CV is the broad reduction peak from P25-TiO₂ at 1.15-1.35 mV which is rather close to the redox potential of the anchored iron complex, which may explain why these species are particularly sensitive to light.

4.5 Conclusion

We were able to synthesize surface bound iron catalysts on a variety of surfaces that exhibited similar behavior to their homogenous counterpart for redox-switchable-NCA polymerization. These surface bound catalysts for NCA polymerization are less active than their homogenous counterpart as has been observed due to mass transport limitations which was observed with our group's previous surface bound iron catalysts.¹⁶ While increasing stir rate is one method to decrease the effects of mass transport, we believe further improvements could be seen if the catalysts are integrated into flow cells. Additionally, the monomer scope must be

expanded beyond poly(sarcosine) in order to access NCAs derived from conventional amino acids. This challenge can be tackled through catalyst design to decrease the favorability of monomer deprotonation. When these limitations are overcome, there will be many directions to pursue in the creation of complex, polyamide-coated surfaces that may prove to be valuable as sensors, anti-fouling agents or protective layers.

4.6 Experimental

General Considerations: Unless stated otherwise, all reactions were carried out in oven-dried glassware in a nitrogen-filled glove box or with standard Schlenk line techniques.⁴⁸ Solvents were used after passage through a solvent purification system consisting of two columns, one of activated manganese oxide and 3 Å molecular sieves, respectively under a blanket of argon. Solvents were then degassed briefly by exposure to vacuum and stored over 3 Å molecular sieves under a nitrogen atmosphere. Complexes **3.1** and **3.2** were synthesized as described previously.^{49,50} Amino acids γ -benzyl-*L*-glutamate and sarcosine were purchased from Acros Organics and used as received. Triphosgene was purchased from Chem-Impex International Inc. and used as received. Tetrabutylammonium hexafluorophosphate was purchased from Oakwood Chemicals and dried over P₂O₅ *in vacuo*. FTO-coated glass slides (300 mm x 300 mm x 2.2 mm, surface resistivity $\sim 7\Omega/\text{sq}$) were obtained from Sigma Aldrich and used as received. P25 TiO₂ powder was dried at 130 °C *in vacuo* before use. Monomers γ -benzyl-*L*-glutamate-*N*-carboxyanhydride⁵¹ and sarcosine-*N*-carboxyanhydride,⁵² were synthesized according to literature procedures. FcBAR^{F24} was synthesized according to literature procedures.⁵³

ICP-OES: Inductively coupled plasma optical emission spectrometry was recorded on an Agilent 5100 instrument that was calibrated using known concentrations of standard solutions to quantify iron. 1000 ppm Fe standard solution was purchased from Sigma Aldrich. To digest iron-complex from Fe(I)-TiO₂, the powder/electrode was soaked in 20 mL 1% nitric acid solution overnight before. Then the solution was subjected to centrifugation and used for ICP-OES test.

SEC: Size-exclusion chromatography (SEC) by permeation chromatography (GPC) was performed on a Tosoh EcoSEC instrument HLC-8320GPC with a refractive index (RI) detector and three Tosoh TSKgel Alpha M columns (7.8mmID × 300 mm, resin type: methacrylate, particle size:13 μm, pore size: mixed bed). These columns were maintained at 50 °C for all analyses. All samples were eluted by DMF + 0.01% LiBr at a flow rate of 0.6 mL/min. Calibration was performed using polystyrene standards (ReadyCal Kit, Sigma-Aldrich #81434). Samples were passed through 0.20 μm nylon filters before being injected into the SEC system.

Nuclear Magnetic Resonance: (NMR) spectra were recorded at ambient temperature on spectrometers at 500 and 600 MHz for ¹H NMR.

Cyclic Voltammetry for molecular catalysts: Cyclic voltammetry and bulk electrolysis were carried out on a potentiostat (Biologic VMP3). Cyclic voltammetry in solution was conducted using a 3- electrode configuration, where glassy carbon was used as the working electrode and the counter electrode while a platinum disc was used as the reference electrode. Potentials were recorded relative to ferrocene/ ferrocenium.

Cyclic Voltammetry for surface bound catalysts. Electrodes were suspended in 0.1 M ⁿBu₄PF₆ solution in THF. The scan rate was 20 mV/s. Cyclic voltammetry on electrodes was conducted

using a 3- electrode configuration, where the anchored iron on titania electrode was used as working electrode, while the reference and counter electrodes were strips of lithium metal.

Representative procedure for anchoring iron complex to P25 TiO₂ powder

P25 TiO₂ powder (200 mg) was heated at 10⁻⁴ torr at 130 °C to remove water on the surface. In a nitrogen-filled glove box, iron bis(imino)pyridine alkyl **3.7** (25.0 mg, 97.6 μmol) was dissolved in diethyl ether (10 ml) at -35 °C. The solution was added to P25 TiO₂ (200 mg) in the dark and allowed to stir at room temperature for 1 hour. The suspension was centrifuged and washed with diethyl ether (2 ml x 3) and then tetrahydrofuran (2 ml) until the supernatant was colorless. The final powder was light blue to purple in color. Yield = 174 mg, 87 %. ICP-OES = 0.25 weight % iron.

Representative procedure for the surface initiated polymerization of sarcosine-NCA with P25 Fe(I)-TiO₂ powder 4.1.

In a nitrogen-filled glove box, sarcosine-*N*-carboxyanhydride (50.0 mg, 434 μmol), cobaltocenium tetrakis[3,5-bis(trifluoromethyl)phenyl]borate (4.6 mg, 4.4 μmol) and 1,3,5-trimethoxybenzene (20.0 mg, 119 μmol) were dissolved in tetrahydrofuran (10.0 ml) in a glass vial. The solution was added to Fe(I)-TiO₂ powder **4.1** (25 mg, 0.25 wt % Fe, 0.11 mmol Fe). An aliquot was taken for a t= 0, time point. A stir bar was added and the suspension which was allowed to stir at 1000 rpm for 24 h. Aliquots were taken periodically for sampling, quenched with a small amount of benzoic acid, filtered over celite to remove the nanoparticles and the solvent was removed *in vacuo*. Conversion was determined by comparing the ratio of methine signal of 1,3,5-trimethoxybenzene to the methine polymer and monomer signals for sarcosine-

NCA by both ^1H NMR. The powder was washed with dichloromethane and centrifuged to remove any residual monomer or free polymer. Sarcosine-NCA conversion (56 %).

Representative procedure for the preparation of doctor-blade P25 TiO₂ electrodes

Commercial P25 TiO₂ powder (1.5 g) was mixed with ethanol (5.0 mL), acetic acid (75 μL) and Triton X-100 (2 drops) to make a uniform slurry. The slurry was then uniformly coated onto the FTO substrate (3.0 cm \times 0.7 cm) by the doctor blade method. Next, the electrode was annealed at 450°C in air for 0.5 h. The electrode was then treated under UV irradiation for 30 minutes.

Representative procedure for the preparation of spin-coated P25 TiO₂ electrodes

Commercial P25 TiO₂ nanopowder (1.5 g) was mixed with ethanol (5.0 mL), acetylacetone (75 μL) and Triton X-100 (2 drops) to make a uniform slurry. The slurry was then uniformly coated onto the FTO substrate (3 cm \times 1 cm)) and then the electrode was spin-coated at 500 rpm for 10 s and then 2000 rpm for 45 s. Next, the electrode was annealed at 450°C in air for 0.5 h. The electrode was then treated under UV irradiation for 30 minutes.

Representative procedure for the synthesis of SAM on P25 TiO₂

Spin-coated P25 TiO₂ electrode obtained by spin-coating method were treated by UV irradiation for 30 min to increase -OH density and then immediately immersed in a solution of 3-bromopropyl trimethoxysilane (0.5 mL) in anhydrous toluene (10 mL) at 80 °C for 3 days. After that, the electrodes were washed with toluene (25 ml). to remove excess silane followed by being rinsed with methanol (3 x 25 ml) and isopropanol (3 x 25 ml). The electrodes were stored in vacuum oven at 80°C overnight. The Br-terminated electrodes were soaked in a 3:7 dioxane/H₂O

(9 ml/ 21ml) solution at 80°C for 4 days. The electrodes were washed by ultrapure millipore water (10 ml x 3) and dried in vacuum oven at 80°C overnight.

Representative procedure for anchoring iron complex onto electrode surfaces

P25 TiO₂ electrodes were heated at 10⁻⁴ torr at 130 °C to remove water on the surface. In a nitrogen-filled glove box, iron bis(imino)pyridine alkyl **3.7** (25.0 mg, 97.6 μmol) was dissolved in 10 ml of diethyl ether at -35 °C. P25 TiO₂ electrodes were added to the solution in the dark and allowed to stir at room temperature for 10 min. The electrode was washed with diethyl ether (2 x 2 ml) and tetrahydrofuran (2 ml) until supernatant was colorless. The resulting electrodes were pale to dark blue in color. ICP-OES = 0.020 μmol iron/ cm².

Representative procedure for surface initiated polymerization of Sarcosine-NCAs with iron complex on electrode surfaces

In a nitrogen-filled glove box, sarcosine-*N*-carboxyanhydride (50.0 mg, 434 μmol), cobaltocenium tetrakis[3,5-bis(trifluoromethyl)phenyl]borate (4.6 mg, 4.4 μmol) and 1,3,5-trimethoxybenzene (20.0 mg, 119 μmol) were dissolved in tetrahydrofuran (10.0 ml) in a glass vial. The solution was added to spin-coated Fe(I)- P25 TiO₂ electrode **4.4** (3 cm², 0.020 μmol iron/ cm²). An aliquot was taken for a t = 0 h, time point. A stir bar was added and the suspension which was allowed to stir at 1000 rpm for 24 h. Aliquots were taken periodically for sampling, quenched with a small amount of benzoic acid and solvent was removed *in vacuo*. Conversion was determined by comparing the ratio of methine signal of 1,3,5-trimethoxybenzene to the methine polymer and monomer signals for sarcosine-*N*-carboxyanhydride by ¹H NMR. Electrode was washed with dichloromethane to remove any residual monomer or free polymer. Sarcosine-NCA conversion = 44 %.

Standard procedure for the electrochemical redox-switching of homogenous iron complex **3.1 in the presence of various monomers.**

In a nitrogen-filled glove box, a 0.1 M solution of electrolyte, tetrabutylammonium hexafluorophosphate was prepared. Reagents were prepared from the same stock electrolyte and made as followed so that each solution contained complex **3.1** (0.49 mM) and monomer ϵ -caprolactone (24.4 mM) or γ -benzyl-*L*-glutamate (24.4 mM). Measurements were taken with a scan rate of 20 mV/s. Electrochemical potential was recorded relative to a ferrocene standard.

Standard procedure for the electrochemical redox-switching of anchored iron complex Fe(I)-TiO₂ electrode, in the presence of sarcosine-NCA.

In a nitrogen-filled glove box, a 0.1 M solution of electrolyte, tetrabutylammonium hexafluorophosphate was prepared. Reagents were prepared from the same stock electrolyte and made as followed so that each solution contained 43.4 mM of sarcosine-*N*-carboxyanhydride and 4.4 mM of cobaltocenium tetrakis[3,5-bis(trifluoromethyl)phenyl]borate. Solution stirred at room temperature for 0.5 hours. The electrode was washed with tetrahydrofuran (5 ml) and added to fresh electrolyte. Measurements were taken with a scan rate of 50 mV/s. Electrochemical potential was recorded relative to a lithium standard. To compare values to ferrocene, -3.67 mV was added to the voltage recorded.

4.7 References

- (1) Rbaa, M.; Fardioui, M.; Verma, C.; Abousalem, A. S.; Galai, M.; Ebenso, E. E.; Guedira, T.; Lakhrissi, B.; Warad, I.; Zarrouk, A. 8-Hydroxyquinoline Based Chitosan Derived

- Carbohydrate Polymer as Biodegradable and Sustainable Acid Corrosion Inhibitor for Mild Steel: Experimental and Computational Analyses. *International Journal of Biological Macromolecules* **2020**, *155*, 645–655. <https://doi.org/10.1016/j.ijbiomac.2020.03.200>.
- (2) Salam Hamdy, A.; Beccaria, A. M.; Temtchenko, T. Corrosion Protection of AA6061 T6 by Fluoropolymer Coatings in NaCl Solution. *Surface and Coatings Technology* **2002**, *155* (2–3), 176–183. [https://doi.org/10.1016/S0257-8972\(02\)00042-7](https://doi.org/10.1016/S0257-8972(02)00042-7).
- (3) Carteau, D.; Vallée-Réhel, K.; Linossier, I.; Quiniou, F.; Davy, R.; Compère, C.; Delbury, M.; Faÿ, F. Development of Environmentally Friendly Antifouling Paints Using Biodegradable Polymer and Lower Toxic Substances. *Progress in Organic Coatings* **2014**, *77* (2), 485–493. <https://doi.org/10.1016/j.porgcoat.2013.11.012>.
- (4) Lorient, M.; Linossier, I.; Vallée-Réhel, K.; Faÿ, F. Influence of Biodegradable Polymer Properties on Antifouling Paints Activity. *Polymers* **2017**, *9* (2). <https://doi.org/10.3390/polym9020036>.
- (5) Bui-Thi-Tuyet, V.; Trippé-Allard, G.; Ghilane, J.; Randriamahazaka, H. Surface and Electrochemical Properties of Polymer Brush-Based Redox Poly(Ionic Liquid). *ACS Applied Materials and Interfaces* **2016**, *8* (42), 28316–28324. <https://doi.org/10.1021/acsami.6b02107>.
- (6) Guo, P. F.; Gong, H. Y.; Zheng, H. W.; Chen, M. L.; Wang, J. H.; Ye, L. Iron-Chelated Thermoresponsive Polymer Brushes on Bismuth Titanate Nanosheets for Metal Affinity Separation of Phosphoproteins. *Colloids and Surfaces B: Biointerfaces* **2020**, *196* (July), 111282. <https://doi.org/10.1016/j.colsurfb.2020.111282>.
- (7) Ayres, N. Polymer Brushes: Applications in Biomaterials and Nanotechnology. *Polymer*

- Chemistry* **2010**, *1* (6), 769–777. <https://doi.org/10.1039/b9py00246d>.
- (8) Chrisey, D. B.; Pique, A.; Modi, R.; Wu, H. D.; Auyeung, R. C. Y.; Young, H. D. Direct Writing of Conformal Mesoscopic Electronic Devices by MAPLE DW. *Applied Surface Science* **2000**, *168* (1–4), 345–352. [https://doi.org/10.1016/S0169-4332\(00\)00824-2](https://doi.org/10.1016/S0169-4332(00)00824-2).
- (9) Moon, H.; Seong, H.; Shin, W. C.; Park, W. T.; Kim, M.; Lee, S.; Bong, J. H.; Noh, Y. Y.; Cho, B. J.; Yoo, S.; et al. Synthesis of Ultrathin Polymer Insulating Layers by Initiated Chemical Vapour Deposition for Low-Power Soft Electronics. *Nature Materials* **2015**, *14* (6), 628–635. <https://doi.org/10.1038/nmat4237>.
- (10) Chen, W. L.; Cordero, R.; Tran, H.; Ober, C. K. 50th Anniversary Perspective: Polymer Brushes: Novel Surfaces for Future Materials. *Macromolecules* **2017**, *50* (11), 4089–4113. <https://doi.org/10.1021/acs.macromol.7b00450>.
- (11) Barbey, R.; Lavanant, L.; Paripovic, D.; Schüwer, N.; Sugnaux, C.; Tugulu, S.; Klok, H. A. Polymer Brushes via Surface-Initiated Controlled Radical Polymerization: Synthesis, Characterization, Properties, and Applications. *Chemical Reviews* **2009**, *109* (11), 5437–5527. <https://doi.org/10.1021/cr900045a>.
- (12) Advincula, R.; Zhou, Q.; Park, M.; Wang, S.; Mays, J.; Sakellariou, G.; Pispas, S.; Hadjichristidis, N. Polymer Brushes by Living Anionic Surface Initiated Polymerization on Flat Silicon (SiO_x) and Gold Surfaces: Homopolymers and Block Copolymers. *Langmuir* **2002**, *18* (22), 8672–8684. <https://doi.org/10.1021/la025962t>.
- (13) Li, B.; Hou, W.; Sun, J.; Jiang, S.; Xu, L.; Li, G.; Memon, M. A.; Cao, J.; Huang, Y.; Bielawski, C. W.; et al. Tunable Functionalization of Graphene Oxide Sheets through Surface-Initiated Cationic Polymerization. *Macromolecules* **2015**, *48* (4), 994–1001.

<https://doi.org/10.1021/ma5026237>.

- (14) Liu, X.; Guo, S.; Mirkin, C. A. Surface and Site-Specific Ring-Opening Metathesis Polymerization Initiated by Dip-Pen Nanolithography. *Angewandte Chemie - International Edition* **2003**, *42* (39), 4785–4789. <https://doi.org/10.1002/anie.200352309>.
- (15) Weck, M.; Jackiw, J. J.; Rossi, R. R.; Weiss, P. S.; Grubbs, R. H. Ring-Opening Metathesis Polymerization from Surfaces. *Journal of the American Chemical Society* **1999**, *121* (16), 4088–4089. <https://doi.org/10.1021/ja983297y>.
- (16) Qi, M.; Zhang, H.; Dong, Q.; Li, J.; Musgrave, R. A.; Zhao, Y.; Dulock, N.; Wang, D.; Byers, J. A. Electrochemically Switchable Polymerization from Surface-Anchored Molecular Catalysts. *Chemical Science* **2021**. <https://doi.org/10.1039/d1sc02163j>.
- (17) Rutot-Houzé, D.; Fris, W.; Degée, P.; Dubois, P. Controlled Ring-Opening (Co)Polymerization of Lactones Initiated from Cadmium Sulfide Nanoparticles. *Journal of Macromolecular Science - Pure and Applied Chemistry* **2004**, *41 A* (6), 697–711. <https://doi.org/10.1081/MA-120034200>.
- (18) Lönnberg, H.; Zhou, Q.; Brumer, H.; Teeri, T. T.; Malmström, E.; Hult, A. Grafting of Cellulose Fibers with Poly(ϵ -Caprolactone) and Poly(L-Lactic Acid) via Ring-Opening Polymerization. *Biomacromolecules* **2006**, *7* (7), 2178–2185. <https://doi.org/10.1021/bm060178z>.
- (19) Zhou, G.; Xu, X.; Wang, S.; He, X.; He, W.; Su, X.; Wong, C. P. Surface Grafting of Epoxy Polymer on CB to Improve Its Dispersion to Be the Filler of Resistive Ink for PCB. *Results in Physics* **2017**, *7*, 1870–1877. <https://doi.org/10.1016/j.rinp.2017.02.018>.
- (20) Shen, Y.; Li, Z.; Klok, H. A. Polypeptide Brushes Grown via Surface-Initiated Ring-Opening

- Polymerization of α -Amino Acid N-Carboxyanhydrides. *Chinese Journal of Polymer Science (English Edition)* **2015**, 33 (7), 931–946. <https://doi.org/10.1007/s10118-015-1654-7>.
- (21) Zdyrko, B.; Luzinov, I. Polymer Brushes by the “Grafting to” Method. *Macromolecular Rapid Communications* **2011**, 32 (12), 859–869. <https://doi.org/10.1002/marc.201100162>.
- (22) Edmondson, S.; Osborne, V. L.; Huck, W. T. S. Polymer Brushes via Surface-Initiated Polymerizations. *Chemical Society Reviews* **2004**, 33 (1), 14–22. <https://doi.org/10.1039/b210143m>.
- (23) Olivier, A.; Meyer, F.; Raquez, J. M.; Damman, P.; Dubois, P. Surface-Initiated Controlled Polymerization as a Convenient Method for Designing Functional Polymer Brushes: From Self-Assembled Monolayers to Patterned Surfaces. *Progress in Polymer Science (Oxford)* **2012**, 37 (1), 157–181. <https://doi.org/10.1016/j.progpolymsci.2011.06.002>.
- (24) Wibowo, S. H.; Sulistio, A.; Wong, E. H. H.; Blencowe, A.; Qiao, G. G. Polypeptide Films via N-Carboxyanhydride Ring-Opening Polymerization (NCA-ROP): Past, Present and Future. *Chemical Communications* **2014**, 50 (39), 4971–4988. <https://doi.org/10.1039/c4cc00293h>.
- (25) Yang, C.; Shi, Z.; Feng, C.; Li, R.; Luo, S.; Li, X.; Ruan, L. An Adjustable PH-Responsive Drug Delivery System Based on Self-Assembly Polypeptide-Modified Mesoporous Silica. *Macromolecular Bioscience* **2020**, 20 (6), 1–10. <https://doi.org/10.1002/mabi.202000034>.
- (26) Lu, L.; Lahasky, S. H.; McCandless, G. T.; Zhang, D.; Garno, J. C. Thermoresponsive

- Behavior of Polypeptoid Nanostructures Investigated with Heated Atomic Force Microscopy: Implications toward the Development of Smart Coatings for Surface-Based Sensors. *ACS Applied Nano Materials* **2019**, *2* (12), 7617–7625.
<https://doi.org/10.1021/acsanm.9b01715>.
- (27) Xu, Z.; Feng, Y.; Liu, X.; Guan, M.; Zhao, C.; Zhang, H. Synthesis and Characterization of Fe₃O₄@SiO₂@poly-L-Alanine, Peptide Brush-Magnetic Microspheres through NCA Chemistry for Drug Delivery and Enrichment of BSA. *Colloids and Surfaces B: Biointerfaces* **2010**, *81* (2), 503–507. <https://doi.org/10.1016/j.colsurfb.2010.07.048>.
- (28) Borase, T.; Heise, A. Hybrid Nanomaterials by Surface Grafting of Synthetic Polypeptides Using N-Carboxyanhydride (NCA) Polymerization. *Advanced Materials* **2016**, *28* (27), 5725–5731. <https://doi.org/10.1002/adma.201504474>.
- (29) Stukenkemper, T.; Paquez, X.; Verhoeven, M. W. G. M.; Hensen, E. J. M.; Dias, A. A.; Brougham, D. F.; Heise, A. Polypeptide Polymer Brushes by Light-Induced Surface Polymerization of Amino Acid N-Carboxyanhydrides. *Macromolecular Rapid Communications* **2018**, *39* (7), 1–5. <https://doi.org/10.1002/marc.201700743>.
- (30) Lu, L.; Lahasky, S. H.; Zhang, D.; Garno, J. C. Directed Growth of Polymer Nanorods Using Surface-Initiated Ring-Opening Polymerization of N-Allyl N-Carboxyanhydride. *ACS Applied Materials and Interfaces* **2016**, *8* (6), 4014–4022.
<https://doi.org/10.1021/acsami.5b11358>.
- (31) Audouin, F.; Fox, M.; Larragy, R.; Clarke, P.; Huang, J.; O'Connor, B.; Heise, A. Polypeptide-Grafted Macroporous PolyHIPE by Surface-Initiated N-Carboxyanhydride (NCA) Polymerization as a Platform for Bioconjugation. *Macromolecules* **2012**, *45* (15),

- 6127–6135. <https://doi.org/10.1021/ma3010263>.
- (32) Witte, P.; Menzel, H. Nickel-Mediated Surface Grafting from Polymerization of α -Amino Acid-N-Carboxyanhydrides. *Macromolecular Chemistry and Physics* **2004**, *205* (13), 1735–1743. <https://doi.org/10.1002/macp.200400100>.
- (33) Chen, C. Redox-Controlled Polymerization and Copolymerization. *ACS Catalysis* **2018**, *8* (6), 5506–5514. <https://doi.org/10.1021/acscatal.8b01096>.
- (34) Gregson, C. K. A.; Gibson, V. C.; Long, N. J.; Marshall, E. L.; Oxford, P. J.; White, A. J. P. Redox Control within Single-Site Polymerization Catalysts. *Journal of the American Chemical Society* **2006**, *128* (23), 7410–7411. <https://doi.org/10.1021/ja061398n>.
- (35) Broderick, E. M.; Guo, N.; Vogel, C. S.; Xu, C.; Sutter, J.; Miller, J. T.; Meyer, K.; Mehrkhodavandi, P.; Diaconescu, P. L. Redox Control of a Ring-Opening Polymerization Catalyst. *Journal of the American Chemical Society* **2011**, *133* (24), 9278–9281. <https://doi.org/10.1021/ja2036089>.
- (36) Biernesser, A. B.; Li, B.; Byers, J. A. Redox-Controlled Polymerization of Lactide Catalyzed by Bis(Imino)Pyridine Iron Bis(Alkoxide) Complexes. *Journal of the American Chemical Society* **2013**, *135* (44), 16553–16560. <https://doi.org/10.1021/ja407920d>.
- (37) Wang, X.; Thevenon, A.; Brosmer, J. L.; Yu, I.; Khan, S. I.; Mehrkhodavandi, P.; Diaconescu, P. L. Redox Control of Group 4 Metal Ring-Opening Polymerization Activity toward ϵ -Lactide and ϵ -Caprolactone. *Journal of the American Chemical Society* **2014**, *136* (32), 11264–11267. <https://doi.org/10.1021/ja505883u>.
- (38) Biernesser, A. B.; Delle Chiaie, K. R.; Curley, J. B.; Byers, J. A. Block Copolymerization of Lactide and an Epoxide Facilitated by a Redox Switchable Iron-Based Catalyst.

- Angewandte Chemie* **2016**, *128* (17), 5337–5340.
<https://doi.org/10.1002/ange.201511793>.
- (39) Delle Chiaie, K. R.; Biernesser, A. B.; Ortuño, M. A.; Dereli, B.; Iovan, D. A.; Wilding, M. J. T.; Li, B.; Cramer, C. J.; Byers, J. A. The Role of Ligand Redox Non-Innocence in Ring-Opening Polymerization Reactions Catalysed by Bis(Imino)Pyridine Iron Alkoxide Complexes. *Dalton Transactions* **2017**, *46* (38), 12971–12980.
<https://doi.org/10.1039/c7dt03067c>.
- (40) Savka, R.; Foro, S.; Gallei, M.; Rehahn, M.; Plenio, H. Oxidation-Triggered Ring-Opening Metathesis Polymerization. *Chemistry - A European Journal* **2013**, *19* (32), 10655–10662.
<https://doi.org/10.1002/chem.201300868>.
- (41) Magenau, A. J. D.; Strandwitz, N. C.; Gennaro, A.; Matyjaszewski, K. Electrochemically Mediated Atom Transfer Radical Polymerization. *Science* **2011**, *332* (April), 81–83.
<https://doi.org/10.4159/harvard.9780674333987.c22>.
- (42) Qi, M.; Dong, Q.; Wang, D.; Byers, J. A. Electrochemically Switchable Ring-Opening Polymerization of Lactide and Cyclohexene Oxide. *Journal of the American Chemical Society* **2018**, *140* (17), 5686–5690. <https://doi.org/10.1021/jacs.8b02171>.
- (43) Lyon, L. A.; Hupp, J. T. Energetics of the Nanocrystalline Titanium Dioxide/Aqueous Solution Interface: Approximate Conduction Band Edge Variations between $H_0 = -10$ and $H_- = +26$. *Journal of Physical Chemistry B* **1999**, *103* (22), 4623–4628.
<https://doi.org/10.1021/jp9908404>.
- (44) Schneider, J.; Matsuoka, M.; Takeuchi, M.; Zhang, J.; Horiuchi, Y.; Anpo, M.; Bahnemann, D. W. Schneider et Al. - 2014 - Understanding TiO₂ Photocatalysis Mechanisms and

- Materials(2).Pdf. *Chem. Rev.* **2014**, *114* (9), 9919–9986.
- (45) Ortuño, M. A.; Dereli, B.; Chiaie, K. R. D.; Biernesser, A. B.; Qi, M.; Byers, J. A.; Cramer, C. J. The Role of Alkoxide Initiator, Spin State, and Oxidation State in Ring-Opening Polymerization of ϵ -Caprolactone Catalyzed by Iron Bis(Imino)Pyridine Complexes. *Inorganic Chemistry* **2018**, *57*, 2064–2071.
- (46) Hosseini, A.; Içli, K.; Özenbaş, M.; Erçelebi. Fabrication and Characterization of Spin-Coated TiO₂ Films. *Energy Procedia* **2014**, *60* (C), 191–198.
<https://doi.org/10.1016/j.egypro.2014.12.332>.
- (47) Wu, C. Y.; Tu, K. J.; Deng, J. P.; Lo, Y. S.; Wu, C. H. Markedly Enhanced Surface Hydroxyl Groups of TiO₂ Nanoparticles with Superior Water-Dispersibility for Photocatalysis. *Materials* **2017**, *10* (5). <https://doi.org/10.3390/ma10050566>.
- (48) Burger, B. J.; Bercaw, J. E. Bercaw Air-Sensitive Chemistry. In *Experimental Organometallic Chemistry*; ACS Symposium Series, 1987; pp 79–115.
- (49) Biernesser, A. B.; Li, B.; Byers, J. A. Redox-Controlled Polymerization of Lactide Catalyzed by Bis(Imino)Pyridine Iron Bis(Alkoxide) Complexes. *Journal of the American Chemical Society* **2013**, *135*, 16553–16560.
- (50) Delle Chiaie, K. R.; Biernesser, A. B.; Ortuño, M. A.; Dereli, B.; Iovan, D. A.; Wilding, M. J. T.; Li, B.; Cramer, C. J.; Byers, J. A. The Role of Ligand Redox Non-Innocence in Ring-Opening Polymerization Reactions Catalysed by Bis(Imino)Pyridine Iron Alkoxide Complexes. *Dalton Trans.* **2017**, *46*, 12971–12980.
- (51) Gradišar, Š.; Žagar, E.; Pahovnik, D. Ring-Opening Polymerization of N-Carboxyanhydrides Initiated by a Hydroxyl Group. *ACS Macro Letters* **2017**, *6*, 637–640.

- (52) Klinker, K.; Schäfer, O.; Huesmann, D.; Bauer, T.; Capelôa, L.; Braun, L.; Stergiou, N.; Schinnerer, M.; Dirisala, A.; Miyata, K.; et al. Secondary-Structure-Driven Self-Assembly of Reactive Polypept(o)ides: Controlling Size, Shape, and Function of Core Cross-Linked Nanostructures. *Angewandte Chemie - International Edition* **2017**, *56*, 9608–9613.
- (53) Le Bras, J.; Jiao, H.; Meyer, W. E.; Hampel, F.; Gladysz, J. . Synthesis, Crystal Structure, and Reactions of the 17-Valence-Electron Rhenium Methyl Complex [(H5-C5Me5)Re(NO)(P(4-C6H4CH3)3)(CH3)]⁺ B(3,5-C6H3(CF3)2)₄⁻: Experimental and Computational Bonding Comparisons with 18-Electron Methyl and Methylidene Complexes. *Journal of Organometallic Chemistry* **2000**, *616*, 54–66.

5.0 Appendix A. NMR Spectra for All Complexes and Polymers

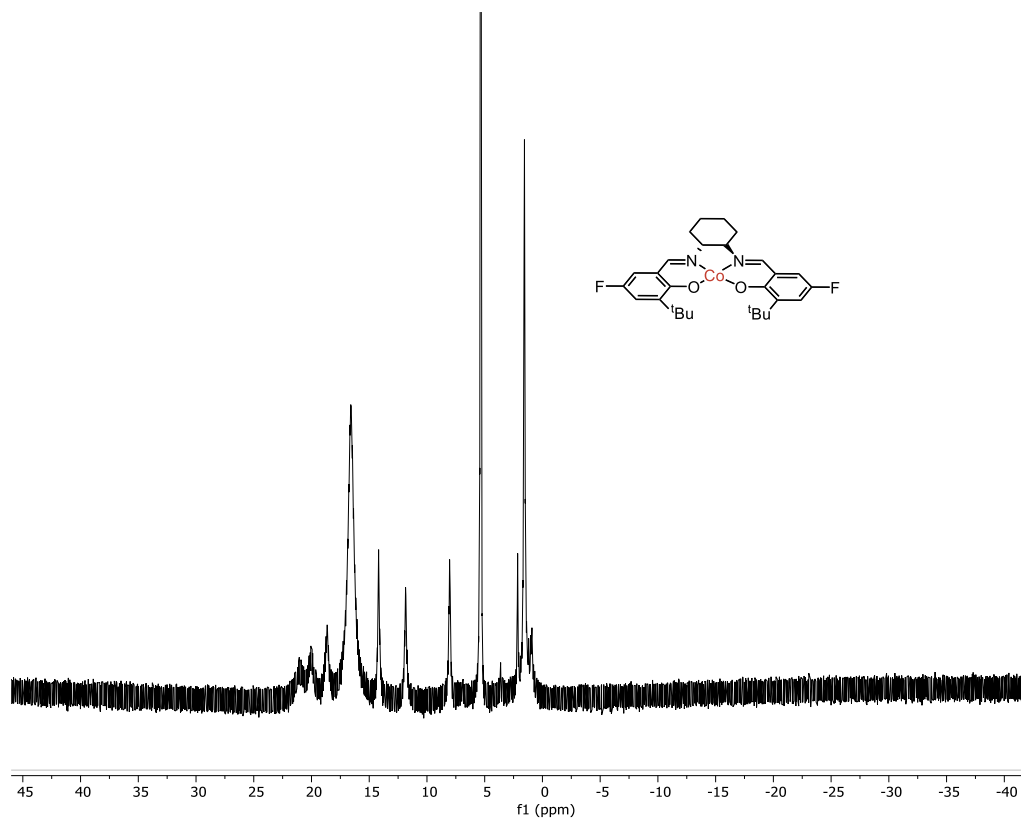


Figure A.1. 500 MHz, ^1H NMR spectrum for complex **2.9** in CDCl_3 .

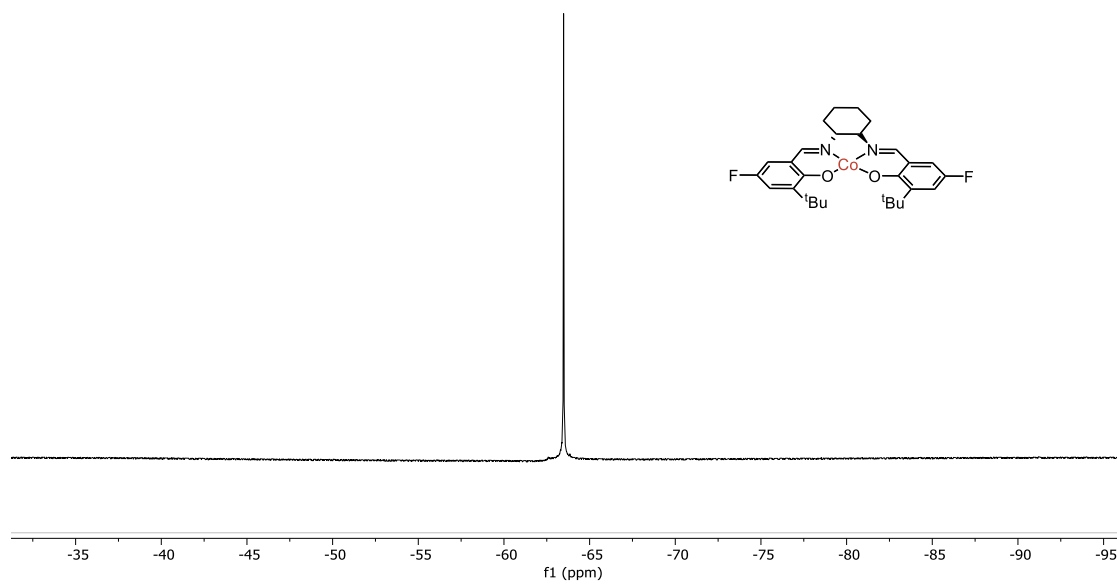


Figure A.2. 470 MHz, ^{19}F NMR spectrum for complex **2.9** in CDCl_3 .

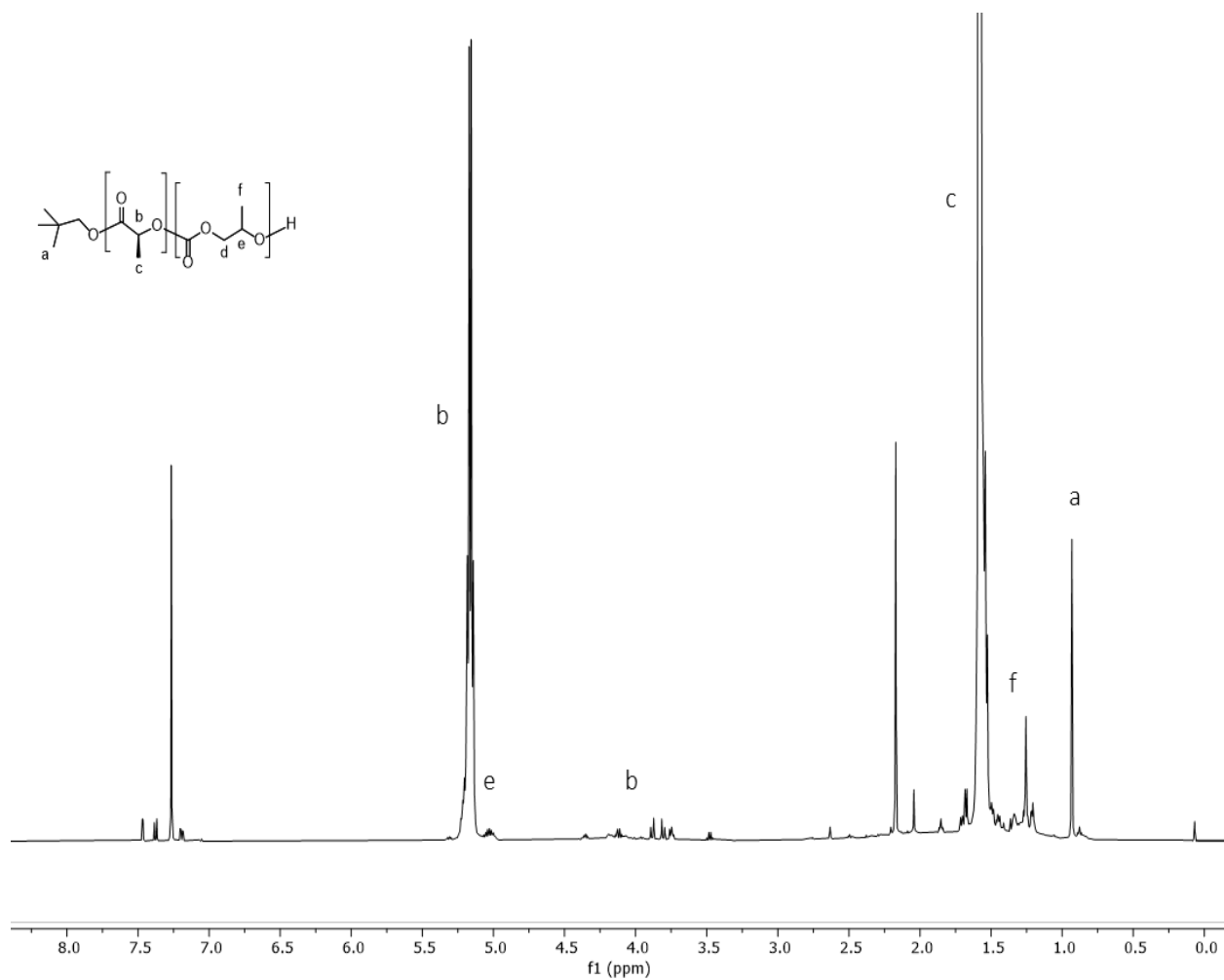


Figure A.3. 500 MHz, ¹H NMR spectrum for poly(L-lactic acid-b-propylene carbonate) from Scheme 2.12a in CDCl₃.

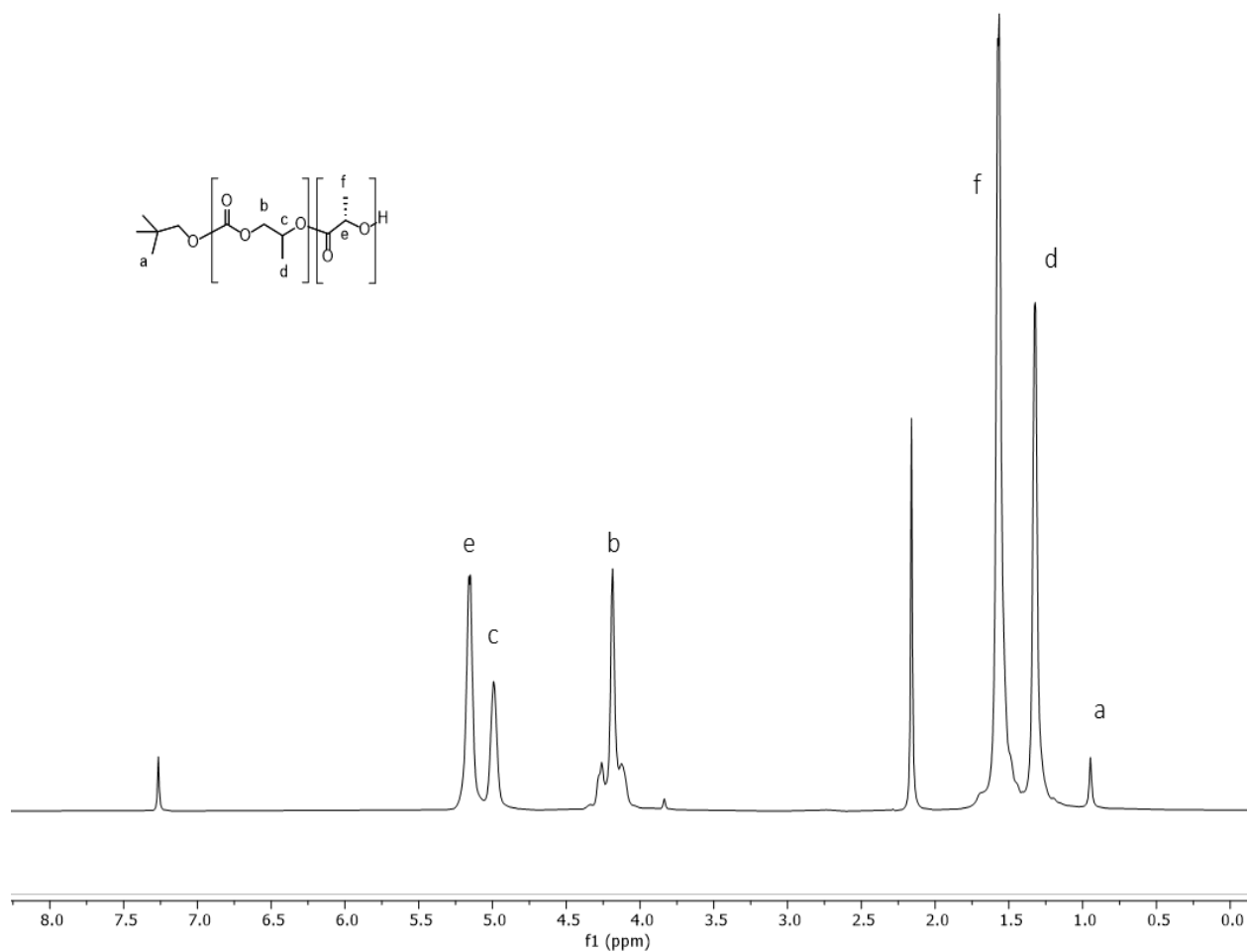


Figure A.4. 500 MHz, ¹H NMR spectrum for poly(propylene carbonate-*b*-L-lactic acid) from Scheme 2.12b in CDCl₃.

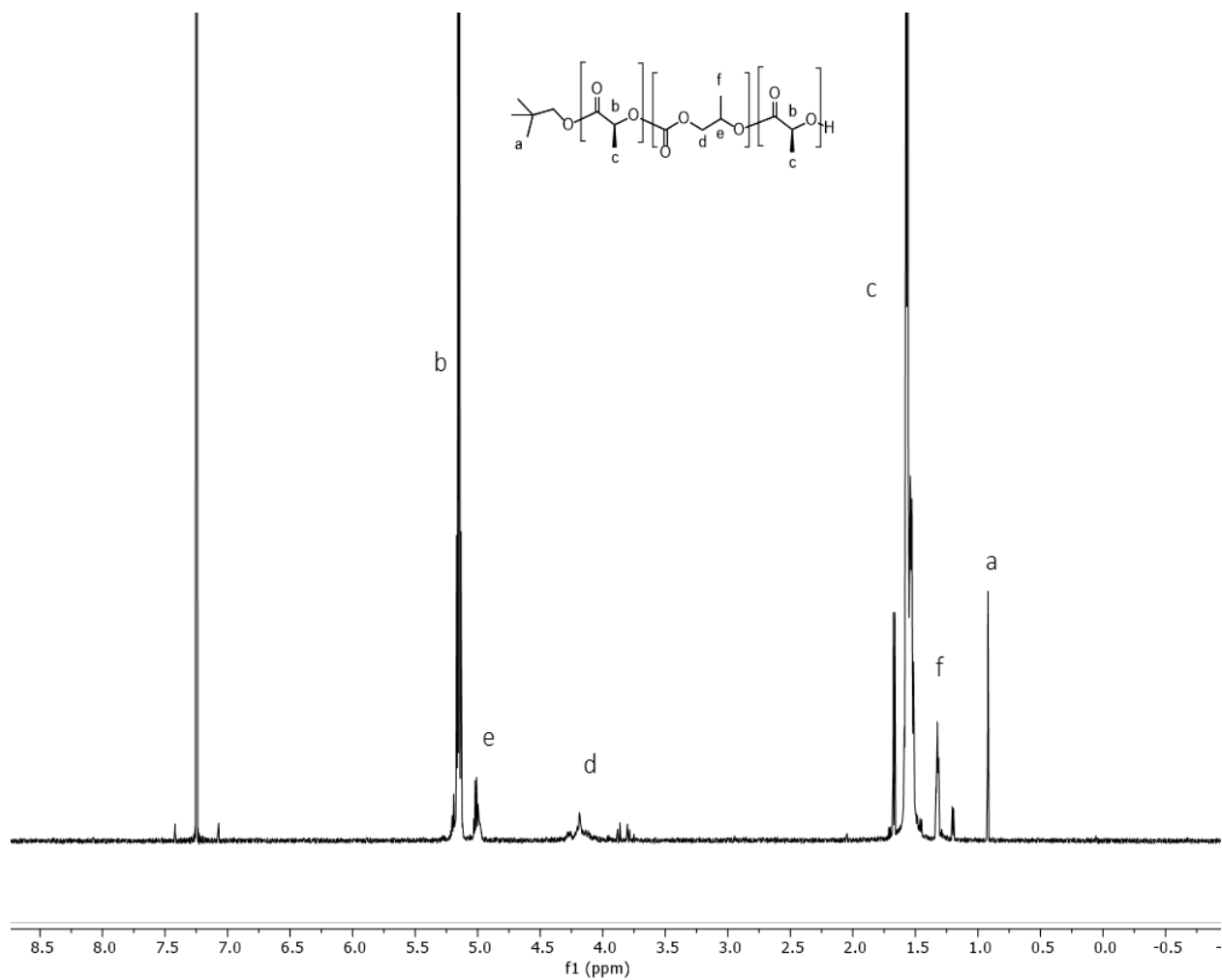


Figure A.5. 500 MHz, ¹H NMR spectrum for poly(L-lactic acid-*b*-propylene carbonate-*b*-L-lactic acid') from Scheme 2.13a in CDCl₃.

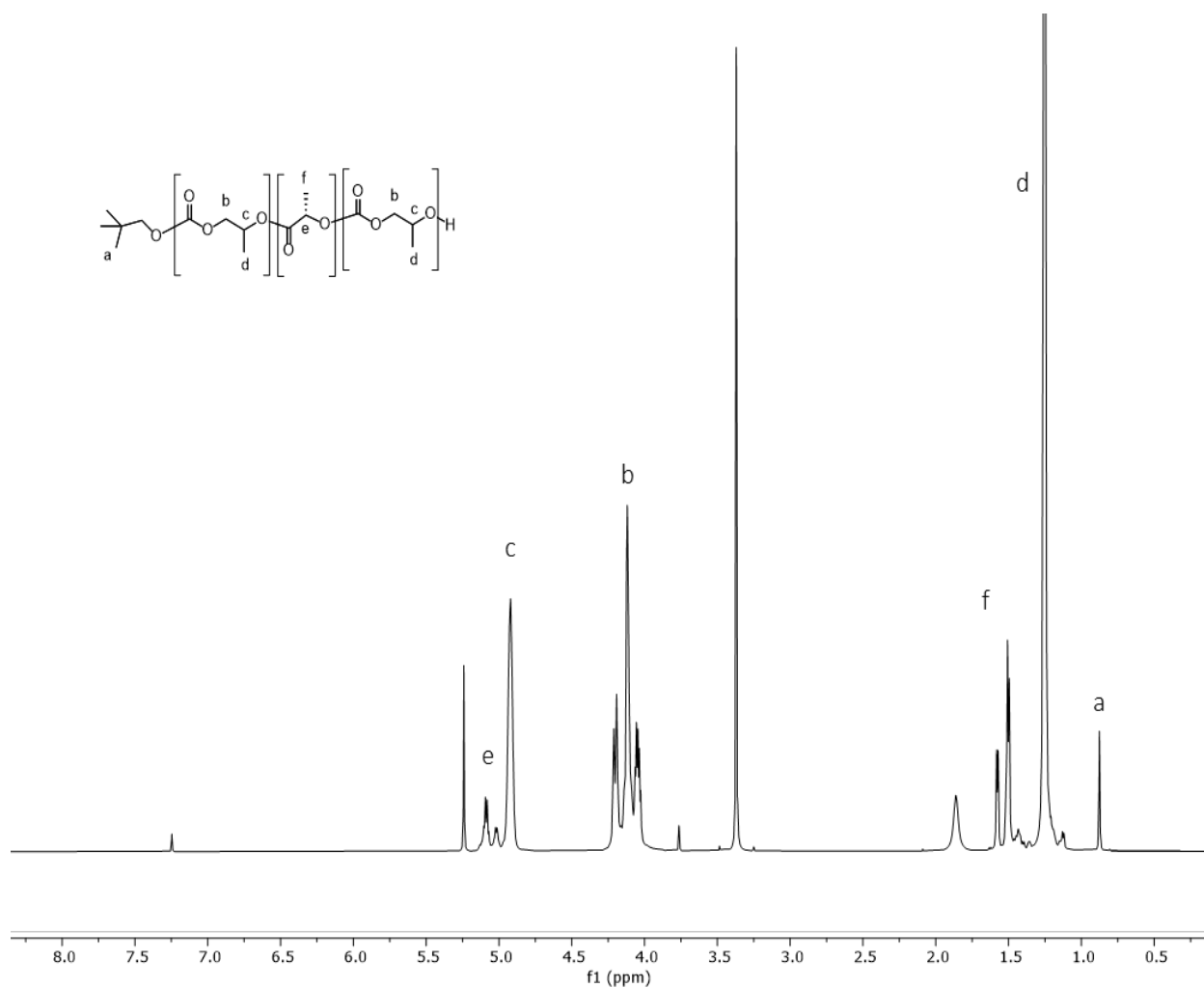


Figure A.6. 500 MHz, ¹H NMR spectrum for poly(propylene carbonate-*b*-L-lactic acid-*b*-propylene carbonate') from Scheme 2.13b in CDCl₃.

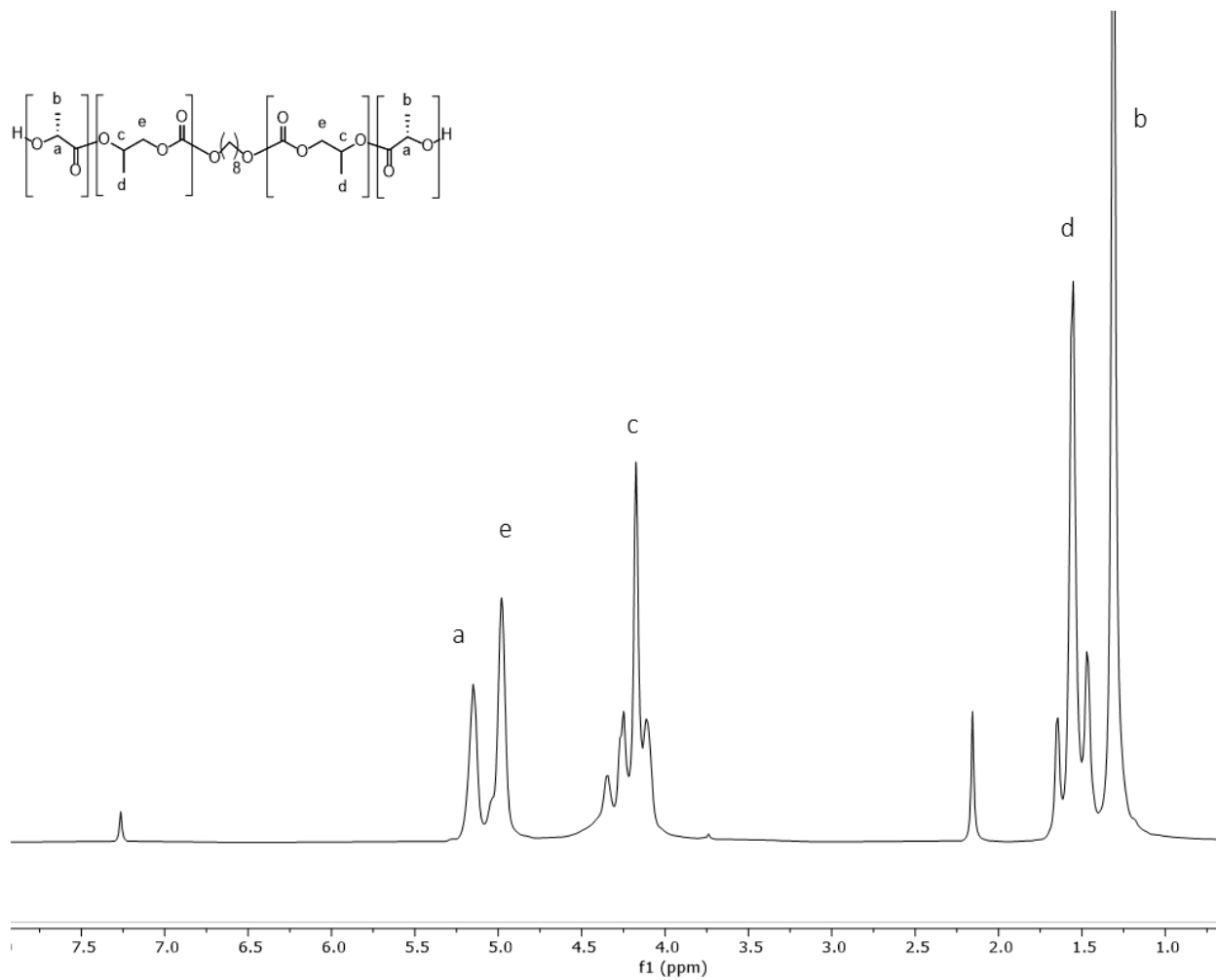


Figure A.7. 500 MHz, ^1H NMR spectrum for telechelic poly(*L*-lactic acid-*b*-propylene carbonate-*b*-*L*-lactic acid) from Scheme 2.14 in CDCl_3 .

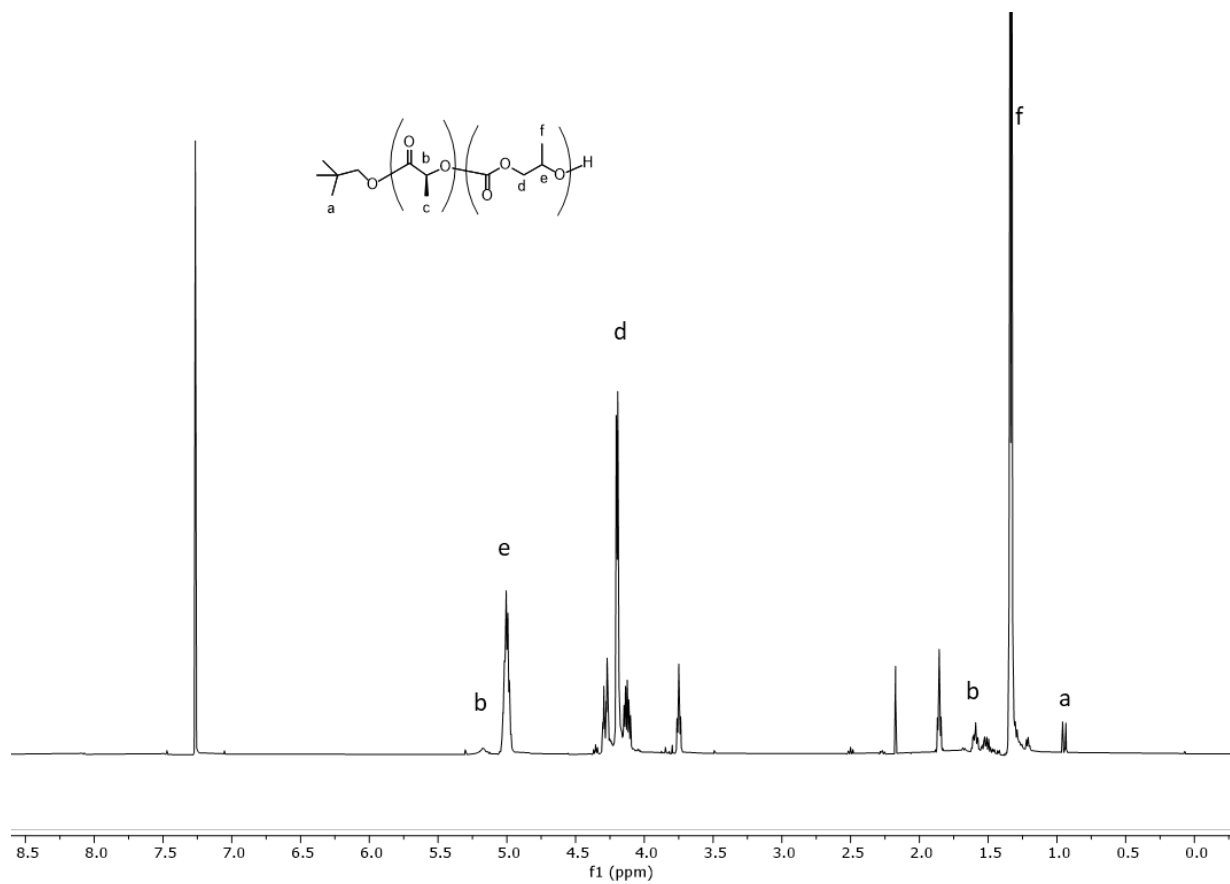


Figure A.8. 500 MHz, ¹H NMR spectrum for poly(L-lactic acid-s-propylene carbonate) from Scheme 2.16a in CDCl₃.

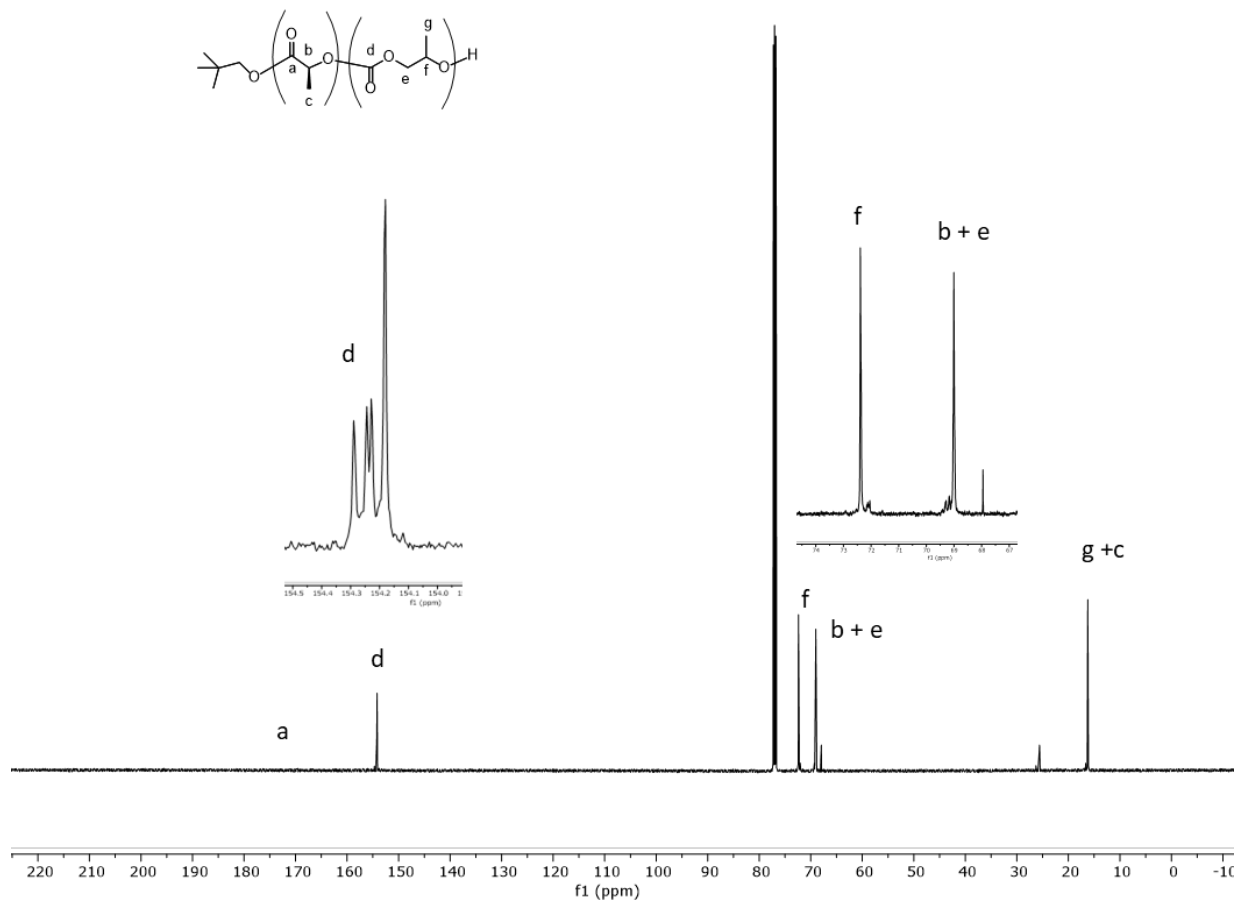


Figure A.9. 125 MHz, ^{13}C NMR spectrum for poly(L-lactic acid-s-propylene carbonate) from Scheme 2.16a in CDCl_3 .

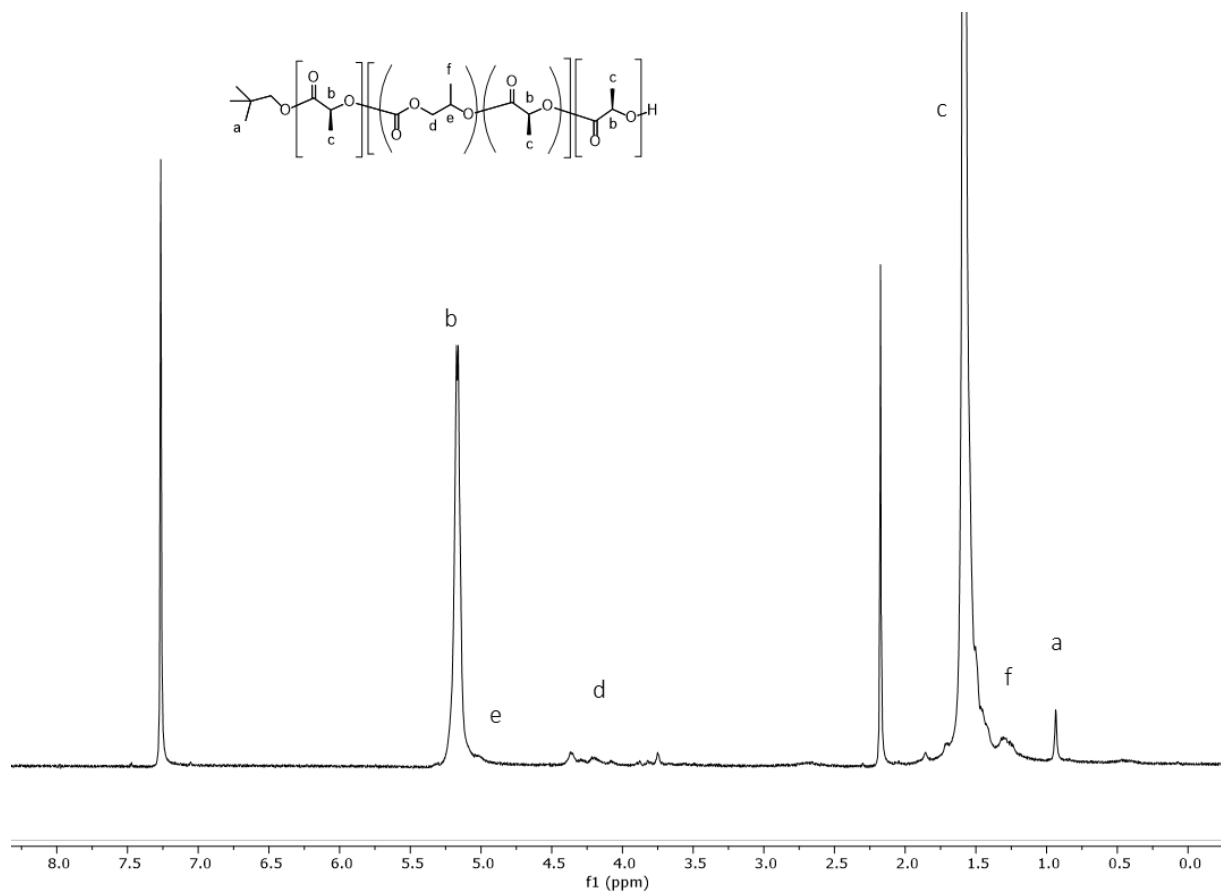


Figure A.10. 500 MHz, ¹H NMR spectrum for poly(*L*-lactic acid-*b*-(*L*-lactic acid-*s*-propylene carbonate)-*b*-*L*-lactic acid') from Scheme 2.17a in CDCl₃.

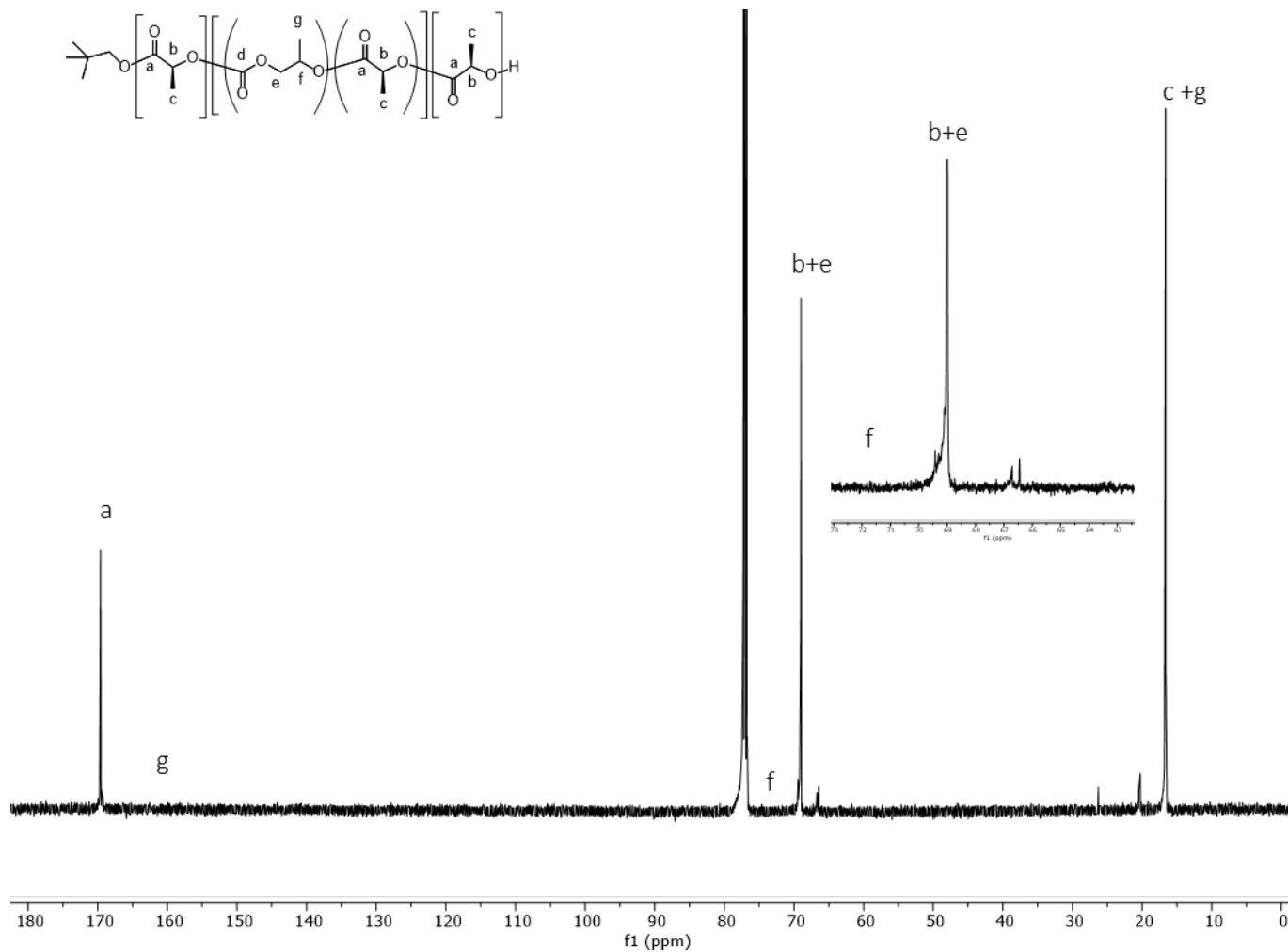


Figure A.11. 125 MHz, ^{13}C NMR spectrum for poly(*L*-lactic acid-*b*-(*L*-lactic acid-*s*-propylene carbonate)-*b*-*L*-lactic acid') from Scheme 2.17a in CDCl_3 .

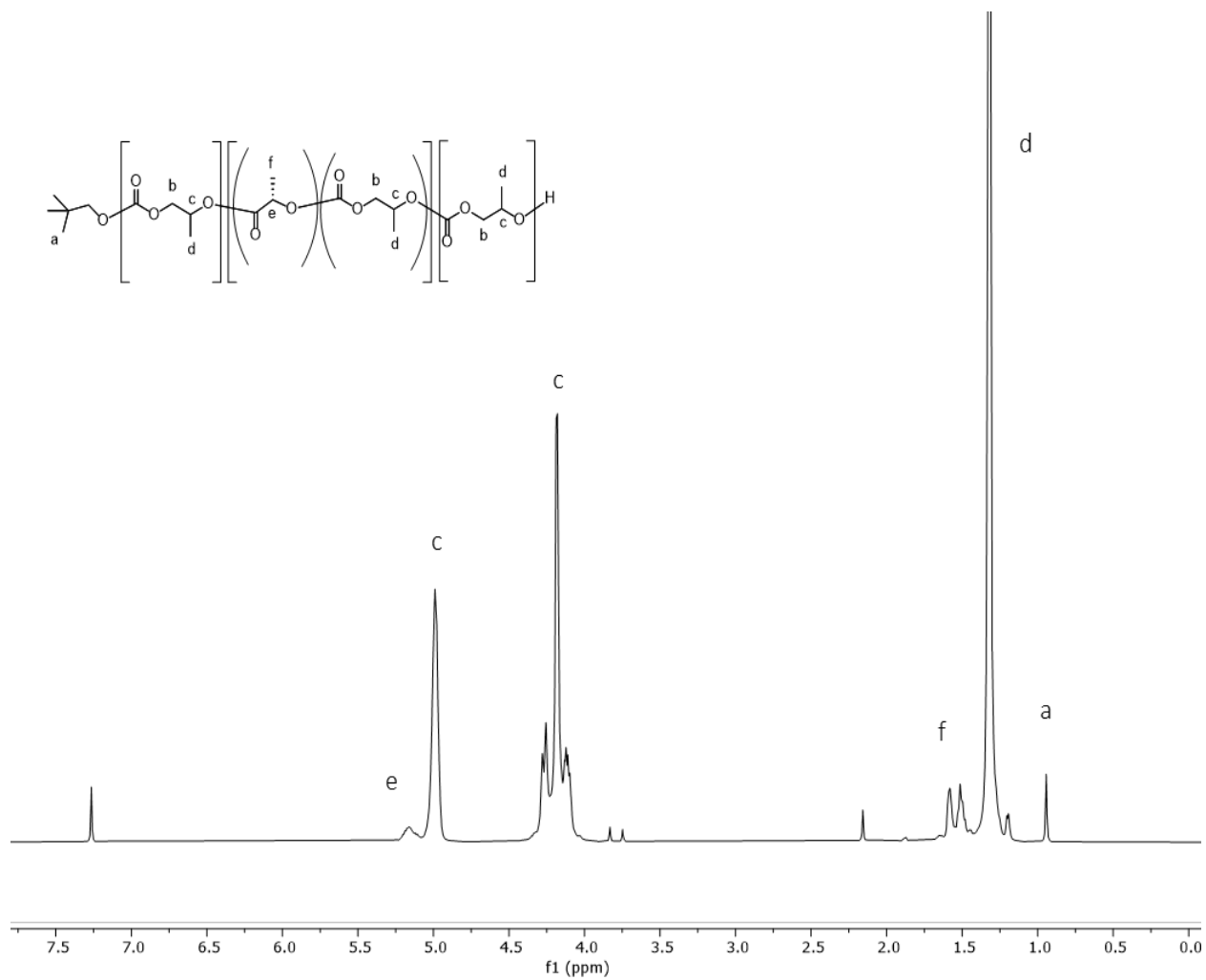


Figure A.12. 500 MHz, ¹H NMR spectrum for poly(propylene carbonate-*b*-(*L*-lactic acid-*s*-propylene carbonate)-*b*-*L*-lactic acid) from Scheme 2.17b in CDCl₃.

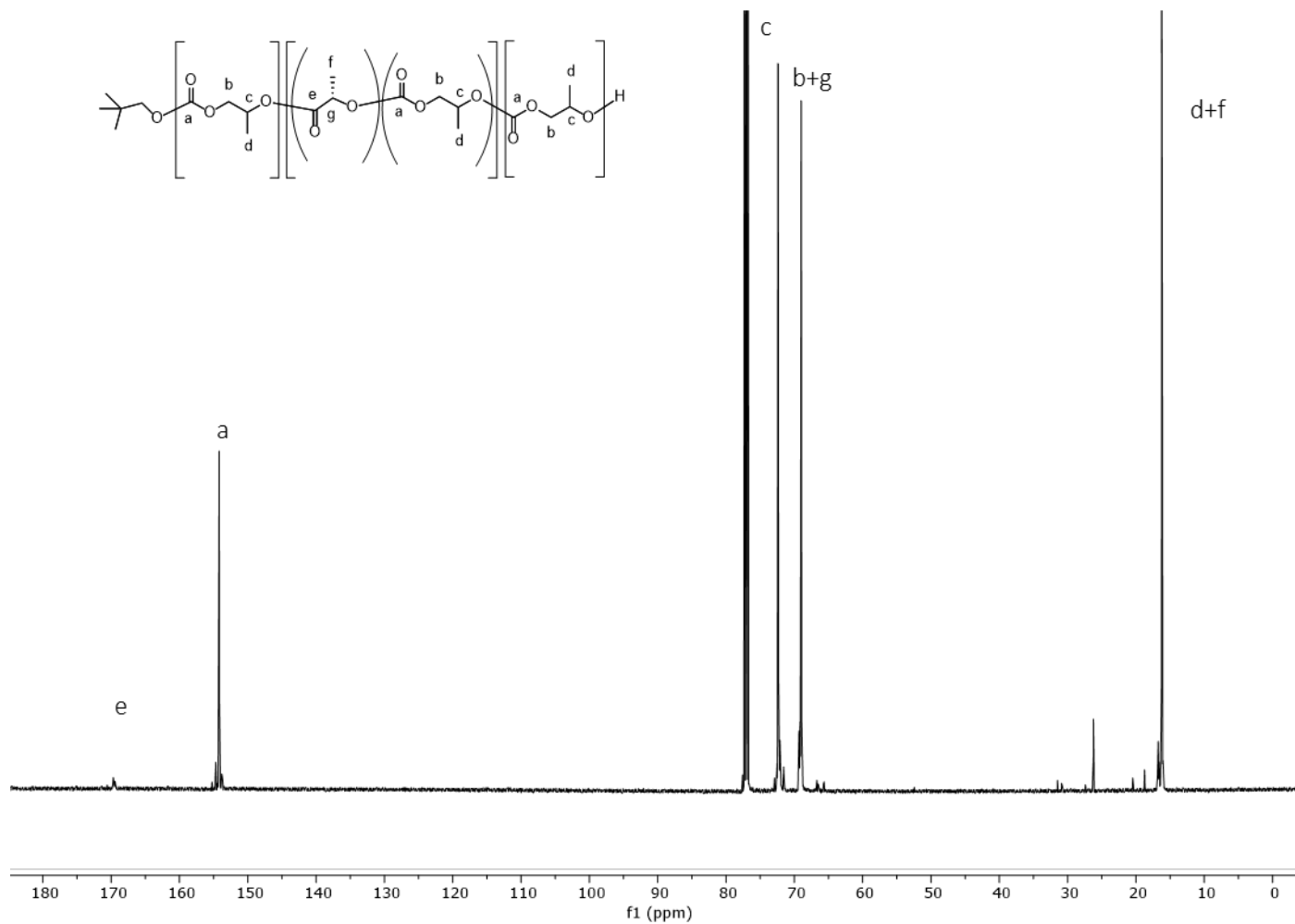


Figure A.13. 125 MHz, ^{13}C NMR spectrum for poly(propylene carbonate-*b*-(*L*-lactic acid-*s*-propylene carbonate)-*b*-*L*-lactic acid) from Scheme 2.17b in CDCl_3 .

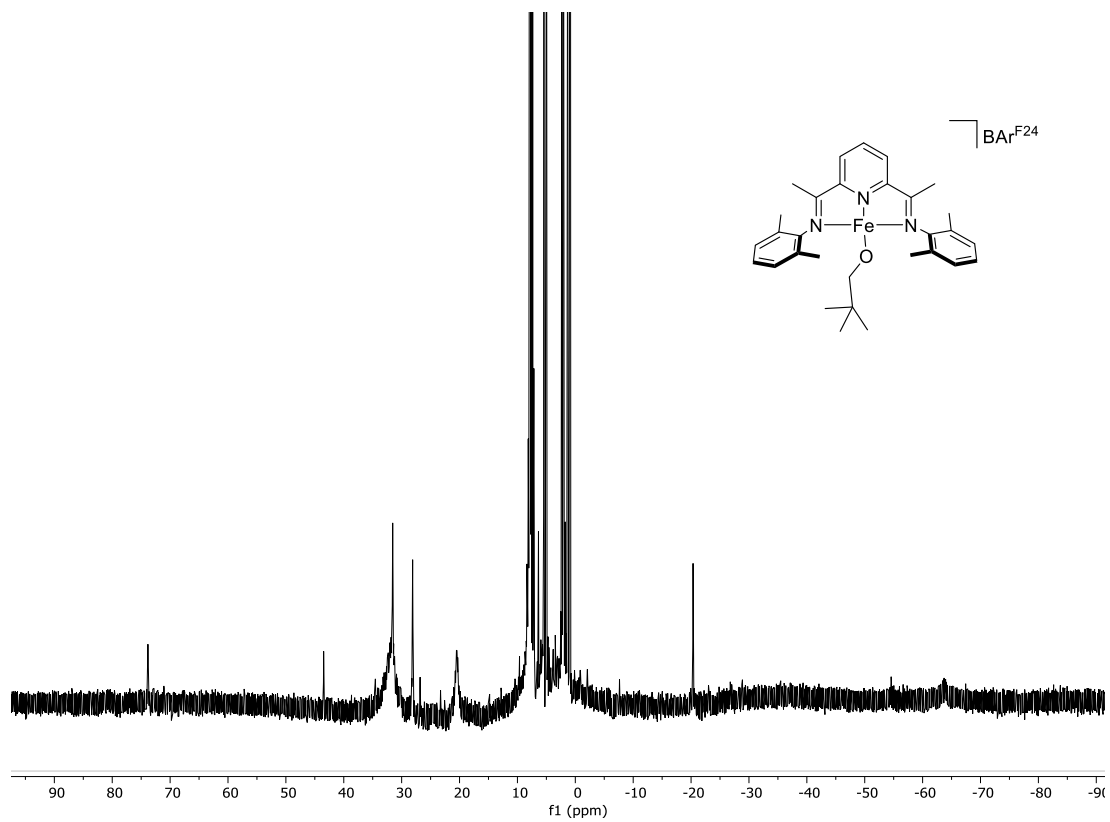


Figure A.14. 500 MHz, ^1H NMR spectrum for complex **3.2** in CD_2Cl_2 .

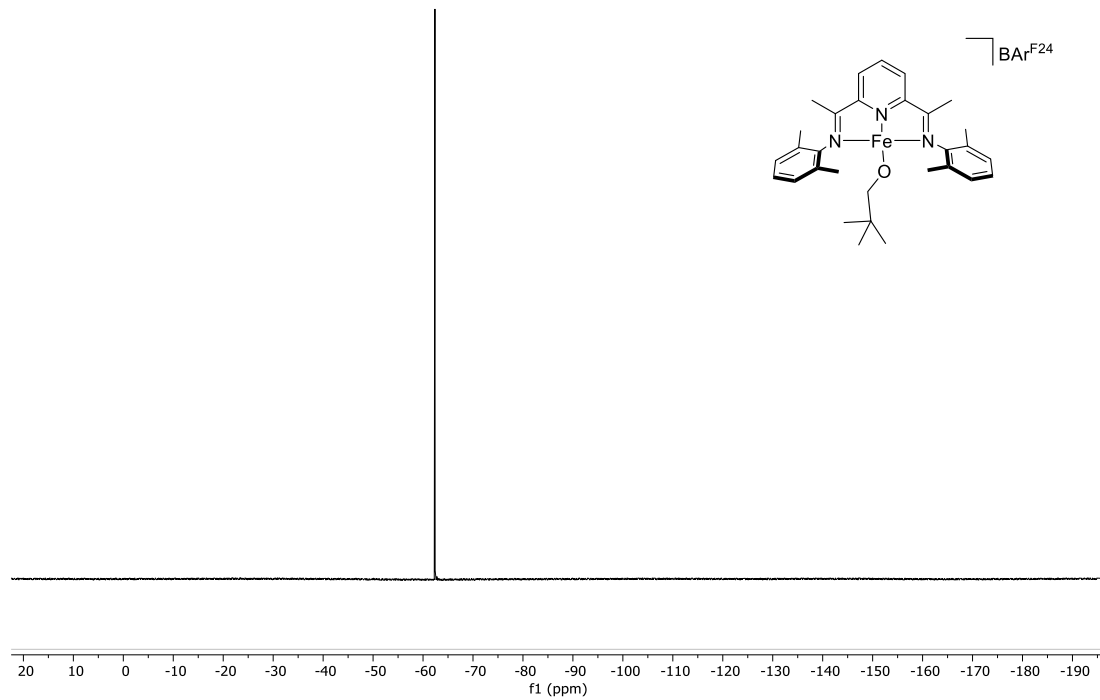


Figure A.15. 470 MHz, ^{19}F NMR spectrum for complex **3.2** in CD_2Cl_2 .

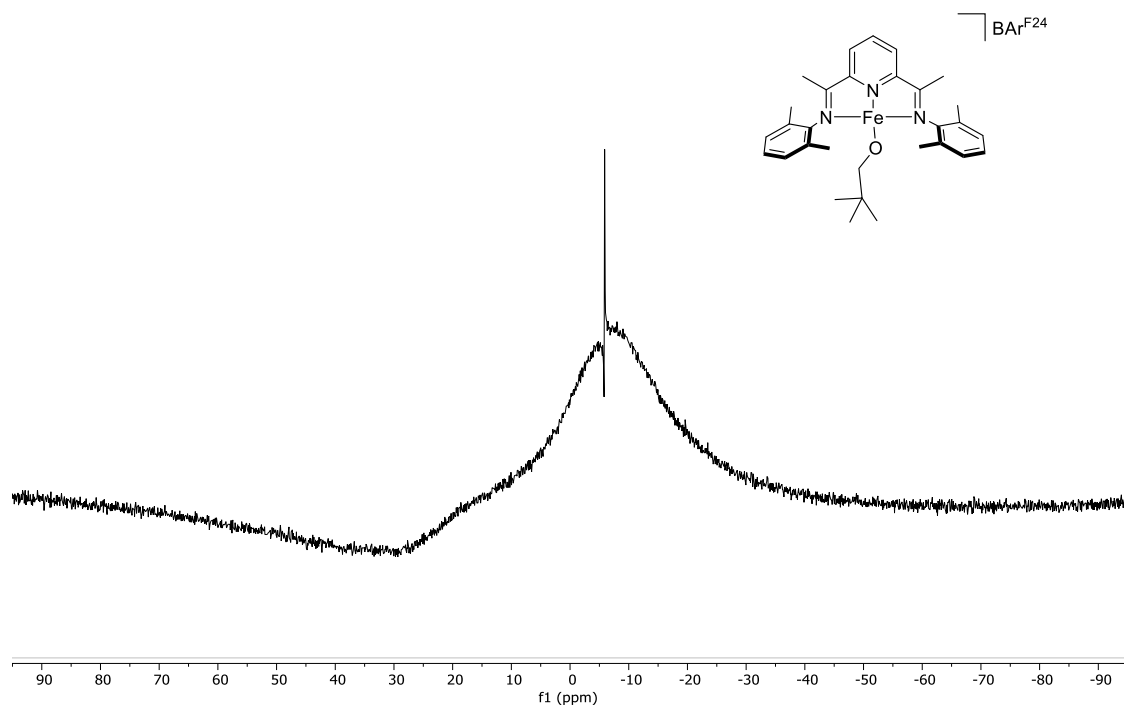


Figure A.16. 128 MHz, ^{11}B NMR spectrum for complex **3.2** in CD_2Cl_2 .

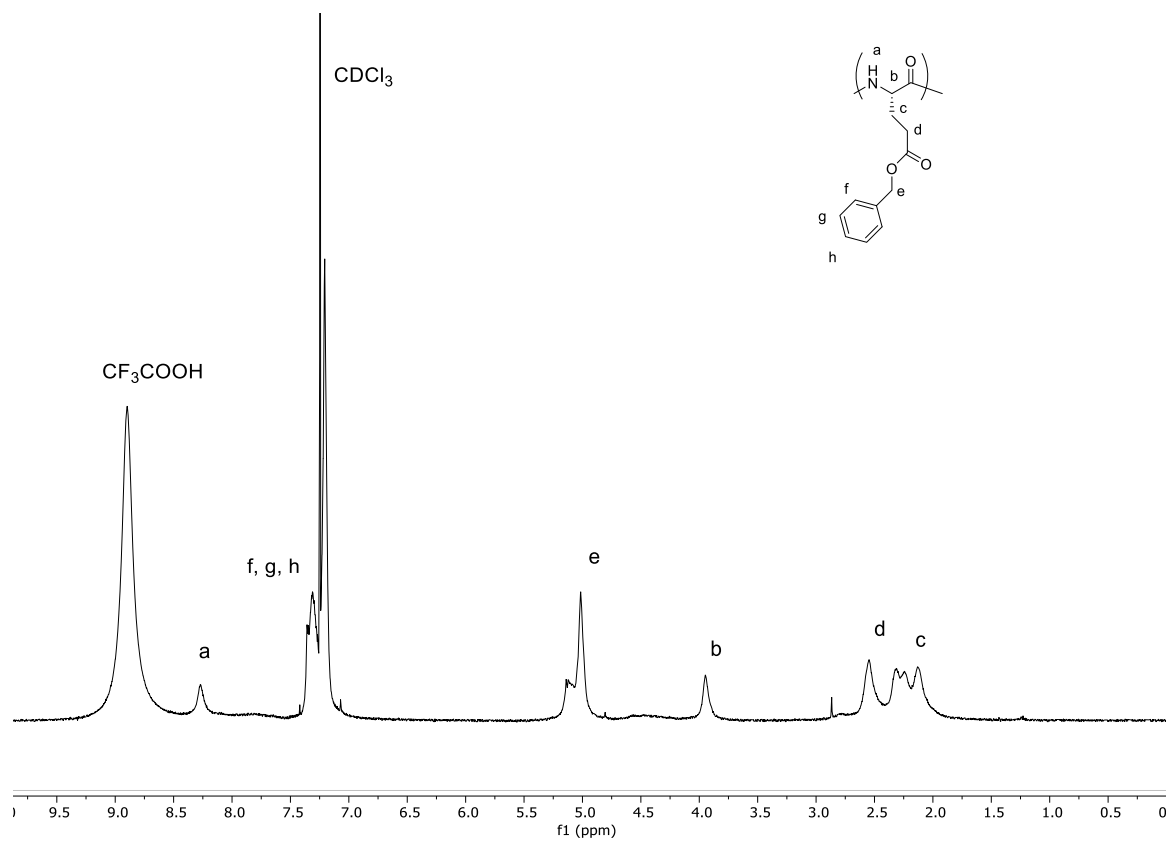


Figure A.17. 500 MHz, ¹H NMR spectrum of precipitated poly(γ-benzyl-L-glutamate) in CDCl₃ and 5 % trifluoroacetic acid from entry 6, Table 3.1.

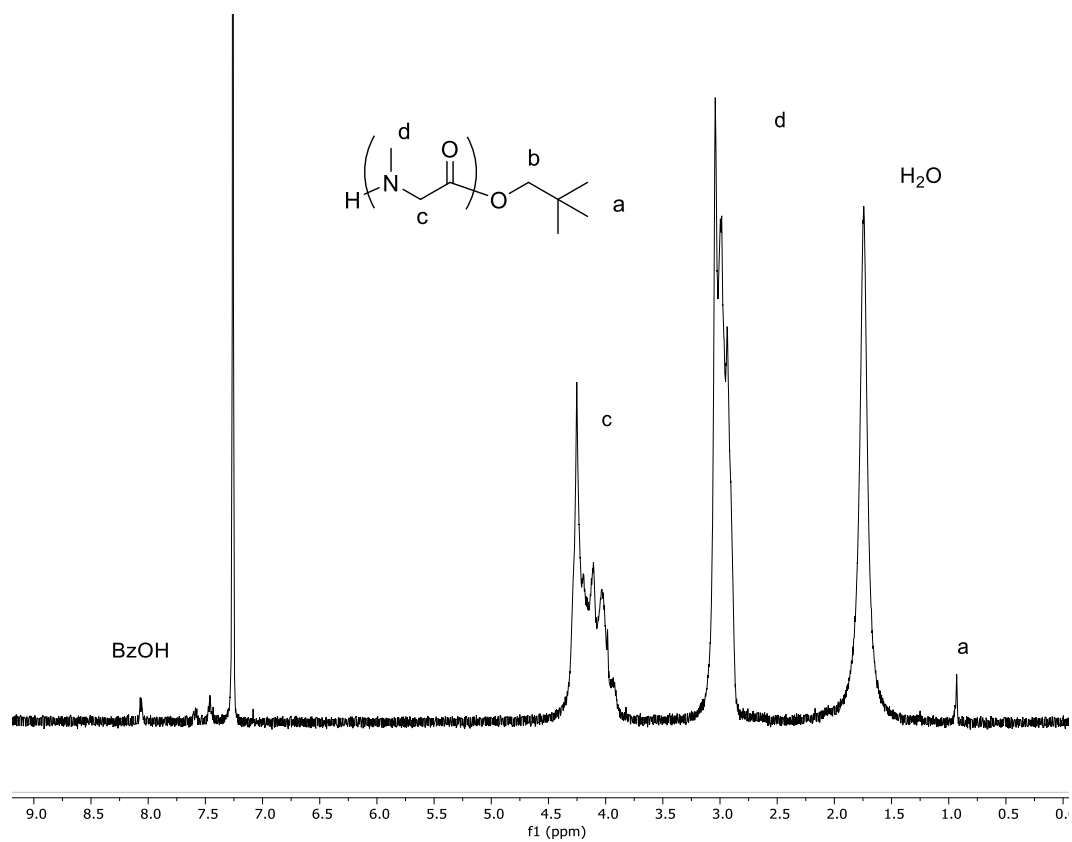


Figure A.18. 500 MHz, ^1H NMR spectrum of poly(sarcosine) from entry 1, Table 3.3 in CDCl_3 .

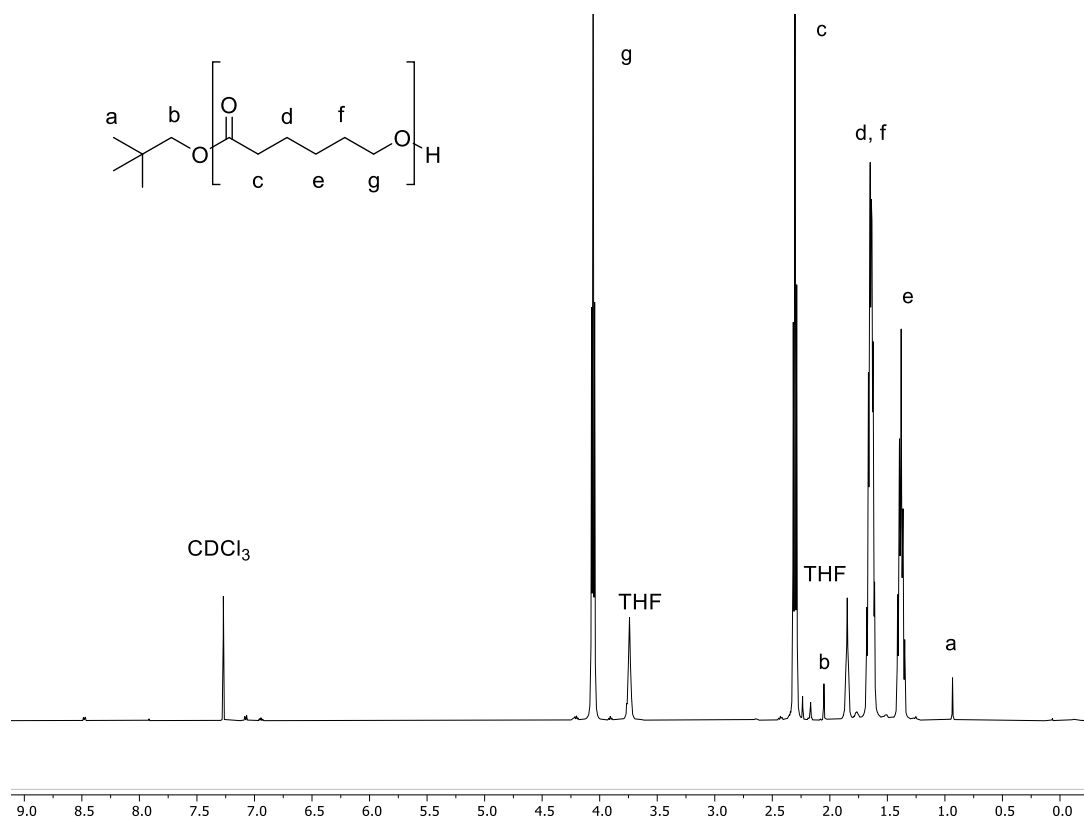


Figure A.18. 500 MHz, ¹H NMR spectrum of poly(ε-caprolactone) from Scheme 3.5a in CDCl₃.

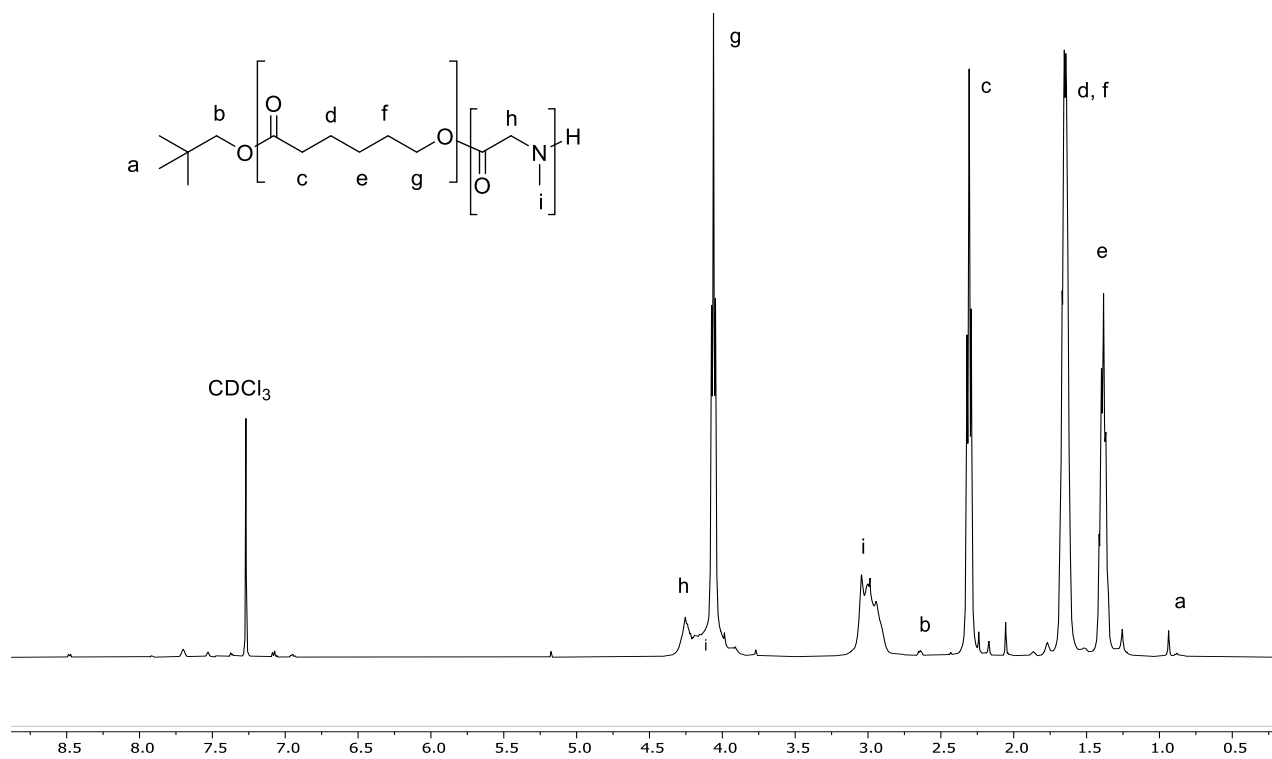


Figure A.20. 600 MHz, ^1H NMR spectrum of poly(ϵ -caprolactone-*b*-sarcosine) from Scheme 3.5a in CDCl_3 .

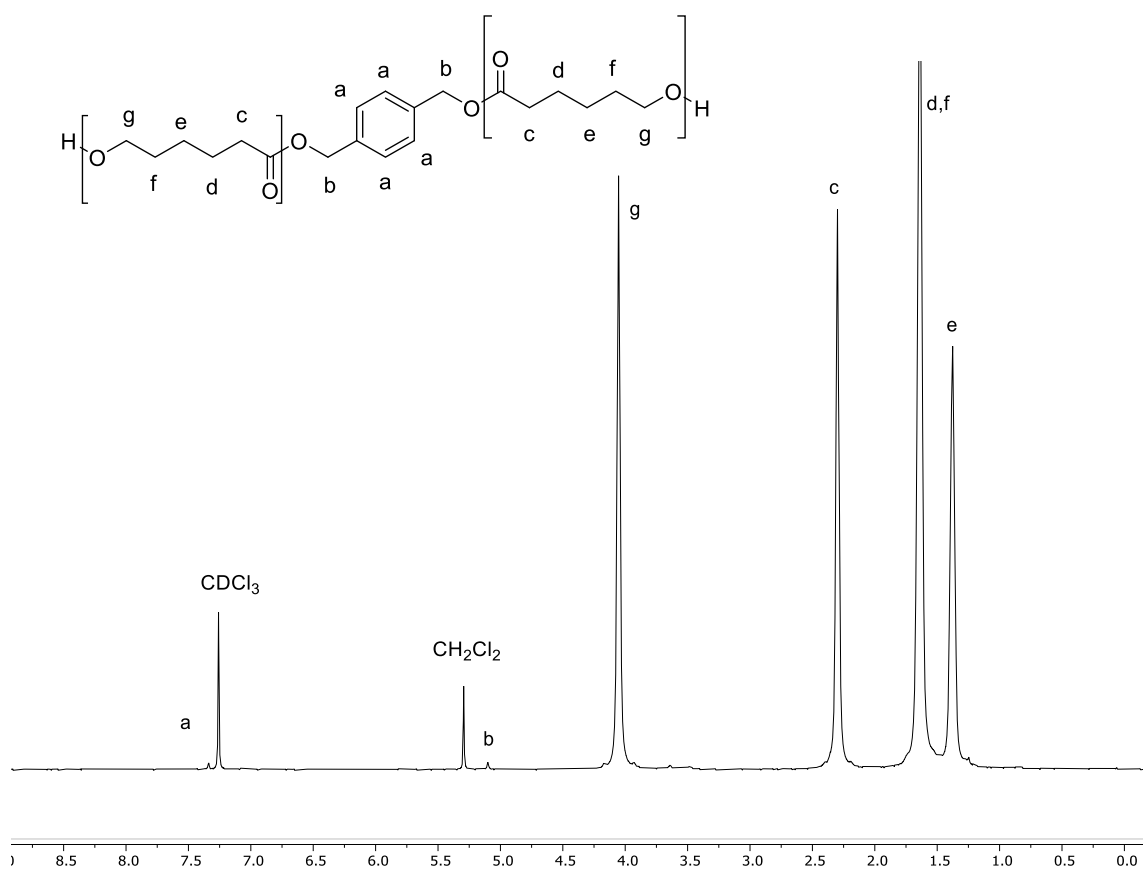


Figure A.21. 500 MHz, ¹H NMR spectrum of poly(ε-caprolactone) from Scheme 3.5c in CDCl₃.

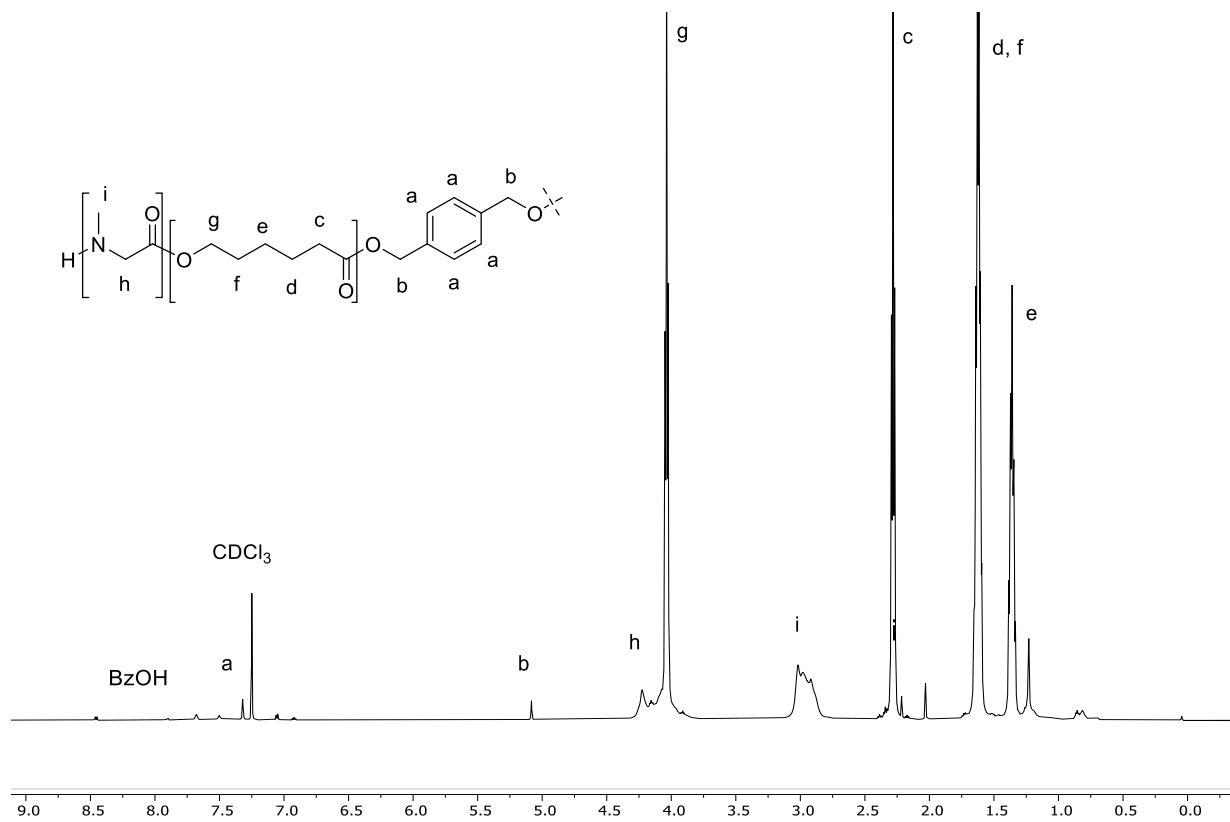


Figure A.22. 600 MHz, ¹H NMR spectra of telechelic poly(sarcosine-*b*-ε-caprolactone-*b*-sarcosine) from Scheme 3.5c in CDCl₃.

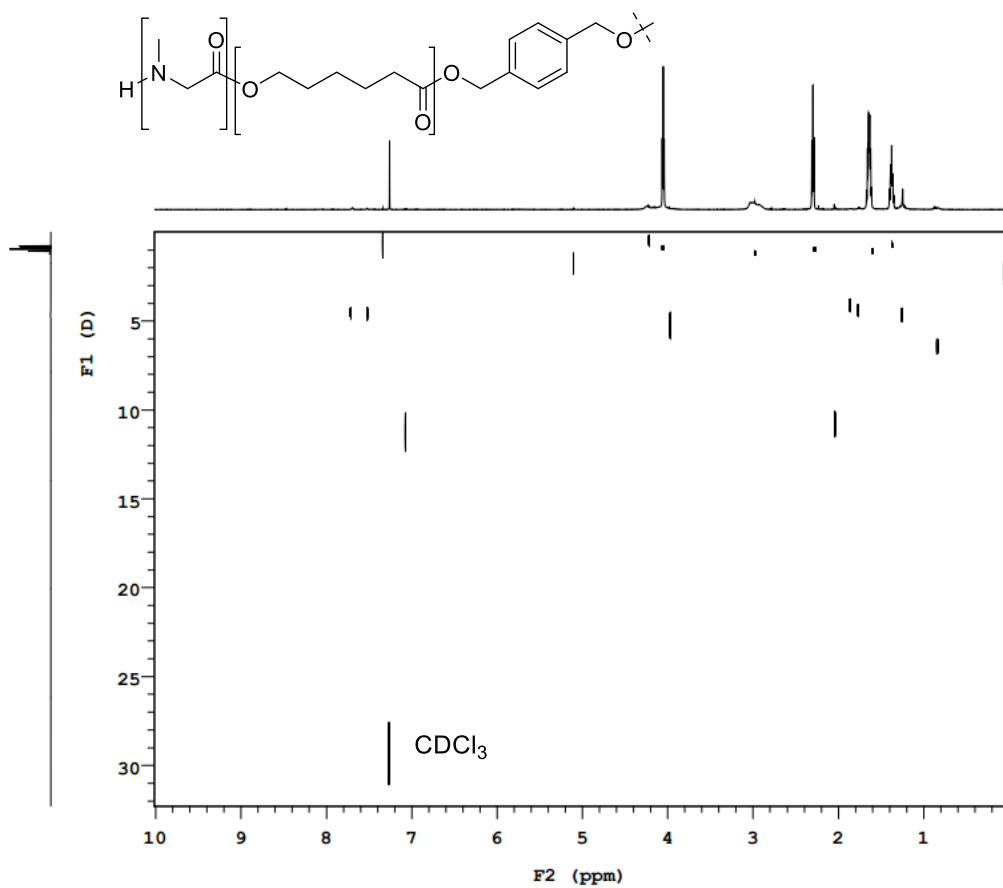


Figure A.23. 600 MHz, ^1H DOSY NMR spectra of poly(sarcosine-*b*-ε-caprolactone-*b*-sarcosine) from Scheme 3.5c in CDCl_3 .

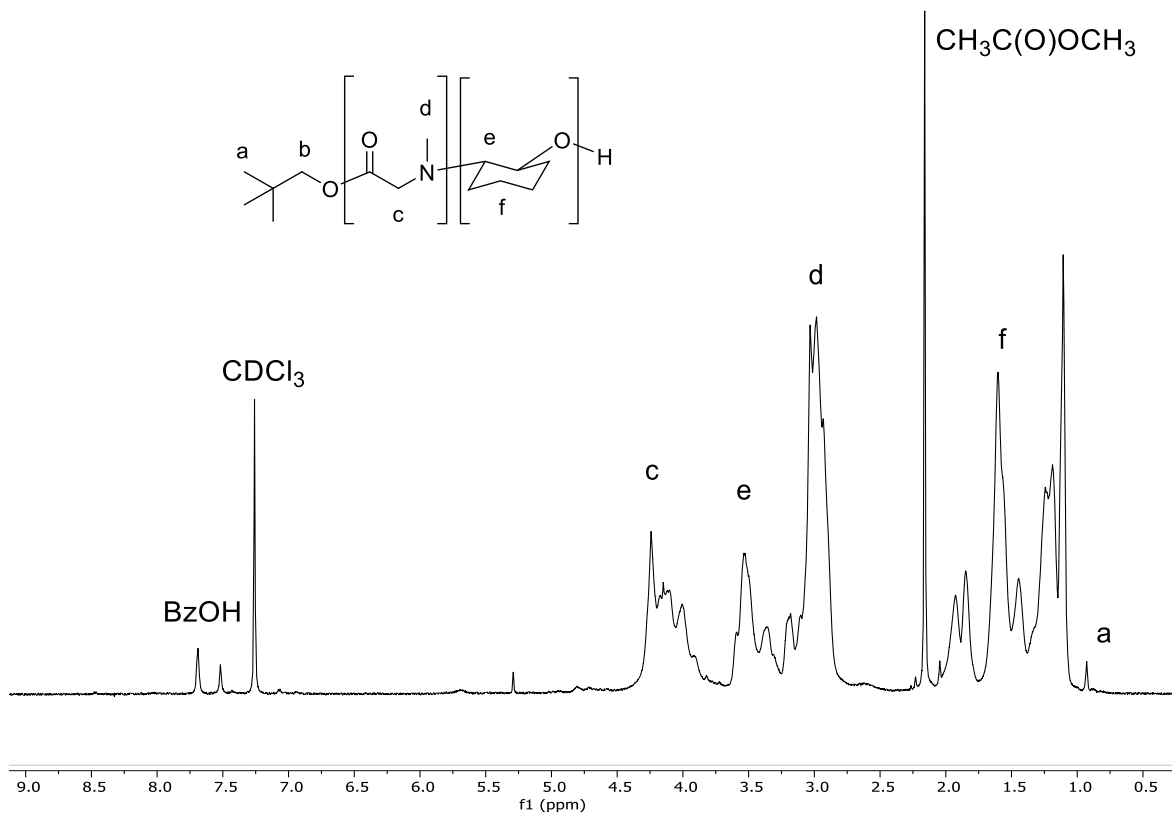


Figure A.24. 500 MHz, ¹H NMR spectrum of poly(sarcosine-*b*-cyclohexene oxide) from Scheme 3.8a in CDCl₃.

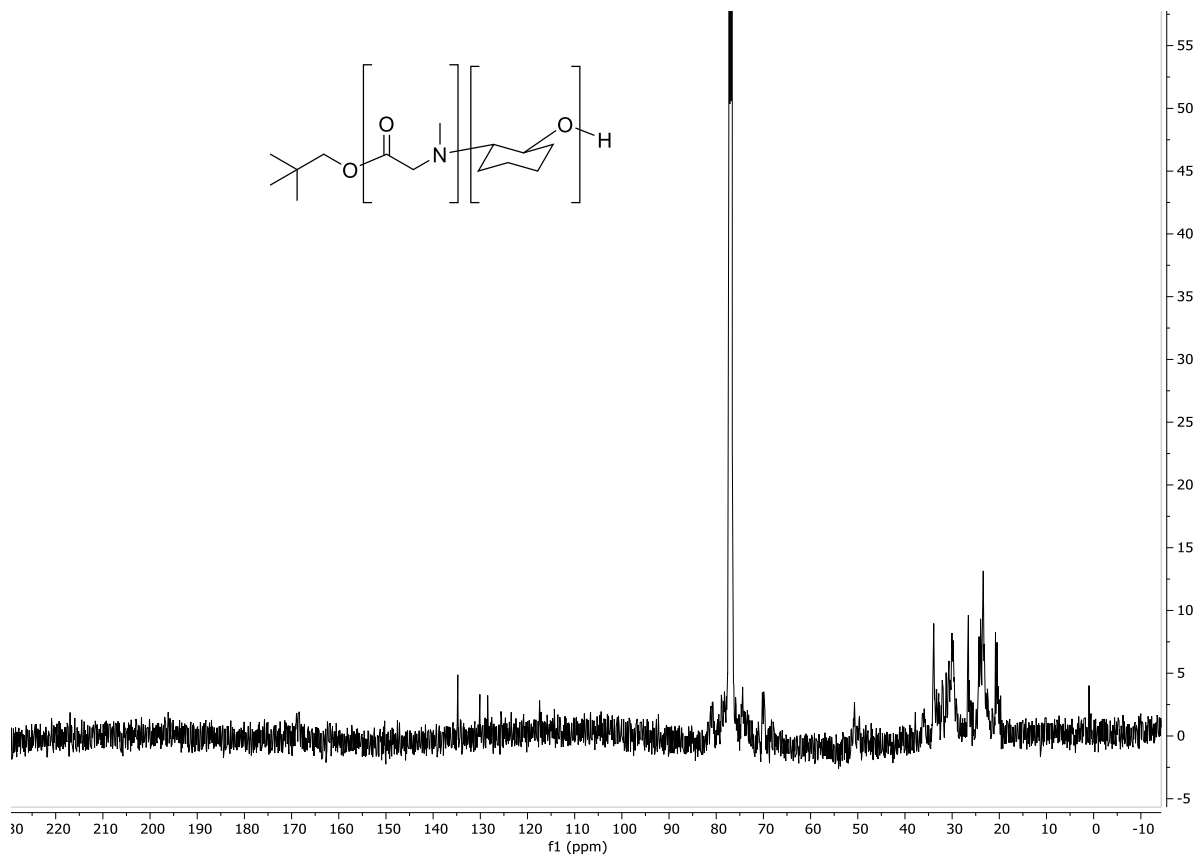


Figure A.25. 500 MHz, ¹³C NMR spectrum of poly(sarcosine-*b*-cyclohexene oxide) from Scheme 3.8a in CDCl₃.

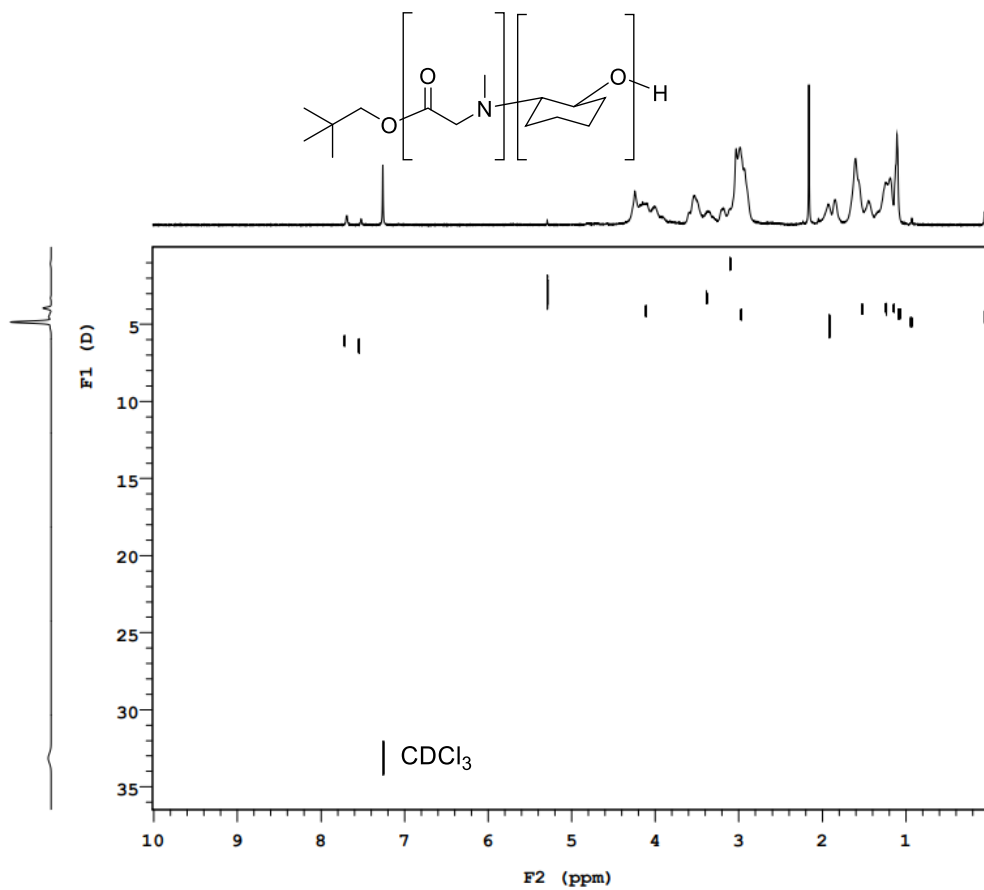


Figure A.26. 500 MHz, ¹H DOSY NMR spectrum of poly(sarcosine-*b*-cyclohexene oxide) from entry Scheme. 3.8a in CDCl₃.

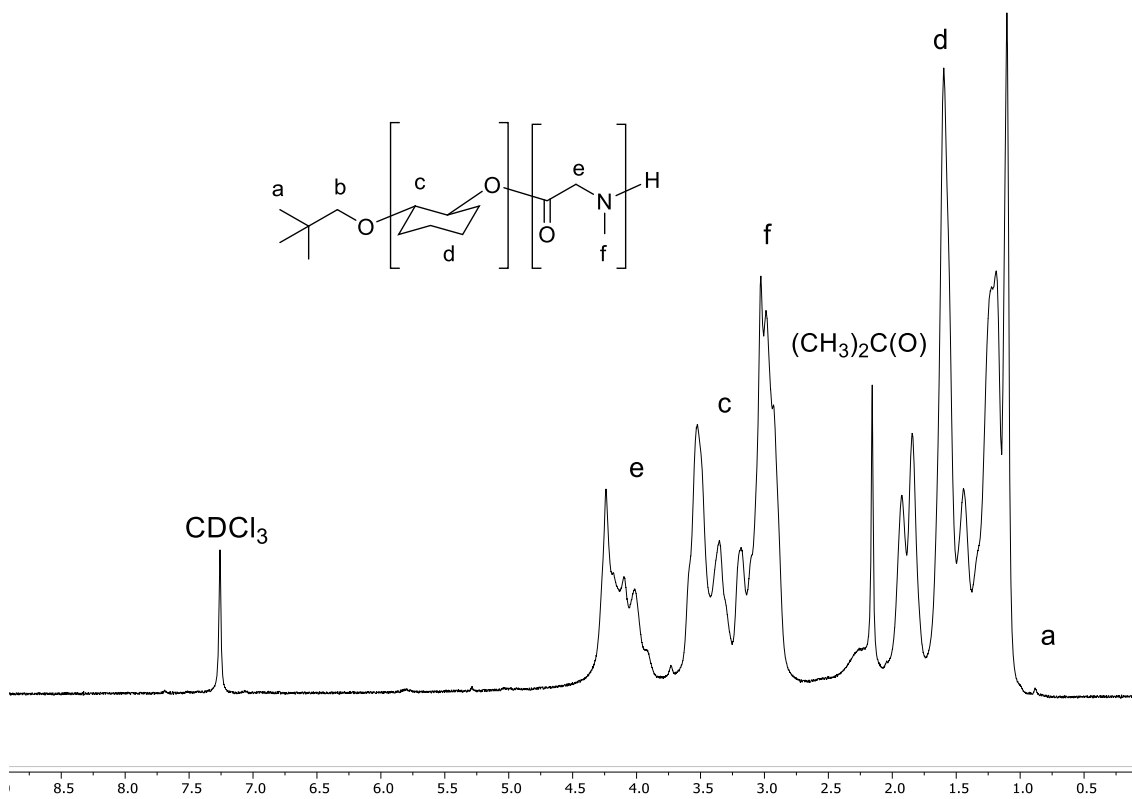


Figure A.27. 600 MHz, ¹H NMR spectrum of poly(cyclohexene oxide-*b*-sarcosine) from Scheme 3.8b in CDCl₃.

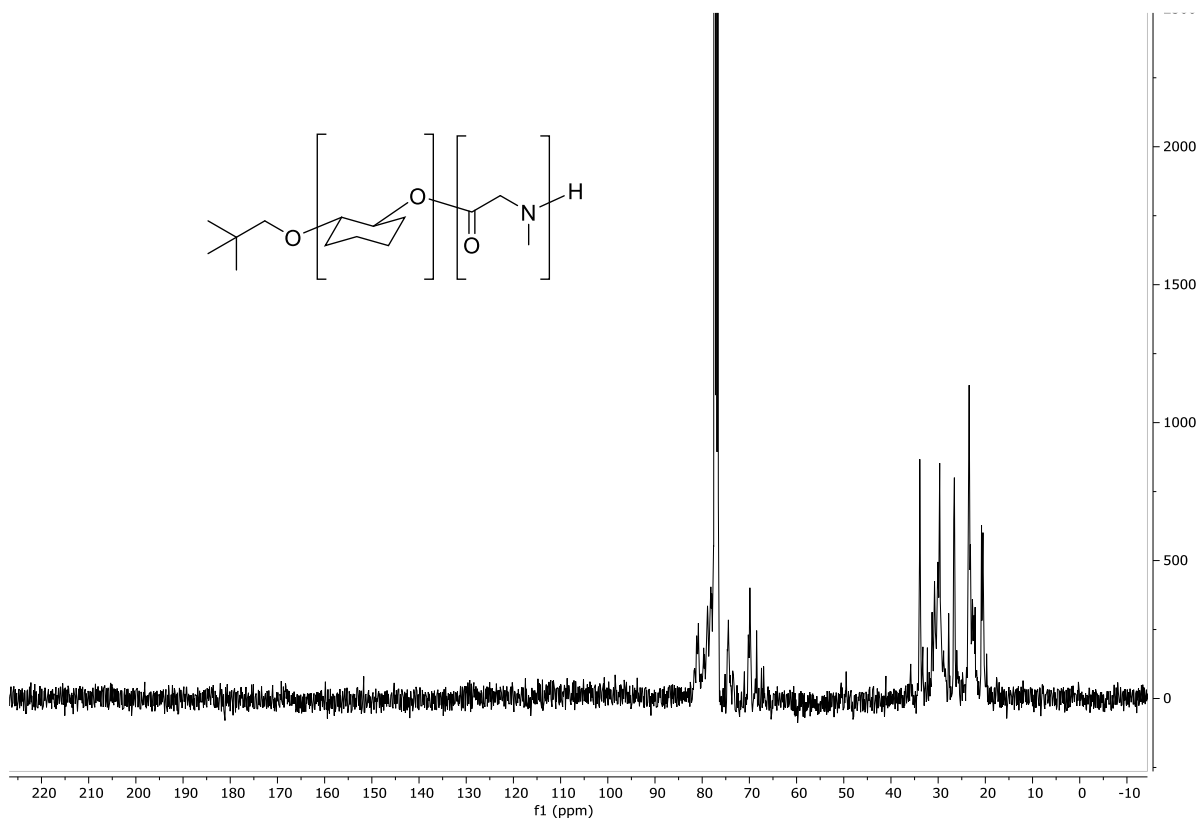


Figure A.28. 125 MHz, ^{13}C NMR spectrum of poly(cyclohexene oxide-*b*-sarcosine) from Scheme 3.8b in CDCl_3 .

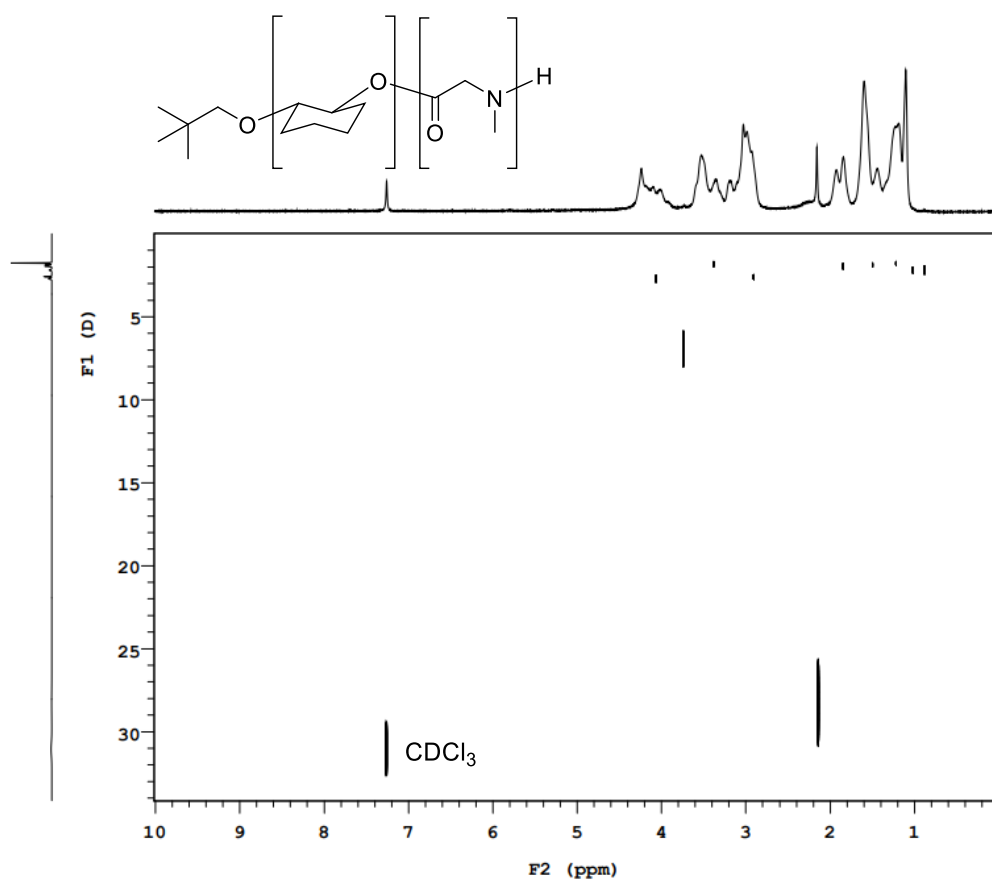


Figure A.29. 600 MHz, ¹H DOSY NMR spectrum of poly(cyclohexene oxide-*b*-sarcosine) from Scheme 3.8b in CDCl₃.

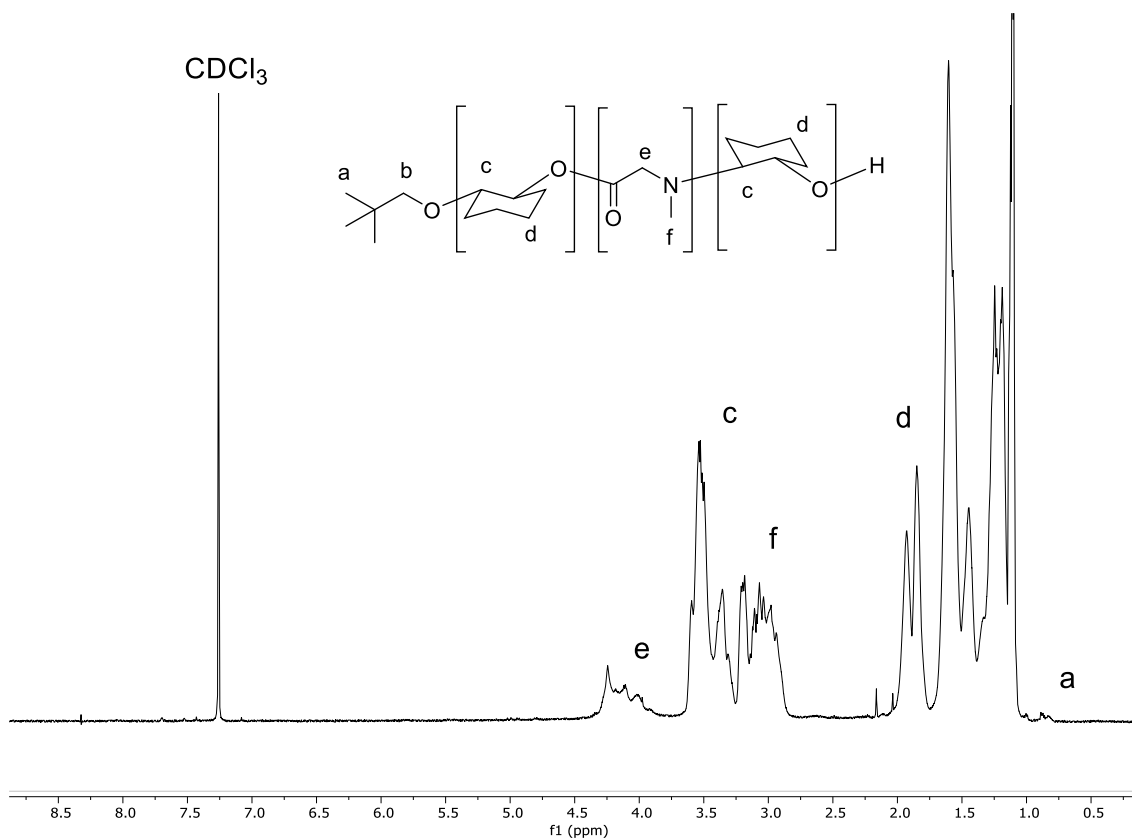


Figure A.30. 500 MHz, ^1H NMR spectrum of poly(cyclohexene oxide-*b*-sarcosine-*b*-cyclohexene oxide') from Scheme 3.9a in CDCl_3 .

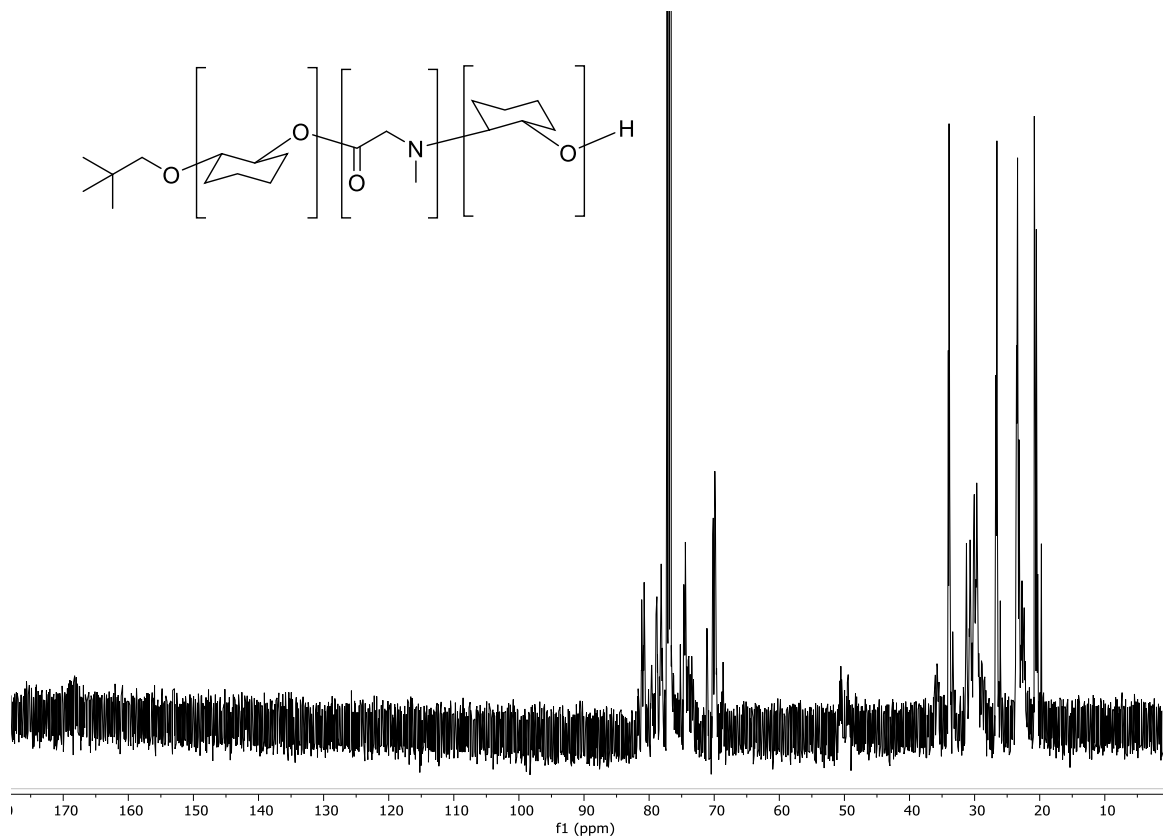


Figure A.31. 125 MHz, ¹³C NMR spectrum of poly(cyclohexene oxide-*b*-sarcosine-*b*-cyclohexene oxide') from Scheme 3.9a in CDCl₃.

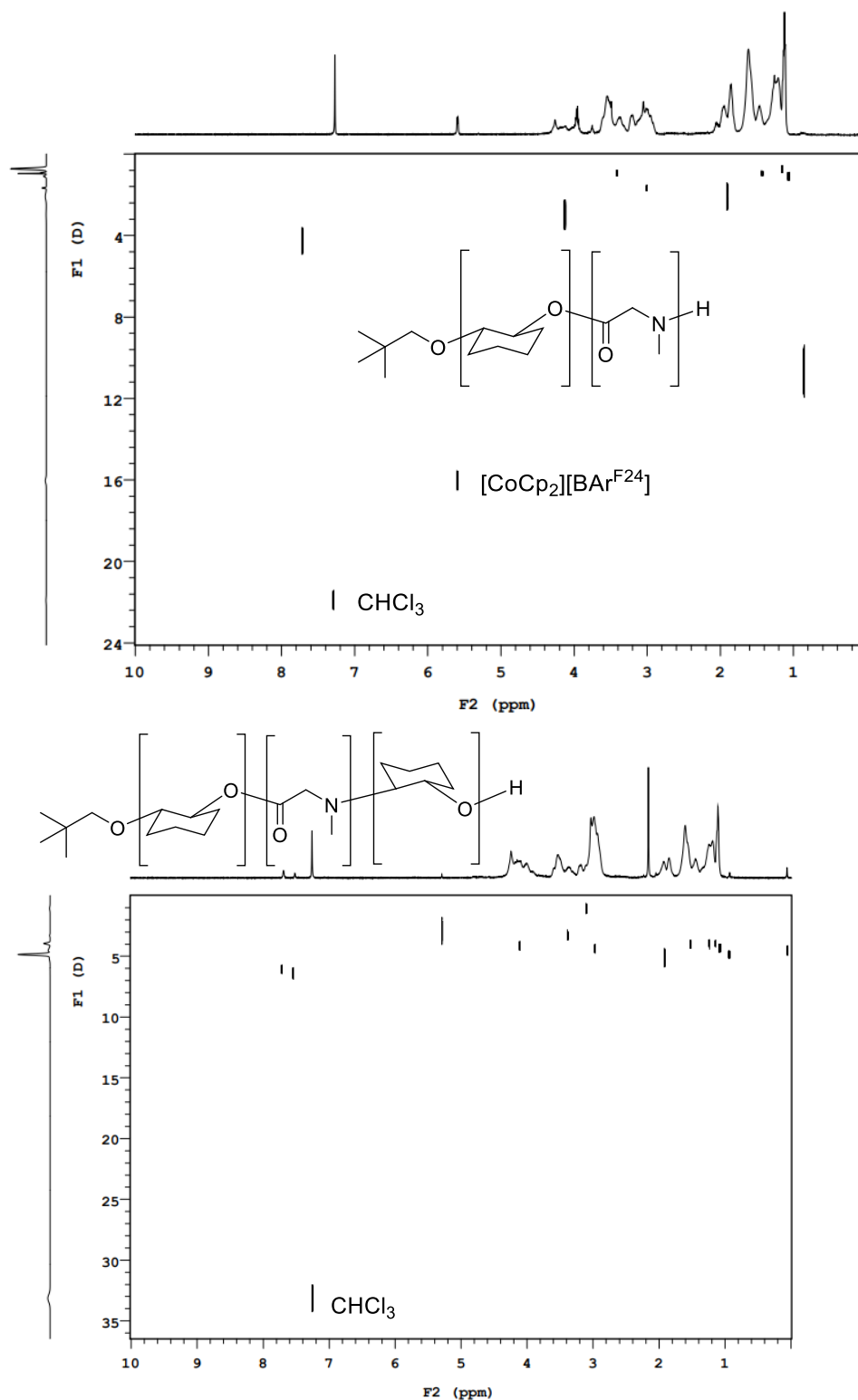


Figure A.32. 500 MHz, ^1H DOSY NMR spectrum of (top) poly(cyclohexene oxide-*b*-sarcosine) and (bottom) poly(cyclohexene oxide-*b*-sarcosine-*b*-cyclohexene oxide') from Scheme 3.9a in CDCl_3 .

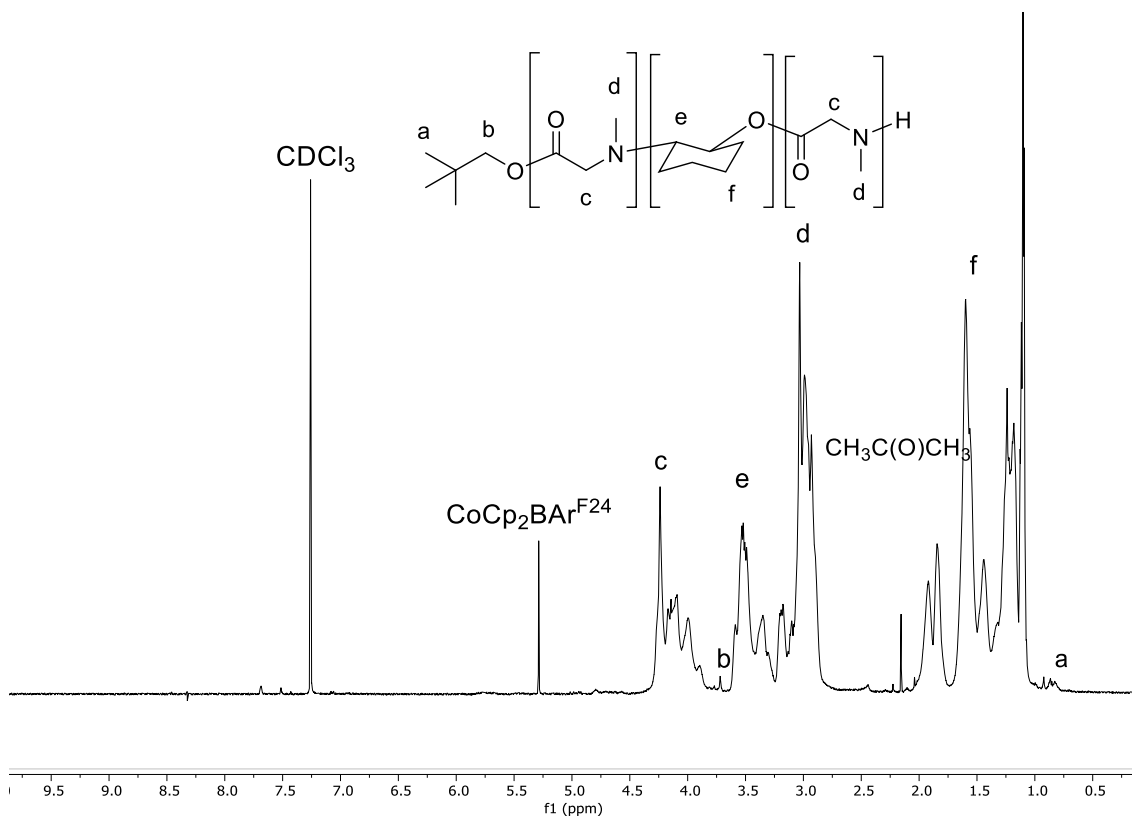


Figure A.33. 500 MHz, ¹H NMR spectrum of poly(sarcosine-*b*-cyclohexene oxide-*b*-sarcosine') from Scheme 3.9b CDCl₃.

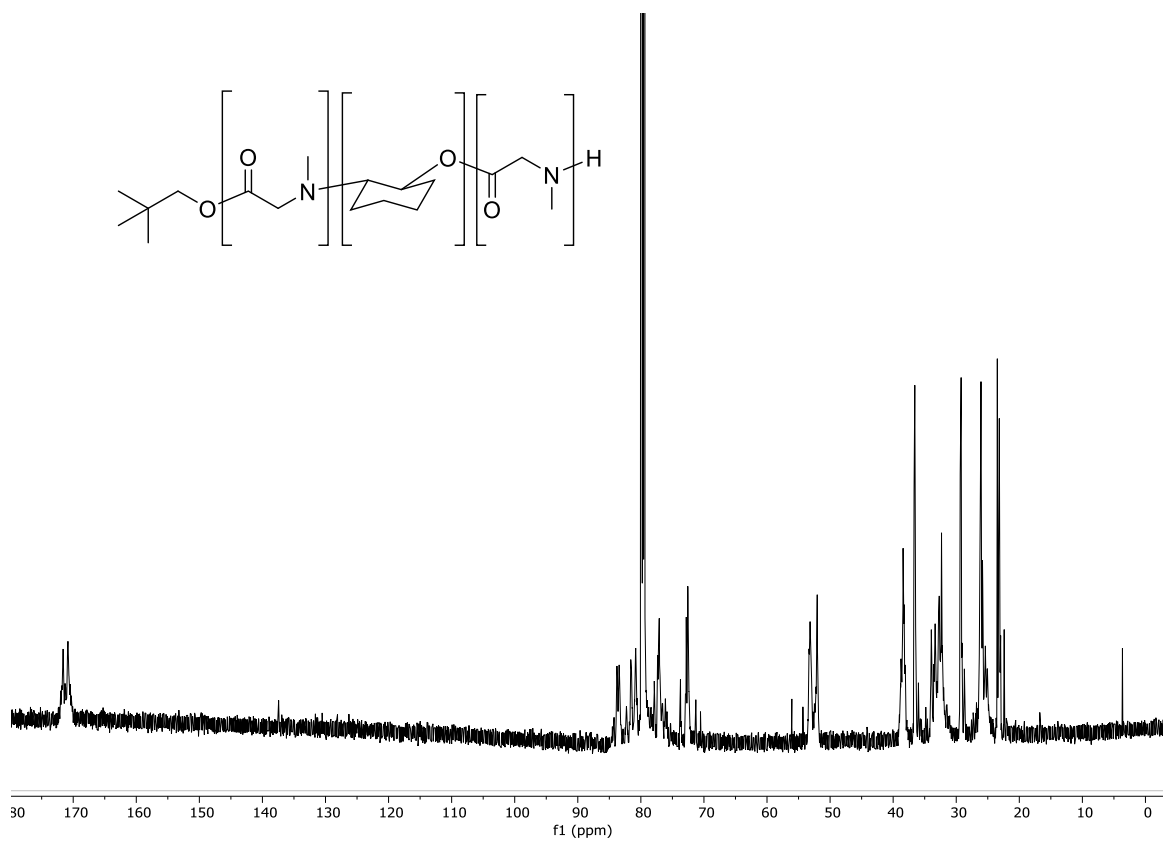


Figure A.34. 125 MHz, ^{13}C NMR spectrum of poly(sarcosine-*b*-cyclohexene oxide-*b*-sarcosine') from Scheme 3.9b in CDCl_3 .

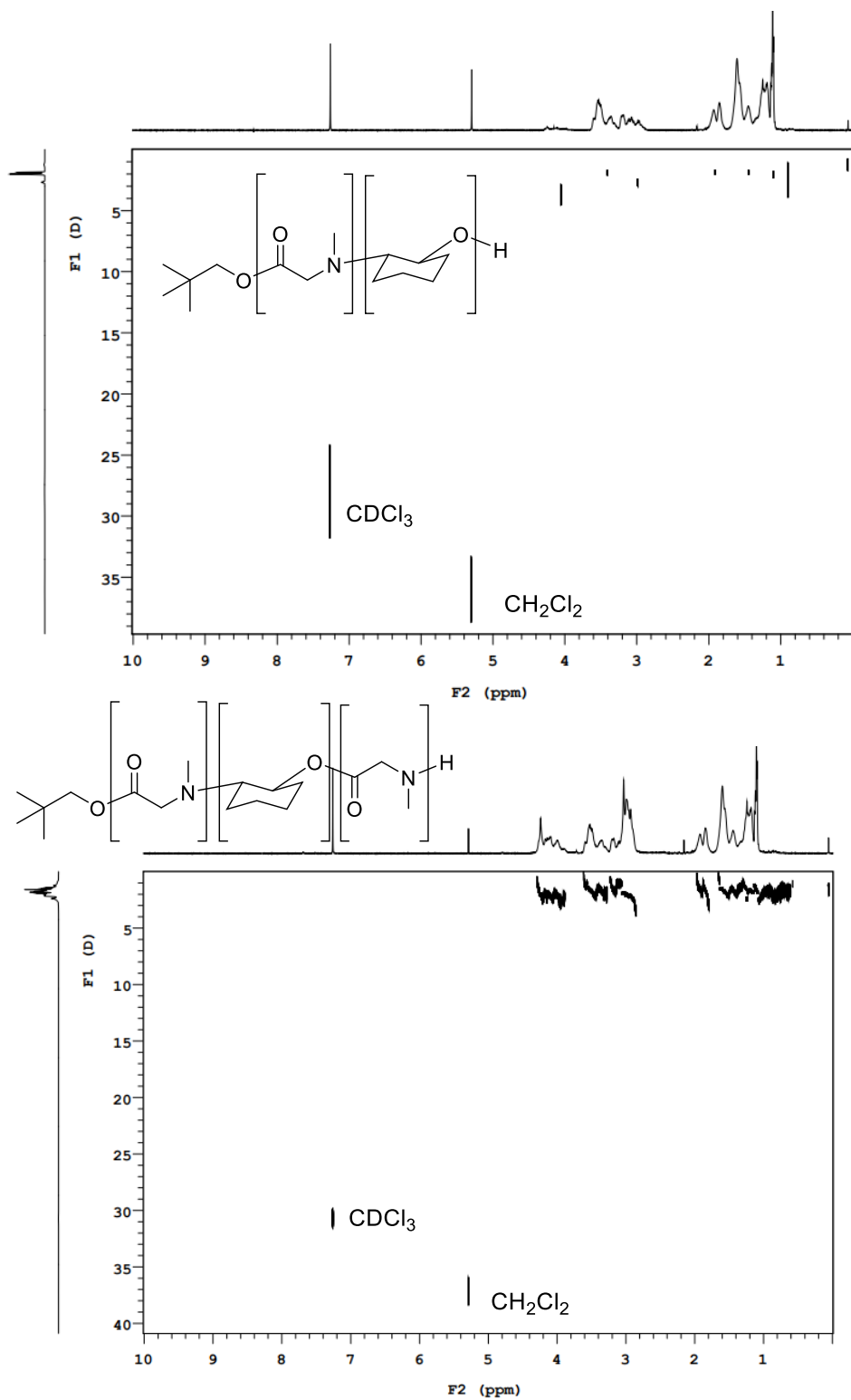


Figure A.35. 500 MHz, ^1H DOSY NMR spectrum of (top) poly(sarcosine-*b*-cyclohexene oxide) and (bottom) poly(sarcosine-*b*-cyclohexene oxide-*b*-sarcosine') from Scheme 3.9b in CDCl_3 .

6.0 Appendix B. GPC Chromatograms for All Polymers

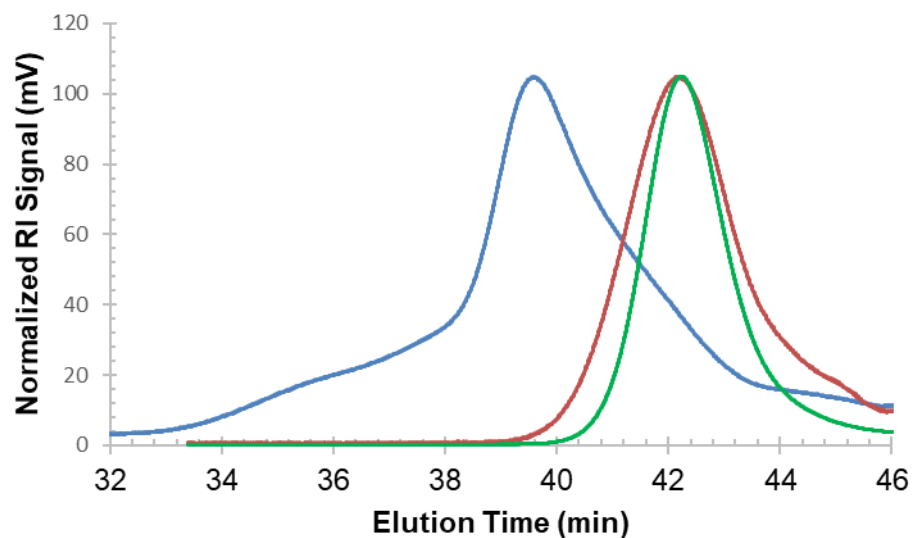


Figure B.1. GPC chromatogram of poly(γ -benzyl-*L*-glutamate) polymerized by complexes **1.48** (green), **3.1** (red) and **1.49** (blue) from entries 3 (green), 6 (red) and 7 (blue), Table 3.1 in DMF at 50 °C recorded by a RI detector.

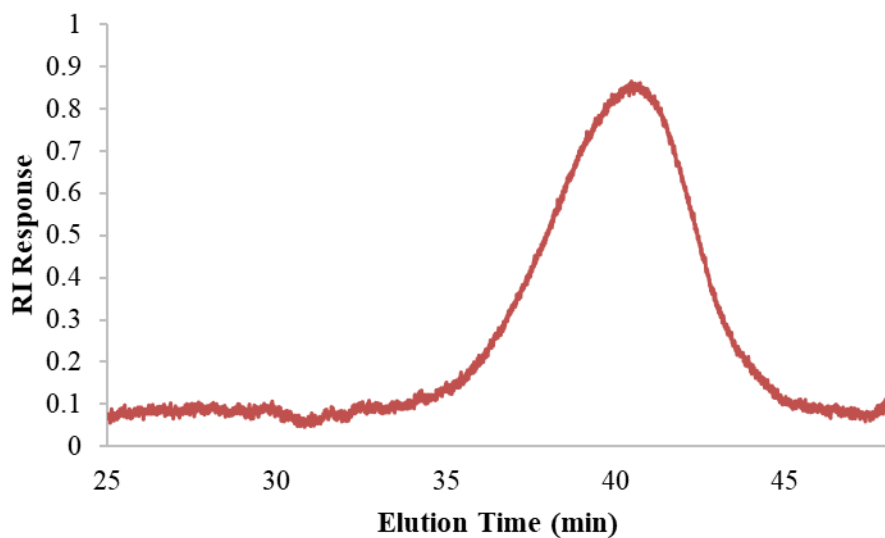


Figure B.2. GPC chromatogram of poly(γ -benzyl-*L*-glutamate) from entry 2, Table 3.2 in DMF at 50 °C recorded by a RI detector.

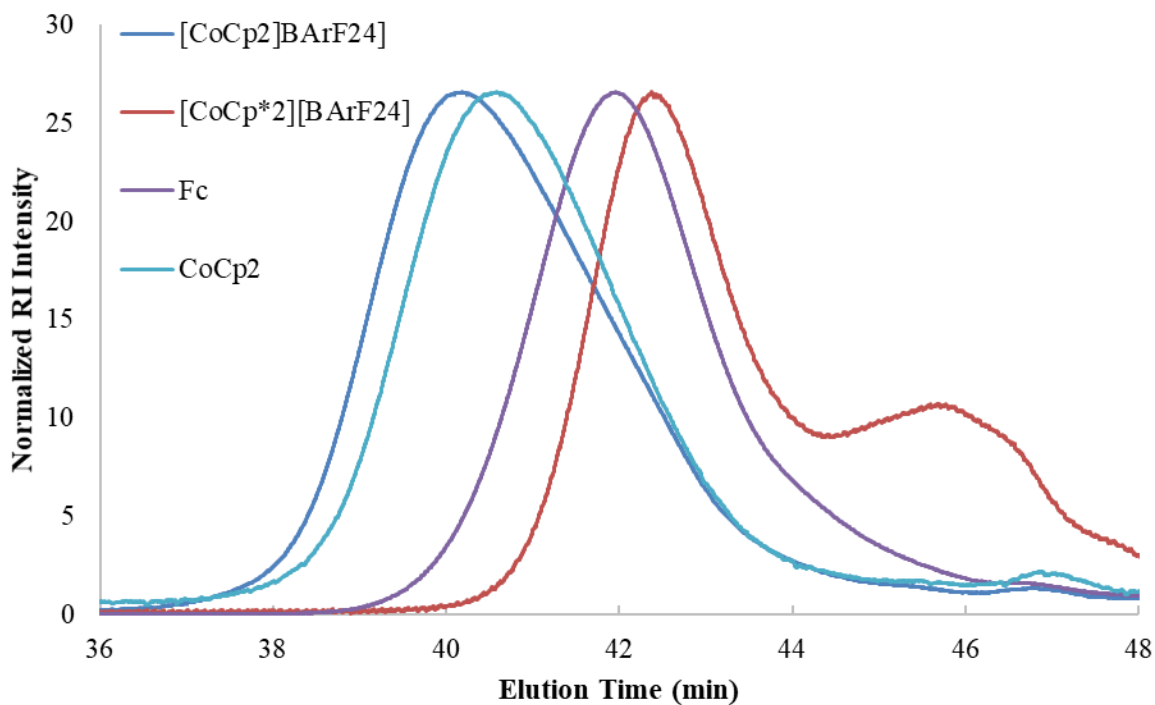


Figure B.3. GPC chromatogram of poly(γ -benzyl-*L*-glutamate) polymerized by **3.1** with different additives from entries 1,2, 4 and 5, Table 3.2. Polymers were measured in DMF at 50 °C recorded by a RI detector.

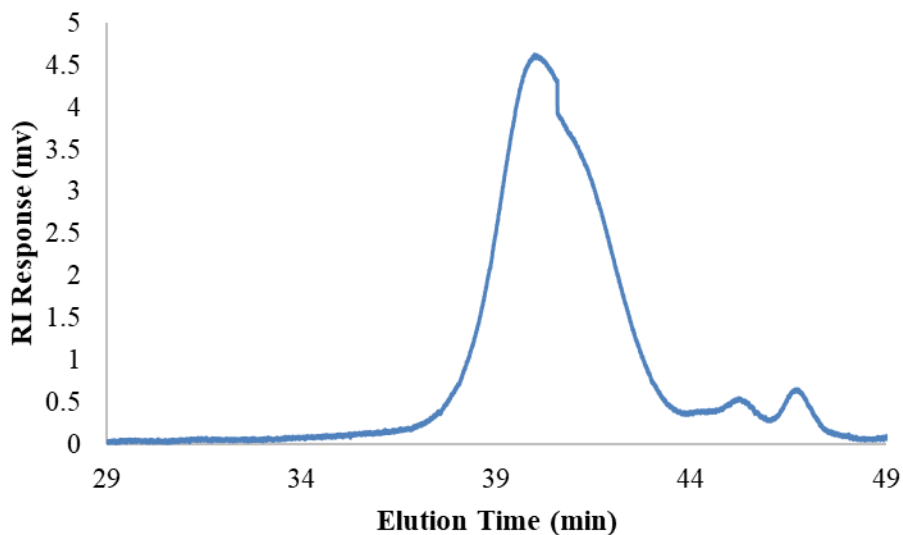


Figure B.4. GPC chromatogram of poly(BLG) from entry 19, Table 3.2 in DMF at 50 °C recorded by a RI detector.

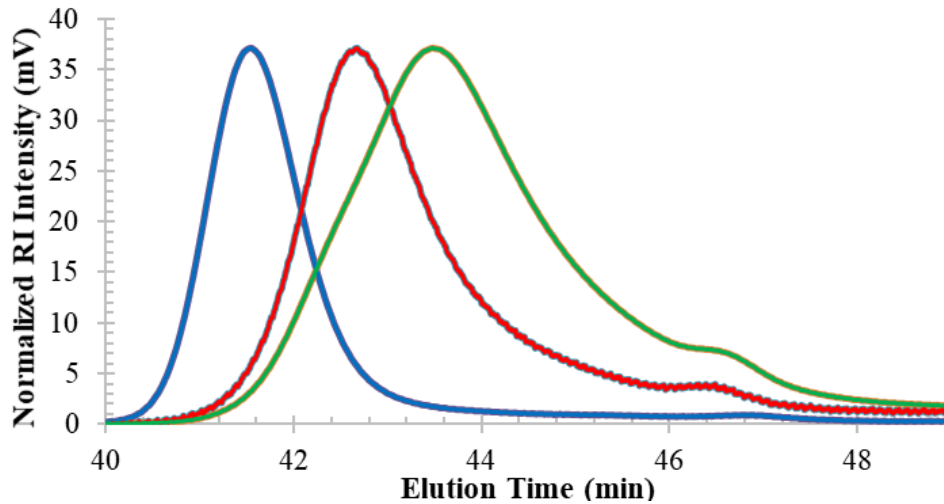


Figure B.5. GPC chromatogram of poly(sarcosine) at various loadings of complex **3.1** to Sar-NCA from entries 1 (1:100 **3.1**:[Sar-NCA], red), 4 (1:50 **3.1**:[Sar-NCA], green) and 5 (1:200 **3.1**:[Sar-NCA], blue), from Table 3.3. Polymers were measured in DMF at 50 °C and recorded by an RI detector.

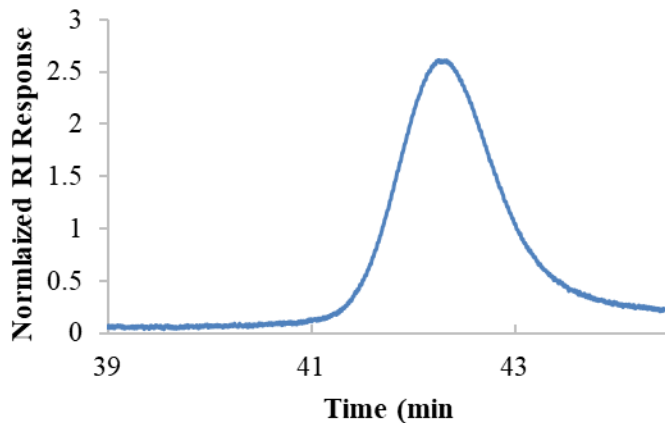


Figure B.6. GPC chromatogram of poly(sarcosine) from entry 6, Table 3.3 in DMF at 50 °C recorded by an RI detector.

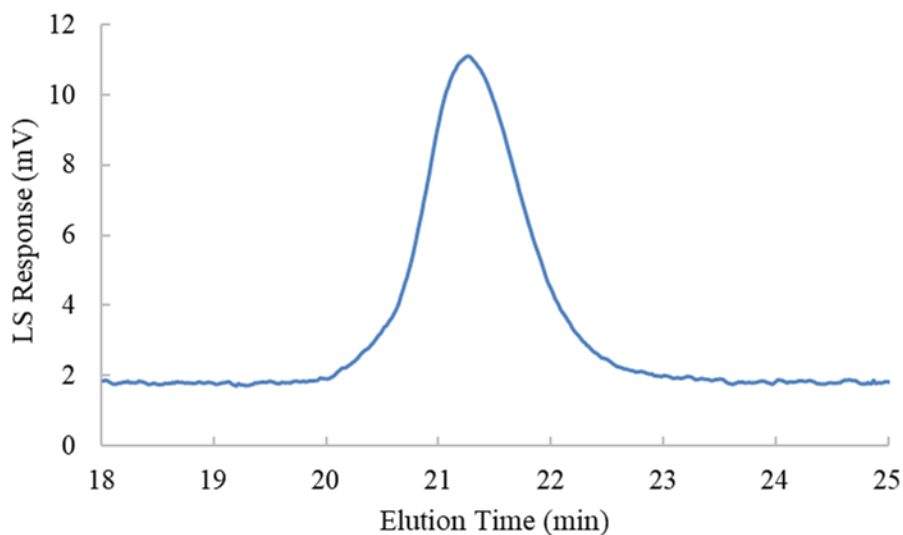


Figure B.7. GPC chromatogram of poly(ϵ -caprolactone) from Scheme 3.4A in THF at 40 °C recorded by a LS detector.

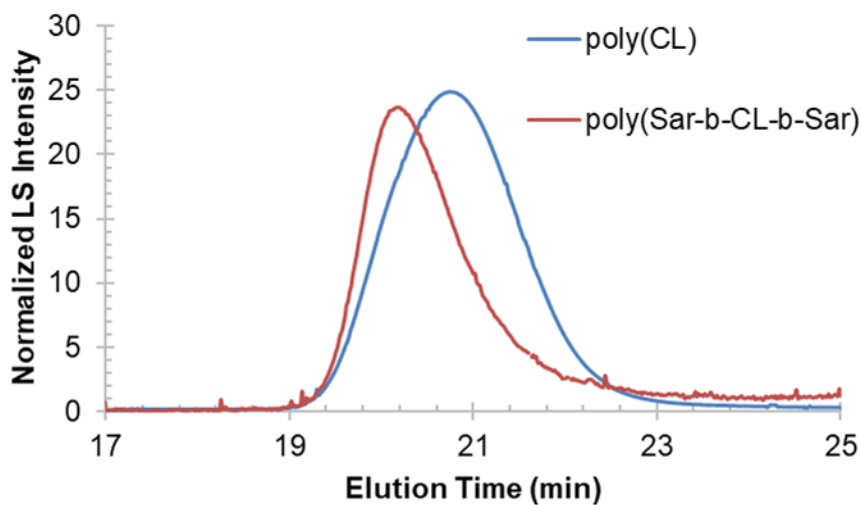


Figure B.8. GPC chromatogram of telechelic poly(ϵ -caprolactone) sequential poly(sarcosine-*b*- ϵ -caprolactone-*b*-sarcosine) from Scheme 3.4c in THF at 40 °C recorded by a LS detector.

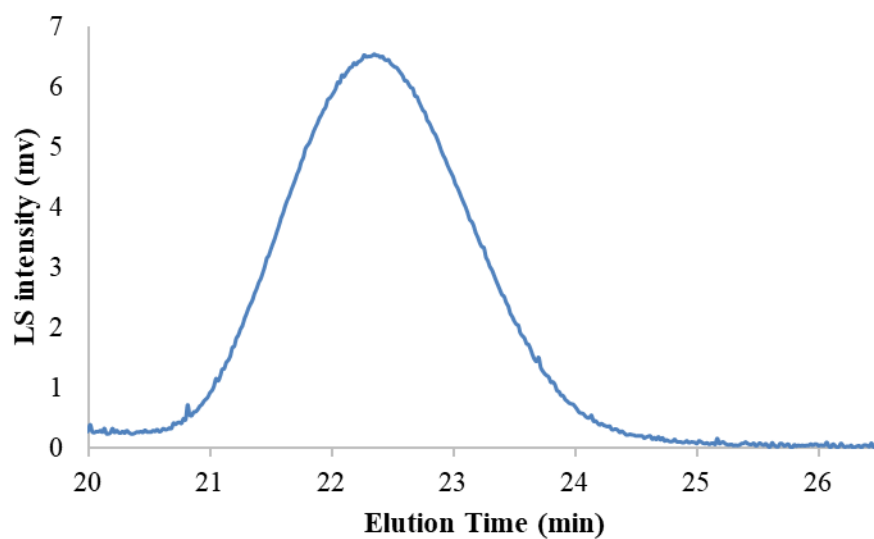
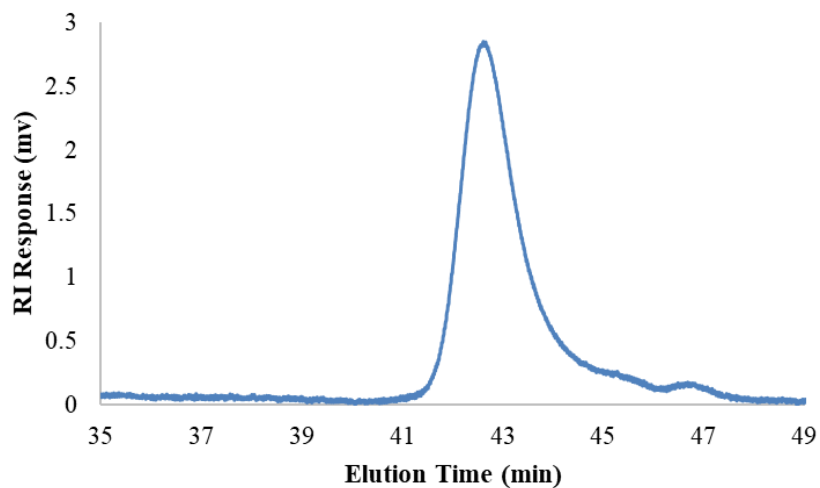


Figure B.9. GPC chromatogram of poly(sarcosine) (top) and poly(sarcosine-*b*-cyclohexene oxide) (bottom) from Scheme 3.8a. Top spectra was recorded using RI detector in DMF at 50 °C. Bottom spectra was recorded using a LS detector in THF at 40 °C.

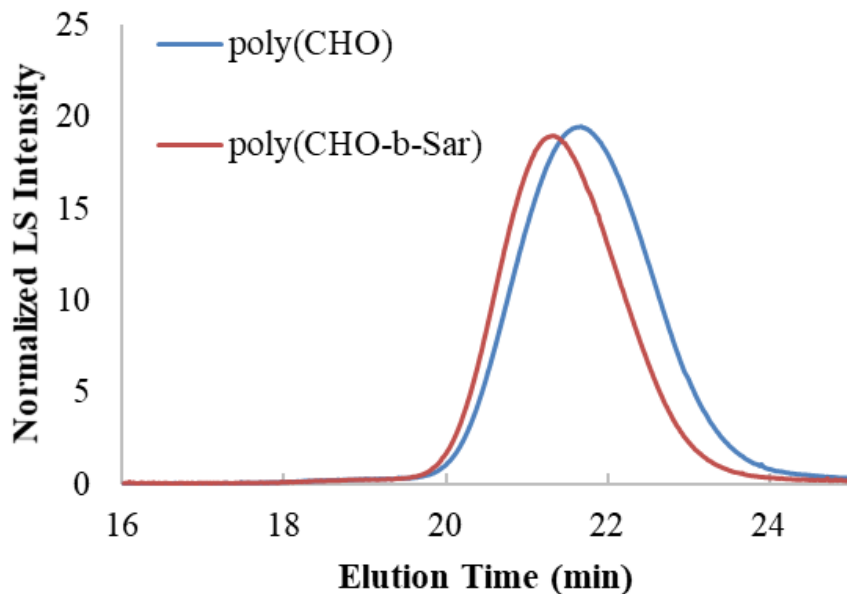


Figure B.10. GPC chromatogram of poly(cyclohexene oxide) and poly(cyclohexene oxide-*b*-sarcosine) from Scheme 3.8b in THF at 40 °C recorded by LS detector.

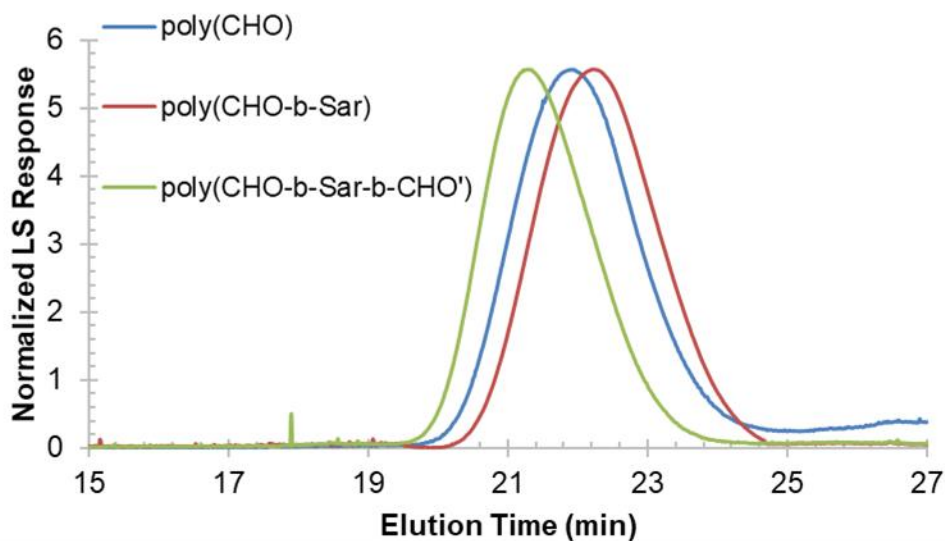


Figure B.11. GPC chromatogram of poly(cyclohexene oxide) (blue), poly(cyclohexene oxide-*b*-sarcosine) (red) and poly(cyclohexene oxide-*b*-sarcosine-*b*-cyclohexene oxide') (green) from Scheme 3.9a.

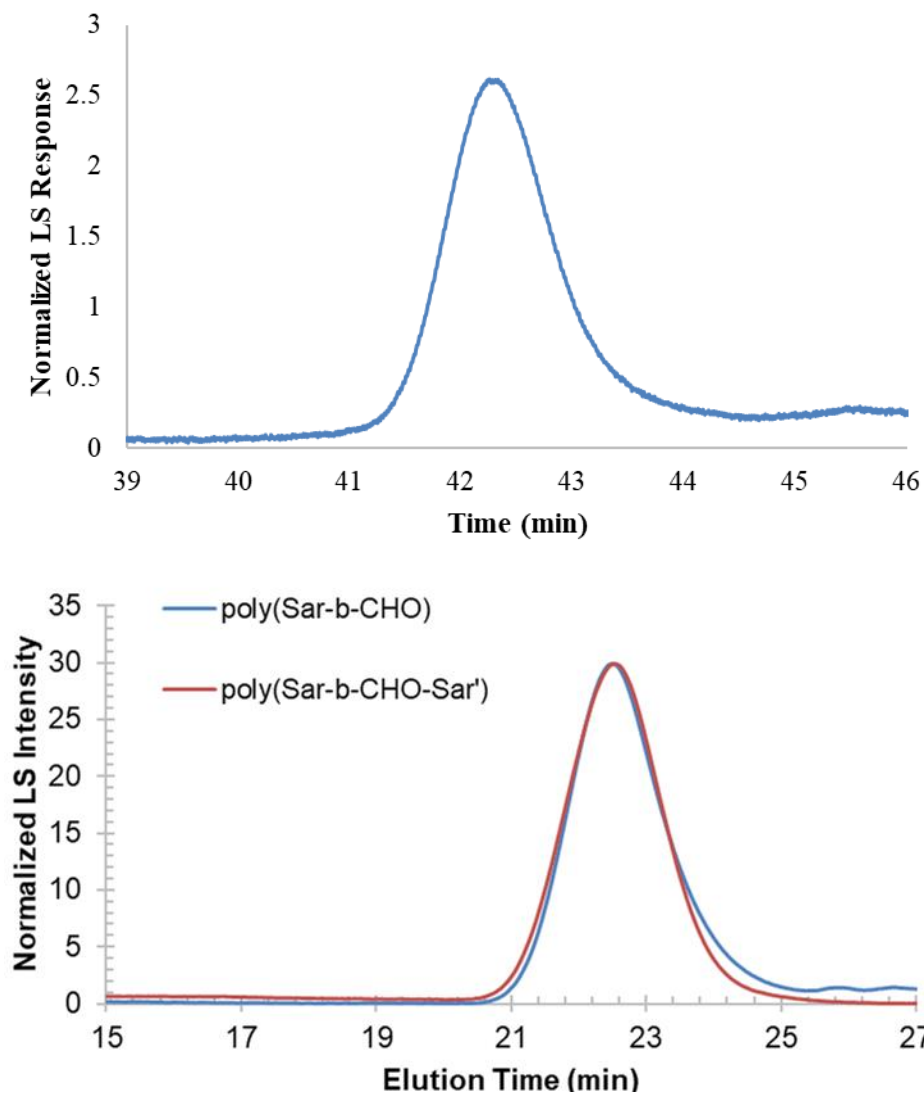


Figure B.12. GPC chromatogram of poly(sarcosine) (top) and poly(sarcosine-*b*-cyclohexene oxide) and poly(sarcosine-*b*-cyclohexene oxide-*b*-sarcosine') (bottom) from Scheme 3.9b. Top spectrum was recorded by RI detector in DMF at 50 °C. Bottom spectra were recorded by a LS detector in THF at 40 °C.

7.0 Appendix C. MALDI Mass Spectrums and Control Reactions from Chapter 3

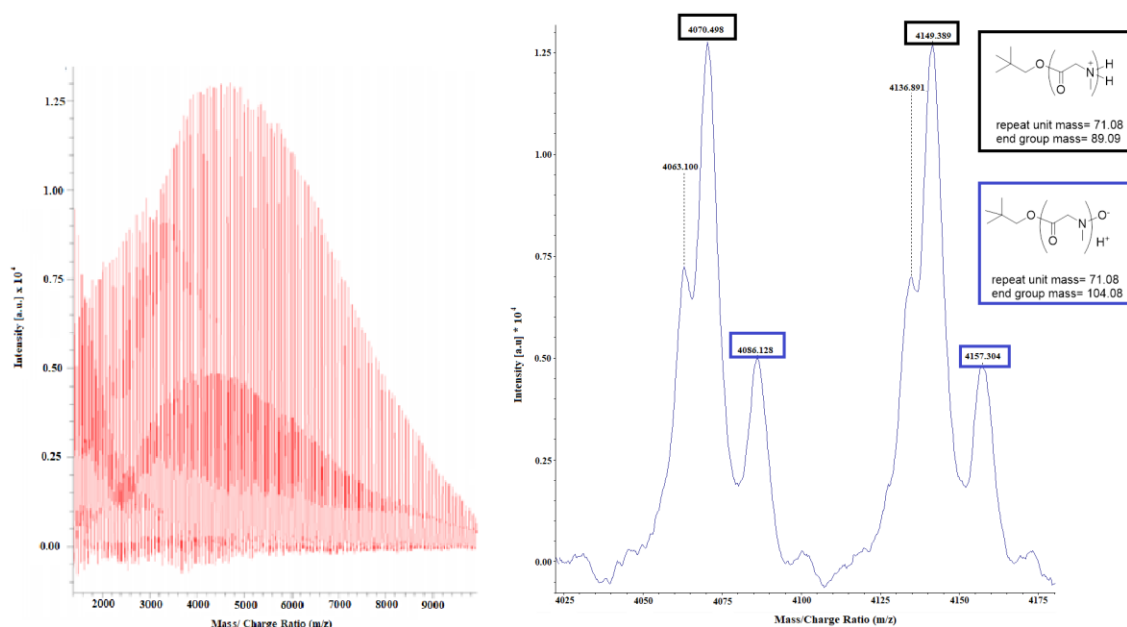


Figure C.1. MALDI spectrum of sarcosine-NCA polymerized by 1 mol % complex **3** for 10 min in THF. Sample was prepared in CHCl_3 at a 1:10 ratio of polymer to trans-2-[3-(4-tert-Butylphenyl)-2-methyl-2-propenylidene]malononitrile with no added cationizing agent. Potentially, excess benzoic acid from quenching of polymerization is acting as the cation source.

Table C.1. Polymerization of cyclohexene oxide by complex **3.2** in various solvents.^a

Solvent	Catalyst loading (mol %)	Time (min)	Conv. ^c (%)	$M_n(\text{theo})^d$ (kDa)	$M_n(\text{exp})^e$ (kDa)	M_w/M_n^f
2-MeTHF	1	60	99	9.8	10.0	1.73
2-MeTHF	0.5	1440	98	19.2	9.1	1.83
PhF	1	60	68	6.7	8.4	1.71
PhCl	1	10	99	9.8	6.3	2.49
PhCl	0.2	10	97	47.6	52.0	2.59

^aReactions were carried out in solvent at using the iron precatalyst at [0.35 M] CHO. ^b

Conversion, determined by ¹H NMR. ^cConversion, determined by both the ¹H NMR and mass of precipitated polymer. ^dTheoretical molecular weight was calculated by $M_n(\text{theo}) = \text{conv.} * \text{MW}_{\text{CHO}} * 200$. ^eExperimental molecular weight and molecular weight distributions were determined by GPC.